B K+− and Form Factors for Semi-Leptonic and Radiative B Decays*

BHARUCHA, AOIFE,KATY,MANEK

$B \to K^* \mu^+ \mu^-$ and Form Factors for Semi-Leptonic and Radiative B Decays

A thesis submitted for the degree of
Doctor of Philosophy
by

Aoife Katy Manek Bharucha

September 2010

Institute for Particle Physics Phenomenology
Department of Physics, Durham University

$B \to K^* \mu^+ \mu^-$ and Form Factors for Semi-Leptonic and Radiative B Decays

Aoife Katy Manek Bharucha

The hadronic environment of the LHC favours the study of exclusive modes, and of these semi-leptonic and radiative B decays will play a leading role in the search for new physics (NP). A prime example is the rare decay $B \to K^*(\to K\pi)\mu^+\mu^-$, where the many measurable quantities offer important new tests of the Standard Model and its extensions. We define sets of CP-conserving and CP-violating observables which are studied in terms of the full form factors, calculated in QCD sum rules on the light-cone (LCSR), and QCD factorisation. Those with reduced dependence on hadronic quantities and sensitivity to NP are identified. In the first few years of data–taking at the LHC, the focus will be on quantities which are simple to extract while maximising the available NP sensitivity. Out of three such observables, two are well known to the experimental community. However a third, one of the CP-conserving angular observables, leads to significant additional constraints on parameter space. We then study form factors for rare semi-leptonic and radiative B decays to $K^{(*)}$, ρ and ϕ_s mesons, combining theoretical and phenomenological constraints from Lattice QCD, LCSR, and dispersive bounds. We pay particular attention to form factor parameterisations which are based on the so-called series expansion, and study the related systematic uncertainties on a quantitative level. Finally we calculate the leading-twist $\mathcal{O}(\alpha_s^2\beta_0)$ corrections to the $B \to \pi$ transition form factor $f_+(0)$ in LCSR, allowing an improved determination of the CKM matrix element $|V_{ub}|$.

Declaration

I declare that no material presented in this thesis has previously been submitted by myself for a degree at this or any other university. This dissertation does not exceed the word limit for the respective Degree Committee. The research described in this thesis has been carried out in collaboration with Patricia Ball, Andrzej Buras and Thorsten Feldmann, as well as Wolfgang Altmannshofer, William Reece, David Straub and Michael Wick, and has been or will be published as follows:

- "Symmetries and Asymmetries of $B \to K^* \mu^+ \mu^-$ Decays in the Standard Model and Beyond"
  W. Altmannshofer, P. Ball, A. Bharucha, A. J. Buras, D. M. Straub and M. Wick
  JHEP **0901**, 019 (2009) [arXiv:0811.1214 [hep-ph]]
- "Constraining new physics with $B \to K^* \mu^+ \mu^-$ in the early LHC era"
  A. Bharucha and W. Reece
  accepted for publication in EPJC
  arXiv:1002.4310 [hep-ph]
- "Theoretical and Phenomenological Constraints on Form Factors for Radiative and Semi-Leptonic B-Meson Decays"
  A. Bharucha, T. Feldmann and M. Wick
  accepted for publication in JHEP
  arXiv:1004.3249 [hep-ph]

Aoife Katy Manek Bharucha

Acknowledgements

Most importantly I would like to express my utmost gratitude to my supervisor Patricia Ball for her invaluable guidance and continual patience over the past four years. I am also grateful to Andrzej Buras and Thorsten Feldmann for welcoming me to the group at Technische Universität München as a visitor in February and March 2009, and for their advice during this period. I am also indebted to my collaborators, William Reece, Michael Wick, Wolfgang Altmannshofer and David Straub, without whom this work would not have been possible. I also must mention Gudrun Hiller and Christoph Bobeth for helpful correspondence with regards to Ch. 2. Similarly, in connection to Ch. 3, I'm obliged to Adrian Signer for advice concerning quark masses, as well as Ulrik Egede and Mitesh Patel for a careful reading of the draft.

I was very fortunate to be a student in the nurturing environment of the IPPP, where members of staff, including the director Nigel Glover and my second supervisor Mike Pennington, were always generous with their time and expertise, and students offered additional assistance when required, especially David Wilson, Eimear O'Callaghan, Jesus Javier Cobos Martinez and Tracey Li, as well as Alison Fowler, Jamie Tattersall, Ciaran Williams and Gareth Jones. I'm also very grateful to the support staff, particularly Linda Wilkinson, Trudy Forster and Phil Roffe, without whom the institute would crumble. My parents and sister Tehmi and my housemates Amanda, Heather, Ana and Sumreni have also been a constant source of support and encouragement. This work was supported in the UK by the Science and Technology Facilities Council (STFC) and also in part by the EU network contract No. MRTN-CT-2006-035482 (Flavianet).

Contents

List of Tables

List of Figures

Chapter 1

Introduction

> '*Grace had stood her ground during that discussion. "There are plenty of things nobody can see," she said. "What about that particle thingy that they're trying to find. That Higgs bison, or whatever."*
>
> *"Boson," Jamie had interjected. "Higgs boson. It's a sort of . . . "*
>
> *"Boson," said Isabel. "I saw Professor Higgs the other day, you know. He was walking along Heriot Row looking down at the pavement."*
>
> *"He won't find his boson down there," said Grace.*
>
> *"He wouldn't have been looking for it," said Jamie. "It exists only in the mathematics he did. It's a theory." '*
>
> —Alexander McCall-Smith in "The Lost Art of Gratitude"

The Large Hadron Collider (LHC) at CERN, Geneva is slowly creeping into public consciousness, being advertised either as a "Big Bang" machine, or as an experiment looking for the Higgs Boson [1], the particle which is responsible for endowing mass on the elements of the Standard Model (SM) [2–9]. This can be inferred from both the 5 million "YouTube" hits of the "Large Hadron Rap" and media coverage the day the LHC switched on. The attention of the press has been in part focused on the anxiety that the high energy of the collisions at the LHC might create a black hole, which could literally mean the end of the world. Strong arguments against these ideas were formulated in Ref. [10], where it was explained that cosmic rays have been colliding with the Earth and Sun etc. at much higher energies for billions of years. From the stability of astronomical bodies we can strongly constrain the rate of accretion of any stable microscopic black

holes that were produced in such collisions. On the other hand, references to the Higgs in books completely unrelated to science, as shown in the quotation above, indicate that some notion of the physics we hope to unravel at the LHC has reached an astonishingly wide audience.

Even if the LHC does detect signs that the Higgs boson exists, and electroweak precision data suggests that it will, there are still many problems of the SM that the Higgs cannot resolve e.g. the origin of flavour, the baryon asymmetry, the presence of dark matter (for a recent review of the SM and its problems see Ref. [11]). In addition, the scalar mass of the Higgs is not protected from quadratic divergences by gauge or chiral symmetries, so in order to avoid fine tuning, i.e. the cancellation of relatively large quantum effects to give a much smaller result, we hope and expect to see signs at the LHC of what lies beyond the frontier of particle physics, as described in Ref. [12]. The detectors which will be probing this frontier directly are ATLAS [13] and CMS [14]. A complementary approach, looking for the unknown via indirect production, is adopted by another detector, LHCb [15], as well as the B physics programs of CMS and ATLAS, reviewed recently in Ref. [16]. More specifically, this involves the study of B meson decays, where non-SM particles might appear in loops, resulting in observed deviations from the SM predictions. Since the size of the effects decreases as the mass scale of the "new physics" (NP) particles increases, high precision B physics measurements can result in sensitivity to a much larger range of scales than via direct production, as elaborated on in the context of effective field theories in Sec. 1.2. This indirect approach has proved invaluable time and again, for example in the prediction of the charm quark mass from the observation of $K^0 - \bar{K}^0$ mixing [17] prior to its discovery by direct production, and similarly for the top quark mass via $B^0 - \bar{B}^0$ mixing [18].

1.1 Flavour structure of the Standard Model

B decays are particularly interesting due to their intrinsic relation to the quark flavour structure of the SM Lagrangian ($\mathcal{L}_{\rm SM}$). For a detailed derivation of $\mathcal{L}_{\rm SM}$ see Ref. [19]. Following Electroweak symmetry breaking, the Yukawa terms $\mathcal{L}_Y^q$, break the SM quark flavour symmetry described by the group $SU(3)_q^3$ [20], via

$$\mathcal{L}_{\rm SM} = \mathcal{L}_K + \mathcal{L}_H - \mathcal{L}_Y^q - \mathcal{L}_Y^l. \tag{1.1}$$

where $\mathcal{L}_K$ contains the kinetic and gauge terms for the electroweak and strong interactions, $\mathcal{L}_H$ the Higgs terms and $\mathcal{L}_Y^l$ the Yukawa terms for the leptons. These $SU(3)_q^3$-breaking terms take the form

$$\mathcal{L}_{\mathrm{Y}}^q = Y_{ij}^d \bar{Q}_{L_i} \cdot \phi D_{R_j} + Y_{ij}^u \bar{Q}_{L_i} \cdot \tilde{\phi} U_{R_j} + h.c. \tag{1.2}$$

where Q_{L_i} is a left handed quark doublet, U_{R_j} is a right handed up-type quark singlet, D_{R_j} is a right handed down-type quark singlet, $Y_{ij}^{u,d}$ are the Yukawa couplings, ϕ is the Higgs scalar, $\tilde{\phi} = i\tau\phi^\dagger$ and i, j indicate the quark generation. $\mathcal{L}_Y^q$ is therefore not invariant under transformations of the form $Q_L \to V_Q Q'_L$, $U_R \to V_U U'_R$ and $D_R \to V_D D'_R$, V_Q, where V_U and V_D are unitary matrices. This called for a convention to be chosen for the quark basis, i.e. $Y^d = \lambda_d$ and $Y^u = V^\dagger \lambda_u$ where $\lambda_{u,d}$ are diagonal, minimising the number of parameters. V is a unitary matrix, known as the Cabibbo-Kobayashi-Maskawa (CKM) matrix [21; 22]. Due to the unitarity of V, at tree level it only affects charged current weak interactions. Here the participating eigenstates (d', s', b') differ from the mass eigenstates (d, s, b). This results in flavour changing charged currents (FCCC's), which play a leading role in B decays. Note that the vanishing of flavour changing neutral currents (FCNC's) at tree level is known as the Glashow-Iliopoulos-Maiani (GIM) mechanism [23].

The CKM matrix can be described by three real angles and a CP-violating phase; the first experimental evidence of this phase was found in $K^0 - \bar{K}^0$ mixing [24] and later in $B^0 - \bar{B}^0$ mixing at Babar and Belle [25; 26]. Note that the only other instance of a CP-violating phase in the SM is the strong CP phase, θ_{QCD}. However, experimental measurements of the neutron electron dipole moment force it to be unnaturally small, resulting in the strong CP problem, for more details see Ref. [27]. The experimental observation in 1983 that b quarks decays predominantly to c, i.e. $|V_{ub}| << |V_{cb}|$, along with the recognition that $|V_{cb}| \sim |V_{us}|^2$, resulted in the parameterisation in terms of λ, A, ρ and η by Wolfenstein [28],

$$V = \begin{pmatrix} V_{ud} & V_{us} & V_{ub} \\ V_{cd} & V_{cs} & V_{cb} \\ V_{td} & V_{ts} & V_{tb} \end{pmatrix} = \begin{pmatrix} 1 - \lambda^2/2 & \lambda & A\lambda^3(\rho - i\eta) \\ -\lambda & 1 - \lambda^2/2 & A\lambda^2 \\ A\lambda^3(1 - \rho - i\eta) & -A\lambda^2 & 1 \end{pmatrix} + \mathcal{O}(\lambda^4), \tag{1.3}$$

expanding in the small parameter $\lambda \approx 0.22$. The unitarity of the CKM matrix results in a number of orthogonality conditions, e.g. between the first and third columns of V,

$$V_{ud}V_{ub}^* + V_{cd}V_{cb}^* + V_{td}V_{tb}^* = 0\,. \tag{1.4}$$

This relation, rescaled by $V_{cd}V_{cb}^*$, is often represented in the complex $\bar{\rho} - \bar{\eta}$ plane by the unitarity triangle, defined by the origin, $\{1, 0\}$ and the point $\{\bar{\rho}, \bar{\eta}\}$ where, for convenience, the phase convention is chosen such that the side of length 1 is real. Note that to ensure that the unitarity of the CKM matrix holds to all orders in λ, ρ and η are rescaled to $\bar{\rho} = \rho\,(1 - \lambda^2/2)$ and $\bar{\eta} = \eta\,(1 - \lambda^2/2)$ [29]. The three angles of the triangle, α, β and γ, are given by

$$\alpha \equiv \arg\left(-\frac{V_{td}V_{tb}^*}{V_{ud}V_{ub}^*}\right)\,, \quad \beta \equiv \arg\left(-\frac{V_{cd}V_{cb}^*}{V_{td}V_{tb}^*}\right)\,, \quad \gamma \equiv \arg\left(-\frac{V_{ud}V_{ub}^*}{V_{cd}V_{cb}^*}\right)\,. \tag{1.5}$$

The major success of the B Factories, the BaBar detector at PEP-II, and the Belle detector at KEK-B, was measuring these angles and the parameters λ, A, ρ and η, in an attempt to overconstrain the unitarity triangle. For example, λ can be determined from $K \to \pi l\nu$, A from $b \to cl\nu$, $\sin 2\beta$ from the CP asymmetry in $B \to \Psi K_s$, $|V_{ub}|$ from inclusive and exclusive $b \to ul\nu$, γ from $B \to DK$ decays, α from $B \to \pi\pi$, $\pi\rho$, $\rho\rho$ decays, $|V_{ts}/V_{td}|$ from the ratio of the mass splitting in B_s and B_d mixing [30]. Any inconsistencies in these measurements would indicate a possible new physics contribution. Constraints on the Unitarity Triangle as imposed from numerous experimental sources have been complied by the UTfit collaboration [31] and the CKMFitter group [32], which adopt a Bayesian and frequentist approach respectively. From these results it is clear that the matter-antimatter asymmetry cannot be explained by electroweak baryogenesis and CP violation in the CKM triangle alone, and physics beyond the SM must contribute either via flavour blind phases in the quark sector, or through leptogenesis (for an overview of electroweak baryogenesis see Ref. [33]).

1.2 Effective Field Theories and Renormalisation

Extracting the desired parameters from experimental observables requires a varying degree of theoretical input, more so in the case of exclusive decays where the perturbative quark interaction must be related to the hadronic matrix element. These hadronic effects are discussed in Secs. 1.3-1.6. First however, we must consider the calculation of heavy

b quark interactions which is greatly simplified by the indispensable tool of effective field theories. This allows the separations of long and short distance contributions into effective operators and perturbatively calculable Wilson coefficients respectively, such that the resulting effective Hamiltonian takes the form

$$\mathcal{H}_{eff} \sim \sum_i C_i \mathcal{O}_i. \tag{1.6}$$

The operators $\mathcal{O}_i$ contain the degrees of freedom relevant below the factorisation or renormalisation scale. The effective couplings for these operators are then the Wilson coefficients C_i, which can be obtained by, in path-integral language, "integrating out" all fields above this scale, i.e. removing such fields as dynamical degrees of freedom [34]. More specifically for $B \to K^* \mu^+ \mu^-$, the subject of Chs. 2 and 3, we require the effective Hamiltonian for $b \to s\mu^+\mu^-$ transitions, given by [35; 36]

$$\mathcal{H}_{\text{eff}} = -\frac{4\, G_F}{\sqrt{2}} \left(\lambda_t \mathcal{H}_{\text{eff}}^{(t)} + \lambda_u \mathcal{H}_{\text{eff}}^{(u)} \right). \tag{1.7}$$

Here λ_i indicates the CKM combination $V_{ib}V_{is}^*$ and the Fermi coupling constant G_F is defined by

$$\frac{G_F}{\sqrt{2}} = \frac{g_2^2}{8 M_W^2}, \tag{1.8}$$

where g_2 is the weak coupling constant and M_W is the mass of the charged weak boson, $W^\pm$. Finally we define

$$\mathcal{H}_{\text{eff}}^{(t)} = C_1 \mathcal{O}_1^c + C_2 \mathcal{O}_2^c + \sum_{i=3}^{10} C_i \mathcal{O}_i \,,$$

$$\mathcal{H}_{\text{eff}}^{(u)} = C_1 (\mathcal{O}_1^c - \mathcal{O}_1^u) + C_2 (\mathcal{O}_2^c - \mathcal{O}_2^u) \,.$$

The operators are as in the basis defined by Chetyrkin, Misiak and Münz (CMM) [37]. These are identical to the P_i given in Ref. [35], and are defined by,

$$\begin{aligned} \mathcal{O}_1^u &= (\bar{s}\gamma_\mu T^a P_L u)(\bar{u}\gamma^\mu T^a P_L b), \\ \mathcal{O}_2^u &= (\bar{s}\gamma_\mu P_L u)(\bar{u}\gamma^\mu P_L b), \end{aligned} \tag{1.9}$$

$$
\begin{aligned}
\mathcal{O}_1^c &= (\bar{s}\gamma_\mu T^a P_L c)(\bar{c}\gamma^\mu T^a P_L b),\\
\mathcal{O}_2^c &= (\bar{s}\gamma_\mu P_L c)(\bar{c}\gamma^\mu P_L b),\\
\mathcal{O}_3 &= (\bar{s}\gamma_\mu P_L b)\textstyle\sum_q(\bar{q}\gamma^\mu q),\\
\mathcal{O}_4 &= (\bar{s}\gamma_\mu T^a P_L b)\textstyle\sum_q(\bar{q}\gamma^\mu T^a q),\\
\mathcal{O}_5 &= (\bar{s}\gamma_{\mu_1}\gamma_{\mu_2}\gamma_{\mu_3} P_L b)\textstyle\sum_q(\bar{q}\gamma^{\mu_1}\gamma^{\mu_2}\gamma^{\mu_3} q),\\
\mathcal{O}_6 &= (\bar{s}\gamma_{\mu_1}\gamma_{\mu_2}\gamma_{\mu_3} T^a P_L b)\textstyle\sum_q(\bar{q}\gamma^{\mu_1}\gamma^{\mu_2}\gamma^{\mu_3} T^a q),\\
\mathcal{O}_7 &= \tfrac{e}{g^2} m_b(\bar{s}\sigma^{\mu\nu} P_R b) F_{\mu\nu},\\
\mathcal{O}_8 &= \tfrac{1}{g} m_b(\bar{s}\sigma^{\mu\nu} T^a P_R b) G^a_{\mu\nu},\\
\mathcal{O}_9 &= \tfrac{e^2}{g^2}(\bar{s}\gamma_\mu P_L b)\textstyle\sum_l(\bar{l}\gamma^\mu l),\\
\mathcal{O}_{10} &= \tfrac{e^2}{g^2}(\bar{s}\gamma_\mu P_L b)\textstyle\sum_l(\bar{l}\gamma^\mu\gamma_5 l),
\end{aligned}
\tag{1.10}
$$

where g is the strong coupling constant, $P_{L,R} = (1 \mp \gamma_5)/2$, $F_{\mu\nu}$ and $G_{\mu\nu}$ are the photonic and gluonic field strengths, and sums over q and l denote sums over light quarks and leptons, respectively. m_b denotes the running b quark mass in the $\overline{\text{MS}}$ scheme described below. Note that $m_s P_L$ contributions to $\mathcal{O}_7$, $\mathcal{O}_8$ are neglected here. The inclusion of the factors $16\pi^2/g^2 = 4\pi/\alpha_s$ in the definition of the operators $\mathcal{O}_{i\geq 7}$ serves to allow a more transparent organisation of the expansion of their associated Wilson coefficients in perturbation theory: all C_i are expanded as

$$
C_i = C_i^{(0)} + \frac{\alpha_s}{4\pi} C_i^{(1)} + \left(\frac{\alpha_s}{4\pi}\right)^2 C_i^{(2)} + O(\alpha_s^3)\,, \tag{1.11}
$$

where $C_i^{(0)}$ is the tree-level contribution, which vanishes for all operators but $\mathcal{O}_2$, and in our notation $C_9^{(0)}$ is also non-zero. $C_i^{(n)}$ denotes an n-loop contribution.

Both the bare operators and Wilson coefficients contain divergences, which must be removed by a process know as renormalisation (for a detailed introduction to renormalisation see Ref. [19]). This is a two step procedure, first the theory is regulated to allow manipulation of quantities, and then the divergent terms are removed. In the following we work in naïve Dimensional regularisation [38–40], where the number of dimension is set to $4 - 2\epsilon$, and γ_5 is treated as in 4 dimensions, though care must be taken when

evaluating certain traces as the cyclicity of the trace is lost [41]. We then use the $\overline{\text{MS}}$ scheme [42], simply subtracting the divergences, as in the minimal subtraction (MS) scheme [43], along with the associated $\ln 4\pi$ and γ_E terms. This involves multiplying the bare quantities by renormalisation constants $Z(\mu)$, which leaves the renormalised quantities finite. A scale μ must also be introduced such that the strong coupling is dimensionless in $4 - 2\epsilon$ dimensions. Explicitly for the strong coupling g and the mass m,

$$g_0 = Z_g g \mu^\epsilon \qquad m_0 = Z_m m. \tag{1.12}$$

One can obtain the scale dependence of the renormalised parameters using the fact that the bare ones must be scale independent [44]. Therefore the strong coupling in particular must be scale dependent, and as the renormalisation constants are perturbatively expanded in the strong coupling, they also acquire a scale dependence,

$$\frac{d\,g}{d\ln\mu} \equiv -g\beta \tag{1.13}$$

$$\frac{d\,m}{d\ln\mu} \equiv -\gamma_m m. \tag{1.14}$$

Here we see that this dependence is described by the QCD β function and the anomalous dimension γ_m of the mass operator respectively. The β function and anomalous dimension γ_m are defined by their relation to the renormalisation constants Z_g and Z_m respectively, by

$$\beta = Z_g^{-1} \frac{d\,Z_g}{d\ln\mu}\,,$$

$$\gamma_m = Z_m^{-1} \frac{d\,Z_m}{d\ln\mu} \tag{1.15}$$

It is often more convenient to define the running of α_s instead of g, where $\alpha_s = g^2/(4\pi)$,

$$\frac{d\,\alpha_s}{d\ln\mu} \equiv -2\beta\,\alpha_s. \tag{1.16}$$

The functions β and γ_m can be expanded in perturbation theory,

$$\beta = \beta_0 \frac{\alpha_s}{4\pi} + \beta_1 \left(\frac{\alpha_s}{4\pi}\right)^2 + \ldots \quad \text{and} \quad \gamma_m = \gamma_{m,0} \frac{\alpha_s}{4\pi} + \gamma_{m,1} \left(\frac{\alpha_s}{4\pi}\right)^2 + \ldots \tag{1.17}$$

where

$$\beta_0 = 11 - \frac{2}{3}N_f, \qquad \beta_1 = 102 - 10N_f - 2C_F N_f,$$

$$\gamma_{m,0} = 6C_F \qquad \text{and} \qquad \gamma_{m,1} = 3C_F^2 + 97C_F - \frac{10}{3}C_F N_f, \tag{1.18}$$

with N_f being the number of active flavours.

We can use Eqs. (1.14) and (1.16) to obtain the running of m and α_s with respect to the scale, e.g. for α_s,

$$\alpha_s(\mu) = \frac{\alpha_s(\mu_0)}{v(\mu)}\left(1 - \frac{\beta_1}{\beta_0}\frac{\alpha_s(\mu_0)}{4\pi}\frac{\ln v(\mu)}{v(\mu)}\right) \tag{1.19}$$

with

$$v(\mu) = 1 - \beta_0 \frac{\alpha_s(\mu_0)}{4\pi}\ln\frac{\mu_0^2}{\mu^2}. \tag{1.20}$$

If we expand the leading term in Eq. (1.19) in $\alpha_s(\mu_0)$ we get

$$\alpha_s(\mu) = \alpha_s(\mu_0)\sum_{m=0}^{\infty}\left(\beta_0 \frac{\alpha_s(\mu_0)}{4\pi}\ln\frac{\mu_0^2}{\mu^2}\right)^m \tag{1.21}$$

Thus Eq. (1.19) automatically sums the logarithms $\ln(\mu_0^2/\mu^2)$ which become large for $\mu \ll \mu_0$, spoiling the convergence of the perturbation series. In general solving the RGE equations to leading order in α_s allows us, in the leading logarithmic (LL) approximation, to sum up the terms $(\alpha_s \ln(M_W/\mu))^n$ to all orders in n. In the next-to-leading logarithmic (NLL) approximation, going to NLO in the RGE equation means that terms $\alpha_s(\alpha_s \ln(M_W/\mu))^n$ are summed to all orders in n, etc.. This leads to the RG improved perturbation theory (for an introduction see Ref. [34].

Coming back to the renormalisation of the operators, this requires renormalisation constants which have associated anomalous dimensions. However, the mixing of the operators under renormalisation results in the scale dependence of the associated Wilson coefficients being described by an anomalous dimension matrix,

$$\mu\frac{dC_i(\mu)}{d\mu} = \gamma_{ij}C_j(\mu), \quad \text{where} \quad \gamma_{ji} = Z_{ik}^{-1}\frac{\mathrm{d}\, Z_{jk}}{\mathrm{d}\ln\mu}. \tag{1.22}$$

The Wilson coefficients are usually calculated by matching to the full theory at the scale M_W, in a perturbative expansion in powers of $\alpha_s(m_W)$. These can be evolved down to the required scale $\mu \sim m_b$ using

$$C_i(\mu) = U_{ij}(\mu, M_W)C_j(M_W), \tag{1.23}$$

where RG improved perturbation theory is employed to sum large logs. The next-to-next-to-leading logarithmic (NNLL) accuracy of our calculations in Chs. 2 and 3 requires the matching conditions at $\mu = m_W$ to two-loop accuracy, as calculated in Ref. [35]. Two-loop accuracy in the matching requires the inclusion of anomalous dimensions in the renormalisation-group equations to three-loop accuracy given by the 10×10 SM anomalous dimension matrix calculated in Refs. [45; 46]. Additional scale dependence in C_9 and C_{10} comes from the factor $1/g^2$, which otherwise would be scale independent. This procedure is discussed in further detail in App. C of Ref. [47].

Using effective field theories means that effects beyond the SM correspond to changes to the Wilson coefficients, or to new operators becoming relevant. Constraints on the Wilson coefficients therefore translate into constraints on NP models. For example, the precise measurement of the branching ratio of the flavour changing neutral current process $b \to s\gamma$ at the B Factories and the TeVatron has greatly restricted the flavour structure of physics beyond the SM. At leading order, neglecting the mass of the strange quark, the decay amplitude for $b \to s\gamma$ depends largely on $\mathcal{O}_7$, therefore, in order to see visible effects, NP would need to induce changes to C_7. These effects would be suppressed by the NP scale, $\Lambda_{\rm NP}$, and multiplied by a coupling specific to the model. In the SM, the FCNC nature of the decay means that it is suppressed by the CKM elements, and the electroweak scale, i.e. $G_F\, V_{ts}^* V_{tb}/M_W^2$. There is no reason to expect such a Cabibbo suppression for NP, however if the NP coupling is of $\mathcal{O}(1)$, then $\Lambda_{\rm NP}$ is pushed up to 10-100 TeV [20]. This is in conflict with expectations from electroweak constraints, and is known as the "flavour problem" [48], spurring the proposal of a class of models that display Minimal Flavour Violation (MFV) [49; 50], in which the flavour structure of the new theory mirrors the flavour structure of the SM. Two possible extensions of MFV which have consequences for flavour observables are an additional Higgs doublet, or flavour blind CP-violating phases as in Ref. [51; 52]. Note that hints of a large NP B_s mixing phase at the TeVatron [53; 54] are not compatible with MFV, and that the flavour structure of TeV scale physics is distinct from that of the SM is still very much a possibility. This can be further explored by making precise measurements of observables sensitive to this structure, and comparing with theoretical predictions

in the SM. At the LHC, marked improvements in the measurement of $B \to K^* \mu^+ \mu^-$ observables, $\mathcal{B}(B_{s,d} \to \mu^+ \mu^-)$, $S(B_s \to \psi\phi)$ and γ via $B \to DK$ will hopefully result in the observation of deviations from the SM. If not it will make the case for MFV much stronger. In order to maximise the success of the LHC, the above mentioned theoretical predictions should be as accurate as possible. To this end, in the following we concentrate on exclusive decays for semi-leptonic and radiative decays.

1.3 Motivation for Studying Exclusive B Decays

Inclusive B decays involve a summation over all possible final states. This is theoretically straightforward in principle but in practise involves corrections via heavy quark expansion (see e.g. Ref. [55]). Experimentally these decays are more challenging than their exclusive counterparts. Particularly due the hadronic environment of the LHC, and notably at LHCb, exclusive B meson decays will play one of the major roles for precision tests of the flavour sector in the Standard Model (SM) and its possible New Physics (NP) extensions [48; 56]. However, to make theoretical predictions for these decays we need to take hadronic effects into account, and in Sec. 1.4 we will introduce the techniques used to achieve this. First however, we will discuss why exclusive semi-leptonic and radiative* exclusive processes are particularly interesting.

1.3.1 Determination of CKM Parameters

Semi-leptonic decays play an important role in the determination of parameters of the CKM matrix defined in Eq. (1.3). $|V_{cb}|$ was determined at the B Factories to $< 2\%$ from inclusive decays [57], however the inclusive determination of $|V_{ub}|$ is experimentally more difficult due to the large $b \to c\, l\nu$ background,and instead can be extracted from the exclusive channels $B \to \pi l\nu$ or $B \to \rho l\nu$, using the absolute prediction of the hadronic decay, and the absolute branching fraction. $|V_{ub}|$ from $B \to \pi l\nu$ is currently known at the 10% level [56] and, as the B Factory measurement for the $B \to \pi$ semileptonic branching ratio is likely to be improved at Super-B, this should be reduced to $\sim 4\%$ [58]. Theoretical improvements are therefore required to compete with experiment, the subject of Ch. 5. Together the experimental and theoretical advances might even resolve the tension, i.e. the 2σ discrepancy, between the latest averages [57] for the inclusive

*By the term "radiative decays" we mean B decays to a final state containing a photon or an excited photon which thereafter decays to a lepton pair.

and exclusive determinations of $|V_{ub}|$. Note that the current estimated uncertainty on $|V_{ub}|$ from inclusive decays is similar to that from exclusive decays, but interestingly the value of $|V_{ub}|$ obtained using $\sin 2\beta$ is closer to the exclusive result [59], so the exclusive determination is thought to be more promising.

1.3.2 Study of Flavour Changing Neutral Currents

The FCNC decay $b \to s\gamma$, first observed experimentally as $B \to K^*\gamma$ at CLEO in 1993 [60], provides one of the most stringent constraints on physics beyond the SM, as discussed in Sec. 1.1. However, it only gives rise to a limited number of observables– the branching ratio and CP asymmetries, e.g. the time-dependent CP asymmetry in $B \to K^*\gamma$ [52; 61]. Instead, the focus at the LHC will be on rare $b \to s(d)l^+l^-$ exclusive decays as these, and in particular decays to muons, can be measured with unprecedented accuracy. Known as "rare decays" due to their suppression in the SM, these are a challenge to experimentalists due to large backgrounds from semi-leptonic B and D decays and long-distance contributions e.g. $B \to J/\Psi\, X_s$. These problems however are manageable in the case of exclusive decays to the simplest final states e.g. $B \to K^{(*)}l^+l^-$, $B \to \rho l^+l^-$ and $B_s \to \phi\, l^+l^-$, where l is restricted to e, μ [48]. As opposed to $b \to s\gamma$, the three or four body final state gives rise to a multitude of promising angular observables. In addition, many more of these rare decays will be seen at the LHC than were observed at the B Factories, for example an order of magnitude more $B \to K^{(*)}l^+l^-$ events will be seen at LHCb [62]; these decays are the subject of Chs. 2 and 3. From measurements of interesting $B \to K^{(*)}l^+l^-$ observables and the branching ratio for $B_{s(d)} \to l^+l^-$ (on which the current upper bound is an order of magnitude above the SM prediction) invaluable information on the the flavour structure of TeV scale physics as well as the Higgs structure and any flavour-diagonal CP-violating phases present can be obtained [52].

1.4 Understanding Exclusive Processes

In heavy-to-light semi-leptonic and radiative B decays, the b quark decays to a light quark (the recoiling quark), with which the spectator (i.e. the light quark in the B meson) must combine to form the final state meson (for a detailed description and diagrams see e.g. Ref. [63]). The dominant configuration is that in which the B and final

state mesons contain the minimum number of Fock constituents. Such a configuration is characterised by the wave function $\Phi(u, k_\perp)$, where u is the momentum fraction carried by the quark, and $k_\perp$ its transverse momentum. In order to form such a state, the recoiling quark must transfer energy to the "soft cloud". This is difficult as it is usually much more energetic than the spectator.

If a hard gluon transfers momentum from the b or recoiling quark to the spectator, this ensures that the transverse separation between the two final state quarks is small, facilitating the production of the final state meson. This is known as the hard mechanism, and can be calculated by the convolution of a perturbative hard-scattering kernel T_H with the distribution amplitudes of the mesons involved $\phi(u, \mu^2)$ at the scale μ, as initially advocated by Brodsky and Lepage. They found that this mechanism is dominant in the Sudakov limit, applicable to exclusive interactions of light hadrons in the limit of large momentum transfer, and could therefore be used to describe the electromagnetic pion form factor [64]. As the transverse momentum is restricted, one can calculate the distribution amplitude for the mesons by integrating the Bethe-Salpeter wavefunction $\Phi(u, k_\perp)$ up to $k_\perp = \mu$. As this approach was successful for light mesons, it was extended in Ref. [65] to B meson decays. For example, schematically, the matrix element for the process $B \to M\gamma^{(*)}$ would be expressed as

$$\langle M\gamma^{(*)}|H_{\text{eff}}|B\rangle \sim \phi_B \otimes T_H \otimes \phi_M + \mathcal{O}(1/m_b), \tag{1.24}$$

However, at $m_b \approx 5$GeV the Sudakov limit does not apply and this approach neglects an important contribution. This other contribution important for heavy meson decays is the soft mechanism, where the final state meson is formed in an end-point configuration, such that $1 - x \sim \mathcal{O}(1/m_b)$. As this does not impose any conditions on the transverse momentum between the recoiling quark and spectator, the wavefunction should be known as a function of $k_\perp$. A comprehensive description of B decays must include both these mechanisms.

For semi-leptonic decays, one can simply factorise the decay amplitude into two matrix elements, one describing the hadronic matrix element and the other the leptonic current. This "naïve factorisation" approach is justified here, as gluons between the two matrix elements do not arise. Matrix elements for the decay of a B to a light meson are described by quantities known as form factors (FFs). The form factors therefore contain all hadronic information for semi-leptonic decays, including the soft and hard mechanisms described above. Being non-perturbative quantities, they must be calculated using

non-perturbative techniques as discussed in Sec. 1.5. Applying "Naïve factorisation" to radiative decays is less successful, as the non-factorisable gluons between the two matrix elements below the scale $\mu \sim m_b$ cannot be ignored. Without these additional strong corrections the scale dependence of the form factors and Wilson coefficients do not reproduce the correct scale dependence of the original matrix element. In addition, the renormalisation scheme dependence of the Wilson coefficients cannot cancel in the amplitude as the form factors are renormalisation scheme independent. This calls for a more careful approach to factorisation which we will introduce in Sec. 1.6.

1.5 Form Factors and QCD Sum Rules on the Light-Cone

As stated earlier, being non-perturbative hadronic quantities, the theoretical calculation of FFs requires techniques such as Lattice QCD (see e.g. Refs. [66–70]) or QCD sum rules on the light cone (LCSR, see e.g. [71; 72], and [73] and references therein). Before we discuss these methods, particularly LCSR, we first define the form factors in order to introduce notation which will be referred to throughout this thesis. For the decay to a generic pseudoscalar meson P, three FFs are required, $f_0(q^2)$, $f_+(q^2)$ and $f_T(q^2)$, which depend on the momentum transfer $q^2 = (p-k)^2$,

$$\begin{aligned}\langle P(k)|\bar{q}\gamma_\mu b|B(p)\rangle &= \left(p_\mu + k_\mu - q_\mu \frac{m_B^2 - m_P^2}{q^2}\right) f_+(q^2) + \frac{m_B^2 - m_P^2}{q^2}\, q_\mu\, f_0(q^2)\,,\\ \langle P(k)|\bar{q}\sigma_{\mu\nu}q^\nu b|B(p)\rangle &= \frac{i}{m_B + m_P}\left(q^2(p+k)_\mu - (m_B^2 - m_P^2)\, q_\mu\right) f_T(q^2)\,. \end{aligned} \tag{1.25}$$

At zero momentum transfer, the additional relation $f_+(0) = f_0(0)$ holds.

Similarly, the matrix elements for the transition between a B meson and a generic vector meson V[†] can be written in terms of FFs $V(q^2)$, $A_{0-3}(q^2)$, $T_{1-3}(q^2)$, which are conventionally defined as

$$\langle V(k,\varepsilon)|\bar{q}\gamma_\mu b|\bar{B}(p)\rangle = i\epsilon_{\mu\nu\rho\sigma}\,\varepsilon^{*\nu}(k)\, p^\rho k^\sigma\, \frac{2V(q^2)}{m_B + m_V}\,,$$

[†]Here our phase convention for the vector state, to be used in Ch. 4, differs by a relative factor of i from the conventional definition that is used in Chs. 2 and 3.

$$\langle V(k,\varepsilon)|\bar{q}\gamma_\mu\gamma_5 b|\bar{B}(p)\rangle = -\varepsilon_\mu^*(k)\,(m_B+m_V)\,A_1(q^2) + (p+k)_\mu\,(\varepsilon^*(k)\cdot q)\,\frac{A_2(q^2)}{m_B+m_V}$$

$$+q_\mu\,(\varepsilon^*(k)\cdot q)\,\frac{2m_V}{q^2}\left(A_3(q^2)-A_0(q^2)\right)\,, \qquad (1.26)$$

where $A_0(0) = A_3(0)$. For transitions involving a tensor current, the matrix elements are characterised by the tensor FFs,

$$\langle V(k,\varepsilon)|\bar{q}\sigma_{\mu\nu}q^\nu b|\bar{B}(p)\rangle = i\epsilon_{\mu\nu\rho\sigma}\,\varepsilon^{*\nu}\,p^\rho k^\sigma\,2T_1(q^2)\,,$$

$$\langle V(k,\varepsilon)|\bar{q}\sigma_{\mu\nu}q^\nu\gamma_5 b|\bar{B}(p)\rangle = T_2(q^2)\left(\varepsilon_\mu^*(k)\,(m_B^2-m_V^2) - (\varepsilon^*(k)\cdot q)\,(p+k)_\mu\right)$$

$$+T_3(q^2)(\varepsilon^*(k)\cdot q)\left(q_\mu - \frac{q^2}{m_B^2-m_V^2}\,(2p-q)_\mu\right)\,, \qquad (1.27)$$

where $T_1(0) = T_2(0)$. The equations of motion for the quarks imply the additional constraint

$$A_3(q^2) = \frac{m_B+m_V}{2m_V}\,A_1(q^2) - \frac{m_B-m_V}{2m_V}\,A_2(q^2)\,, \qquad (1.28)$$

and therefore the $B \to V$ transitions are characterised by seven independent FFs.

It is worth mentioning that certain decays, e.g. decays to unstable hadrons, are more challenging in Lattice QCD, and in some cases only quenched results exist for a subset of the FFs. On the other hand all relevant heavy–to–light form factors can be calculated in the LCSR framework, incorporating both soft and hard mechanisms discussed in Sec. 1.4. Light-cone sum rules evolved from the traditional QCD sum rules approach [74; 75], which concerns the evaluation of correlators of quark currents between vacuum states. This is possible on one hand in terms of a sum over hadronic states, where around m_B the B meson pole is dominant, and above which a continuum of resonances contributes. On the other hand the correlation function can be calculated by way of an operator expansion in terms of non-local condensates, the coefficients of which are calculated perturbatively. LCSR takes a different approach, considering instead correlators of the T product of two quark currents sandwiched between a final on-shell meson and the vacuum [76; 77]. This can be expanded about the light-cone, in terms of perturbatively calculable hard scattering kernels convoluted with non-perturbative, universal light-cone distribution amplitudes. The correlator can also be expressed as the sum over excited states, the first being the B meson, followed by the continuum. Then assuming quark hadron duality above a certain continuum threshold, one can equate the continuum

contributions on both sides. Borel transforming this relation improves the sum rule by ensuring that this assumption, and the truncation of the series, has a minimal effect on the result.

To illustrate the LCSR approach to the calculation of the form factor $f_+(q^2)$, and introduce the notation which will be required in Ch. 5, we consider the correlator of two quark currents sandwiched between the vacuum and pion,

$$\Pi_\mu = i\, m_b \int d^D x e^{-i\, p_B \cdot x} \langle \pi(p)|T\{\bar{u}(0)\gamma_\mu b(0)\bar{b}(x) i\gamma_5 d(x)\}|0\rangle \tag{1.29}$$

$$= (p_B + p)_\mu \Pi_+(p_B^2, q^2) + (p_B - p)_\mu \Pi_-(p_B^2, q^2). \tag{1.30}$$

This will have a pole due to the B meson contribution at $p_B^2 = m_B^2$. In the region around the pole, $\Pi_+(p_B^2, q^2)$ can be factorised into two matrix elements, one corresponding to the $B \to \pi$ transition, described by $f_+(q^2)$ and $f_-(q^2)$

$$\langle \pi(p)|\bar{u}\gamma_\mu b|B(p_B)\rangle = (p_B + p)_\mu f_+(q^2) + (p_B - p)_\mu f_-(q^2), \tag{1.31}$$

where p_B and p are the momenta of the B and π mesons respectively and $q^2 = (p_B - p)^2$[‡], and the other corresponding to the decay of the B meson, described by the decay constant f_B,

$$m_b \langle 0|\bar{d} i\gamma_5 b|B\rangle = m_B^2 f_B. \tag{1.32}$$

This leads to an expression for the correlator of the form

$$\Pi_+(p_B^2, q^2) = f_B m_B^2 \frac{f_+(q^2)}{m_B^2 - p_B^2} + \int_{s > m_B^2} ds \frac{\rho_{\rm had}}{s - p_B^2}, \tag{1.33}$$

where $\rho_{\rm had}$ is the spectral density of the higher-mass hadronic states.

Alternatively, the correlator can be calculated in the Euclidean region, where $p_B^2 - m_B^2$ is large and negative, using a light-cone expansion about $x^2 = 0$. Integrating out the transverse and minus degrees of freedom below the scale μ, the longitudinal momentum

[‡]Due to differences in notation in Chs. 4 and 5, Eq. (1.31) is not identical to Eq. (1.25); the two definitions can be related by making the replacement $f_-(q^2) \to f_0(q^2) - f_+(q^2)$. In addition, here we define the B and π meson momenta to be p_B and p respectively, as opposed to p and k in Eq. (1.25).

fraction u remains relevant. The transverse degrees of freedom are included below the scale μ as higher twist contributions, and above μ as perturbative effects. This leads to the collinearly factorised expression

$$\Pi_+(p_B^2, q^2) = \sum_n \int du\, \mathcal{T}^{(n)}(u, p_B^2, q^2, \mu^2)\phi^{(n)}(u, \mu^2) \tag{1.34}$$

where $\mathcal{T}^{(n)}(u, \mu^2)$ are the perturbatively calculable hard kernels, and $\phi^{(n)}(u, \mu^2)$ are the non-perturbative light-cone distribution amplitudes (DA's) for a given twist n. This factorisation theorem is not proven for all orders, but can be verified for a given order by the cancellation of IR and soft divergences, the latter arising when the convolution does not converge at the endpoints.

As mentioned earlier, in the following we will be interested in the leading-twist contribution, such that $b(0)\bar{b}(x)$ is simply the perturbative propagator. At tree-level, we find the trivial result

$$\Pi_+(p_B^2, q^2) = \frac{1}{2} f_\pi m_b^2 \int_0^1 du\, \frac{\phi(u, \mu^2)}{m_b^2 - u p_B^2 - \bar{u} q^2}. \tag{1.35}$$

Here $\phi(u, \mu^2)$ is the leading-twist pion distribution amplitude (DA), which contains the distribution of the momentum fraction u of partons in the pion's infinite momentum frame for the lowest Fock state. We postpone the discussion of DA's to Sec. 5.5.1, and here simply state the definition to be

$$\langle \pi(p)|\bar{u}(0)\gamma_\mu\gamma_5[0, x]\, d(x)|0\rangle = -i f_\pi p_\mu \int_0^1 du\, e^{i\bar{u}p\cdot x}\phi(u, \mu^2) + \ldots, \tag{1.36}$$

where f_π is the decay constant of the pion, $\bar{u} = 1 - u$, μ is the renormalisation scale, $[0, x]$ is the Wilson line connecting the points 0 and x, and the ellipses indicate the contributions at higher-twist[§]. In the following we work in the in the Fock-Schwinger or light-cone gauge where the Wilson lines are 1. Making the substitution $u = (m_b^2 - q^2)/(s - q^2)$ in Eq. (1.35), and taking the imaginary part, we can define the spectral density ρ_{T2} at leading-twist, which can be extended to include higher order perturbative corrections,

$$\Pi_+(p_B^2, q^2) = \int_0^\infty ds \frac{\rho_{\mathrm{T2}}}{s - p_B^2} + \ldots, \tag{1.37}$$

[§]The explicit form of these terms can be found in Ref. [71]

where again the ellipses indicate the contributions at higher-twist. Equating the expressions for $\Pi_+(p_B^2, q^2)$ in Eqs. (1.33) and (1.37), results in

$$f_B m_B^2 \frac{f_+(q^2)}{m_B^2 - p_B^2} + \int_{s>m_B^2} ds \frac{\rho_{\rm had}}{s - p_B^2} = \int_0^\infty ds \frac{\rho_{\rm T2}}{s - p_B^2}. \tag{1.38}$$

Above the continuum threshold s_0, a continuum of states contribute and the approximation of quark-hadron duality is thought to be reasonable, such that

$$\rho_{\rm had} = \rho_{\rm T2}\, \Theta(s - s_0). \tag{1.39}$$

Subtracting this term arising from the continuum from Eq. (1.38) leads to the relation

$$f_B m_B^2 \frac{f_+(q^2)}{m_B^2 - p_B^2} = \int_{m_b^2}^{s_0} ds\, \frac{\rho_{\rm T2}}{s - p_B^2}. \tag{1.40}$$

Now applying a Borel transform $\hat{B}$ to both sides using

$$\hat{B} \frac{1}{s - p_B^2} = \frac{1}{M^2} e^{-s/M^2}, \tag{1.41}$$

results in the sum rule for $f_+(q^2)$,

$$f_+(q^2) = \frac{1}{f_B m_B^2} \int_{m_b^2}^{s_0} ds\, \rho_{\rm T2}\, e^{-(s - m_B^2)/M^2}, \tag{1.42}$$

where M^2 is the Borel parameter. The approximation of quark-hadron duality introduces an unavoidable uncertainty into the sum rule, but this is reduced by taking the Borel transform, and making appropriate choices for s_0 and M^2 such that the result for $f_+(q^2)$ is flat with respect to these parameters. The LCSR method can be applied to all heavy to light form factors for B decays, and can be systematically improved by going to higher orders in twist and the perturbative expansion.

1.6 QCD Factorisation and Radiative Decays

As mentioned in Sec. 1.4, radiative B decays cannot be described entirely by form factors due to strong interaction effects, known as non-factorisable corrections. These take the form of electromagnetic corrections to the matrix elements of purely hadronic operators, i.e. O_{1-6} and O_8, of the weak effective Hamiltonian defined in Eq. (1.9). QCD

factorisation (QCDF) is a framework by which these can be computed in the combined heavy quark and large energy limit [47]. Here large energy refers to that of the final state meson, $E \sim \mathcal{O}(m_B/2)$. The discussion of QCDF here will be confined to the context of $B \to K^* \mu^+ \mu^-$, where E is related to q^2, the dilepton invariant mass, and m_{K^*}, the mass of the K^*, by

$$2m_B E = m_B^2 + m_{K^*}^2 - q^2 \,. \tag{1.43}$$

The extension to other radiative decays is straightforward, e.g. to $B \to \rho l^+ l^-$ in Ref. [78]. The calculation of hard scattering effects is similar to that of light hadronic exclusive processes in the Brodsky-Lepage formalism, as in Eq. (1.24), computing the perturbative $\mathcal{O}(\alpha_s)$ hard scattering kernel which must be convoluted with the distribution amplitude of the B meson and the K^*. As described earlier,the "hard mechanism" is not the full description for B decays; the soft mechanism cannot be neglected as it contributes at the same (leading) order in $1/m_b$. Therefore QCDF proposes an expression for the decay amplitude consisting of two terms, separating soft and hard perturbative contributions into $C_a^{(i)}$ and $T_a^{(i)}$, and extending Eq. (1.24) schematically we find,

$$\langle M\gamma^* | \mathcal{H}_{\text{eff}}^{(i)} | B \rangle \sim \xi_a C_a^{(i)} + \phi_B \otimes T_a^{(i)} \otimes \phi_{a,K^*} + O(1/m_b), \tag{1.44}$$

with $a = \perp, \parallel$ and $i = u, t$. Here ϕ_B and ϕ_{a,K^*} are light-cone distribution amplitudes for the B meson and the K^* respectively. Note that non-factorisable corrections do not affect $\mathcal{O}_{9/10}$, but only contribute to the decay amplitude through the production of a virtual photon, which then decays into the lepton pair, therefore in Eq. (1.44) we consider the decay amplitude to a virtual photon.

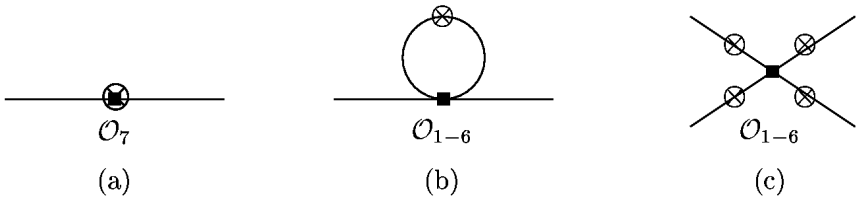

Figure 1.1: Leading contributions to $\langle \gamma^* \bar{K}^* | H_{\text{eff}} | \bar{B} \rangle$ where the crossed circles indicate possible virtual photons (from Ref [79]).

In Eq. (1.44), as in Refs. [47; 78; 79], the $C_a^{(i)}$ are multiplied by $\xi_\perp$ and $\xi_\parallel$, known as soft form factors, which correspond to the polarisation of the vector meson. These

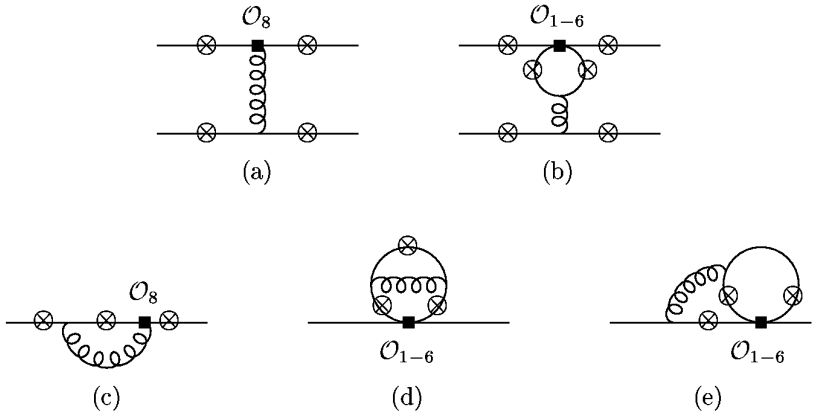

Figure 1.2: Non-factorisable contributions to $\langle\gamma^*\bar{K}^*|H_{\rm eff}|\bar{B}\rangle$, where the crossed circles indicate possible virtual photons (from Ref [79]).

are defined in the heavy quark and large energy limit, where the number of independent form factors reduces from 7 to 2. Neglecting $\mathcal{O}(\alpha_s)$ corrections, the ξ's are defined in Ref. [78] to leading order as

$$\xi_\perp(q^2) = \frac{m_B}{m_B + m_{K^*}}\, V(q^2)\,, \tag{1.45}$$

$$\xi_\parallel(q^2) = \frac{m_B + m_{K^*}}{2E}\, A_1(q^2) - \frac{m_B - m_{K^*}}{m_B}\, A_2(q^2)\,. \tag{1.46}$$

We can express the matrix element for the $B \to K^*\gamma^*$ transition more specifically in terms of the functions $\mathcal{T}_{1-3}^{(i)}(q^2)$,

$$\begin{aligned}\langle\gamma^*(q,\mu)\bar{K}^*(k,\varepsilon^*)|\mathcal{H}_{\rm eff}^{(i)}|\bar{B}(p)\rangle = \frac{ig_{\rm em}m_b}{\pi^2}\Bigg\{ & 2\,\mathcal{T}_1^{(i)}(q^2)\,\epsilon^{\mu\nu\rho\sigma}\varepsilon_\nu^* p_\rho p'_\sigma \\ & -i\,\mathcal{T}_2^{(i)}(q^2)\left[(m_B^2 - m_{K^*}^2)\,\varepsilon^{*\mu} - (\varepsilon^*\cdot q)\,(p^\mu + p'^\mu)\right] \\ & -i\,\mathcal{T}_3^{(i)}(q^2)\,(\varepsilon^*\cdot q)\left[q^\mu - \frac{q^2}{m_B^2 - m_{K^*}^2}(p^\mu + p'^\mu)\right]\Bigg\},\end{aligned} \tag{1.47}$$

where $i = u, t$, p and k are the momenta of the B and K^* mesons and ϵ^* is the polarisation vector of the K^*. The factor of m_b is defined to be the pole mass. In the case of the

effective Lagrangian defined in Sec. 1.2,

$$\mathcal{H}_{\rm eff} = -\frac{4\,G_F}{\sqrt{2}}\left(\lambda_t \mathcal{H}_{\rm eff}^{(t)} + \lambda_u \mathcal{H}_{\rm eff}^{(u)}\right), \tag{1.48}$$

including the contribution from the electromagnetic dipole operator $\mathcal{O}_7$ shown in Fig. 1.1(a) as well as the diagrams involving the four-quark operators $\mathcal{O}_{1-6}$ shown in Fig. 1.1(b) (but not annihilation contributions shown in Fig. 1.1(c)), the leading logarithmic expressions are [80]

$$\mathcal{T}_1^{(t)}(q^2) = C_7^{\rm eff}\, T_1(q^2) + Y(q^2)\,\frac{q^2}{2m_b(m_B + m_{K^*})}\,V(q^2), \tag{1.49}$$

$$\mathcal{T}_2^{(t)}(q^2) = C_7^{\rm eff}\, T_2(q^2) + Y(q^2)\,\frac{q^2}{2m_b(m_B - m_{K^*})}\,A_1(q^2), \tag{1.50}$$

$$\mathcal{T}_3^{(t)}(q^2) = C_7^{\rm eff}\, T_3(q^2) + Y(q^2)\,\left[\frac{m_B - m_{K^*}}{2m_b}\,A_2(q^2) - \frac{m_B + m_{K^*}}{2m_b}\,A_1(q^2)\right]. \tag{1.51}$$

$C_{7,9}$ always appear in a particular combination with other C_i, so we define effective coefficients $C_{7,9}^{\prime\rm eff}$, and also $C_{8,10}^{\prime\rm eff}$, given by [81],

$$\begin{aligned}
C_7^{\rm eff} &= \frac{4\pi}{\alpha_s}\,C_7 - \frac{1}{3}\,C_3 - \frac{4}{9}\,C_4 - \frac{20}{3}\,C_5 - \frac{80}{9}\,C_6\,,\\
C_8^{\rm eff} &= \frac{4\pi}{\alpha_s}\,C_8 + C_3 - \frac{1}{6}\,C_4 + 20C_5 - \frac{10}{3}\,C_6\,,\\
C_9^{\rm eff} &= \frac{4\pi}{\alpha_s}\,C_9 + Y(q^2)\,,\\
C_{10}^{\rm eff} &= \frac{4\pi}{\alpha_s}\,C_{10}
\end{aligned} \tag{1.52}$$

$$\begin{aligned}
\text{with}\quad Y(q^2) = {}& h(q^2, m_c)\left(\frac{4}{3}\,C_1 + C_2 + 6C_3 + 60C_5\right)\\
&- \frac{1}{2}\,h(q^2, m_b)\left(7C_3 + \frac{4}{3}\,C_4 + 76C_5 + \frac{64}{3}\,C_6\right)\\
&- \frac{1}{2}\,h(q^2, 0)\left(C_3 + \frac{4}{3}\,C_4 + 16C_5 + \frac{64}{3}\,C_6\right)\\
&+ \frac{4}{3}\,C_3 + \frac{64}{9}\,C_5 + \frac{64}{27}\,C_5\,.
\end{aligned} \tag{1.53}$$

Note that these definitions differ from those in Ref. [47], due to a different normalisation of the operators $\mathcal{O}_{7-10}$. As explained in Sec. 1.2, we include a factor $16\pi^2/g^2 = 4\pi/\alpha_s$ in the definition of the operators $\mathcal{O}_{i\geq 7}$ to allow a more transparent organisation of the expansion of their Wilson coefficients in perturbation theory. The function

$$h(q^2, m_q) = -\frac{4}{9}\left(\ln\frac{m_q^2}{\mu^2} - \frac{2}{3} - z\right) - \frac{4}{9}(2+z)\sqrt{|z-1|}\begin{cases} \arctan\dfrac{1}{\sqrt{z-1}} & z > 1 \\ \ln\dfrac{1+\sqrt{1-z}}{\sqrt{z}} - \dfrac{i\pi}{2} & z \leq 1 \end{cases} \tag{1.54}$$

is related to the basic fermion loop, and z is defined as $4m_q^2/s$. The contributions from the four-quark operators $\mathcal{O}_{1-6}$ are usually combined with the coefficient C_9 into an "effective" (basis- and scheme-independent) Wilson coefficient $C_9^{\text{eff}}(q^2) = C_9 + Y(q^2)$.

In Ref. [79], the full form factors are replaced by the soft form factors, such that Eqs.(1.49-1.51) simplify to

$$\mathcal{T}_1^{(t)}(q^2) \equiv \mathcal{T}_\perp^{(t)}(q^2) = \xi_\perp(q^2)\left[C_7^{\text{eff}}\,\delta_1 + \frac{q^2}{2m_b m_B}\,Y(q^2)\right], \tag{1.55}$$

$$\mathcal{T}_2^{(t)}(q^2) = \frac{2E}{m_B}\,\mathcal{T}_\perp^{(t)}(q^2), \tag{1.56}$$

$$\mathcal{T}_3^{(t)}(q^2) - \frac{m_B}{2E}\,\mathcal{T}_2^{(t)}(q^2) \equiv \mathcal{T}_\parallel^{(t)}(q^2) = -\xi_\parallel(q^2)\left[C_7^{\text{eff}}\,\delta_2 + \frac{m_B}{2m_b}\,Y(q^2)\,\delta_3\right]. \tag{1.57}$$

The factors δ_i are defined such that $\delta_i = 1 + \mathcal{O}(\alpha_s)$, where the α_s-corrections are the $\mathcal{O}(\alpha_s)$ contributions to Eqs. (1.46), computed in [79]. The results of Ref. [47] can therefore presented in terms of two invariant amplitudes $\mathcal{T}_{\perp,\parallel}(q^2)$, instead of three, which refer to the decay into a transversely and longitudinally polarised vector meson (virtual photon), respectively. In QCDF, the next-to-leading order extensions of these quantities, including both hard and soft contributions in analogy to Eq. (1.44), take the form

$$\begin{aligned}\mathcal{T}_a^{(i)} &= \xi_a\left(C_a^{(0,i)} + \frac{\alpha_s C_F}{4\pi}\,C_a^{(1,i)}\right) \\ &\quad + \frac{\pi^2}{N_c}\,\frac{f_B f_{K^*,a}}{m_B}\,\Xi_a \sum_\pm \int \frac{d\omega}{\omega}\,\phi_{B,\pm}(\omega)\int_0^1 du\,\phi_{K^*,a}(u)\,T_{a,\pm}^{(i)}(u,\omega),\end{aligned} \tag{1.58}$$

where $C_F = 4/3$, $N_c = 3$, $\Xi_\perp \equiv 1$, $\Xi_\parallel \equiv m_{K^*}/E$, and $T_{a,\pm}(u,\omega)$ is expanded as

$$T^{(i)}_{a,\pm}(u,\omega) = T^{(0,i)}_{a,\pm}(u,\omega) + \frac{\alpha_s C_F}{4\pi} T^{(1,i)}_{a,\pm}(u,\omega). \tag{1.59}$$

Here the usual K^* decay constant f_{K^*} is given by $f_{K^*,\parallel}$, and $f_{K^*,\perp}$ is the (scale-dependent) transverse decay constant defined by the matrix element of the tensor current. Note that one can obtain the leading-order coefficient $C_a^{(0,t)}$ by comparing Eqs. (1.55) and (1.57) setting $\delta_i = 1$. The leading -order coefficient $T^{(0,t)}_{a,\pm}(u,\omega)$ was obtained in Ref. [47] by calculating the non-factorisable weak annihilation contribution as in Fig. 1.1. The diagrams in Fig. 1.2, involving the four-quark operators and the chromomagnetic dipole operator with virtual photon emission, were also calculated, and result in non-factorisable corrections to both $C_a^{(t)}$ and $T_a^{(t)}$¶. Here the numerically small vertex corrections to the weak annihilation diagram in Fig. 1.1(c) are neglected. Extending the relations in Eq. (1.45) to $\mathcal{O}(\alpha_s)$ [79] in the heavy quark limit, results in factorisable corrections to $C_a^{(t)}$.

For the decay $B \to K^*\mu^+\mu^-$, CP violation in the SM is only induced by the weak phase present in $\lambda_u = V_{ub}V_{us}^*$. Therefore the calculation of CP asymmetries in Ch. 2 requires the inclusion of the doubly Cabibbo suppressed $\mathcal{H}_{\rm eff}^{(u)}$ contribution, and the necessary results for $C_a^{(u)}$ and $T^{(u)}_{a,\pm}(u,\omega)$ can be found in the appendix of Ref. [78]. On the other hand, the $B \to K^*\mu^+\mu^-$ observables studied in the first few years at the LHC (as investigated in Ch. 3) will not be sensitive to these effects, so $\mathcal{H}_{\rm eff}^{(u)}$ is neglected. Note that extending the $b \to s$ formalism to $b \to d$ decays is straightforward [78], and in this case both $\mathcal{H}_{\rm eff}^{(u)}$ and $\mathcal{H}_{\rm eff}^{(t)}$ are CKM suppressed, so both must be taken into account. For decays to charged ρ mesons the $1/m_b$ suppressed weak annihilation effects must be included as they are enhanced by the large Wilson coefficient C_2, and therefore affect the isospin asymmetries [78]. Altogether QCDF provides a framework for the calculation of non-factorisable strong interaction corrections (i.e. those corrections not related to form factors) in the heavy quark limit. This is complete to $\mathcal{O}(\alpha_s)$, with the exception of the suppressed weak annihilation contribution which is included to leading order.

We are now armed with the tools required to obtain predictions for exclusive semileptonic and radiative processes, namely effective field theories (Sec. 1.2), QCD sum rules on the light cone and QCD factorisation (Sec. 1.6). From the discussion in Sec. 1.3, it is clear that a particular decay deserving attention at the LHC is $B \to K^*\mu^+\mu^-$, and in Ch. 2 we will present observables for this decay in the SM and beyond, followed in

¶Note that $\mathcal{O}_{7,9,10}$ do not induce non-factorisable corrections, as they are 2-quark operators

Ch. 3 by a study of the potential to constrain NP in the early LHC era using these observables. Form factors (Sec. 1.5) are key in the calculation of semi-leptonic and radiative exclusive decays, and the non-perturbative techniques used to calculate them such as Lattice QCD and LCSR are often only valid in certain ranges of momentum transfer. In Ch. 4 we therefore explore the extrapolation of predictions for these form factors, using theoretical constraints from dispersive bounds. Finally in Ch. 5 we consider twist-2 $\mathcal{O}(\alpha_s^2\beta_0)$ corrections to the form factor $f_+(q^2)$ at zero recoil for $B \to \pi l\nu$, using light cone sum rules, relevant to the extraction of the CKM element $|V_{ub}|$ (see Sec. 1.1), and conclude in Ch. 6.

Chapter 2

Symmetries and Asymmetries of $B_d \to K^{*0}\mu^+\mu^-$

2.1 Introduction

The exclusive rare decay $B \to K^*\ell^+\ell^-$ is a golden channel for LHCb, due to its sensitivity to non-standard flavour and CP-violating effects combined with the vast array of possible observables. For example, a number of asymmetries, like the well-known forward-backward asymmetry ($A_{\rm FB}$), can be constructed with sensitivity to a variety of NP effects. Excluding the resonance-dominated region around the charmonium resonances with $B \to K^*\psi(\to \ell^+\ell^-)$, $B \to K^*\ell^+\ell^-$ is one of the rarest B decays ever observed; the first $B \to K^*(\to K\pi)\ell^+\ell^-$ events were first seen at the B factories BaBar and Belle, (230 at Belle [82]). Current experimental results are compiled in Tab. 2.1. The LHC hopes to improve on these results by an order of magnitude, and a recent study by the LHCb collaboration [62] predicts 7200 signal events with a data set of $2\,\text{fb}^{-1}$, which corresponds to one nominal year of running. It was shown that this would enable a determination of the zero-crossing point of $A_{\rm FB}$ with the expected precision of 0.46 GeV^2.

We present an analysis of this channel, based on QCD factorisation and including the full set of LCSR form factors (as discussed in Secs. 1.5, 1.6), whereby we include the dominant effects suppressed by the b quark mass. We focus on the decays of neutral B's, $\bar{B}^0 \to \bar{K}^{*0}(\to K^-\pi^+)\mu^+\mu^-$ and its CP-conjugate $B^0 \to K^{*0}(\to K^+\pi^-)\mu^+\mu^-$, as the LHC has a preference for charged particles in the final state, and such that the flavour of the decaying B meson (B^0 or $\bar{B}^0$) is unambiguously tagged. We also focus on

Experiment	BaBar [83]	Belle [82]	CDF [84]
$\mathrm{BR}(B \to K^*\mu^+\mu^-) \times 10^7$	$11.1 \pm 1.9 \pm 0.7$	$10.8^{+1.0}_{-1.0} \pm 0.9$	$8.1 \pm 3.0 \pm 1.0$
Number of $B\bar{B}$ events	384×10^6	657×10^6	–

Table 2.1: Experimental results for the branching ratio of $B \to K^*\mu^+\mu^-$; the region around the charm resonances with $B \to K^*\psi(\to \mu^+\mu^-)$ is excluded. The first error is statistics, the second systematics.

$\ell = \mu$ which can be cleanly measured at the LHC; see Ref. [85] for a discussion of effects arising by considering instead $\ell = e$.

A wealth of literature exists on $B \to K^*\mu^+\mu^-$ decays. Notably in 1999, Ali et al. calculated the dilepton mass spectrum and A_{FB} in the SM and various SUSY scenarios using naïve factorisation and QCD sum rules on the light cone [86]. QCD factorisation in the heavy quark limit was first applied to $B \to K^*\mu^+\mu^-$ by Beneke et al. [47; 78]. Here the size of the $\mathcal{O}(1/m_B)$ effects is not yet fully known. In Ref. [87], a calculation of $B \to K^*\mu^+\mu^-$ using soft-collinear theory (SCET) was presented. Two recent analyses also use QCD factorisation, the first focused on possible NP effects in CP asymmetries [88] and the second on observables available from angular distributions [89]. There are also many papers investigating the sensitivity of this channel to NP effects. Most of these however, except Ref. [90], focus on the effects of NP on A_{FB}, while we shall argue that there could be large effects in many angular observables not considered before, see Sec. 2.3.

We aim to improve on previous studies as follows:

- we include the full set of 7 form factors, rather than the 2 form factors in the heavy quark limit, calculated from QCD sum rules on the light-cone*;
- we give an up-to-date prediction of the $B \to K^*(\to K\pi)\mu^+\mu^-$ observables in the SM and shall argue that the bulk of power-suppressed corrections is due to the difference between the full QCD form factors and their heavy quark limit;
- we study all angular observables in the decay $B \to K^*(\to K\pi)\mu^+\mu^-$ and identify those with small sensitivity to hadronic and large sensitivity to NP effects;
- we include the effects of scalar and pseudoscalar operators, which are extremely suppressed in the SM, on all angular observables;

*Our set of form factors is shown to fulfil all correlations required in the heavy quark limit in Ref. [52].

The rest of the chapter is organised as follows: in Sec. 2.2 we review the theoretical framework, based on the trinity of effective Hamiltonian, form factors and QCD factorisation. In Sec. 2.3 we discuss the kinematics of the decay and define the basic observables in the process. In Sec. 2.3.5 we define observables satisfying the requirements of theoretical cleanliness and sensitivity to NP effects. Sec. 2.4, the centre part of our paper, contains the phenomenological analysis of those observables in the SM, and in a model-independent way. We conclude in Sec. 2.5, briefly reviewing our main results.

2.2 Theoretical Framework

The calculation of the $B \to K^*\mu^+\mu^-$ decay amplitude consists of three steps, as outlined in Ch. 1, and further details specific to our calculation are described in this section:

- the definition of additional operators required in the effective Hamiltonian $\mathcal{H}_{\text{eff}}$ for a generic new physics model;
- the discussion of specific details about the LCSR form factors employed;
- the approach taken to include QCD factorisation (QCDF) corrections in our calculation.

QCDF is only valid for small invariant dilepton mass $q^2 \sim O(1\,\text{GeV}^2)$, or, equivalently, large K^* energy $E \sim O(m_B/2)$. For this reason, and others discussed in Sec. 2.2.4 we concentrate on the region $1\,\text{GeV}^2 < q^2 < 6\,\text{GeV}^2$. After having discussed the above steps we will explain our strategy for calculating the $B \to K^*\mu^+\mu^-$ amplitude.

2.2.1 Effective Hamiltonian

In order to investigate the effects of New Physics, we extend the operator basis defined in Eq. (1.9) to include primed operators, which have opposite chirality to the unprimed ones, and vanish or are highly suppressed in the SM. We also include the scalar and pseudoscalar operators $\mathcal{O}_{S,P}$, and their primed equivalents $\mathcal{O}'_{S,P}$, which vanish in the SM. We neglect the contributions of $\mathcal{O}'_i$ for $1 \leq i \leq 6$, as, although they may be generated in certain NP scenarios e.g. left-right symmetric models or the general MSSM, their impact is either greatly constrained or very small. Therefore we now define $\mathcal{H}_{\text{eff}}^{(t)}$ and

$\mathcal{H}_{\rm eff}^{(u)}$,

$$\mathcal{H}_{\rm eff}^{(t)} = C_1\mathcal{O}_1^c + C_2\mathcal{O}_2^c + \sum_{i=3}^{6} C_i\mathcal{O}_i + \sum_{i=7-10,P,S} (C_i\mathcal{O}_i + C_i'\mathcal{O}_i')\,, \tag{2.1}$$

$$\mathcal{H}_{\rm eff}^{(u)} = C_1(\mathcal{O}_1^c - \mathcal{O}_1^u) + C_2(\mathcal{O}_2^c - \mathcal{O}_2^u)\,. \tag{2.2}$$

where the remaining operators are given by

$$\mathcal{O}_7' = \frac{e}{g^2} m_b(\bar{s}\sigma_{\mu\nu}P_L b)F^{\mu\nu}, \qquad \mathcal{O}_8' = \frac{1}{g} m_b(\bar{s}\sigma_{\mu\nu}T^a P_L b)G^{\mu\nu\,a}, \tag{2.3}$$

$$\mathcal{O}_9' = \frac{e^2}{g^2}(\bar{s}\gamma_\mu P_R b)(\bar{\mu}\gamma^\mu\mu), \qquad \mathcal{O}_{10}' = \frac{e^2}{g^2}(\bar{s}\gamma_\mu P_R b)(\bar{\mu}\gamma^\mu\gamma_5\mu), \tag{2.4}$$

$$\mathcal{O}_S = \frac{e^2}{16\pi^2} m_b(\bar{s}P_R b)(\bar{\mu}\mu), \qquad \mathcal{O}_S' = \frac{e^2}{16\pi^2} m_b(\bar{s}P_L b)(\bar{\mu}\mu), \tag{2.5}$$

$$\mathcal{O}_P = \frac{e^2}{16\pi^2} m_b(\bar{s}P_R b)(\bar{\mu}\gamma_5\mu), \qquad \mathcal{O}_P' = \frac{e^2}{16\pi^2} m_b(\bar{s}P_L b)(\bar{\mu}\gamma_5\mu), \tag{2.6}$$

and again, g is the strong coupling constant, $P_{L,R} = (1 \mp \gamma_5)/2$ and m_b denotes the running b quark mass in the $\overline{\rm MS}$ scheme.

Any NP contributions to the decay enter through $C_i(m_W)$, which is then evolved to lower scales as in the SM. As described in Sec. 1.2, the next-to-next-to-leading logarithmic (NNLL) accuracy of our calculation in the SM requires the matching conditions at $\mu = m_W$ to two-loop accuracy, as calculated in Ref. [35]. NP contributions, on the other hand, will be included to one-loop accuracy only.[†]

Two-loop accuracy in the matching requires the inclusion of anomalous dimensions in the renormalisation-group equations to three-loop accuracy given by the 10×10 SM anomalous dimension matrix calculated in Refs. [45; 46]. The operators $\mathcal{O}_{S,P}^{(\prime)}$, being conserved currents, are scale-independent and do not mix such that their Wilson coefficients are given by the coefficients at the matching scale. $\mathcal{O}_9$ mixes with $\mathcal{O}_{1,\ldots,6}$, via diagrams with a virtual photon decaying into $\mu^+\mu^-$. Additional scale dependence in C_9 and C_{10} comes from the factor $1/g^2$, which otherwise would be scale independent.

Tab. 2.2 contains all the SM values of the Wilson coefficients to NNLL accuracy. As in Eq. (1.53) where we defined $C_{7,9}^{\rm eff}$ and $C_{8,10}^{\rm eff}$, we define effective coefficients $C_{7,9}^{\prime\rm eff}$, and

[†]An explicit calculation of two-loop corrections in the MSSM [36] shows that they are small.

$C_1(\mu)$	$C_2(\mu)$	$C_3(\mu)$	$C_4(\mu)$	$C_5(\mu)$	$C_6(\mu)$	$C_7^{\rm eff}(\mu)$	$C_8^{\rm eff}(\mu)$	$C_9^{\rm eff}(\mu) - Y(q^2)$	$C_{10}^{\rm eff}(\mu)$
-0.257	1.009	-0.005	-0.078	0.000	0.001	-0.304	-0.167	4.211	-4.103

$\bar{C}_1(\mu)$	$\bar{C}_2(\mu)$	$\bar{C}_3(\mu)$	$\bar{C}_4(\mu)$	$\bar{C}_5(\mu)$	$\bar{C}_6(\mu)$	$C_7'^{\rm eff}(\mu)$	$C_8'^{\rm eff}(\mu)$
-0.128	1.052	0.011	-0.032	0.009	-0.037	-0.006	-0.003

Table 2.2: SM Wilson coefficients at the scale $\mu = m_b = 4.8\,\text{GeV}$, to NNLL accuracy. All other Wilson coefficients are heavily suppressed in the SM. The "barred" $\bar{C}_i$ are related to C_i as defined in Ref. [47]. Input: $\alpha_s(m_W) = 0.120$, $\alpha_s(m_b) = 0.214$, obtained from $\alpha_s(m_Z) = 0.1176$ [30], using three-loop evolution. We also use $m_t(m_t) = 162.3\,\text{GeV}$ [91], $m_W = 80.4\,\text{GeV}$ and $\sin^2\theta_W = 0.23$.

also $C_{8,10}'^{\rm eff}$, given by

$$C_{7,8,9,10}'^{,\rm eff} = \frac{4\pi}{\alpha_s}\, C'_{7,8,9,10}\,. \tag{2.7}$$

Later it will become clear that in the $B \to K^*(\to K\pi)\mu^+\mu^-$ decay amplitude certain Wilson coefficients only arise in combinations, e.g. $C_S - C'_S$, and cannot be accessed separately.

2.2.2 Form Factors

The $B \to K^*$ matrix elements of the operators $\mathcal{O}^{(\prime)}_{7,9,10,S,P}$ can be expressed in terms of seven form factors $V(q^2)$, $A_{1-3}(q^2)$ and $T_{1-3}(q^2)$, as defined in Eqs. (1.26,1.27). As usual we define the momentum transfer q^2, where $q^\mu = p^\mu - k^\mu$, between the B and the K^*, with momentum p and k respectively. No lattice calculation of a full set of form factors is available yet, although recent (quenched) results for $T_1(0)$ relevant for $B \to K^*\gamma$ give: $T_1(0) = 0.24 \pm 0.03^{+0.04}_{-0.01}$ [92]. Preliminary results from an alternative lattice calculation of $T_1(0)$ have been reported in Ref. [93]. At present, a more promising method for calculating form factors at large energies of the final-state meson (i.e. at small q^2) is offered by QCD sum rules on the light-cone (LCSRs) as introduced in Sec. 1.5. The LCSR approach was applied to $B \to K^*$ form factors in, for instance, Refs. [72; 94]. LCSRs for all 7 form factors except for A_0 are available at $O(\alpha_s)$ accuracy for twist-2 and-3 and tree-level accuracy for twist-4 contributions [72]. In Ref. [52], the LCSR for A_0 was also calculated to the same accuracy.

B parameters			
f_B [95]	$\lambda_B(\mu_h)$ [96]	μ_h	
200(25) MeV	0.51(12) GeV	2.2 GeV	
K^* parameters			
$f_{K^*}^{\parallel}$	$f_{K^*}^{\perp}(2\text{GeV})$	$a_1^{\perp,\parallel}(2\text{GeV})$	$a_2^{\perp,\parallel}(2\text{GeV})$
220(5) MeV	163(8) MeV	0.03(3)	0.08(6)
quark masses			
$m_b(m_b)$ [97]	$m_c(m_c)$ [97]	$m_t(m_t)$ [91]	
4.20(4) GeV	1.30(2) GeV	162.3(1.1) GeV	

Table 2.3: Numerical values of hadronic input parameters. $a_i^{\perp,\parallel}$ are parameters of the twist-2 K^* DAs and are taken from Ref. [98–101],as well as all higher-twist parameters not included in the table.

Higher twist contributions are suppressed by a factor m_{K^*}/m_b, such that the next term in the light-cone expansion contains twist-3, -4 and -5 DAs and at $q^2 = 0$ is of order $(m_{K^*}/m_b)^3$. Note that for $q^2 > 0$, the expansion parameter is $m_b m_{K^*}/(m_b^2 - q^2) \approx m_{K^*}/(2E)$, where E is the energy of the K^*. The light-cone expansion is therefore restricted to large E i.e. small q^2. However, the LCSR method does not rely on m_b being a large (or hard) scale.

The form factors used in the analysis are the same as those calculated in Ref. [52], and further details about the calculation can be found there. The resulting values of the form factors at $q^2 = 0$ are given in Tab. 2.4. With f_B fixed, the errors of the form factors become rather small and are below 20%. The q^2-dependence follows directly from the sum rules. In Fig. 2.1 we plot the central values of all form factors as functions of q^2.

2.2.3 QCD Factorisation

As explained in Sec. 1.6, in addition to terms proportional to the form factors, we also need to include "non-factorisable" contributions to the $B \to K^*\mu^+\mu^-$ amplitude, involving the purely hadronic operators $\mathcal{O}_1$ to $\mathcal{O}_6$ and the chromomagnetic-dipole operator $\mathcal{O}_8$ with additional (virtual) photon emission. These effects were calculated in QCD factori-

$A_0(0)$	$A_1(0)$	$A_2(0)$	$V(0)$
0.333 ± 0.033	0.233 ± 0.038	0.190 ± 0.039	0.311 ± 0.037
$T_1(0)$	$T_3(0)$	$\xi_\parallel(0)$	$\xi_\perp(0)$
0.268 ± 0.045	0.162 ± 0.023	0.118 ± 0.008	0.266 ± 0.032

Table 2.4: LCSR results for $q^2 = 0$. $T_2(0) = T_1(0)$. The scale-dependent form factors T_i and $\xi_{\parallel,\perp}$ are evaluated at $\mu = 4.8\,\text{GeV}$. The soft form factors $\xi_{\perp,\parallel}$ are introduced in Sec. 2.2.3. The error is calculated from varying s_0 by $\pm 2\,\text{GeV}^2$, M^2 by $\pm 2\,\text{GeV}^2$ and all hadronic input parameters according to their uncertainties given in Tab. 2.3, except for f_B [52]..

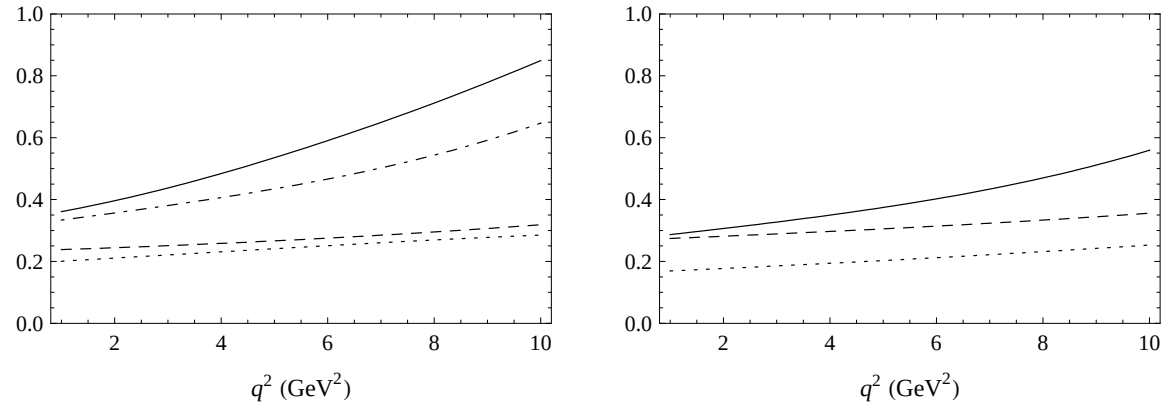

Figure 2.1: Form factors from LCSRs for central values of input parameters. Left: Solid curve: A_0, long dashes: A_1, short dashes: A_2, dot-dashed curve: V. Right: Solid curve: T_1, long dashes: T_2, short dashes: T_3 [52].

sation in Refs. [47; 78; 79] which, as mentioned earlier, is valid in the limit of large energy of the K^*, $E \sim O(m_B/2)$, and the heavy quark limit (E is as defined in Eq. (1.43)). As QCDF is not valid above the charm threshold, for the phenomenological analysis, we require $E > 2.1\,\text{GeV}$, which corresponds to $q^2 < 6\,\text{GeV}^2$, well below the charm threshold. Above the charm resonances other techniques are required to predict the $B \to K^*\mu^+\mu^-$ matrix element. Naïve factorisation is probably a reasonable approximation at the 10 to 20% level. Corrections to the decay amplitude in the large q^2 region were calculated in Ref. [102], computing long-distance effects from quark loops using an operator product expansion in $1/Q$, where $Q = m_b, q^2$. Here terms of $\mathcal{O}(m_c^2/Q^2)$ and $\mathcal{O}(1/Q)$ are included up to α_s. The scale and scheme independence of the results for physical observables indicates that this approach is an improvement on the naïve factorisation.

As the QCDF corrections are calculated in the heavy quark limit, the success of this technique relies on the $\mathcal{O}(1/m_b)$ corrections being small. One source of corrections arises from using the soft form factors instead of the full form factors. Therefore if we use the full LCSR form factors we can automatically include these $\mathcal{O}(1/m_b)$ corrections, the importance of which is discussed in App. B of Ref. [52]. However, we still need to consider the remaining α_s^0/m_b corrections. Weak annihilation contributes at this order, but is suppressed due to the small size of the Wilson coefficients it depends on, C_3 and C_4, so here the $\mathcal{O}(1/m_b)$ terms can be safely neglected. Finally certain diagrams, formally of $\mathcal{O}(\alpha_s/m_b)$, might become relevant due to an end-point divergence in the convolution. Such a divergence would signal that additional soft contributions should also be considered, of $O(1/m_b)$ as α_s is non-perturbative. However, in light-cone sum rules, similar contributions described by three-particle DA's of type $\langle 0|\bar{q}\,G\,s|\bar{K}^*\rangle$, with G the gluonic field-strength tensor are numerically small [98–101]. This leads us to believe that we are justified in neglecting such soft terms. Further details, and the exact form of the QCDF corrections we include, are found in Sec. 2.3.4.

2.2.4 Our Strategy

Based on the above discussion, our strategy for calculating $B \to K^*(\to K\pi)\mu^+\mu^-$ decays is the following:

- we predict observables in the dilepton mass range $1\,\text{GeV}^2 < q^2 < 6\,\text{GeV}^2$;
- we include the main source of power-suppressed corrections by using the full QCD form factors in the naïvely factorised amplitude, and the ξ form factors in the QCDF corrections;
- we concentrate on the prediction of observables which are independent of the absolute values of form factors, and only depend on their ratios;
- for the error analysis, we employ correlated errors between form factors, which follow from the light-cone sum rules;
- we include new-physics effects in the Wilson coefficients $C_{7,9,10,S,P}$, and their primed counterparts, but not in the other C_i.

As mentioned earlier, QCDF breaks down close to the charm resonances, resulting in a threshold at $q^2 = 4m_c^2$. In order to stay sufficiently below the threshold, we set $q^2_{\text{max}} = 6\,\text{GeV}^2$. Meanwhile at q^2 close to the kinematical minimum, the decay amplitude is dominated by the photon pole and by just one Wilson coefficient, C_7^{eff}. Hence, in

this region one cannot gain any information not already known from the well-studied radiative decay $b \to s\gamma$. Further, there could be (unknown) resonance contributions from ρ or other mesons, and for these reasons we set $q^2_{\text{min}} = 1\,\text{GeV}^2$.

2.3 Differential Decay Distribution and Spin Amplitudes

In this section we discuss the kinematics of the 4-body decay $B \to K^*(\to K\pi)\mu^+\mu^-$, define the angular observables in the spectrum and derive explicit formulae in terms of form factors and Wilson coefficients.

2.3.1 Differential Decay Distribution

The decay actually being observed in experiment is not $B \to K^*\mu^+\mu^-$, but $B \to K^*(\to K\pi)\mu^+\mu^-$. As discussed in Ref. [103], the additional information provided by the angle between K and π is sensitive to the polarisation of the K^* and thus provides an additional probe of the effective Hamiltonian.

The matrix element of the effective Hamiltonian for the decay $B \to K^*(\to K\pi)\mu^+\mu^-$ can be written, in naïve factorisation, as

$$\begin{aligned}\mathcal{M} \;=&\frac{G_F\alpha}{\sqrt{2}\pi}V_{tb}V_{ts}^*\Bigg\{\Bigg[\langle K\pi|\bar{s}\gamma^\mu(C_9^{\text{eff}}P_L + C_9^{\prime\text{eff}}P_R)b|\bar{B}\rangle \\ &- \frac{2m_b}{q^2}\langle K\pi|\bar{s}i\sigma^{\mu\nu}q_\nu(C_7^{\text{eff}}P_R + C_7^{\prime\text{eff}}P_L)b|\bar{B}\rangle\Bigg](\bar{\mu}\gamma_\mu\mu) \\ &+ \langle K\pi|\bar{s}\gamma^\mu(C_{10}^{\text{eff}}P_L + C_{10}^{\prime\text{eff}}P_R)b|\bar{B}\rangle(\bar{\mu}\gamma_\mu\gamma_5\mu) \\ &+\langle K\pi|\bar{s}(C_SP_R + C_S'P_L)b|\bar{B}\rangle(\bar{\mu}\mu)+\langle K\pi|\bar{s}(C_PP_R + C_P'P_L)b|\bar{B}\rangle(\bar{\mu}\gamma_5\mu)\Bigg\}.\end{aligned} \tag{2.1}$$

To express the $B \to K\pi$ matrix elements in terms of the $B \to K^*$ form factors discussed in Sec. 2.2.2, one assumes that the K^* decays at resonance[‡]. Then, one can use a

[‡]For a study of off-resonance effects, see Ref. [104].

narrow-width approximation by making the following replacement in the squared K^* propagator:

$$\frac{1}{(k^2 - m_{K^*}^2)^2 + (m_{K^*}\Gamma_{K^*})^2} \xrightarrow{\Gamma_{K^*} \ll m_{K^*}} \frac{\pi}{m_{K^*}\Gamma_{K^*}} \delta(k^2 - m_{K^*}^2). \tag{2.2}$$

In this way, the form factors are independent of the $K^*K\pi$ coupling $g_{K^*K\pi}$ [103; 105], because it cancels between the vertex factor and the width

$$\Gamma_{K^*} = \frac{g_{K^*K\pi}^2}{48\pi} m_{K^*} \beta^3, \tag{2.3}$$

where

$$\beta = \frac{1}{m_{K^*}^2} \left[m_{K^*}^4 + m_K^4 + m_\pi^4 - 2(m_{K^*}^2 m_K^2 + m_K^2 m_\pi^2 + m_{K^*}^2 m_\pi^2) \right]^{1/2}. \tag{2.4}$$

Writing the matrix elements in Sec. 2.2.2 as

$$\langle \bar{K}^*(k) | J_\mu | \bar{B}(p) \rangle = \epsilon^{*\nu} A_{\nu\mu}, \tag{2.5}$$

where $A_{\nu\mu}$ contains the $B \to K^*$ form factors, the corresponding $B \to K\pi$ matrix element can then be expressed as

$$\langle \bar{K}(k_1)\pi(k_2) | J_\mu | \bar{B}(p) \rangle = -D_{K^*}(k^2)\, W^\nu A_{\nu\mu}, \tag{2.6}$$

where [103]

$$|D_{K^*}(k^2)|^2 = g_{K^*K\pi}^2 \frac{\pi}{m_{K^*}\Gamma_{K^*}} \delta(k^2 - m_{K^*}^2) = \frac{48\pi^2}{\beta^3 m_{K^*}^2} \delta(k^2 - m_{K^*}^2), \tag{2.7}$$

$$W^\mu = K^\mu - \frac{m_K^2 - m_\pi^2}{k^2}\, k^\mu, \qquad k^\mu = k_1^\mu + k_2^\mu, \qquad K^\mu = k_1^\mu - k_2^\mu. \tag{2.8}$$

With an on-shell K^*, the decay is completely described by four independent kinematical variables: the dilepton invariant mass squared q^2 and the angles θ_{K^*}, θ_l and ϕ. The three angles are defined as follows: θ_{K^*} is the angle between the K^- and $\bar{B}$ in the rest frame of the $\overline{K}^*$, and is defined in the range $-1 \leq \cos\theta_{K^*} \leq 1$; θ_l is defined as the angle between the μ^- and $\bar{B}$ in the di-muon centre of mass frame, and is defined in the range $-1 \leq \cos\theta_l \leq 1$. ϕ is the angle between the normal to the K-π plane and the normal to the di-muon plane, and is defined in the range $0 \leq \phi \leq 2\pi$. For the conjugate decay,

the angles are defined analogously, but with reference to the K^+ and μ^+. Squaring the matrix element, summing over spins of the final state particles and making use of the kinematical identities given in the same appendix, one obtains the full angular decay distribution of $\bar{B}^0 \to \bar{K}^{*0}(\to K^-\pi^+)\mu^+\mu^-$:

$$\frac{d^4\Gamma}{dq^2\, d\cos\theta_l\, d\cos\theta_{K^*}\, d\phi} = \frac{9}{32\pi} I(q^2, \theta_l, \theta_{K^*}, \phi)\,, \tag{2.9}$$

where

$$\begin{aligned} I(q^2, \theta_l, \theta_{K^*}, \phi) &= I_1^s \sin^2\theta_{K^*} + I_1^c \cos^2\theta_{K^*} + (I_2^s \sin^2\theta_{K^*} + I_2^c \cos^2\theta_{K^*})\cos 2\theta_l \\ &+ I_3 \sin^2\theta_{K^*} \sin^2\theta_l \cos 2\phi + I_4 \sin 2\theta_{K^*} \sin 2\theta_l \cos\phi \\ &+ I_5 \sin 2\theta_{K^*} \sin\theta_l \cos\phi \\ &+ (I_6^s \sin^2\theta_{K^*} + I_6^c \cos^2\theta_{K^*})\cos\theta_l + I_7 \sin 2\theta_{K^*} \sin\theta_l \sin\phi \\ &+ I_8 \sin 2\theta_{K^*} \sin 2\theta_l \sin\phi + I_9 \sin^2\theta_{K^*} \sin^2\theta_l \sin 2\phi\,. \end{aligned} \tag{2.10}$$

The corresponding expression for the CP-conjugated mode $B^0 \to K^{*0}(\to K^+\pi^-)\mu^+\mu^-$ is

$$\frac{d^4\bar{\Gamma}}{dq^2\, d\cos\theta_l\, d\cos\theta_{K^*}\, d\phi} = \frac{9}{32\pi} \bar{I}(q^2, \theta_l, \theta_{K^*}, \phi)\,. \tag{2.11}$$

The function $\bar{I}(q^2, \theta_l, \theta_{K^*}, \phi)$ is obtained from (2.10) by the replacements [103]

$$I^{(a)}_{1,2,3,4,7} \longrightarrow \bar{I}^{(a)}_{1,2,3,4,7}\,, \qquad I^{(a)}_{5,6,8,9} \longrightarrow -\bar{I}^{(a)}_{5,6,8,9}\,, \tag{2.12}$$

where $\bar{I}_i^{(a)}$ equals $I_i^{(a)}$ with all weak phases conjugated. The minus sign in (2.12) is a result of our convention that, while θ_{K^*} is the angle between the $\bar{K}^{*0}$ and the K^- flight direction or between the K^{*0} and the K^+, respectively, the angle θ_l is measured between the $\bar{K}^{*0}$ (K^{*0}) and the lepton μ^- in *both* modes. Thus, a CP transformation interchanging lepton and antilepton leads to the transformations $\theta_l \to \theta_l - \pi$ and $\phi \to -\phi$. This convention agrees with Refs. [88; 103; 106], but is different from the convention used in some experimental publications [62], where θ_l is defined as the angle between K^{*0} and μ^+ in the B^0 decay, but between $\bar{K}^{*0}$ and μ^- in the $\bar{B}^0$ decay.

The angular coefficients $I_i^{(a)}$, which are functions of q^2 only, are usually expressed in terms of $\bar{K}^*$ transversity amplitudes. Since we want to explicitly keep lepton-mass effects and include also contributions from scalar and pseudoscalar operators, this step deserves a closer look.

2.3.2 Transversity Amplitudes

To introduce the transversity amplitudes, consider for the moment the decay $B \to K^*V^*$, with the B meson decaying to an on-shell K^* and a virtual photon or Z boson (which can later decay into a lepton-antilepton pair). The amplitude for this process can be written as

$$\mathcal{M}_{(m,n)}(B \to K^*V^*) = \epsilon^{*\mu}_{K^*}(m)\, M_{\mu\nu}\, \epsilon^{*\nu}_{V^*}(n) \tag{2.13}$$

where $\epsilon^{\mu}_{V^*}(n)$ is the polarisation vector of the virtual gauge boson, which can be transverse ($n = \pm$), longitudinal ($n = 0$) or timelike ($n = t$). In the B meson rest frame, the four basis vectors can be written as [105; 107]

$$\epsilon^{\mu}_{V^*}(\pm) = (0, 1, \mp i, 0)/\sqrt{2}, \tag{2.14}$$

$$\epsilon^{\mu}_{V^*}(0) = (-q_z, 0, 0, -q_0)/\sqrt{q^2}, \tag{2.15}$$

$$\epsilon^{\mu}_{V^*}(t) = (q_0, 0, 0, q_z)/\sqrt{q^2}, \tag{2.16}$$

where $q^\mu = (q_0, 0, 0, q_z)$ is the four-momentum vector of the gauge boson. They satisfy the orthonormality and completeness relations

$$\epsilon^{*\mu}_{V^*}(n)\epsilon_{V^*\,\mu}(n') = g_{nn'}, \tag{2.17}$$

$$\sum_{n,n'} \epsilon^{*\mu}_{V^*}(n)\epsilon^{\nu}_{V^*}(n')g_{nn'} = g^{\mu\nu}, \tag{2.18}$$

where $n, n' = t, \pm, 0$ and $g_{nn'} = \mathrm{diag}(+, -, -, -)$.

The K^*, on the other hand, is on shell and thus has only three polarisation states, $\epsilon^{\mu}_{K^*}(m)$ with $m = \pm, 0$, which read in the B rest frame

$$\epsilon^{\mu}_{K^*}(\pm) = (0, 1, \pm i, 0)/\sqrt{2}, \tag{2.19}$$

$$\epsilon^{\mu}_{K^*}(0) = (k_z, 0, 0, k_0)/m_{K^*}, \tag{2.20}$$

where $k^\mu = (k_0, 0, 0, k_z)$ is the four-momentum vector of the K^* (note that $k_z = -q_z$). They satisfy the relations

$$\epsilon^{*\mu}_{K^*}(m)\epsilon_{K^*\,\mu}(m') = -\delta_{mm'}, \tag{2.21}$$

$$\sum_{m,m'} \epsilon^{*\mu}_{K^*}(m)\epsilon^{\nu}_{K^*}(m')\,\delta_{mm'} = -g^{\mu\nu} + \frac{k^\mu k^\nu}{m^2_{K^*}}. \tag{2.22}$$

The helicity amplitudes H_0, H_+ and H_- can now be projected out from $M_{\mu\nu}$ by contracting with the explicit polarisation vectors in (2.13),

$$H_m = \mathcal{M}_{(m,m)}(B \to K^*V^*), \qquad m = 0, +, -. \tag{2.23}$$

Alternatively, one can work with the transversity amplitudes defined as [106]

$$A_{\perp,\parallel} = (H_{+1} \mp H_{-1})/\sqrt{2}, \quad A_0 \equiv H_0. \tag{2.24}$$

In contrast to the decay of B to two (on-shell) vector mesons, to which this formalism can also be applied, there is an additional transversity amplitude in the case of $B \to K^*V^*$ because the gauge boson is virtual, namely

$$A_t = \mathcal{M}_{(0,t)}(B \to K^*V^*), \tag{2.25}$$

which corresponds to a K^* polarisation vector which is longitudinal in the K^* rest frame and a V^* polarisation vector which is timelike in the V^* rest frame.[§]

If we now consider the subsequent decay of the gauge boson into a lepton-antilepton pair, the amplitude becomes

$$\mathcal{M}(B \to K^*V^*(\to \mu^+\mu^-))(m) \propto \epsilon^{*\mu}_{K^*}(m)\, M_{\mu\nu} \sum_{n,n'} \epsilon^{*\nu}_{V^*}(n)\epsilon^{\rho}_{V^*}(n')\, g_{nn'}\, (\bar{\mu}\gamma_\rho P_{L,R}\mu). \tag{2.26}$$

This amplitude can now be expressed in terms of six transversity amplitudes $A^L_{\perp,\parallel,0}$ and $A^R_{\perp,\parallel,0}$, where L and R refer to the chirality of the leptonic current, as well as the seventh

[§]Unlike sometimes stated in the literature, A_t does not correspond to a timelike polarisation of the K^* meson. As mentioned above, the K^* decays on the mass shell and thus has only three polarisation states.

transversity amplitude A_t. The reason that for A_t no separate left-handed and right-handed parts have to be considered can be seen as follows. Noticing that the timelike polarisation vector in (2.16) is simply given by $\epsilon^\mu_{V^*}(t) = q^\mu/\sqrt{q^2}$, one can see from current conservation,

$$q^\mu(\bar{\mu}\gamma^\mu\mu) = 0, \qquad q^\mu(\bar{\mu}\gamma^\mu\gamma_5\mu) = 2im_\mu(\bar{\mu}\gamma_5\mu), \tag{2.27}$$

that the timelike component of the V^* can only couple to an axial-vector current. In addition, this shows that A_t vanishes in the limit of massless leptons.

Now, having shown that the amplitude of the sequential decay $B \to K^*V^*(\to \mu^+\mu^-)$ can be expressed in terms of seven transversity amplitudes, it is clear that this is true for all contributions of the operators $\mathcal{O}_7^{(\prime)}$, $\mathcal{O}_9^{(\prime)}$ and $\mathcal{O}_{10}^{(\prime)}$ to the decay of interest, $B \to K^*(\to K\pi)\mu^+\mu^-$, regardless of whether they originate from virtual gauge boson exchange (i.e. photon or Z penguin diagrams) or from box diagrams.

Does this also apply to decays mediated not by a vector, but a scalar and pseudoscalar operator? Inspecting Eqs. (2.5), (2.6) and (2.27), one can see that the combination $(\mathcal{O}_P - \mathcal{O}'_P)$ can be absorbed into the transversity amplitude A_t, because it couples to axial-vector currents, just like the timelike component of a virtual gauge boson. However, this is not possible for the scalar operators $\mathcal{O}_S^{(\prime)}$. Therefore, the inclusion of scalar operators in the decay $B \to K^*(\to K\pi)\mu^+\mu^-$ requires the introduction of a an additional, "scalar" transversity amplitude, which we denote A_S.

To summarise, the treatment of the decay $B \to K^*(\to K\pi)\mu^+\mu^-$ by decomposition of the amplitude into seven transversity amplitudes $A^{L,R}_{\perp,\parallel,0}$ and A_t is sufficient as long as the operators $\mathcal{O}^{(\prime)}_{7,9,10}$ and $\mathcal{O}_P^{(\prime)}$ are considered, but has to be supplemented by an additional, eighth transversity amplitude A_S once contributions from scalar operators are taken into account.

Finally, we give the explicit form of the eight transversity amplitudes (up to corrections of $O(\alpha_s)$, whose discussion we postpone until Sec. 2.3.4):

$$A_{\perp L,R} = N\sqrt{2}\lambda^{1/2}\left[\left[(C_9^{\text{eff}} + C_9^{\text{eff}\prime}) \mp (C_{10}^{\text{eff}} + C_{10}^{\text{eff}\prime})\right]\frac{V(q^2)}{m_B + m_{K^*}} + \frac{2m_b}{q^2}(C_7^{\text{eff}} + C_7^{\text{eff}\prime})T_1(q^2)\right], \tag{2.28}$$

$$A_{\parallel L,R} = -N\sqrt{2}(m_B^2 - m_{K^*}^2)\left[\left[(C_9^{\text{eff}} - C_9^{\text{eff}\prime}) \mp (C_{10}^{\text{eff}} - C_{10}^{\text{eff}\prime})\right]\frac{A_1(q^2)}{m_B - m_{K^*}}\right.$$

$$+ \frac{2m_b}{q^2}(C_7^{\rm eff} - C_7^{\rm eff\prime})T_2(q^2)\Bigg], \tag{2.29}$$

$$\begin{aligned} A_{0L,R} = -\frac{N}{2m_{K^*}\sqrt{q^2}}\Bigg\{ & \left[(C_9^{\rm eff} - C_9^{\rm eff\prime}) \mp (C_{10}^{\rm eff} - C_{10}^{\rm eff\prime})\right] \\ & \times \left[(m_B^2 - m_{K^*}^2 - q^2)(m_B + m_{K^*})A_1(q^2) - \lambda\frac{A_2(q^2)}{m_B + m_{K^*}}\right] \\ & + 2m_b(C_7^{\rm eff} - C_7^{\rm eff\prime})\left[(m_B^2 + 3m_{K^*}^2 - q^2)T_2(q^2) - \frac{\lambda}{m_B^2 - m_{K^*}^2}T_3(q^2)\right]\Bigg\}, \end{aligned} \tag{2.30}$$

$$A_t = \frac{N}{\sqrt{q^2}}\lambda^{1/2}\left[2(C_{10}^{\rm eff} - C_{10}^{\rm eff\prime}) + \frac{q^2}{2m_\mu}(C_P - C_P')\right]A_0(q^2), \tag{2.31}$$

$$A_S = -N\lambda^{1/2}(C_S - C_S')A_0(q^2), \tag{2.32}$$

where

$$N = V_{tb}V_{ts}^*\left[\frac{G_F^2\alpha^2}{3\cdot 2^{10}\pi^5 m_B^3}q^2\lambda^{1/2}\beta_\mu\right]^{1/2}, \tag{2.33}$$

with $\lambda = m_B^4 + m_{K^*}^4 + q^4 - 2(m_B^2 m_{K^*}^2 + m_{K^*}^2 q^2 + m_B^2 q^2)$ and $\beta_\mu = \sqrt{1 - 4m_\mu^2/q^2}$.

2.3.3 Angular Coefficients

With the eight transversity amplitudes defined in the preceding subsection, the angular coefficients I_i in (2.10) can be written as

$$I_1^s = \frac{(2+\beta_\mu^2)}{4}\left[|A_\perp^L|^2 + |A_\parallel^L|^2 + (L\to R)\right] + \frac{4m_\mu^2}{q^2}{\rm Re}\left(A_\perp^L A_\perp^{R*} + A_\parallel^L A_\parallel^{R*}\right), \tag{2.34}$$

$$I_1^c = |A_0^L|^2 + |A_0^R|^2 + \frac{4m_\mu^2}{q^2}\left[|A_t|^2 + 2{\rm Re}(A_0^L A_0^{R*})\right] + \beta_\mu^2|A_S|^2, \tag{2.35}$$

$$I_2^s = \frac{\beta_\mu^2}{4}\left[|A_\perp^L|^2 + |A_\parallel^L|^2 + (L\to R)\right], \tag{2.36}$$

$$I_2^c = -\beta_\mu^2\left[|A_0^L|^2 + (L\to R)\right], \tag{2.37}$$

$$I_3 = \frac{1}{2}\beta_\mu^2 \left[|A_\perp^L|^2 - |A_\parallel^L|^2 + (L \to R)\right], \tag{2.38}$$

$$I_4 = \frac{1}{\sqrt{2}}\beta_\mu^2 \left[\mathrm{Re}(A_0^L A_\parallel^{L\,*}) + (L \to R)\right], \tag{2.39}$$

$$I_5 = \sqrt{2}\beta_\mu \left[\mathrm{Re}(A_0^L A_\perp^{L\,*}) - (L \to R) - \frac{m_\mu}{\sqrt{q^2}}\,\mathrm{Re}(A_\parallel^L A_S^* + A_\parallel^R A_S^*)\right], \tag{2.40}$$

$$I_6^s = 2\beta_\mu \left[\mathrm{Re}(A_\parallel^L A_\perp^{L\,*}) - (L \to R)\right], \tag{2.41}$$

$$I_6^c = 4\beta_\mu \frac{m_\mu}{\sqrt{q^2}}\,\mathrm{Re}\left[A_0^L A_S^* + (L \to R)\right], \tag{2.42}$$

$$I_7 = \sqrt{2}\beta_\mu \left[\mathrm{Im}(A_0^L A_\parallel^{L\,*}) - (L \to R) + \frac{m_\mu}{\sqrt{q^2}}\,\mathrm{Im}(A_\perp^L A_S^* + A_\perp^R A_S^*)\right], \tag{2.43}$$

$$I_8 = \frac{1}{\sqrt{2}}\beta_\mu^2 \left[\mathrm{Im}(A_0^L A_\perp^{L\,*}) + (L \to R)\right], \tag{2.44}$$

$$I_9 = \beta_\mu^2 \left[\mathrm{Im}(A_\parallel^{L\,*} A_\perp^L) + (L \to R)\right]. \tag{2.45}$$

A few comments are in order:

- In contrast to the transversity amplitudes themselves, the angular coefficients I_i are all physical observables. In fact, they contain the complete information that can be extracted from the measurement of the decay $\bar{B}^0 \to \bar{K}^{*0}(\to K^-\pi^+)\mu^+\mu^-$. We will discuss in Sec. 2.3.5 which combinations of the angular coefficients constitute *theoretically clean* observables.
- In the limit of massless leptons, the well-known relations $I_1^s = 3I_2^s$ and $I_1^c = -I_2^c$ hold.
- The coefficient I_6^c vanishes unless contributions from scalar operators *and* lepton mass effects are taken into account. Therefore, to our knowledge, it has never been considered in the literature before. However, it is a potentially good observable for scalar currents. We will come back to this point in Sec. 2.4.2.

2.3.4 Additional Corrections to Transversity Amplitudes

As mentioned in Sec. 2.3.2, the transversity amplitudes defined in Eqs. (2.28) to (2.32) do not include effects from spectator interactions, which do induce, on the one hand, $O(\alpha_s)$ corrections and, on the other hand, corrections from weak annihilation (WA). These corrections have been calculated within the QCD factorisation (QCDF) framework in Refs. [47] and [78] in terms of the soft form factors $\xi_\perp$ and $\xi_\parallel$, as defined to leading order in Eq. (1.45). In Ref. [47], two types of $O(\alpha_s)$ corrections, factorisable and non-factorisable, are presented, of which we only require the latter. The factorisable corrections arise when expressing the full form factors in terms of $\xi_\parallel$ and $\xi_\perp$, are given by the radiative corrections in Eqs. (B.1)–(B.4) in App. B of Ref. [52] and since we use the full form factors at LO these are redundant in our set-up[¶].

The second QCDF correction to the transversity amplitude in Sec. 2.3.2 is given by the WA contribution, $T^{(0)}_{\parallel,-}(u,\omega)$ in the notation of Ref. [47]. It is induced by the penguin operators $\mathcal{O}_3$ and $\mathcal{O}_4$ and hence is numerically small, see Tab. 2.2. This is a term which is leading in $1/m_b$ and $O(\alpha_s)$, so in principle one should also include power-suppressed and radiative corrections. However, in view of its small size at L.O., we feel justified in neglecting these corrections. Note that the WA contribution to the λ_u amplitude for $B^+ \to K^{*+}\mu^+\mu^-$, contains the factor $C_2 \approx 1$ and hence should be included for this process. However this is not of consequence for our study as we focus on neutral meson decays.

On introducing the chirality-flipped operators, the $\mathcal{T}^{(t,u)}_{\perp,\parallel}$ introduced in Eq. (1.58), and also mentioned in Sec. 2.2.3, are promoted to $\mathcal{T}^{\pm(t,u)}_{\perp,\parallel}$ corresponding to the notations of Ref. [108]. In terms of these quantities, we can define the additional corrections to the transversity amplitudes[‖]:

$$\Delta A^{\rm QCDF}_{\perp L,R} = \sqrt{2}N\,\frac{2m_b}{q^2}\,(m_B^2-q^2)(\mathcal{T}_\perp^{+(t),\rm WA+nf} + \hat{\lambda}_u \mathcal{T}_\perp^{+(u)})\,,$$

$$\Delta A^{\rm QCDF}_{\parallel L,R} = -\sqrt{2}N\,\frac{2m_b}{q^2}\,(m_B^2-q^2)(\mathcal{T}_\perp^{-(t),\rm WA+nf} + \hat{\lambda}_u \mathcal{T}_\perp^{-(u)})\,,$$

[¶]In Ref. [47] factorisable corrections also arise due expressing the $\overline{\rm MS}$ b quark mass in the operators $\mathcal{O}_{7,8}$, Eq. (1.9), by a mass parameter in a different renormalisation scheme. In our numerical analysis, however, we use the running b quark mass in the $\overline{\rm MS}$ scheme throughout so these factorisable $O(\alpha_s)$ corrections calculated in Refs. [47; 78] are also dropped

[‖]It should be noted that the functions $F^{(7,9)}_{1,2,u}$ entering the non-factorisable corrections are defined with a different overall sign in Refs. [78] and [109]

$$\Delta A_{0L,R}^{\rm QCDF} = \frac{N(m_B^2-q^2)^2}{m_{K^*}m_B^2\sqrt{q^2}}\, m_b(\mathcal{T}_\parallel^{-(t),\rm WA+nf} + \hat\lambda_u \mathcal{T}_\parallel^{-(u)})\,. \tag{2.46}$$

The superscript, WA+nf, on $\mathcal{T}_\perp^{\pm(t)}$ indicates that only contributions from WA and non-factorisable $O(\alpha_s)$ corrections are to be included. In accordance with Ref. [88], we define $\hat\lambda_u = \lambda_u/\lambda_t$. The total transversity amplitudes are given by the expressions in (2.28)–(2.30) plus the above terms $\Delta A^{\rm QCDF}$. Note there are no corrections to A_t or A_S.

2.3.5 Observables

As discussed in Sec. 2.3, the decay $\bar B^0 \to \bar K^{*0}(\to K^-\pi^+)\mu^+\mu^-$ is completely described in terms of twelve angular coefficient functions $I_i^{(a)}$. The corresponding CP-conjugate mode $B^0 \to K^{*0}(\to K^+\pi^-)\mu^+\mu^-$ gives access to twelve additional observables, the CP-conjugate angular coefficient functions $\bar I_i^{(a)}$. These quantities have a clear relation to both experiment and theory: theoretically they are expressed in terms of transversity amplitudes, and experimentally they describe the angular distribution. A physical interpretation of these $I_i^{(a)}$ can be drawn from Eqs. (2.34) to (2.45). For example, I_6^c depends on scalar operators and I_7 to I_9 depend on the imaginary part of the transversity amplitudes, and consequently on their phases, which come either from QCD effects and enter the QCD factorisation expressions at $O(\alpha_s)$, see Sec. 2.2, or are CP-violating SM or NP phases.

To separate CP-conserving and CP-violating NP effects, we find it more convenient to consider the twelve CP averaged angular coefficients

$$S_i^{(a)} = \left(I_i^{(a)} + \bar I_i^{(a)}\right) \Big/ \frac{d(\Gamma+\bar\Gamma)}{dq^2} \tag{2.47}$$

as well as the twelve CP asymmetries**

$$A_i^{(a)} = \left(I_i^{(a)} - \bar I_i^{(a)}\right) \Big/ \frac{d(\Gamma+\bar\Gamma)}{dq^2}\,. \tag{2.48}$$

These are our primary observables to be used in the phenomenological analysis in Sec. 2.4. They offer a clean and comprehensive way to analyse the full richness of angular distributions in $B \to K^*(\to K\pi)\mu^+\mu^-$ decays. We shall show below that all previously studied observables, for example the forward-backward asymmetry $A_{\rm FB}$, can

** Note that our definition of the CP asymmetries differs from Ref. [88] by a factor of $\frac{3}{2}$.

	$m_\mu = 0$	$m_\mu \neq 0$
SM	18	22
SM + $\mathcal{O}_S^{(\prime)}$	20	24

Table 2.5: Number of independent observables in $B \to K^*(\to K\pi)\mu^+\mu^-$, depending on whether lepton mass effects and/or scalar operators are taken into account.

be easily expressed in terms of our new observables. $S_i^{(a)}$ and $A_i^{(a)}$ are normalised to the CP-averaged dilepton mass distribution to reduce both experimental and theoretical uncertainties. Taking the CP average means that CP-violating effects in the $S_i^{(a)}$ are washed out, resulting in a cleaner observable. Taking the CP asymmetry, on the other hand, means that any non-standard CP violation can be easily identified.

These CP asymmetries, i.e. $A_i^{(a)}$, are expected to be small in the SM, as previously noted in Ref. [88]. This is because the only CP-violating phase affecting the decay enters via λ_u and is doubly Cabibbo-suppressed. Therefore we are particularly keen to examine these asymmetries in the context of CP-violating phases in NP models.

It should be stressed that out of these 24 observables, two vanish in the SM, namely S_6^c and A_6^c, which are generated only by scalar operators, and four are related in the limit of massless leptons through $S_1^s = 3S_2^s$, $S_1^c = -S_2^c$ and $A_1^s = 3A_2^s$, $A_1^c = -A_2^c$ (see Sec. 2.3.3). Tab. 2.5 summarises the number of independent observables in these limits.

In addition, even for non-zero lepton mass, only three of the four $S_{1,2}^{s,c}$ are independent, which can be seen as follows. The dilepton mass distribution can be expressed in terms of angular coefficients as

$$\frac{d\Gamma}{dq^2} = \frac{3}{4}(2\,I_1^s + I_1^c) - \frac{1}{4}(2\,I_2^s + I_2^c). \tag{2.49}$$

Therefore, due to the normalisation given in Eq. (2.47), there is the relation

$$\frac{3}{4}(2\,S_1^s + S_1^c) - \frac{1}{4}(2\,S_2^s + S_2^c) = 1. \tag{2.50}$$

Consequently, the complete set of 24 independent observables would be given by the twelve $A_i^{(a)}$, eleven $S_i^{(a)}$ and the CP-averaged dilepton mass distribution $d(\Gamma + \bar{\Gamma})/dq^2$. However, the latter is the only observable for which the normalisation of the form factors is relevant, so theoretically it is not as clean.

In our opinion, the quantities $S_i^{(a)}$ and $A_i^{(a)}$ are the natural starting point for an experimental analysis. In Ref. [89], a detailed investigation was carried out showing that a full angular fit was the preferred way to extract observables. This would involve fitting Eqs. (2.9) and (2.11) to data. From such a fit the $I_i^{(a)}$ and $\bar{I}_i^{(a)}$ would be found directly, and could be combined using Eqs. (2.47) and (2.48) to give the desired quantities. We suggest that a similar full angular fit could be carried out for the four-fold spectrum $d^4(\Gamma \pm \bar{\Gamma})$, so $S_i^{(a)}$ and $A_i^{(a)}$ would be instantly accessible. Note that, due to Eq. (2.12), the CP-averaged decay distribution $d^4(\Gamma + \bar{\Gamma})$ gives access to $S^{(a)}_{1,2,3,4,7}$ and $A^{(a)}_{5,6,8,9}$, while the remaining observables can be obtained from $d^4(\Gamma - \bar{\Gamma})$.

Alternatively, $S_i^{(a)}$ and $A_i^{(a)}$ can be found by taking asymmetries and/or integrating $d^4(\Gamma \pm \bar{\Gamma})$ over the angles θ_l, θ_K and ϕ. Details for the extraction of some of the $A_i^{(a)}$ are given in Ref. [88], but we stress that all our observables can be determined in a similar manner. To illustrate this point, one case not mentioned in Ref. [88] is S_5, which can be obtained by integrating over two angles:

$$S_5 = -\frac{4}{3}\left(\int_{\pi/2}^{3\pi/2} - \int_0^{\pi/2} - \int_{3\pi/2}^{2\pi}\right) d\phi \left(\int_0^1 - \int_{-1}^0\right) d\cos\theta_K \frac{d^3(\Gamma - \bar{\Gamma})}{dq^2\, d\cos\theta_K d\phi} \Big/ \frac{d(\Gamma + \bar{\Gamma})}{dq^2}. \tag{2.51}$$

As stated above, we normalise the $S_i^{(a)}$ and $A_i^{(a)}$ to the CP-averaged dilepton mass distribution in order to reduce the dependence on the form factors. Our approach described in Secs. 2.3.2 and 2.3.4 makes use of the full form factors for the dominant leading-order contribution and the soft form factors for additional suppressed contributions. Therefore our results are largely independent of the relation between the soft form factors and the full form factors. However, it is still interesting to note that in App. B of Ref. [52] it was found that relations involving $\xi_\perp$ are almost independent of q^2, whereas those involving $\xi_\parallel$ have a considerable dependence on q^2 due to the neglected $1/m_b$ terms. Therefore we stress that the transversity amplitudes $A_{\perp,\parallel}^{L,R}$ of Sec. 2.3.2, and all angular observables built from them, should be more or less insensitive to $1/m_b$ corrections, i.e. corrections to QCDF, while $A_0^{L,R}$ and all corresponding angular variables will be slightly more affected by such corrections. These findings impact on prior work carried out in this channel, where the transversity amplitudes were given entirely in terms of the soft form factors using QCDF.

All established observables can be expressed in terms of $S_i^{(a)}$ and $A_i^{(a)}$. For example, the CP asymmetry in the dilepton mass distribution is given by (see Eq. (2.50))

$$A_{\rm CP} = \frac{d(\Gamma-\bar\Gamma)}{dq^2}\bigg/\frac{d(\Gamma+\bar\Gamma)}{dq^2} = \frac{3}{4}(2\,A_1^s + A_1^c) - \frac{1}{4}(2\,A_2^s + A_2^c). \tag{2.52}$$

We prefer to define the normalised forward-backward asymmetry as a ratio of CP-averaged quantities, to wit

$$A_{\rm FB} = \left(\int_0^1 - \int_{-1}^0\right) d\cos\theta_l \frac{d^2(\Gamma-\bar\Gamma)}{dq^2\, d\cos\theta_l}\bigg/\frac{d(\Gamma+\bar\Gamma)}{dq^2} = \frac{3}{8}(2\,S_6^s + S_6^c). \tag{2.53}$$

The CP average is numerically irrelevant in the SM, but makes the connection to experiment more transparent. In addition, this definition is complementary to the forward-backward CP asymmetry [110],

$$A_{\rm FB}^{\rm CP} = \left(\int_0^1 - \int_{-1}^0\right) d\cos\theta_l \frac{d^2(\Gamma+\bar\Gamma)}{dq^2\, d\cos\theta_l}\bigg/\frac{d(\Gamma+\bar\Gamma)}{dq^2} = \frac{3}{8}(2\,A_6^s + A_6^c). \tag{2.54}$$

Additional well-established observables are the K^* longitudinal and transverse polarisation fractions F_L, F_T, which are usually defined in terms of transversity amplitudes. We prefer to directly express them in terms of CP-averaged observables and *define*

$$F_L = -S_2^c, \qquad F_T = 4S_2^s. \tag{2.55}$$

The well-known relation $F_T = 1 - F_L$ is then a consequence of Eq. (2.50) in the limit of vanishing lepton mass.

In Refs. [89; 106], the transverse asymmetries $A_T^{(i)}$ were introduced. They can be expressed in terms of our observables as

$$\begin{aligned}
A_T^{(2)} &= \frac{S_3}{2\,S_2^s}\,,\\
A_T^{(3)} &= \left(\frac{4\,S_4^2 + S_7^2}{-2\,S_2^c\,(2\,S_2^s + S_3)}\right)^{1/2},\\
A_T^{(4)} &= \left(\frac{S_5^2 + 4\,S_8^2}{4\,S_4^2 + S_7^2}\right)^{1/2}.
\end{aligned} \tag{2.56}$$

Finally, for some observables it is useful to consider their q^2 average. We define

$$\left\langle S_i^{(a)} \right\rangle = \int_{1\,\mathrm{GeV}^2}^{6\,\mathrm{GeV}^2} dq^2 \left(I_i^{(a)} + \bar{I}_i^{(a)} \right) \Big/ \int_{1\,\mathrm{GeV}^2}^{6\,\mathrm{GeV}^2} dq^2 \frac{d(\Gamma + \bar{\Gamma})}{dq^2}\,, \tag{2.57}$$

$$\left\langle A_i^{(a)} \right\rangle = \int_{1\,\mathrm{GeV}^2}^{6\,\mathrm{GeV}^2} dq^2 \left(I_i^{(a)} - \bar{I}_i^{(a)} \right) \Big/ \int_{1\,\mathrm{GeV}^2}^{6\,\mathrm{GeV}^2} dq^2 \frac{d(\Gamma + \bar{\Gamma})}{dq^2}\,. \tag{2.58}$$

The reasons for choosing the interval $1\,\mathrm{GeV}^2 \leq q^2 \leq 6\,\mathrm{GeV}^2$ are discussed in Sec. 2.2.4.

We proceed in the next section by studying the predictions for $S_i^{(a)}$ and $A_i^{(a)}$, keeping in mind the sensitivity to hadronic effects. This is carried out first in the SM and later in a model independent NP study.

2.4 Phenomenological Analysis

We are now in a position to perform a phenomenological analysis of the observables defined in Sec. 2.3.5, first in the SM, then in a model-independent manner, and finally for specific NP scenarios.

2.4.1 Standard Model

The importance of the observables discussed in the present paper for tests of the SM originates from the following facts:

- Several of the observables we consider are predicted to be strongly suppressed in the SM or even vanish so that New Physics (NP) effects can be seen more easily than in the branching ratio of $B \to K^*\mu^+\mu^-$ which is measured to be consistent with the SM expectations.
- The relatively small number of relevant SM parameters which are already well constrained by a number of processes allows rather definitive predictions for many observables subject mainly to the theoretical uncertainty of form factors.
- In certain cases the sign of a given observable has a unique prediction in the SM, which can be tested more easily than the magnitude itself.

However, to use these facts in a meaningful way, it is essential to have reliable calculations of the relevant form factors. In fact the use of the improved form factors presented here and the consideration of correlations between the uncertainties of the different form factors allows one to obtain rather reliable predictions for angular coefficients in the SM. Our predictions for the CP-averaged angular coefficients $S_i^{(a)}$ in the SM are shown in Fig. 2.2. S_1^s and S_1^c have been omitted since the relations $S_1^s = 3S_2^s$ and $S_1^c = -S_2^c$ (see Sec. 2.3.3) are fulfilled up to lepton-mass effects, which amount to at most 1%. $S_{1,2}^{s,c}$ are numerically large as expected. S_4, S_5, S_6^s are similar in magnitude, but are particularly interesting as they each have a zero in q^2. All these predictions are seen to have small uncertainties, as the normalisation results in a cancellation of hadronic effects. In Tab. 2.6, we show our predictions for the positions of the zeros of S_4, S_5 and S_6^s, denoted by $q_0^2(S_i^{(a)})$ from now on. S_3 is numerically small in the SM since it is approximately proportional to the chirality-flipped Wilson coefficient C_7', which is suppressed by a factor m_s/m_b. S_7, S_8 and S_9 are small as well and have a larger error-band as they arise from the imaginary part of the transversity amplitudes.

The error bands have been obtained by adding various uncertainties in quadrature. We estimate the uncertainty due to the form factors by varying the Borel parameter and continuum threshold as discussed in Sec. 2.2.2. The renormalisation-scale uncertainty is found by varying μ between 4.0 and 5.6 GeV, where μ is the scale at which the Wilson coefficients, α_s and the $\overline{\text{MS}}$ masses are evaluated. We also include parametric uncertainties which are estimated by varying the hadronic parameters as indicated in Tab. 2.3, the ratio m_c/m_b between 0.25 and 0.33, and the CKM angle γ, which is particularly important for the doubly Cabibbo-suppressed contribution to the CP asymmetries, between 60° and 80°.[††] In addition, we show the leading-order prediction as a dashed line. We find that the impact of radiative QCDF corrections is moderate for observables like $S_{2,3,4,5,6}$ that, in the SM, are largely independent of weak or strong phases, but becomes more prominent for observables built from imaginary parts, like $S_{7,8,9}$ and A_i, where the main contribution comes from strong phases induced by $O(\alpha_s)$ corrections in QCDF.

Some of these $S_i^{(a)}$ can be directly compared to previous results in the literature. S_2^s and S_2^c correspond to the K^* longitudinal and transverse polarisation fractions F_L and F_T, see Eq. (2.55), and S_6^s yields the forward-backward asymmetry A_{FB}, see Eq. (2.53). In particular, $q_0^2(S_6^s)$ in Tab. 2.6 is identical to the zero of the forward-backward asymmetry which has been extensively studied in the literature. For completeness, in the last

[††]The discontinuity in some of the error bands just below 6 GeV^2 is an unphysical artifact resulting from small charm quark masses ~ 1.2 GeV allowed in the estimation of the error. This feature was already observed in Ref. [47].

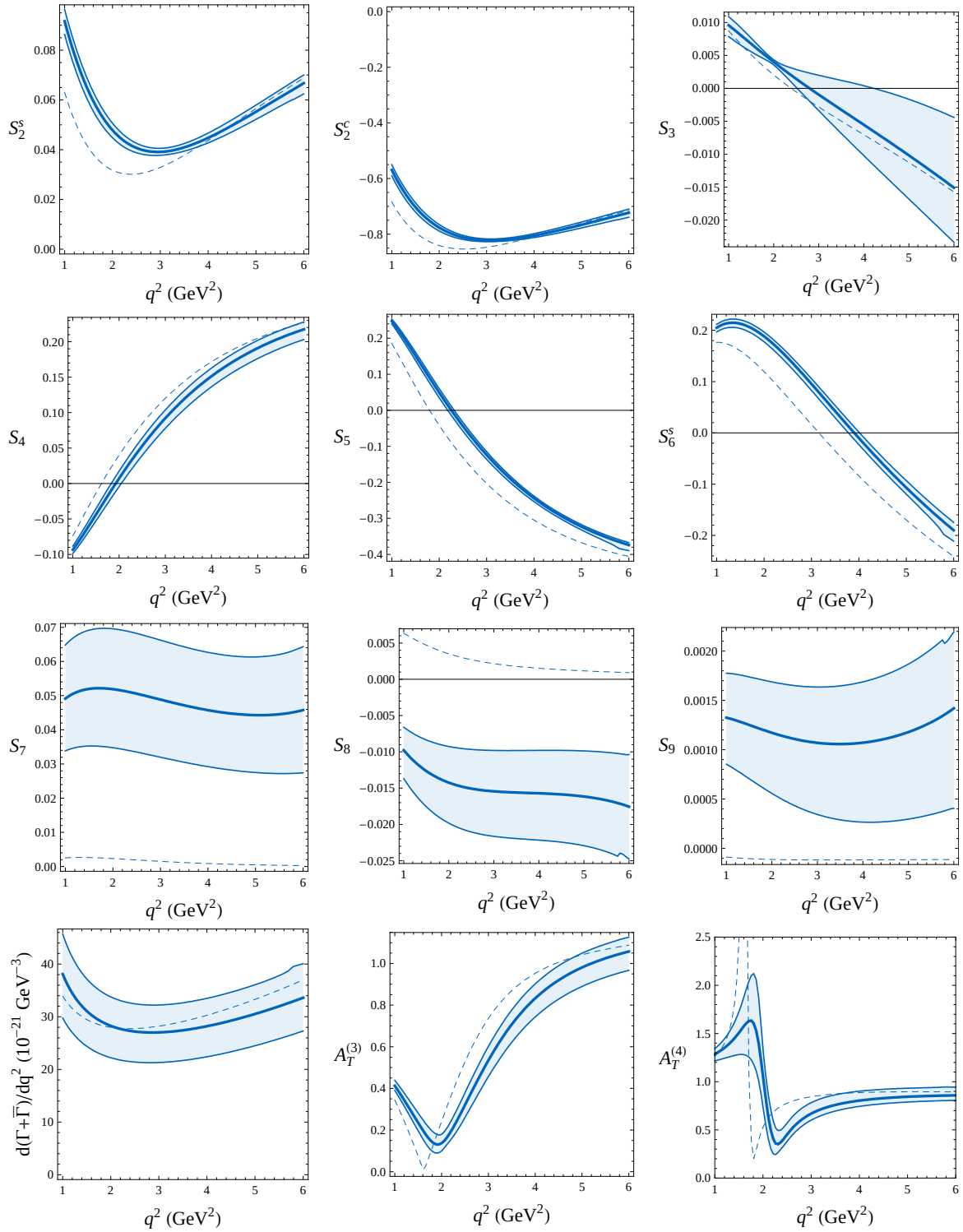

Figure 2.2: CP-averaged angular coefficients $S_i^{(a)}$, CP-averaged dilepton mass distribution $d(\Gamma + \bar{\Gamma})/dq^2$ and transverse asymmetries $A_T^{(3,4)}$ in the SM as a function of q^2. The dashed lines are the leading-order (LO) contributions, obtained in naïve factorisation. The thick solid lines are the full next-to-leading order (NLO) predictions from QCD factorisation (QCDF), as described in Sec. 2.2.4. The blue band defines the total error for the NLO result as described in the text.

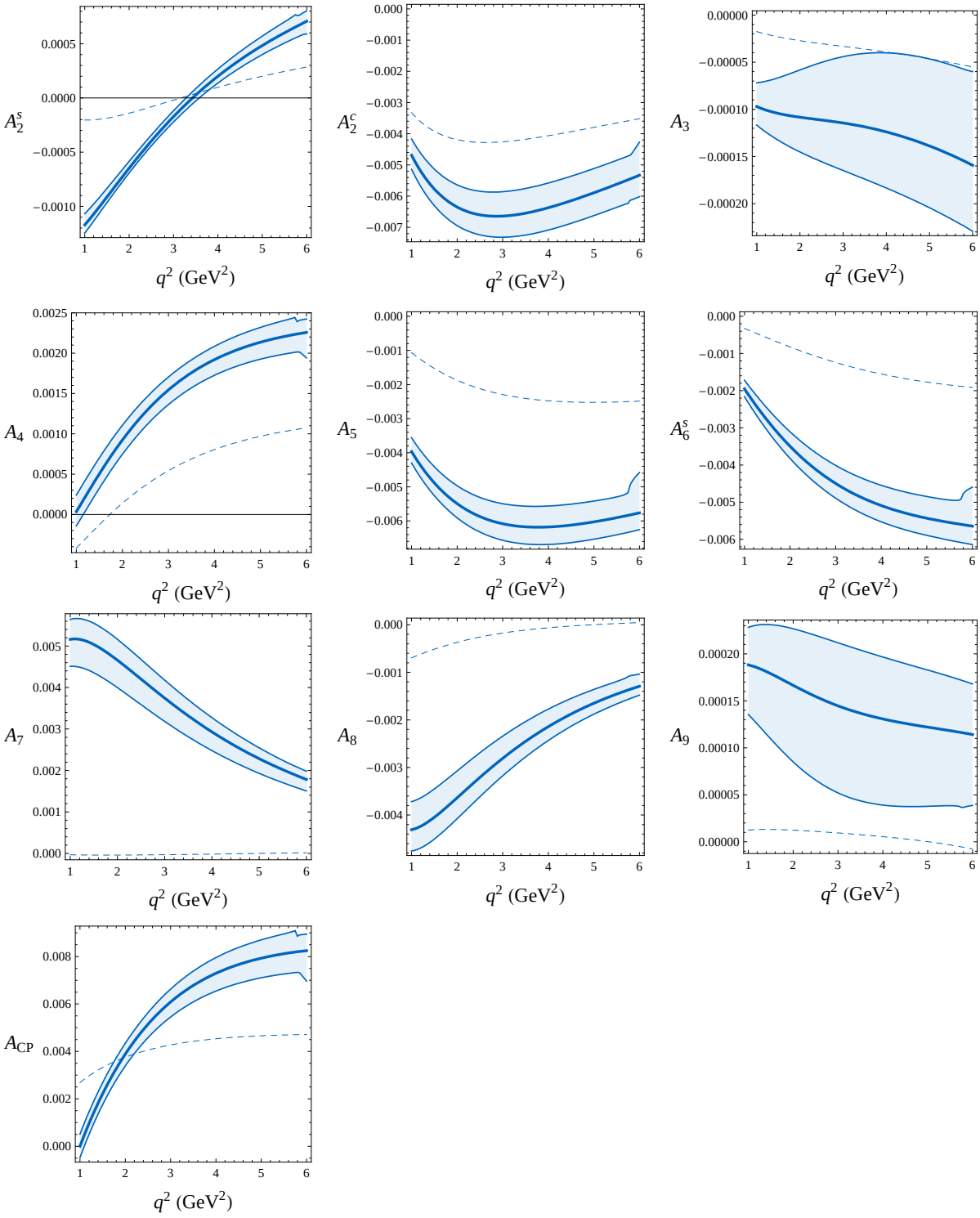

Figure 2.3: CP asymmetries $A_i^{(a)}$ and $A_{\rm CP}$ in the SM as a function of q^2. The meaning of the curves and bands is as in Fig. 2.2.

row of Fig. 2.2 we also show the CP averaged dilepton mass distribution $d(\Gamma + \bar{\Gamma})/dq^2$ and the observables $A_T^{(3)}$ and $A_T^{(4)}$ defined in Ref. [89], see Sec. 2.3.5. We find that our results for all these observables compare well to those in the literature. However, we note that the peak in the plot of $A_T^{(4)}$ is a manifestation of the zero $q_0^2(S_4)$ of S_4, see Eq. (2.56). This division by a near-zero quantity induces a large theoretical uncertainty both in the position of the peak and its height. We stress that such uncertainties do not arise if the observables S_4 and S_5 are considered instead of $A_T^{(3)}$ and $A_T^{(4)}$. In fact, as $d\Gamma/dq^2$ is a smooth function in the range of q^2 considered, none of our observables S_i and A_i is affected by accidental and delicate cancellations in the denominator.

As explained in Sec. 2.3.5, the CP asymmetries are close to zero in the SM, which is evident from Fig. 2.3, where we show all the $A_i^{(a)}$ (again except for $A_1^{s,c}$) and the CP asymmetry in the decay distribution, $A_{\rm CP}$. As explained above, the shift from LO to NLO is substantial. Our results are in good agreement with Ref. [88], but do not coincide exactly. This can be understood by recalling that we use the full LCSR form factors and that our normalisation of the soft form factors, especially $\xi_\parallel$, is different from that used in Ref. [88]. Also our choice of quark masses, in particular m_c/m_b and m_t, as well as the scale μ at which the QCDF hard-scattering corrections are evaluated, differs from [88]. We stress that, in view of the smallness of the SM values of A_i, these discrepancies become irrelevant once large NP contributions start to dominate these observables, as we shall see in the remainder of this section.

In Tab. 2.7, we list our predictions for the q^2-integrated CP-averaged angular coefficients and CP asymmetries as defined in Eqs. (2.57) and (2.58). $\langle S_2^c \rangle$, $\langle S_6^s \rangle$ and $\langle A_{\rm CP} \rangle$ can be directly compared to existing experimental results from BaBar and Belle [111; 112].

Obs.	S_4	S_5	S_6^s
q_0^2 [GeV^2]	$1.94^{+0.12}_{-0.10}$	$2.24^{+0.06}_{-0.08}$	$3.90^{+0.11}_{-0.12}$

Table 2.6: Predictions for the zero positions $q_0^2(S_i^{(a)})$ of S_4, S_5 and S_6^s in the SM.

Obs.	$10^{-2} \times \ldots$	Obs.	$10^{-2} \times \ldots$	Obs.	$10^{-3} \times \ldots$	Obs.	$10^{-3} \times \ldots$
$\langle S_1^s \rangle$	$16.0^{+0.6}_{-0.6}$	$\langle S_5 \rangle$	$-14.2^{+0.8}_{-1.2}$	$\langle A_1^s \rangle$	$-0.2^{+0.2}_{-0.1}$	$\langle A_5 \rangle$	$-5.7^{+0.6}_{-0.5}$
$\langle S_1^c \rangle$	$79.3^{+0.8}_{-0.8}$	$\langle S_6^s \rangle$	$3.5^{+0.8}_{-1.1}$	$\langle A_1^c \rangle$	$6.3^{+0.7}_{-0.8}$	$\langle A_6^s \rangle$	$-4.5^{+0.5}_{-0.4}$
$\langle S_2^s \rangle$	$5.3^{+0.2}_{-0.2}$	$\langle S_7 \rangle$	$4.8^{+1.7}_{-1.7}$	$\langle A_2^s \rangle$	$-0.1^{+0.1}_{-0.0}$	$\langle A_7 \rangle$	$3.4^{+0.4}_{-0.5}$
$\langle S_2^c \rangle$	$-76.6^{+0.7}_{-0.7}$	$\langle S_8 \rangle$	$-1.5^{+0.6}_{-0.6}$	$\langle A_2^c \rangle$	$-6.1^{+0.7}_{-0.6}$	$\langle A_8 \rangle$	$-2.6^{+0.4}_{-0.3}$
$\langle S_3 \rangle$	$-0.3^{+0.4}_{-0.3}$	$\langle S_9 \rangle$	$0.1^{+0.1}_{-0.1}$	$\langle A_3 \rangle$	$-0.1^{+0.1}_{-0.1}$	$\langle A_9 \rangle$	$0.1^{+0.1}_{-0.1}$
$\langle S_4 \rangle$	$10.1^{+1.0}_{-1.2}$			$\langle A_4 \rangle$	$1.5^{+0.2}_{-0.2}$	$\langle A_{\rm CP} \rangle$	$5.9^{+0.6}_{-0.6}$

Table 2.7: Predictions for the integrated CP-averaged angular coefficients $\langle S_i^{(a)} \rangle$ (in units of 10^{-2}) and the integrated CP asymmetries $\langle A_i^{(a)} \rangle$ (in units of 10^{-3}) in the SM. Note the different normalisation of the $\langle A_i^{(a)} \rangle$ with respect to Ref. [88], see footnote $**$.

Wilson coefficients	largest effect in
C_7, C_7'	S_1^s, S_1^c, S_2^s, S_2^c, S_3, S_4, S_5, S_6^s, A_7, A_8, A_9, BR($B \to X_s\gamma$), BR($B \to X_s\mu^+\mu^-$)
C_9, C_9', C_{10}, C_{10}'	S_1^s, S_1^c, S_2^s, S_2^c, S_3, S_4, S_5, S_6^s, A_7, A_8, A_9, BR($B \to X_s\mu^+\mu^-$)
$C_S - C_S'$	S_6^c, BR($B_s \to \mu^+\mu^-$)
$C_P - C_P'$	$S_1^c + S_2^c$, BR($B_s \to \mu^+\mu^-$)

Table 2.8: The Wilson coefficients relevant in $B \to K^*\mu^+\mu^-$ and the observables they have the largest impact on.

2.4.2 Model-independent Considerations

Before turning to specific NP scenarios, we investigate the model-independent impact of the Wilson coefficients on our observables.

Observable	mostly affected by
S_1^s, S_1^c, S_2^s, S_2^c	C_7, C_7', C_9, C_9', C_{10}, C_{10}'
S_3	C_7', C_9', C_{10}'
S_4	C_7, C_7', C_{10}, C_{10}'
S_5	C_7, C_7', C_9, C_{10}'
S_6^s	C_7, C_9
A_7	C_7, C_7', C_{10}, C_{10}'
A_8	C_7, C_7', C_9, C_9', C_{10}'
A_9	C_7', C_9', C_{10}'
S_6^c	$C_S - C_S'$

Table 2.9: The most interesting angular observables in $B \to K^*\mu^+\mu^-$ and the Wilson coefficients they are most sensitive to.

Impact of Wilson Coefficients on Observables

The impact of NP on the angular observables discussed in our paper is given by the changes of the Wilson coefficients of the affected operators. One can group these Wilson coefficients into three classes:

- Dipole coefficients: C_7, C_7', C_8 and C_8'. The role of the gluon dipole operators is subleading in the decay considered.
- Semileptonic coefficients: C_9, C_9', C_{10} and C_{10}'.
- Scalar coefficients: $C_S - C_S'$ and $C_P - C_P'$.

Before entering the discussion of various NP scenarios, it is useful to study the correlation between the angular coefficients and the Wilson coefficients. In Tab. 2.8 we show which observables are most affected by a significant change of a given coefficient. In Tab. 2.9 we show, on the other hand, which Wilson coefficients should be altered to produce a large effect in specific observables.

We observe:

- C_7, C_7', C_9, C_9', C_{10} and C_{10}' can induce large effects in many observables, or at least in those that do not require the presence of strong phases. To be precise, the A_i are mainly induced by imaginary parts of the Wilson coefficients, while the S_i are induced by their real parts.

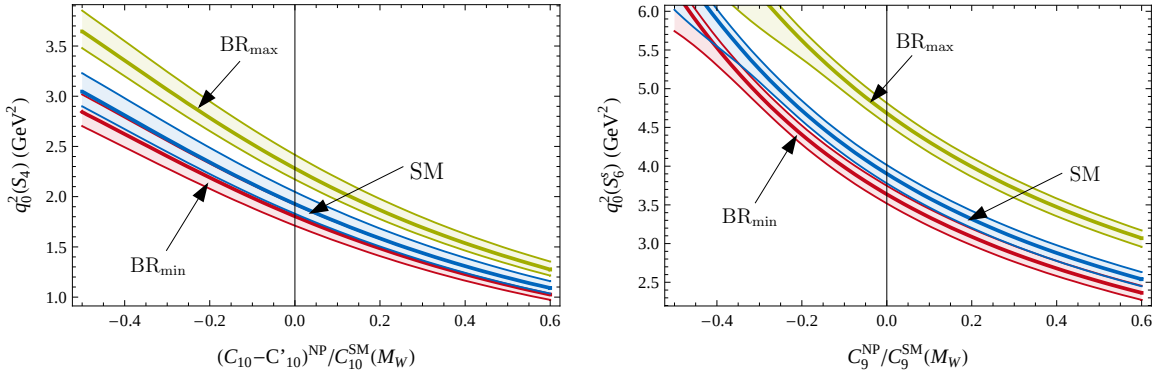

Figure 2.4: Left: correlation between $q_0^2(S_4)$, the position of the zero of S_4, and the NP contribution to $C_{10} - C'_{10}$. Right: correlation between $q_0^2(S_6^s)$ and the NP contribution to C_9. We use the branching ratio for $B \to X_s\gamma$ to constrain the NP contributions to C_7 and C'_7. The green (red) band corresponds to a value of BR$(B \to X_s\gamma)$ at the upper (lower) end of the experimental 2σ range, the blue band to SM values for C_7, C'_7.

- Only the primed coefficients C'_7, C'_9 and C'_{10} can significantly affect the observables S_3 and A_9. As can be seen from Eq. (2.56), S_3 corresponds to the transverse asymmetry $A_T^{(2)}$ and the impact of NP physics contributions to C'_7 on this observable has been studied for example in Refs. [89; 106; 108].
- The scalar operators affect mainly S_6^c and the branching ratio for $B_s \to \mu^+\mu^-$. This implies interesting correlations between these two observables as discussed in Sec. 2.4.2.

Model-independent Analysis of S_4, S_5 and S_6^s

The zero of the forward-backward asymmetry has been the focus of many experimental and theoretical studies (see for example Refs. [62; 113]) as it is established as being an observable free from hadronic effects and capable of distinguishing between NP scenarios. In Sec. 2.3.5 we expressed the CP-averaged forward-backward asymmetry in terms of S_6^s through Eq. (2.53), so S_6^s could clearly be studied instead of $A_{\rm FB}$. In addition, from Fig. 2.2, we find there are two more observables with such a zero in q^2, S_4 and S_5. A study of these three observables in a model-independent way could allow us to constrain the NP contributions to the Wilson coefficients.

From Tab. 2.9 we see that the zero of S_4, $q_0^2(S_4)$, is largely sensitive to C_7, C'_7, C_{10} and C'_{10}. This dependence arises only through $C_7 - C'_7$ and $C_{10} - C'_{10}$. We therefore explore how the position of the zero in q^2 is affected by NP modifications to $C_{10} - C'_{10}$ and C_7.

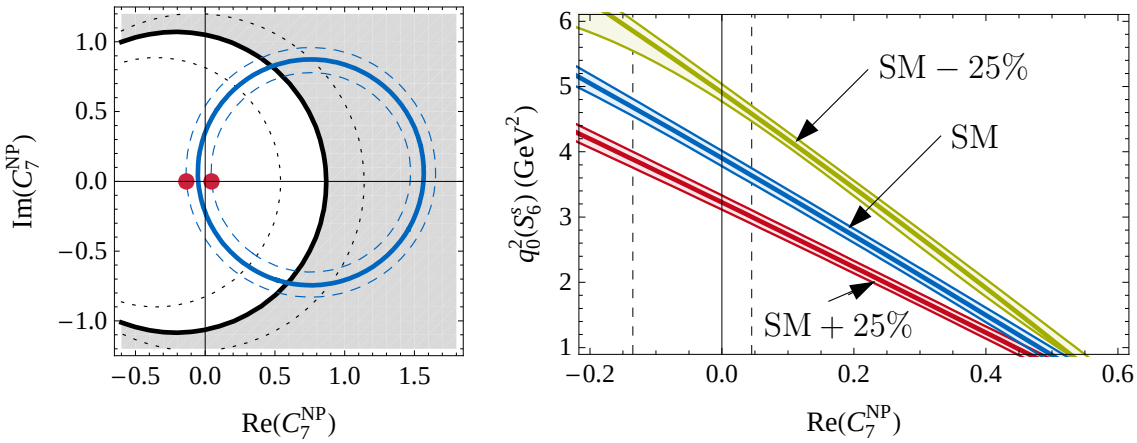

Figure 2.5: Left: Experimental constraints on the NP contribution to C_7. The blue circles show the constraint from the central and $\pm 2\sigma$ values of $\mathrm{BR}(B \to X_s\gamma)$, assuming $C_7'^{\mathrm{NP}} = 0$. The black circle corresponds to the 2σ bound from $\mathrm{BR}(B \to X_s\ell^+\ell^-)$, assuming $C_{10}^{(\prime)\mathrm{NP}} = 0$. The solid thick and the dotted lines have been obtained assuming SM and SM$\pm$25% values for C_9, respectively. Right: Correlation of the zero in S_6^s with the NP contribution to $\mathrm{Re}(C_7)$. The blue, red and green bands indicate SM, SM+25% and SM−25% values for C_9 with the associated theoretical uncertainty. The vertical dashed lines correspond to the upper and lower bounds on $\mathrm{Re}(C_7)$ in the absence of an imaginary part of C_7. (The corresponding points in the left-hand plot are highlighted by red dots.) For an arbitrary imaginary part, the upper bound on $\mathrm{Re}(C_7)$ is removed, and $q_0^2(S_6^s)$ can be at or below $1\,\mathrm{GeV}^2$.

The current experimental value of the branching ratio of $B \to X_s\gamma$ provides a constraint on C_7 and C_7'. We find a strong dependence of $q_0^2(S_4)$ on $C_{10} - C_{10}'$, and its measurement would provide very interesting information about these Wilson coefficients. In Fig. 2.4, we show this dependence for real values of C_7.

If the NP introduces an imaginary part to C_7, the bound from $B \to X_s\gamma$ is weakened, allowing large effects in the zeros. In fact, large values of $\mathrm{Im}(C_7)$ significantly enhance the branching ratio of the decay $B \to X_s\gamma$ and in order to be in agreement with the experimental data, large positive contributions to $\mathrm{Re}(C_7)$ that interfere destructively with C_7^{SM} are required. For such values of the Wilson coefficients, the branching ratio of the decay $B \to X_s\mu^+\mu^-$ is largely enhanced, effectively setting a new upper bound on $\mathrm{Re}(C_7)$. In the left-hand plot in Fig. 2.5, we show these combined constraints on C_7 in the complex plane. Exactly the large positive contributions to $\mathrm{Re}(C_7)$, which are allowed in the presence of phases in C_7^{NP}, then unambiguously shift the zeros of S_4, S_5

and S_6^s towards lower values. In the right-hand plot in Fig. 2.5, we show as an example that the allowed range for $q_0^2(S_6^s)$ is greatly enhanced in the case of complex C_7.

This analysis can also be applied to S_6^s, which depends strongly on C_7 and C_9. We examine the dependence of $q_0^2(S_6^s)$ on NP contributions to C_9 and C_7. This again is restricted by the experimental value of the branching ratio of $B \to X_s\gamma$. We find a strong dependence on C_9, and for real values of C_7 this would be a clean way to determine information about a possible NP contribution to C_9 as seen in Fig 2.4. Again, if NP induces a complex phase of C_7, the range in $q_0^2(S_6^s)$ increases dramatically.

It is a greater challenge to extract information about the Wilson coefficients from S_5 due to its dependence on C_7, C_7', C_9 and C_{10}'. However, a measurement of $q_0^2(S_5)$ could provide a consistency check with $C_{10} - C_{10}'$ and C_9 determined from S_4 and S_6, provided C_7, C_7' are real. In addition, this might allow one to untangle the effects of $C_{10}^{\rm NP}$ and $C_{10}'^{\rm NP}$ in Fig. 2.4.

Impact of Scalar Currents

As mentioned in the introduction, the impact of the scalar and pseudoscalar operators $\mathcal{O}_{S,P}^{(\prime)}$ on the angular distribution of $B \to K^*(\to K\pi)\mu^+\mu^-$ has been considered before [105], and no relevant effects on the observables of interest were found. However, as shown in Sec. 2.3.2, the inclusion of lepton-mass effects*, which were neglected in previous studies, gives rise to an additional observable in models with scalar currents, which can serve as a precision null-test of the SM and, as we will show, in principle allows one to distinguish between different NP models.

To assess the size of the possible effects generated by these operators, we first consider the allowed ranges for the Wilson coefficients $C_{S,P}^{(\prime)}$. The most stringent constraint on these coefficients comes from the measurement of $B_s \to \mu^+\mu^-$, which is strongly helicity suppressed in the SM, with a predicted branching ratio of [114; 115]

$$\mathrm{BR}(B_s \to \mu^+\mu^-) = (3.37 \pm 0.31) \times 10^{-9}. \tag{2.59}$$

The most recent experimental upper bound still lies, at the 95% confidence level, one order of magnitude above the SM [116]:

$$\mathrm{BR}(B_s \to \mu^+\mu^-) < 5.8 \times 10^{-8}\,. \tag{2.60}$$

*We stress that we restricted ourselves to muons in our numerical analysis.

However, in many models, e.g. the MSSM at large $\tan\beta$, this branching ratio can be greatly enhanced.

In a generic NP model, the branching ratio is given by

$$\mathrm{BR}(B_s \to \mu^+\mu^-) = \tau_{B_s} f_{B_s}^2 m_{B_s} \frac{\alpha_{\mathrm{em}}^2 G_F^2}{16\pi^3} |V_{tb}V_{ts}^*|^2 \sqrt{1-\frac{4m_\mu^2}{m_{B_s}^2}} \left[|S|^2 \left(1-\frac{4m_\mu^2}{m_{B_s}^2}\right) + |P|^2 \right], \tag{2.61}$$

where

$$S = \frac{m_{B_s}^2}{2}(C_S - C_S'), \qquad P = \frac{m_{B_s}^2}{2}(C_P - C_P') + m_\mu (C_{10} - C_{10}'). \tag{2.62}$$

Considering the experimental bound in Eq. (2.60), these formulae imply the approximate bounds

$$|C_S - C_S'| \lesssim 0.12\ \mathrm{GeV}^{-1}, \qquad -0.09\ \mathrm{GeV}^{-1} \lesssim C_P - C_P' \lesssim 0.15\ \mathrm{GeV}^{-1}, \tag{2.63}$$

barring large NP contributions to the Wilson coefficients $C_{10}^{(\prime)}$.

Now, inspecting the formulae for the angular coefficients, Eqs. (2.34)–(2.45), one can see that the only terms in which $C_S^{(\prime)}$ and $C_P^{(\prime)}$ are not suppressed by the lepton mass enter in the angular coefficient I_1^c. However, due to the small size of the Wilson coefficients themselves, see (2.63), these terms turn out to be numerically irrelevant in general once the bound from $B_s \to \mu^+\mu^-$ is taken into account.

Since the pseudoscalar operators do not contribute to any other angular coefficient, this implies that they are indeed irrelevant in the phenomenological study of $B \to K^*(\to K\pi)\mu^+\mu^-$. For the scalar operators, however, the situation is different, because of the new angular coefficient I_6^c, Eq. (2.41), which is directly proportional to the real part of $(C_S - C_S')$ and thus vanishes in the SM. So, although numerically small, this angular coefficient is an appealing observable because any measurement of a non-zero value would constitute an unambiguous signal of scalar currents at work.

This is in contrast to the process $B_s \to \mu^+\mu^-$, where a large enhancement of the branching ratio compared to the SM could be caused by both scalar and pseudoscalar currents. In addition, the measurement of a non-zero S_6^c (the CP-averaged counterpart of I_6^c) would allow to determine the sign of $\mathrm{Re}(C_S - C_S')$. In fact, by a combined study of $B_s \to \mu^+\mu^-$ and the observable S_6^c, one would be able to constrain the relative sizes of

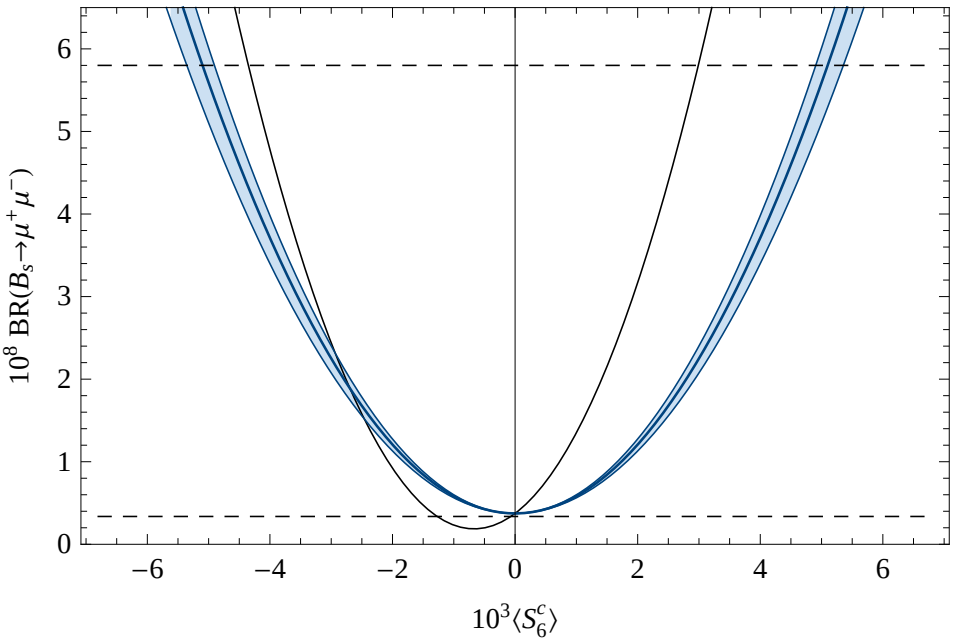

Figure 2.6: Correlation between the observable $\langle S_6^c \rangle$ and the branching ratio for $B_s \to \mu^+\mu^-$. The blue band is obtained by assuming NP contributions only to the Wilson coefficient C_S, the black curve (where error bars are omitted) by assuming $C_P = -C_S$. The horizontal dashed lines indicate the SM prediction for BR($B_s \to \mu^+\mu^-$) (2.59) and the current experimental upper bound (2.60).

the scalar and pseudoscalar Wilson coefficients, which can serve to distinguish different models of NP. For example, in the MSSM, the ratio of C_S and C_P is

$$\frac{C_P}{C_S} \approx -\frac{M_{A^0}^2}{M_{H^0}^2} \approx -1 \tag{2.64}$$

to a very good accuracy, a relation which could be tested by a measurement of BR($B_s \to \mu^+\mu^-$) and S_6^c.

To illustrate this point, we show, in Fig. 2.6, the correlation between BR($B_s \to \mu^+\mu^-$) and $\langle S_6^c \rangle$ (as defined in Eq. (2.57)). The blue band has been obtained by assuming that NP contributions enter only through C_S, i.e. setting $C_P/C_S = 0$, and varying C_S accordingly; the error band takes into account all the sources of error as discussed in Sec. 2.4.1. Assuming, in contrast, $C_P/C_S = -1$, as would be the case in the MSSM, one obtains the black parabola.

To summarise, while pseudoscalar operators are numerically irrelevant in the decay $B \to K^*(\to K\pi)\mu^+\mu^-$, a study of the angular distribution allows one to probe the scalar

sector of a theory beyond the SM, in a way that is theoretically clean and complementary to $B_s \to \mu^+\mu^-$.

2.5 Summary

In this chapter we have analysed the angular distribution of the rare decay $B \to K^*(\to K\pi)\mu^+\mu^-$, and identified a complete set of variables, $S_i^{(a)}$ and $A_i^{(a)}$ which are defined in Sec. 2.3.5. These variables emphasise CP-conserving and CP-violating effects, and are normalised by the total decay rate which results in a cancellation of hadronic uncertainties. The angular observables offer new important tests of the SM and its extentions, as explored in [52]. The next chapter will focus on the measurement of some of these observables in the early LHC era, but an accurate measurement of some will only be possible at an upgraded Belle and a Super-B facility. We have studied the effect of NP on our chosen observables in a model independent way. To this end we have improved on previous studies in a number of ways that have been listed in Sec. 2.1.

The main messages from this study are as follows:

- Our predictions for the CP-averaged angular coefficients $S_i^{(a)}$ in the SM are shown in Fig. 2.2. Some of these $S_i^{(a)}$ are found to be large.
- On the other hand, as evident from Fig. 2.3, the CP asymmetries $A_i^{(a)}$ are close to zero in the SM.
- The observables S_4, S_5 and S_6^c show zero-crossing points which are insensitive to hadronic effects. It is shown that in MFV scenarios the position of the zero-crossing is well-constrained by $b \to s\gamma$. However, additional CP phases contributing to the Wilson coefficient C_7 can result in large deviations from the SM as seen in Figs. 2.4 and 2.5.
- Our model independent study shows that pseudoscalar operators are numerically irrelevant in the decay $B \to K^*\mu^+\mu^-$. On the other hand a study of the angular distributions allows, in a way which is theoretically clean and complementary to $B_s \to \mu^+\mu^-$, to probe the scalar sector of a theory beyond the SM.

Clearly, it will be very exciting to monitor the upcoming LHC, Belle upgrade and eventually Super-B factory in this and in the next decade to see whether the angular observables discussed in our paper will give a hint for any of the extensions of the SM.

Chapter 3

Prospects for $B_d \to K^{*0}\mu^+\mu^-$ in the first few years

3.1 Introduction

The properties of the angular distribution for $B_d \to K^{*0}\mu^+\mu^-$ were introduced Ch. 2 where a number of interesting potential measurements identified (also see Refs. [52; 88; 89; 106; 117; 118]). Particular emphasis has so far been placed on finding angular observables with reduced theoretical uncertainties or sensitivity to particular classes of NP. However, in the first few years of LHC data–taking the dominant sources of uncertainty will be experimental, meaning that the emphasis should be on finding quantities which can be cleanly extracted with relatively small uncertainty. With very large data sets it will be possible to use a full angular analysis to extract the various underlying amplitudes directly, [89; 119]. This will allow a determination of many theoretically clean observables. However performing this kind of analysis will not be possible until detectors are very well understood and the number of collected signal events are in the thousands. Before this, asymmetries of the angular distribution can be used to extract some observables individually, [52; 62; 88; 120; 121].

In this chapter we focus on observables which can be extracted from the $\overline{B}_d \to \overline{K}^{*0}\mu^+\mu^-$ angular distribution by counting the number of signal events as a function of one or two decay angles. The rest of the chapter is structured as follows. In the next section we give a brief overview of the theoretical framework employed with details of the calculation of the decay amplitude involving Wilson coefficients, form–factors and QCD factorisation corrections. In Sec. 3.3.1 observables which will be relevant

$C_1(\mu)$	$C_2(\mu)$	$C_3(\mu)$	$C_4(\mu)$	$C_5(\mu)$
-0.135	1.054	0.012	-0.033	0.009
$C_6(\mu)$	$C_7^{\rm eff}(\mu)$	$C_8^{\rm eff}(\mu)$	$\Delta C_9^{\rm eff}(\mu)$	$C_{10}^{\rm eff}(\mu)$
-0.039	-0.306	-0.159	4.220	-4.093

Table 3.1: SM Wilson coefficients at $\mu = m_b = 4.52\,\text{GeV}/c^2$, where $\Delta C_9^{\rm eff}(\mu) \sim C_9^{\rm eff}(\mu) - Y(q^2)$.

for analyses with the first few years data are discussed, and details of benchmark NP models which we use to study these observables provided. We summarise the impact of existing experimental measurements on constraining the NP contribution to the Wilson coefficients. In Sec. 3.4, we then assess how such measurements would further constrain the effect of NP on the Wilson coefficients. Finally, in Sec. 3.5 a short summary is given.

3.2 Theoretical Details

A decay model following Ref. [86] has become the standard tool for studies of $\overline{B}_d \to \overline{K}^{*0}\mu^+\mu^-$ within the experimental community due to its inclusion in the decay simulator EvtGen [122]. Here we have developed a significantly updated version of that model with much improved support for the simulation of NP. Hence, we present our theoretical framework in a way which allows direct comparison with Ref. [86], where it is shown that it is possible to express the decay amplitude in terms of auxiliary functions. The calculation of these requires Wilson coefficients, form factors and QCD factorisation (QCDF) corrections, as described in the previous chapters. Here we provide details specific to this calculation.

In this chapter we neglect doubly Cabibbo–suppressed contributions $\mathcal{H}_{\rm eff}^{(u)}$, as these will not be detectable in an early analysis of the observables. The weak effective Hamiltonian reduces to $\mathcal{H}_{\rm eff}^{(t)}$ defined in Eq. (2.1). The primed operators $\mathcal{O}'_{7-10}$, the scalar and the pseudoscalar operators, $\mathcal{O}_{S/P}$, and their primed equivalents are included, which vanish or are suppressed in the SM but may become important in certain NP scenarios. The Wilson coefficients are calculated as described in Sec. 2.2.1. Tab. 3.1 gives the values of the Wilson coefficients at $\mu = m_{b,\rm PS}(2\text{GeV})$ in the SM*. The treatment of quark masses in the PS scheme is discussed in Sec. 3.2.2.

*Note that the Wilson coefficients are evaluated at a different scale from Ch. 2, as discussed in Sec. 3.2.2

	Model			
	SM	FBMSSM	GMSSM	UED
$C_7^{\rm eff}(\mu)$	-0.306	0.031+0.475i	-0.186+0.002i	-0.297
$C_7'^{\rm eff}(\mu)$	-0.007	0.008+0.003i	0.155+0.160i	-0.007
$C_8^{\rm eff}(\mu)$	-0.159	-0.085+0.149i	-0.062+0.004i	-0.137
$C_8^{\rm eff}(\mu)$	-0.004	-0.000+0.001i	0.330+0.336i	-0.003
$\Delta C_9^{\rm eff}(\mu)$	4.220	4.257 +0.000i	4.231+0.000i	4.230
$C_9'^{\rm eff}(\mu)$	0.000	0.002+0.000i	0.018+0.000i	0.000
$C_{10}^{\rm eff}(\mu)$	-4.093	-4.063 +0.000i	-4.241+0.000i	-4.212
$C_{10}'^{\rm eff}(\mu)$	0.000	0.004 +0.000i	0.003+0.003i	0.000
$(C_S - C_S')(\mu)$	0.000	-0.044-0.056i	0.000+0.001i	0.000
$(C_P - C_P')(\mu)$	0.000	0.043+0.054i	0.001+0.001i	0.000

Table 3.2: NP Wilson coefficients at $\mu = m_{b,\rm PS}(2\,\text{GeV}/c^2) = 4.52\,\text{GeV}/c^2$.

QCD sum rules on the light cone (LCSR) provides results for the desired range in q^2 [72]. We use the full set of LCSR form factors in the model [123] and estimate uncertainty using the errors provided in Ref. [72] for $q^2 = 0$.We express our leading order results for the decay amplitude in terms of the full form factors, making these factorisable corrections redundant as well as including the main source of $\mathcal{O}(1/m_b)$ corrections, as argued in Ch. 2. The weak annihilation correction is leading order in $1/m_b$ and $\mathcal{O}(\alpha_s)$, but is dependent on the numerically small C_3 and C_4 so can be neglected.

We define $\mathcal{T}_\parallel^{\rm NLO}(q^2)$ and $\mathcal{T}_\perp^{\rm NLO}(q^2)$ to include the relevant $\mathcal{O}(\alpha_s)$ contributions to $\mathcal{T}_\parallel(q^2)$ and $\mathcal{T}_\perp(q^2)$, as in Ref. [47]. We also define the analogous $\mathcal{T}_\parallel'^{\rm NLO}(q^2)$ and $\mathcal{T}_\perp'^{\rm NLO}(q^2)$ where the primes denote that the unprimed Wilson coefficients should be replaced by their primed equivalents. This means that in order to extend the results in Ref. [86] to include NLO corrections, we must make the following replacements:

$$
\begin{aligned}
C_7^{(\prime)\,\rm eff} T_1(q^2) &\to C_7^{(\prime)\,\rm eff} T_1(q^2) + \mathcal{T}_\perp^{(\prime)\,\rm NLO}(q^2) \\
C_7^{(\prime)\,\rm eff} T_2(q^2) &\to C_7^{(\prime)\,\rm eff} T_2(q^2) + 2\frac{E}{m_B}\mathcal{T}_\perp^{(\prime)\,\rm NLO}(q^2) \\
C_7^{(\prime)\,\rm eff} T_3(q^2) &\to C_7^{(\prime)\,\rm eff} T_3(q^2) + \mathcal{T}_\perp^{(\prime)\,\rm NLO}(q^2) + \mathcal{T}_\parallel^{(\prime)\,\rm NLO}(q^2)
\end{aligned}
\tag{3.1}
$$

Here E is the energy of the K^*, as defined in Eq. (1.43), and m_B is the mass of the B meson. These replacements are in keeping with Ref. [47].

3.2.1 Decay amplitudes

The Hamiltonian defined in Eq. (1.7), in combination with the standard definitions for the form factors, leads to the following decay amplitude, as in Refs. [86; 124],

$$\mathcal{M} \propto \left[\mathcal{T}^1_\mu\,(\bar{\mu}\,\gamma^\mu\,\mu) + \mathcal{T}^2_\mu\,(\bar{\mu}\,\gamma^\mu\gamma_5\,\mu) + \mathcal{S}(\bar{\mu}\,\mu)\right] \tag{3.2}$$

where

$$\begin{aligned}
\mathcal{T}^1_\mu &= A(q^2)\epsilon_{\mu\rho\alpha\beta}\epsilon^{*\rho}\,\hat{p}_B^\alpha\,\hat{p}_{K^*}^\beta - iB(q^2)\,\epsilon^*_\mu + iC(q^2)(\epsilon^*\cdot\hat{p}_B)\,\hat{p}_\mu + iD(q^2)(\epsilon^*\cdot\hat{p}_B)\,\hat{q}_\mu \\
\mathcal{T}^2_\mu &= E(q^2)\epsilon_{\mu\rho\alpha\beta}\,\epsilon^{*\rho}\hat{p}_B^\alpha\,\hat{p}_{K^*}^\beta - iF(q^2)\,\epsilon^*_\mu + iG(q^2)(\epsilon^*\cdot\hat{p}_B)\,\hat{p}_\mu + iH(q^2)(\epsilon^*\cdot\hat{p}_B)\,\hat{q}_\mu
\end{aligned} \tag{3.3}$$

and

$$\mathcal{S} = i2\hat{m}_{K^*}(\epsilon^*\cdot\hat{p}_B)\,I(q^2).$$

Here p_B, p_{K^*} and m_B, m_{K^*} are the four–momenta in the B meson rest frame and the masses of the respective particles, $p \equiv p_B + p_{K^*}$, $q \equiv p_B - p_{K^*}$ and ϵ^*_μ is the K^*polarisation vector. The circumflex denotes division by m_B, so for example $\hat{m}_{K^*} \equiv m_{K^*}/m_B$. The auxiliary functions A-$I(q^2)$ follow Ref. [86], but we have updated the previous expressions by including additional primed, scalar and pseudoscalar operators, and the QCDF correction via $\mathcal{T}_\parallel^{(\prime)\mathrm{NLO}}(q^2)$ and $\mathcal{T}_\perp^{(\prime)\mathrm{NLO}}(q^2)$ as outlined in Sec. 3.2.

$$\begin{aligned}
A(q^2) =& \frac{2}{1+\hat{m}_{K^*}}(C_9^{\mathrm{eff}} + C_9^{\prime\,\mathrm{eff}})V(q^2) + \frac{4\hat{m}_b}{\hat{q}^2}\Bigg((C_7^{\mathrm{eff}} + C_7^{\prime\,\mathrm{eff}})T_1(q^2) \\
&+ \mathcal{T}_\perp^{\mathrm{NLO}}(q^2) + \mathcal{T}_\perp^{\prime\,\mathrm{NLO}}(q^2)\Bigg) \\
B(q^2) =& (1+\hat{m}_{K^*})\Bigg\{(C_9^{\mathrm{eff}} - C_9^{\prime\,\mathrm{eff}})A_1(q^2) + \frac{2\hat{m}_b}{\hat{q}^2}(1-\hat{m}_{K^*})\Bigg((C_7^{\mathrm{eff}} - C_7^{\prime\,\mathrm{eff}})T_2(q^2)
\end{aligned}$$

$$+ 2\hat{E}(\mathcal{T}_\perp^{\rm NLO}(q^2) - \mathcal{T}_\perp'^{\rm NLO}(q^2))\Bigg)\Bigg\}$$

$$C(q^2) = \frac{1}{1-\hat{m}_{K^*}^2}\Bigg\{(1-\hat{m}_{K^*})(C_9^{\rm eff} - C_9'^{\rm eff})A_2(q^2)$$
$$+ 2\hat{m}_b\Bigg((C_7^{\rm eff} - C_7'^{\rm eff})(T_3(q^2) + \frac{1-\hat{m}_{K^*}^2}{\hat{q}^2}T_2(q^2))$$
$$+ (1 + \frac{(1-\hat{m}_{K^*}^2)\,2\hat{E}}{\hat{q}^2})(\mathcal{T}_\perp^{\rm NLO}(q^2) - \mathcal{T}_\perp'^{\rm NLO}(q^2)) + \mathcal{T}_\parallel^{\rm NLO}(q^2) - \mathcal{T}_\parallel'^{\rm NLO}(q^2)\Bigg)\Bigg\}$$

$$E(q^2) = \frac{2}{(1+\hat{m}_{K^*})}(C_{10}^{\rm eff} + C_{10}'^{\rm eff})V(q^2)$$

$$F(q^2) = (1+\hat{m}_{K^*})(C_{10}^{\rm eff} - C_{10}'^{\rm eff})A_1(q^2)$$

$$G(q^2) = (C_{10}^{\rm eff} - C_{10}'^{\rm eff})\frac{A_2(q^2)}{(1+\hat{m}_{K^*})}$$

$$H(q^2) = \frac{1}{\hat{q}^2}(C_{10}^{\rm eff} - C_{10}'^{\rm eff})\Bigg((1+\hat{m}_{K^*})A_1(q^2) - (1-\hat{m}_{K^*})A_2(q^2)$$
$$- 2\hat{m}_{K^*}A_0(q^2)\Bigg) - \frac{\hat{m}_{K^*}m_B}{2\hat{m}_\mu}A_0(q^2)(C_P - C_P')$$

$$I(q^2) = -A_0(q^2)(C_S - C_S'). \tag{3.4}$$

Note that using the equations of motion for the muons,

$$q^\mu(\bar{\mu}\gamma_\mu\,\mu) = 0 \qquad \text{and} \qquad q^\mu(\bar{\mu}\gamma_\mu\gamma_5\,\mu) = -2m_\mu\bar{\mu}\gamma_5\,\mu, \tag{3.5}$$

where m_μ is the muon mass, we see that $D(q^2)$ vanishes and $H(q^2)$ is suppressed by a power of m_μ. However $H(q^2)$ receives a pseudoscalar contribution inversely proportional to m_μ allowing for some sensitivity to $C_P - C_P'$, [124]. The observables described in Sec. 3.3.1 may be calculated directly from the amplitudes defined above in Eq. (3.4), and the necessary formulae are presented in App. A. The results can then be compared with those extracted from the angular distribution produced by our Monte–Carlo model.

Parameter	Value	Ref.
m_s	0.104	[125]
$m_{c,\mathrm{PS}}(0.7\,\mathrm{GeV})$	1.5 GeV	[126]
$m_{b,\mathrm{PS}}(2\,\mathrm{GeV})$	4.52 GeV	[127]
$\hat{m}_t(\hat{m}_t)$	162.3 GeV	[91]

Table 3.3: Quark masses

3.2.2 Numerical Input

Quark Masses: The calculation of these auxiliary functions requires the bottom quark pole mass, which is known to contain large long distance corrections. To avoid this issue a renormalisation scheme known as the potential subtraction scheme (PS) was introduced in Ref. [128]. The quark mass defined in the PS scheme has the advantage that the large infrared contributions are absent, while numerically being relatively close to the pole mass. It is suitable for calculations in which the quark is nearly on-shell. Following Ref. [47], although note this differs from the procedure used in Ch. 2, we therefore replace the pole mass by the PS mass $m_{\mathrm{PS}}(\mu_f)$ given in Tab. 3.3, using

$$m = m_{\mathrm{PS}}(\mu_f) + \frac{4\alpha_s}{3\pi}\mu_f + \mathcal{O}(\alpha_s^2) \tag{3.6}$$

and any resulting terms of $\mathcal{O}(\alpha_s^2)$ may be neglected. Here μ_f is the scale at which the PS mass is calculated. Therefore all occurrences of m_b in our results refer to the PS mass at the scale m_b, $m_{b,\mathrm{PS}}(m_b)$.

Note that the operator $\mathcal{O}_7$ is defined in terms of the $\overline{\mathrm{MS}}$ mass. Therefore, when the b quark mass arises in combination with C_7^{eff}, we replace the $\overline{\mathrm{MS}}$ mass, $\bar{m}$, by the pole mass, using

$$\bar{m}(\mu) = m\left(1 + \frac{\alpha_s}{3\pi}\left(3\ln\frac{m_b^2}{\mu^2} - 4\right) + \mathcal{O}(\alpha_s^2)\right). \tag{3.7}$$

This leads to factorisable $\mathcal{O}(\alpha_s)$ corrections to $\mathcal{T}_{\perp/\parallel}^{\mathrm{NLO}}(q^2)$ and $\mathcal{T}_{\perp/\parallel}^{\prime\mathrm{NLO}}(q^2)$ as found in Ref. [47].

For consistency, we calculate the charm quark pole mass using Eq. (3.6). Here the PS mass is taken from the most recent calculation as in Tab. 3.3. The resulting pole mass agrees with results in Ref. [125] where it is calculated from the $\overline{\mathrm{MS}}$ mass. The top

Parameter	Value	Parameter	Value
m_B	5.28 GeV	$V_{\rm us}$	0.226 ± 0.002
m_{K^*}	0.896 GeV	$V_{\rm ub}$	$(3.93 \pm 0.36)10^{-3}$
m_μ	0.106 GeV	γ	$(77^{+30}_{-32})^\circ$
M_W	80.4 GeV	G_F	$(1.166)10^{-5}$

Table 3.4: CKM matrix parameters, additional masses and constants from Ref. [125].

quark mass enters the calculation of the Wilson coefficients, and for this it is suitable to use the $\overline{\rm MS}$ mass in Tab. 3.3, as in Ch. 2.

Hadronic Parameters: In addition to the form factors described in Sec. 3.2, the QCDF corrections require light-cone distribution amplitudes and decay constants. The light-cone distribution amplitude for both the B and K^*mesons enter the hard scattering corrections. For the B meson we follow the prescription in Ref. [47] using the values for Λ_B given in Tab. 2.3. For the K^*meson we use the standard Gegenbauer expansion,

$$\Phi^m_{K^*} = 6u(1-u)(1 + a^m_{1,K^*}C_1^{(3/2)}(2u-1) + a^m_{2,K^*}C_2^{(3/2)}(2u-1)) \tag{3.8}$$

for $m = \perp, \parallel$, taking the coefficients from Tab. 2.3 in Ch. 2. We also require the decay constant for both the B and K^*mesons, and use latest results as in Tab. 2.3. Additional parameters are summarised in Tab. 3.4.

3.3 Observables and New physics

Having established the basic theoretical framework, we proceed to discuss experimental observables for $\overline{B}_d \to \overline{K}^{*0}\mu^+\mu^-$.

3.3.1 Observables

The full angular decay distribution can be interpreted as in Eqs. (2.9) and (2.10), where it is described in terms of the angular coefficients $I_i^{(a)}$, for $i = 1$ to 9 and $a = s$ or c. A natural set of observables was identified in Eqs. (2.47,2.48) by taking combinations of

these $I_i^{(a)}$'s that emphasise CP-conserving and CP-violating effects. In addition to these observables we introduce the rate average, which for a variable $V(q^2)$ is given by

$$\langle V \rangle_{1-6\,\mathrm{GeV}^2} = \int_{1\,\mathrm{GeV}^2}^{6\,\mathrm{GeV}^2} dq^2 \left(V(q^2)\, \frac{d(\Gamma+\bar{\Gamma})}{dq^2} \right) \Bigg/ \int_{1\,\mathrm{GeV}^2}^{6\,\mathrm{GeV}^2} dq^2 \frac{d(\Gamma+\bar{\Gamma})}{dq^2}. \tag{3.9}$$

Using the above, it is possible to reconstruct standard observables such as the forward-backward asymmetry, A_{FB}, and the longitudinal polarisation fraction, F_{L}:

$$A_{\mathrm{FB}} = \frac{3}{8}(2S_6^s + S_6^c) \qquad \text{and} \qquad F_{\mathrm{L}} = -S_2^c. \tag{3.10}$$

As explained in Sec. 3.1, our focus is on those observables that will be measurable at LHCb without a full-angular analysis. In order to keep the experimental complexity to a minimum, these observables should require information on only one or two of the angles. A_{FB}, which depends only on θ_l, and F_{L}, which depends only on θ_{K^*}, are well known examples. Note that in order to extract a simple expression for F_L, one requires the relations, valid in the limit of massless leptons,

$$S_1^s = 3S_2^s\,, \quad S_1^c = -S_2^c \quad \text{and} \quad \frac{3}{4}(2\,S_1^s + S_1^c) - \frac{1}{4}(2\,S_2^s + S_2^c) = 1.$$

A_{FB} and F_{L} can then be expressed as:

$$\begin{aligned} A_{\mathrm{FB}} =& \frac{4}{3}\left(\int_0^1 - \int_{-1}^0 \right) d\theta_l \frac{d^2(\Gamma+\bar{\Gamma})}{d\mathrm{q}^2\, d\theta_l} \Bigg/ \frac{d(\Gamma+\bar{\Gamma})}{dq^2} \\ F_{\mathrm{L}} =& \frac{1}{9}\left(16 \int_{-1/2}^{1/2} \frac{d(\Gamma+\bar{\Gamma})}{d\mathrm{q}^2\, d\cos\theta_{K^*}} \Bigg/ \frac{d(\Gamma+\bar{\Gamma})}{dq^2} - 11 \right) \end{aligned} \tag{3.11}$$

We can also study the possibility of an early measurement of S_5, which can all be extracted with information about $\cos\theta_{K^*}$ and ϕ. It is possible to express this, as in Eq. (2.51), as

$$S_5 = \frac{4}{3}\left(\int_0^{\pi/2} + \int_{3\pi/2}^{2\pi} - \int_{\pi/2}^{3\pi/2} \right) d\phi \left(\int_0^1 - \int_{-1}^0 \right) d\cos\theta_{K^*} \frac{d^3(\Gamma-\bar{\Gamma})}{dq^2\, d\cos\theta_{K^*}\, d\phi} \Bigg/ \frac{d(\Gamma+\bar{\Gamma})}{dq^2}\,. \tag{3.12}$$

A comprehensive study of the effects of the Wilson coefficients on the above observables, and vice–versa can be found in Tabs. 2.8 and 2.9. We note that S_3, A_7, and A_9 can

Observable	Wilson Coefficients
$A_{\rm FB}$	$C_7^{\rm eff}$, $C_9^{\rm eff}$
$F_{\rm L}$	$C_7^{\rm eff}$, $C_7^{\prime\,\rm eff}$,$C_8^{\rm eff}$,$C_9^{\prime\,\rm eff}$, $C_{10}^{\rm eff}$, $C_{10}^{\prime\,\rm eff}$
S_5	$C_7^{\rm eff}$, $C_7^{\prime\,\rm eff}$, $C_9^{\rm eff}$, $C_{10}^{\prime\,\rm eff}$

Table 3.5: Relevant observables and the Wilson coefficients they most strongly depend on [52].

also be extracted by the counting of signal events over one or two angles. S_3 is related to the well known and theoretically clean observable $A_T^{(2)}$ [106]; to be precise, S_3 equals $\frac{1}{2}(1-F_{\rm L})A_T^{(2)}$ in the massless lepton limit. While significant enhancement of $A_T^{(2)}$ is possible in the presence of non–SM $C_7^{\prime\,\rm eff}$ [108], the $\frac{1}{2}(1-F_{\rm L})$ prefactor means that the enhancement is less pronounced in S_3 [121]. The smallness of S_3 means that the experimental sensitivity to $\langle S_3\rangle_{1-6\,{\rm GeV}^2}$ will be limited in the first few years of LHCb data taking. The study of S_3 is thus left for other works [89]. Enhancements to A_7 and A_9 in the presence NP phases can however be sizable [88] and could in principle lead to reasonable experimental resolutions, particularly for $\langle A_9\rangle_{1-6\,{\rm GeV}^2}$. However, these measurements will still be experimentally challenging in the first few years. For these reasons we choose to focus on $A_{\rm FB}$, $F_{\rm L}$ and S_5 for early study at LHCb.

As stated earlier, NP enters the calculation through contributions to the Wilson coefficients, and constraints on these contributions are described in the following subsection. It is well known that for certain values of q^2, the observables $A_{\rm FB}$ and S_5 vanish. We refer to these values of q^2 as the zero-crossing points, $q_0^2(A_{\rm FB})$ and $q_0^2(S_5)$. They are particularly sensitive to NP, and can be used to further constrain the values of the Wilson Coefficients. At leading order, in the large recoil limit, and for real values of the Wilson coefficients, it is possible to obtain simple expressions for $q_0^2(A_{\rm FB})$ [47] and $q_0^2(S_5)$,

$$q_0^2(A_{\rm FB}) = -2m_B\, m_b \frac{C_7^{\rm eff}}{C_9^{\rm eff}} \qquad \text{and} \qquad q_0^2(S_5) = \frac{-m_B\, m_b (C_7^{\rm eff} + C_7^{\prime\,\rm eff})}{C_9^{\rm eff} + \hat{m}_b (C_7^{\rm eff} + C_7^{\prime\,\rm eff})}\,. \tag{3.13}$$

Here we make use of the soft form factors, following Refs. [47; 78]. We can define the slope of $A_{\rm FB}$ and S_5 at the zero-crossing point,

$$G_0(\mathcal{O}) = \left.\frac{d\mathcal{O}}{dq^2}\right|_{q_0^2(\mathcal{O})}, \tag{3.14}$$

where $\mathcal{O}$ is the observable $A_{\rm FB}$ or S_5.

3.3.2 Overview of Specific Models and Effects on Wilson Coefficients

We have investigated three sets of Wilson coefficients in a variety of NP scenarios. The observables for $\overline{B}_d \to \overline{K}^{*0}\mu^+\mu^-$ are most sensitive to the Wilson coefficients $C_7^{\rm eff}$, $C_9^{\rm eff}$, $C_{10}^{\rm eff}$, C_S, C_P and their primed equivalents, so we concentrate on the NP contributions to these.

- **Universal Extra Dimensions** (UED): This model proposes that all SM particles can propagate freely in additional dimensions. Following the model described in Ref. [129] with a single extra dimension, orbifold compactification at the scale R results in a tower of Kaluza-Klein excitations for each SM particle. The simplicity of this model, requiring only a single extra parameter R, is appealing. Here, in order to create maximal effects while respecting existing experimental constraints, we use $1/R = 400\,\mathrm{GeV/c^2}$. UED does not result in any additional operators or CP/flavour violation beyond Minimal Flavour Violation (MFV), so C_S =0 and C_P =0, primed operators are suppressed and there are no additional complex phases contributing to the Wilson coefficients. There can however be large deviations from the SM in $C_7^{\rm eff}$, $C_9^{\rm eff}$ and $C_{10}^{\rm eff}$, as shown in Ref. [130]. This is similar to the case of the constrained MFV models discussed in Ref. [52].
- **Flavour Blind MSSM** (FBMSSM): Here the MFV version of the Minimal Supersymmetric Standard Model (MSSM) is modified by some flavour conserving but CP violating phases in the soft SUSY breaking trilinear couplings [51]. The Wilson coefficients we use correspond to those calculated in scenario FBMSSM II defined in Tab. 11 in Ref. [52]. The additional CP violation contributes substantial complex phases to $C_7^{\rm eff}$, however there is no flavour structure beyond the SM, so primed operators are suppressed as in the SM. As in all supersymmetry (SUSY) models, scalar and pseudoscalar operators arise due to the additional Higgs doublet.
- **General MSSM** (GMSSM): Minimal flavour violation is not imposed, and generic flavour- and CP-violating soft SUSY-breaking terms are allowed [131]. The Wilson coefficients we use are in close correspondence to the scenario GMSSM IV in Ref. [52], corresponding to large NP contributions to both $C_7^{\rm eff}$ and $C_7'^{\rm eff}$ which are allowed by existing experimental bounds [132]. This scenario is not possible in any of the other models mentioned.

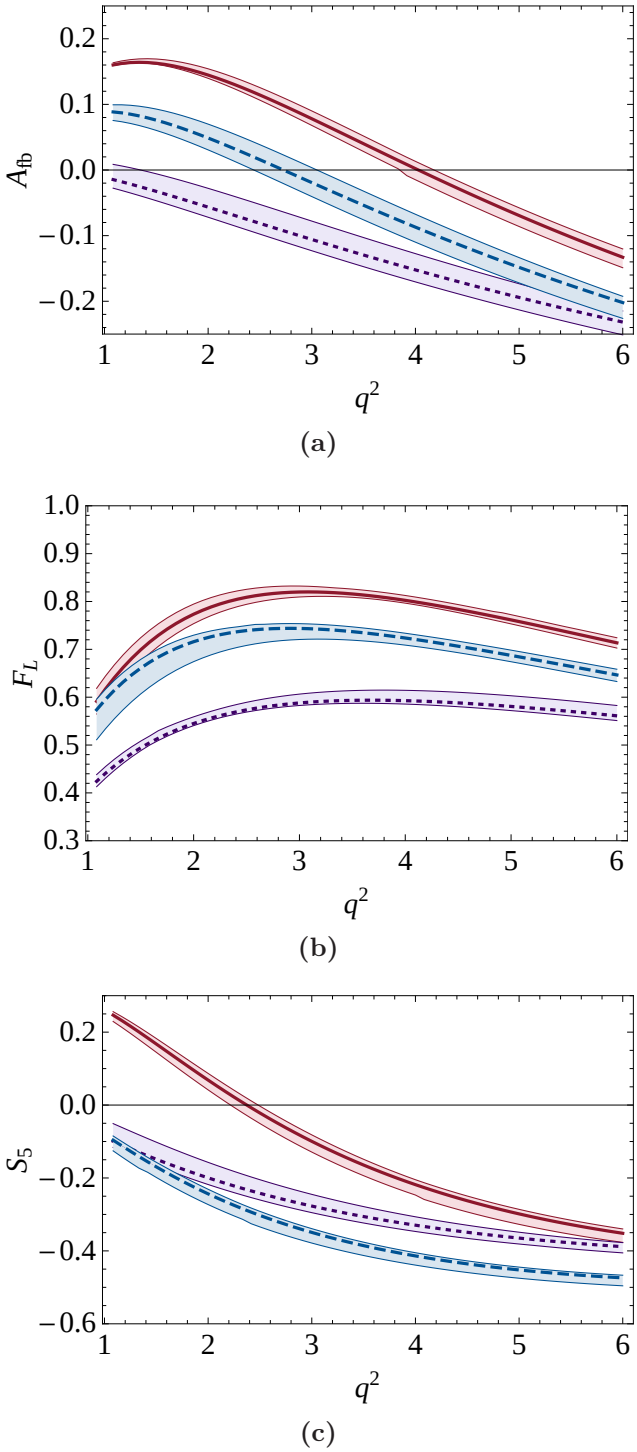

Figure 3.1: Theoretical predictions for (a) $A_{\rm FB}$, (b) F_L and (c) S_5. The red (continuous) line is the SM, the blue (dashed) line is the GMSSM, and the purple (dotted) line is the FBMSSM.

3.3.3 Theory Predictions

The Wilson coefficients in the above scenarios are given explicitly in Tab. 3.2. The central values for the distributions of $A_{\rm FB}$, $F_{\rm L}$, and S_5 are shown in Fig. 3.1 for the SM, the GMSSM, and FBMSSM, along with estimates of the theoretical uncertainties. The agreement with previous results is good. The predominant sources of the uncertainties are the form factors, hadronic parameters, and quark masses, which are determined as discussed in Sec. 3.2. We also include the uncertainty arising from varying the factorisation scale, μ, in the range $\mu \in [\mu/2, 2\mu]$. Note that these uncertainties improve on the previous model. Quantitatively, the position of the zero for A_{FB} found in Ref. [86] is $s_0 = 2.88^{+0.44}_{-0.28}\,\text{GeV}^2$, as opposed to our NLO result $s_0 = 4.03 \pm 0.12\,\text{GeV}^2$; the reduction in the uncertainty is evident[†]. The three distributions all show significant variation for the models considered here, as do the position or absence of the zero-crossing points in $A_{\rm FB}$ and S_5 in the range $q^2 \in [1, 6]\,\text{GeV}^2$.

3.3.4 Constraints

Experimental results can be used to constrain NP contributions, $C_i^{\rm NP}$, to the Wilson coefficients, C_i, where $C_i = C_i^{\rm SM} + C_i^{\rm NP}$. We can then determine possible model-independent effects of NP on $\overline{B}_d \to \overline{K}^{*0}\mu^+\mu^-$. The most important constraints on the Wilson coefficients are from the following measurements:

- **Branching Ratio for $B_s \to \mu^+\mu^-$**: This is used to constrain the possible NP contribution to the scalar and pseudoscalar operators. To calculate the branching ratio we use the standard result as in Eq. (2.61),

$$\mathcal{B}(B_s \to \mu^+\mu^-) = \tau_{B_s} f_{B_s}^2 m_{B_s} \frac{\alpha_{EM}^2 G_F^2}{16\pi^3} |V_{tb}V_{ts}^*|^2 \sqrt{1 - \frac{4m_\mu^2}{m_{B_s}^2}} (|S|^2 \left(1 - \frac{4m_\mu^2}{m_{B_s}^2}\right) + |P|^2), \tag{3.15}$$

  with the definitions

$$S = \frac{m_{B_s}^2}{2}(C_S - C_S') \qquad \text{and} \qquad P = \frac{m_{B_s}^2}{2}(C_P - C_P') + m_\mu (C_{10}^{\rm eff} - C_{10}^{\prime\,\rm eff}). \tag{3.16}$$

[†]The old model, based on Ref. [86], was updated in preparation for Ref. [133], however this only partially included the NLO QCDF corrections. The resulting SM predictions are closer to our results, but the model still leads to strange effects due to e.g. the scale handling at $q^2 \approx 5.5$. Specifically for $A_{\rm FB}$, $s_0 = 4.1\,\text{GeV}^2$, but the theoretical uncertainty on this number is not obvious due to the partial inclusion of NLO corrections.

In agreement with existing results, we find the SM prediction $\mathrm{BR}(B_s \to \mu^+\mu^-) = (3.70 \pm 0.31) \cdot 10^{-9}$ to be well below the current experimental upper bound $3.6 \cdot 10^{-8}$ [116; 134].

- **Branching Ratio for $B \to X_s l^+ l^-$**: We compare NP predictions for $\mathcal{B}(B \to X_s l^+ l^-)_{1-6\,\mathrm{GeV}^2}$ to the mean experimental value $(1.60 \pm 0.51) \cdot 10^{-6}$, as adopted in Ref. [88] combining the results of *BABAR*, $(1.8 \pm 0.7 \pm 0.5) \cdot 10^{-6}$ [135], and Belle, $(1.49^{+0.41}_{-0.32} \pm 0.50) \cdot 10^{-6}$ [136]. This helps to constrain the NP contribution to $C_{7,9,10}^{(\prime)\,\mathrm{eff}}$ as well as $C_{S,P}^{(\prime)}$. As an inclusive mode, the calculation for the region $q^2 \in [1, 6]\,\mathrm{GeV}^2$ of the branching ratio is theoretically clean. We use the expression for the differential decay distribution in Ref. [85], but also include the NLO corrections computed in Ref. [137], and the contribution of the primed operators as in Ref. [138]. Using our parameters we predict $\mathcal{B}(B \to X_s l^+ l^-) = (1.96 \pm 0.11) \cdot 10^{-6}$, for the SM.
- **Branching Ratio for $B \to X_s \gamma$**: We use the recent theoretical result of Ref. [139], $(3.28 \pm 0.25) \cdot 10^{-4}$, and include NP effects as in Ref. [108]. This can be compared to the current experimental average for $\mathrm{E}_\gamma > 1.6\,\mathrm{GeV}$, $\mathcal{B}(B \to X_s\gamma) = (3.52 \pm 0.23 \pm 0.09) \cdot 10^{-4}$, as calculated by the Heavy Flavor Averaging Group [140].
- **Time dependent CP Asymmetry $S(B \to K^*\gamma)$**: This constraint is sensitive to the photon polarisation, and hence to $C_7^{\prime\,\mathrm{eff}}$. Our result $S(B \to K^*\gamma) = (-0.26 \pm 0.05) \cdot 10^{-1}$ agrees with that of Ref. [88] within uncertainties. This should be compared to $S(B \to K^*\gamma) = (-1.6 \pm 2.2) \cdot 10^{-1}$ from experiment [140].
- **Integrated Forward-Backward Asymmetry $\langle A_{\mathrm{FB}} \rangle_{1-6\,\mathrm{GeV}^2}$ for $\overline{B}_d \to \overline{K}^{*0}\mu^+\mu^-$** : We use existing $\overline{B}_d \to \overline{K}^{*0}\mu^+\mu^-$ measurements as constraints. Recently Belle has made a measurement of the Forward-Backward Asymmetry, and find the integrated A_{FB} in the region $1 - 6\,\mathrm{GeV}^2$ to be -0.26 ± 0.29, [82]. This is to be compared to our SM prediction of 0.04 ± 0.03, which is in agreement with the recent result in Ref. [141]. This observable constrains the Wilson coefficients as seen in Tab. 3.5.
- **Integrated Longitudinal Polarisation Fraction $\langle F_{\mathrm{L}} \rangle_{1-6\,\mathrm{GeV}^2}$ for $\overline{B}_d \to \overline{K}^{*0}\mu^+\mu^-$** : Belle has also recently measured the Longitudinal Polarisation Fraction to be 0.67 ± 0.24, [82]. This should be compared to our SM prediction 0.76 ± 0.08, also in agreement with Ref. [141]. Again this constraint affects Wilson coefficients as seen in Tab. 3.5.

Observable	Experiment	SM Theory
$\mathcal{B}(B_s \to \mu^+\mu^-)$	$3.6 \cdot 10^{-8}$ [116; 134]	$(3.70 \pm 0.31) \cdot 10^{-9}$
$\mathcal{B}(B \to X_s l^+ l^-)_{1-6\,\mathrm{GeV}^2}$	$(1.60 \pm 0.51) \cdot 10^{-6}$ [88]	$(1.97 \pm 0.11) \cdot 10^{-6}$
$\mathcal{B}(B \to X_s \gamma)$	$(3.52 \pm 0.23 \pm 0.09) \cdot 10^{-9}$ [140]	$(3.28 \pm 0.25) \cdot 10^{-4}$
$S(B \to K^*\gamma)$	$(-1.6 \pm 2.2) \cdot 10^{-1}$ [140]	$(-0.28 \pm 0.05) \cdot 10^{-1}$
$\langle A_{\mathrm{FB}} \rangle_{1-6\,\mathrm{GeV}^2}$	-0.26 ± 0.29 [82]	0.04 ± 0.03
$\langle F_L \rangle_{1-6\,\mathrm{GeV}^2}$	0.67 ± 0.24 [82]	0.76 ± 0.08

Table 3.6: Experimental measurements used as constraints, along with theoretical predictions in the SM.

We are interested in assessing the impact of these constraints on the underlying Wilson coefficients in as general a way as possible. Therefore, in order to allow $(C_S - C'_S)$, $(C_P - C'_P)$ and the NP components of $C_{7-10}^{(\prime)\,\mathrm{eff}}$ to vary simultaneously, both in magnitude and phase, we have performed a semi–random walk through parameter space. To our knowledge this has not been done in previous studies. At each randomly chosen point in parameter space, predictions are made for the six observables listed above. The point is then either accepted or rejected using a modified χ^2 metric which treats experimental uncertainties as being normally distributed, but theoretical uncertainties as having uniform probability within the specified range. Following traditional minimisation techniques, the random walk is guided by the value of this modified χ^2 so that regions with lower values may be identified. Using this method, a sample of $\sim 2.5 \cdot 10^5$ independent sets of Wilson coefficients was produced. Each set results in predictions for the observables listed above with better than 2σ agreement with current measurements. It was found that the agreement of existing measurements with the SM is excellent, with a χ^2 per degree of freedom of 0.35.

Fig. 3.2 shows the range of values found for the phase and magnitude of the NP contribution to C_7^{eff} and $C_7^{\prime\,\mathrm{eff}}$ during the parameter space exploration. The colour index shows the mean value of the probability that a point is compatible with current experimental results. Areas with probability greater than 1σ are shaded red, while those with less than 1σ are shaded blue. The outline of the 1σ contour can clearly be seen. This can be compared to similar plot in Ref. [88] of the constraints on NP contributions to C_7^{eff} and $C_7^{\prime\,\mathrm{eff}}$. However, this plot differs from ours as the Wilson coefficients were assumed to be real, and all other Wilson coefficients were assumed to be SM-like. Similar figures are shown for the other Wilson coefficients in Fig. 3.3 and 3.4. The allowed regions of

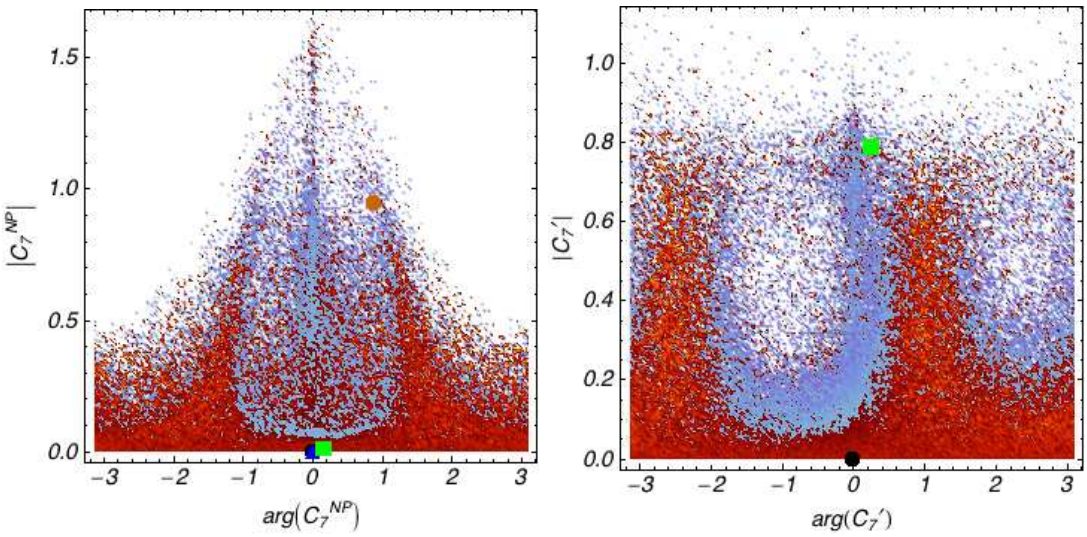

Figure 3.2: Allowed parameter space for the NP contribution to C_7^{eff} and $C_7'^{\text{eff}}$, as described in Sec. 3.3.4. Points with a compatibility with data of 68% or better are drawn with a red (dark grey) colour palette, while those with less than this are drawn with a blue (light grey) palette. The SM point is shown in black at the origin, while the UED point is a blue triangle, the FBMSSM is a green square and the GMSSM is an orange disk.

parameter space are still large. The plot showing the phase and magnitude of the NP contribution to C_{10}^{eff} can also be compared to a similar one in Ref. [88], but this again differs from ours as all other Wilson coefficients were assumed to be SM-like. Note that the latter plot also includes the constraint from A_{FB} at low recoil, which we do not include as we feel that NLO effects are not under control in this region. Nevertheless, the plots show a clear resemblance.

The ensemble of constrained NP models can also be used to explore the likely values of the A_{FB} and S_5 zero–crossing points. It was found that 8% of parameter space points considered had no A_{FB} zero in the range $q^2 \in [0.5, 15]\,\text{GeV}^2$, and 12% for S_5. While it should be noted that theoretical uncertainties are not well controlled over this q^2 range, the majority of points within the 1σ contour lie within the theoretically clean region, $q^2 \in [1, 6]\,\text{GeV}^2$. The distribution can be seen in Fig. 3.5a. Fig. 3.5b shows the distribution of the A_{FB} and S_5 gradients at their zero–crossing points. We find for the majority of points, $G_0(S_5)$ is greater than $G_0(A_{\text{FB}})$. This will have an impact of the $q_0^2(S_5)$ experimental analysis discussed in the next section.

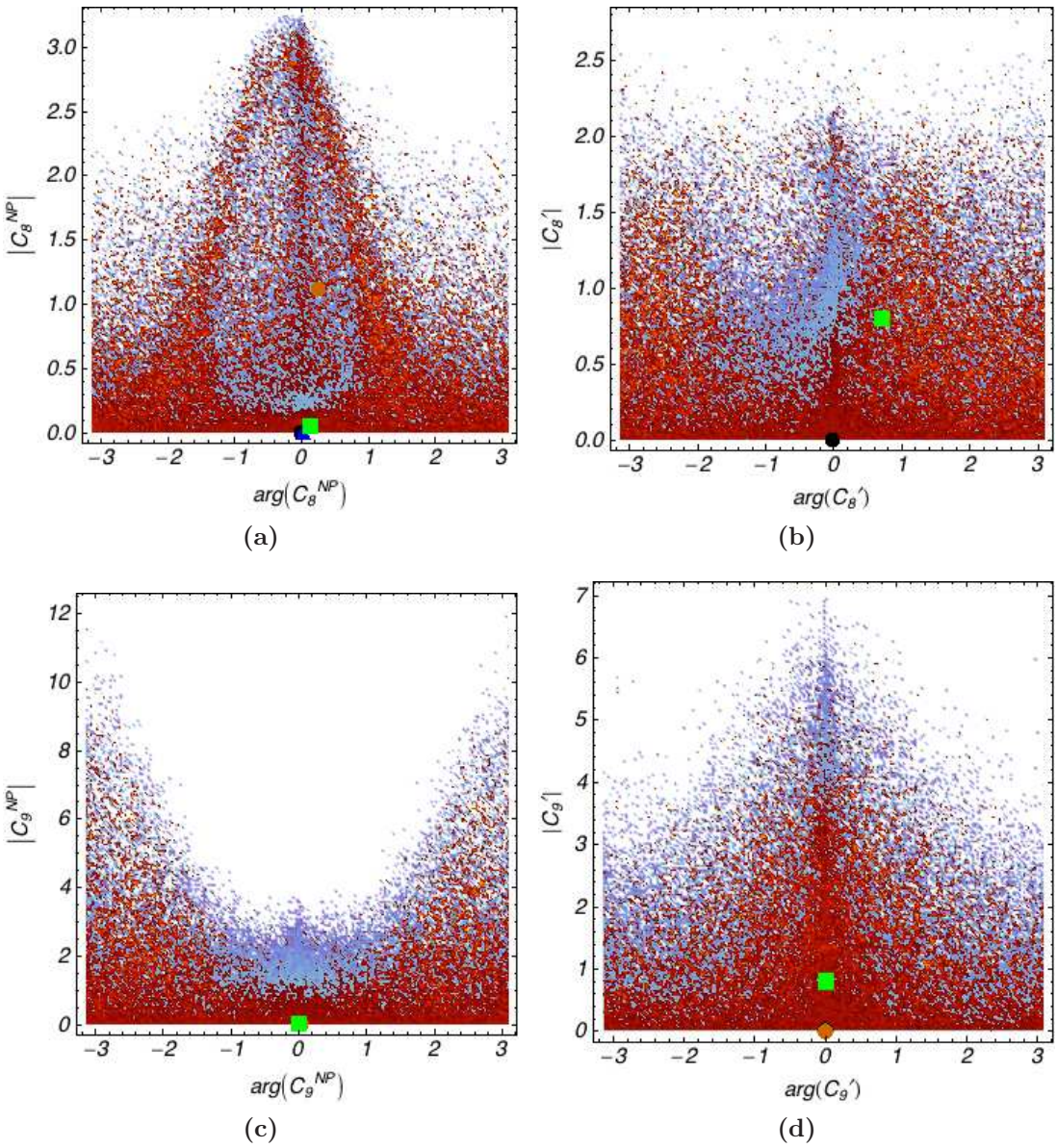

Figure 3.3: Allowed parameter space for the Wilson coefficients $C_{8-9}^{(\prime)\,\mathrm{eff}}$ after applying relevant $b \to s$ experimental constraints. The colour coding is the same as in Fig. 3.2.

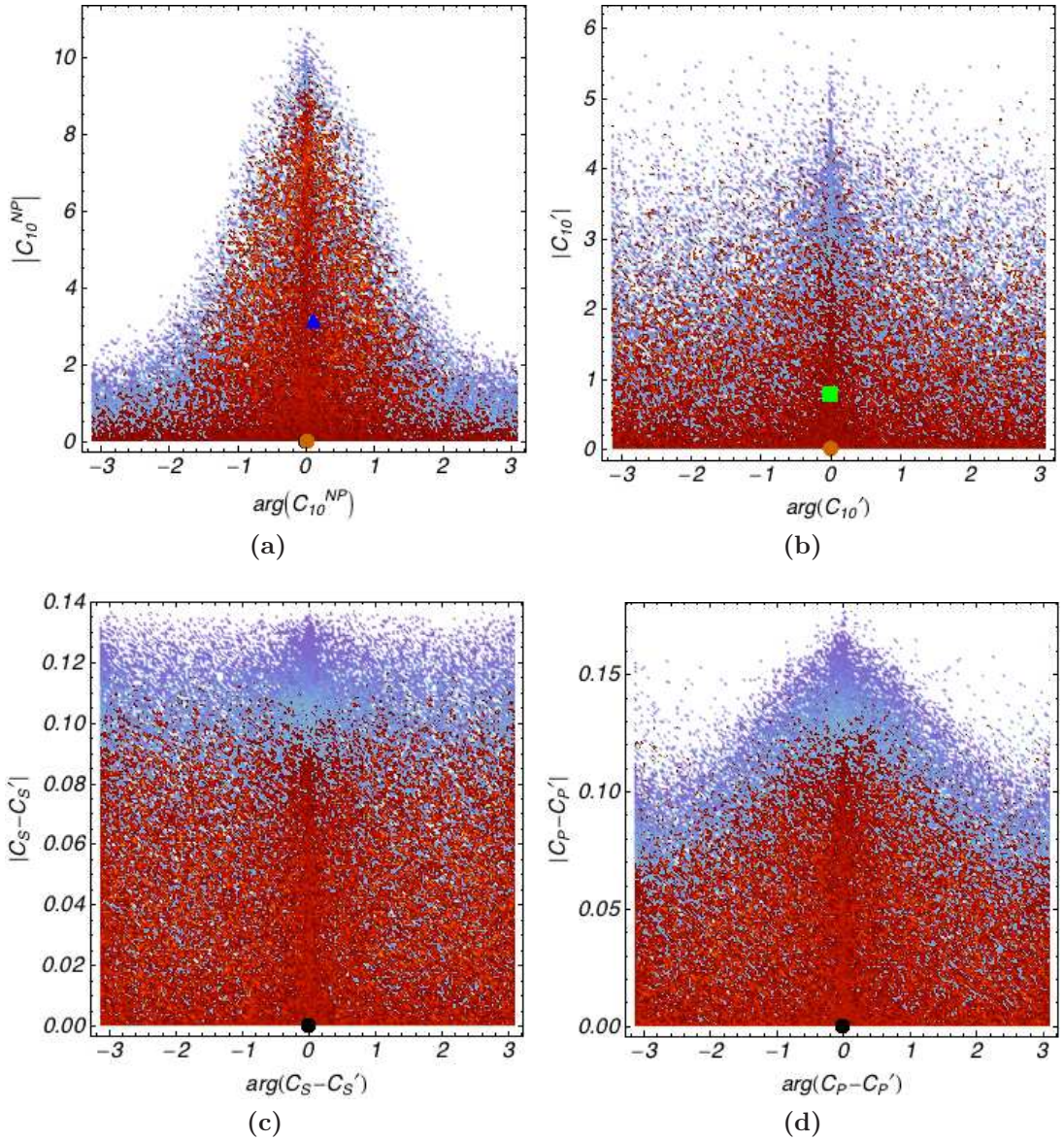

Figure 3.4: Allowed parameter space for the Wilson coefficients $C_{10}^{(\prime)\,\mathrm{eff}}$ and $(C_{S,P} - C'_{S,P})$ after applying relevant $b \to s$ experimental constraints. The colour coding is the same as in Fig. 3.2.

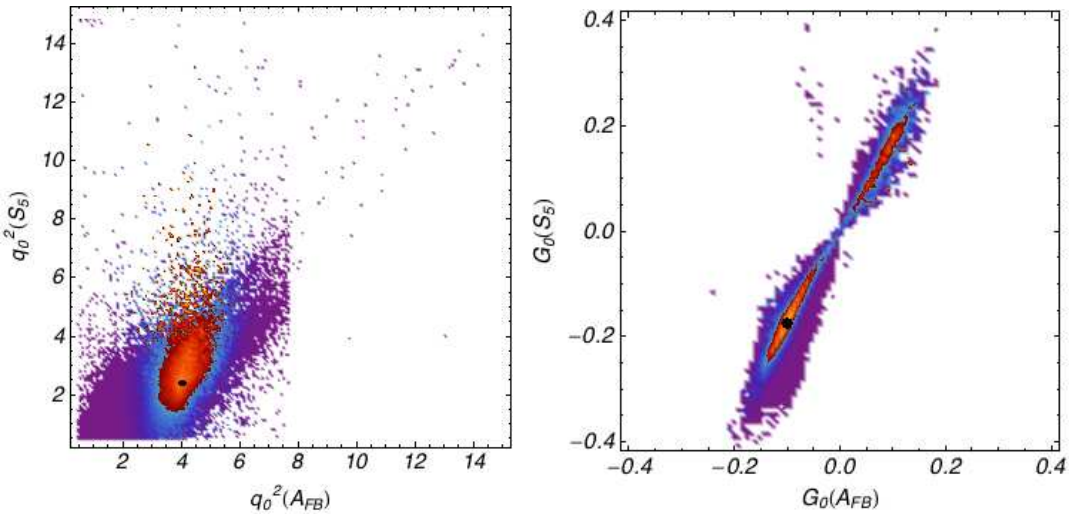

(a) **(b)**

Figure 3.5: Fig. (a) shows allowed values of the $A_{\rm FB}$ and S_5 zero–crossing points in the range $q^2 \in [0.5, 15]\,{\rm GeV}^2$. The SM point and its uncertainty is shown as a black ellipse. Fig. (b) shows the gradient of the $A_{\rm FB}$ and S_5 at the zero–point. In each case the colour index has the same meaning as in Fig. 3.2.

Observable	$2\,{\rm fb}^{-1}$	$1\,{\rm fb}^{-1}$	$0.5\,{\rm fb}^{-1}$
$q_0^2(A_{\rm FB})$	$^{+0.56}_{-0.94}$	$^{+1.27}_{-0.97}$	–
$q_0^2(S_5)$	$^{+0.27}_{-0.25}$	$^{+0.53}_{-0.40}$	–
$\langle A_{\rm FB}\rangle_{1-6\,{\rm GeV}^2}$	$^{+0.03}_{-0.04}$	$^{+0.05}_{-0.03}$	$^{+0.08}_{-0.06}$
$\langle F_{\rm L}\rangle_{1-6\,{\rm GeV}^2}$	$^{+0.02}_{-0.02}$	$^{+0.04}_{-0.03}$	$^{+0.04}_{-0.06}$
$\langle S_5\rangle_{1-6\,{\rm GeV}^2}$	$^{+0.07}_{-0.08}$	$^{+0.09}_{-0.11}$	$^{+0.16}_{-0.15}$

Table 3.7: Estimated 1σ LHCb sensitivities for $2\,{\rm fb}^{-1}$, $1\,{\rm fb}^{-1}$ and $0.5\,{\rm fb}^{-1}$ of integrated luminosity, assuming the SM (taken from Ref. [142]).

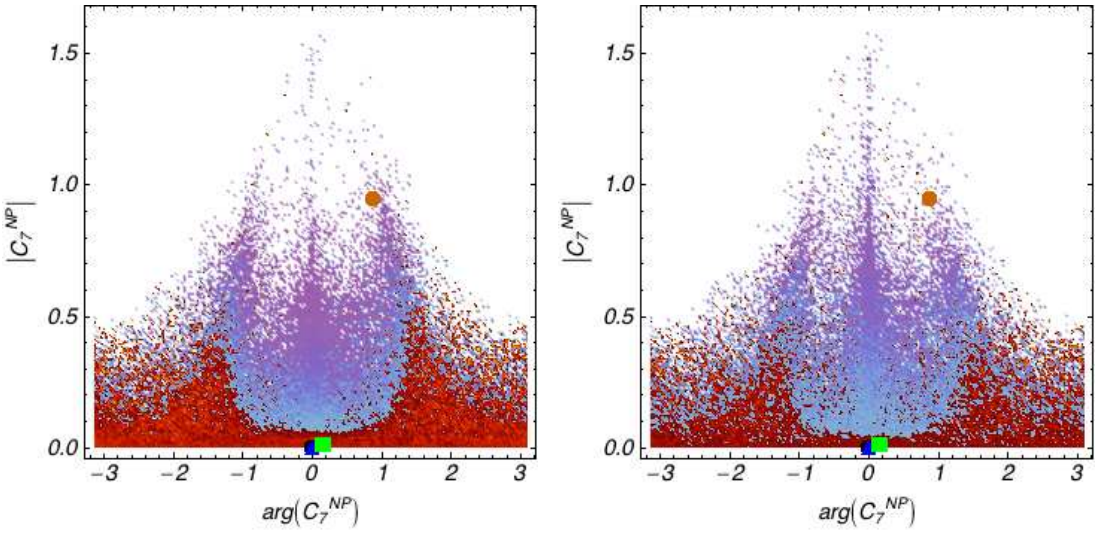

Figure 3.6: The relative impact of different proposed LHCb measurements after $2\,\text{fb}^{-1}$ of integrated luminosity, assuming the SM, on the NP component of C_7^{eff}. Here Fig. 3.6a shows the impact of $\langle A_{\text{FB}}\rangle_{1-6\,\text{GeV}^2}$ and $q_0^2(A_{\text{FB}})$ and Fig. 3.6b $\langle F_{\text{L}}\rangle_{1-6\,\text{GeV}^2}$ and Fig. 3.7 $\langle S_5\rangle_{1-6\,\text{GeV}^2}$ and $q_0^2(S_5)$. In each case the colour index has the same meaning as in Fig. 3.2.

3.4 Experimental Impact

A number of observables have been introduced in Sec. 3.3.1 that can be extracted as a function of q^2 by counting signal events in specific angular bins using Eqs. (3.11)-(3.12). LHCb [15] is expected to collect $\sim 6.2 \cdot 10^3$ signal events per $2\,\text{fb}^{-1}$ of integrated luminosity, with a signal to background ratio of ~ 4 [143]. With relatively small data sets it should be possible to extract the q^2 integrated values of these observables. These measurements offer an early chance to discover NP in $b \to s$ transitions. For larger data sets it will be possible to map out the q^2 distribution too, allowing for additional NP discrimination. Studies of these two approaches can be found in Refs. [62; 120] for the observable A_{FB}.

The relative impact of the different observables, whose sensitivities are shown in Tab. 3.7, can be assessed by revisiting the parameter space exploration performed in Sec. 3.3.4. We are interested in how including these new measurements would affect the current constraints on parameter space. It is assumed that LHCb will make $2\,\text{fb}^{-1}$ measurements of the observables $\langle A_{\text{FB}}\rangle_{1-6\,\text{GeV}^2}$, $\langle S_5\rangle_{1-6\,\text{GeV}^2}$, $\langle F_{\text{L}}\rangle_{1-6\,\text{GeV}^2}$, $q_0^2(A_{\text{FB}})$, and $q_0^2(S_5)$ and that the resultant experimental uncertainties are symmetrised versions of

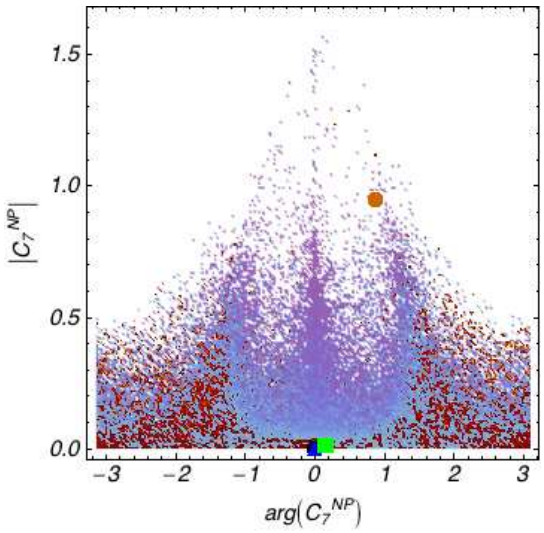

Figure 3.7: The relative impact of the LHCb measurement of Fig. 3.7 $\langle S_5 \rangle_{1-6\,\mathrm{GeV}^2}$ and $q_0^2(S_5)$ after $2\,\mathrm{fb}^{-1}$ of integrated luminosity, assuming the SM, on the NP component of C_7^{eff}. In each case the colour index has the same meaning as in Fig. 3.2.

those given in Tab. 3.7. In addition, we assume that the extracted value of these observables is not affected by NP, and are as given in Tab. 3.6. The total χ^2 for each point in parameter space is then updated to reflect these hypothetical SM measurements. Where individual measurements are superseded by LHCb measurements, they are replaced with no attempt at combination. However, other current constraints such as $\mathcal{B}(B \to X_s\gamma)$ are included as before. In this way the constraining power of each analysis can be compared.

Figs. 3.6, 3.7 show the relative impact of these measurements on the NP component of C_7^{eff}. In Fig. 3.6a, SM values of $\langle A_{\mathrm{FB}} \rangle_{1-6\,\mathrm{GeV}^2}$ and $q_0^2(A_{\mathrm{FB}})$ are imposed with the estimated $2\,\mathrm{fb}^{-1}$ experimental sensitivities taken from Tab. 3.7. Fig. 3.6b shows the impact of $\langle F_{\mathrm{L}} \rangle_{1-6\,\mathrm{GeV}^2}$ and Fig. 3.7 of both $\langle S_5 \rangle_{1-6\,\mathrm{GeV}^2}$ and $q_0^2(S_5)$ for the same LHCb integrated luminosity. These should be compared with the currently allowed C_7^{eff} parameter space shown in Fig. 3.2. The small statistical uncertainty found in Ref. [142] for $q_0^2(S_5)$ allows for the most stringent constraints on parameter space to be made. This emphasises the importance of an early measurement of S_5.

Fig. 3.8 shows the combined effect of the proposed measurements, again assuming the SM and the estimated sensitivities from Tab. 3.7 for the Wilson coefficients C_7^{eff}, $C_7'^{\mathrm{eff}}$, C_9^{eff} and $C_{10}'^{\mathrm{eff}}$. The amount of parameter space left after these measurements would be significantly reduced, with most NP contributions excluded at the 1σ level unless there are large NP phases present. This again illustrates the importance of CP observables as described in [88].

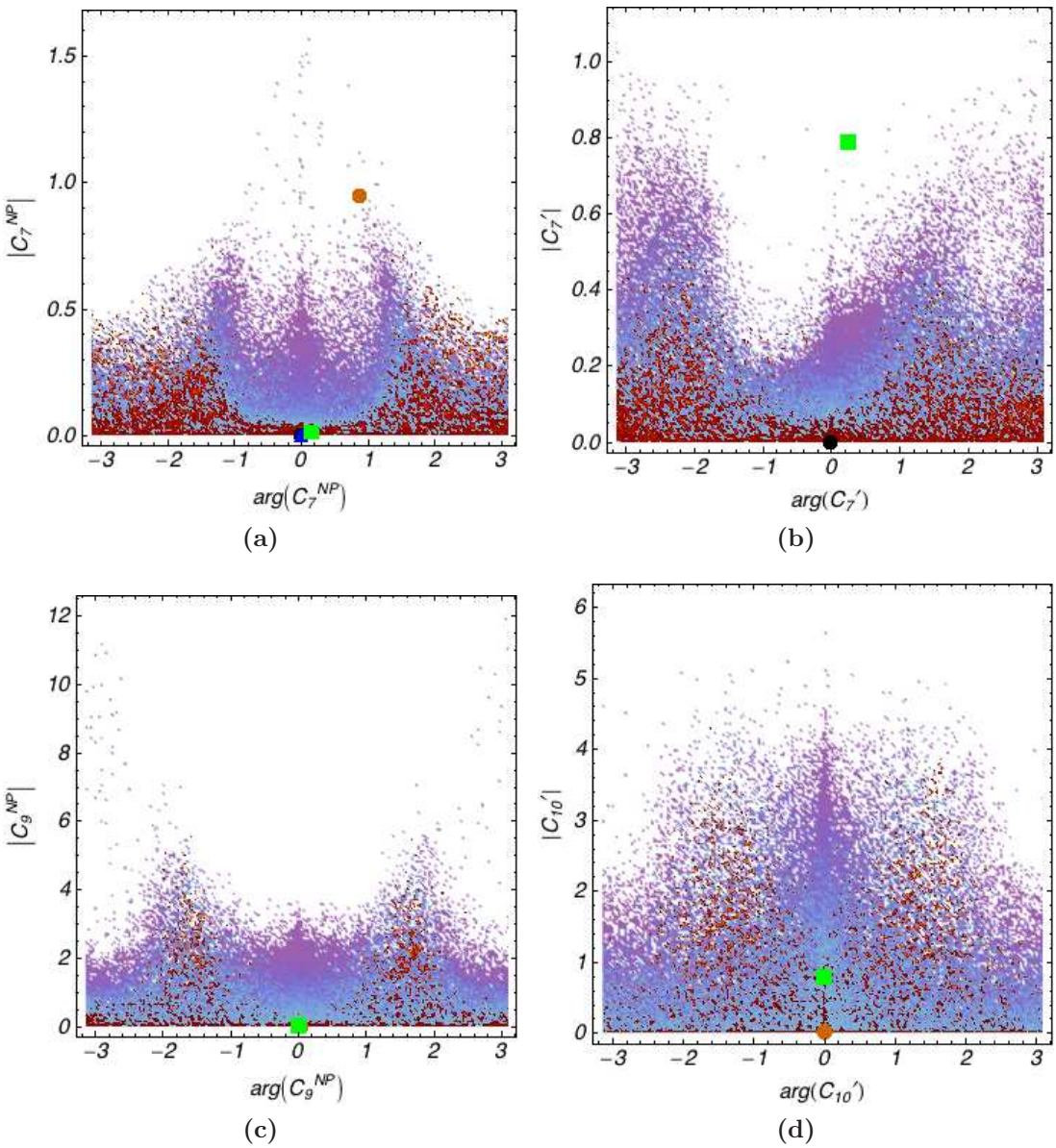

Figure 3.8: Allowed parameter space for the Wilson coefficients C_7^{eff}, $C_7'^{\text{eff}}$, C_9^{eff} and $C_{10}'^{\text{eff}}$ after $2\,\text{fb}^{-1}$ measurements at LHCb of $\langle F_{\text{L}}\rangle_{1-6\,\text{GeV}^2}$, $\langle A_{\text{FB}}\rangle_{1-6\,\text{GeV}^2}$, $q_0^2(A_{\text{FB}})$, $\langle S_5\rangle_{1-6\,\text{GeV}^2}$ and $q_0^2(S_5)$, assuming the SM. The colour coding is the same as in Fig. 3.2.

3.5 Summary

The NP reach of LHCb in the first few years of data taking with the rare decay $B_d \to K^{*0}\mu^+\mu^-$ has been investigated. A new next–to–leading order model which includes QCD factorisation corrections and full LCSR form factors was presented. We have identified observables which are promising for relatively early measurements, as they can be measured with relatively little angular information. We have also provided a simple expression for the position of its zero-crossing point, $q_0^2(S_5)$, at leading order, in terms of $C_7^{\rm eff}$, $C_7^{\prime\,\rm eff}$ and $C_9^{\rm eff}$. In Ref. [142], the sensitivity of LHCb to these observables, in particular S_5 and its zero–crossing was estimated. Based on this work, using a combination of $\langle F_{\rm L}\rangle_{1-6\,{\rm GeV}^2}$, $\langle A_{\rm FB}\rangle_{1-6\,{\rm GeV}^2}$, $q_0^2(A_{\rm FB})$, $\langle S_5\rangle_{1-6\,{\rm GeV}^2}$, and $q_0^2(S_5)$, $2\,{\rm fb}^{-1}$ of LHCb data is shown to reduce the allowed parameter space significantly. The contribution of S_5 to this is significant and can in part be attributed to the small statistical uncertainty expected on $q_0^2(S_5)$. In addition, if the decay is SM-like, the GMSSM and FBMSSM points considered should be ruled out by LHCb with $2\,{\rm fb}^{-1}$. We conclude by stressing that making measurements of S_5 and its zero–crossing would provide a interesting and complementary measurement to others currently planned. $B_d \to K^{*0}\mu^+\mu^-$ is a promising channel for constraining models or making a NP discovery. We look forward to the first LHC results for this decay.

Chapter 4

Form Factors for Radiative and Semi-Leptonic B Decays

4.1 Introduction

In order to extract information about the underlying short-distance flavour transitions from measurements of exclusive decays, hadronic matrix elements are required as theoretical input. As explained in Sec. 1.5, transition form factors (FFs) describe hadronic matrix elements for B meson decays into light mesons, and these are the subject of this chapter. The two main methods successfully applied to the calculations of the FFs are applicable in complementary regions of the momentum transfer q^2 between the initial and final-state mesons. In Lattice QCD, results are more easily obtainable at high values of q^2, as discretisation effects can only be controlled for small momenta of the final state in units of the Lattice spacing. This is in contrast to the LCSR method, which involves an expansion in inverse powers of the energy of the light daughter meson valid for low values of q^2.

Different FF parameterisations, which can be used to interpolate between the results for small and large momentum transfer, have been suggested in the literature; a good review can be found in Ref. [69]. These include simple pole-type parameterisations, like the Bećirević–Kaidalov (BK) approach [144], or variations like the Ball–Zwicky (BZ) parameterisation [71]. Another representation is derived from the Omnes solution to the dispersion relation, a detailed discussion can be found in Ref. [145; 146]. In this paper, we will make use of the so-called Series Expansion (SE), which was advocated in Refs. [147–151]. Here, one can make use of dispersive bounds to obtain additional

theoretical constraints on the expansion coefficients. A simplified version of the SE (SSE) was recently suggested in Ref. [146]. The aim of this chapter is to use the SE/SSE to describe the transition FFs by fitting to recent Lattice and LCSR results; we also include a detailed analysis of systematic errors. We will focus in particular on the FFs for $B \to V\gamma$, $B \to L\,\ell^+\ell^-$, $B \to L\nu\bar{\nu}$ decays, where $L = P, V$ is a light vector or pseudoscalar meson. We will give numerical results for $B \to \rho, K, K^*$ and $B_s \to \phi$ transitions, which are particularly interesting with respect to NP studies, see e.g. Refs. [48; 52; 56; 78; 89; 152; 153]. Detailed phenomenological studies for FFs relevant to the determination of the CKM elements $|V_{ub}|$ and $|V_{cb}|$ from semi-leptonic B decays can be found in the recent literature [66–68; 146; 154]. For the discussion of dispersive bounds for tensor FFs, we will include the result of a precise calculation of the tensor current two-point correlator at NLO in the QCD coupling constant.

The rest of this chapter is organised as follows. In Sec. 4.2, we provide convenient definitions for the B meson FFs and introduce the idea of the SE/SSE. In Sec. 4.3, we review the derivation of dispersive bounds from current-correlation functions and summarise the results for the profile functions obtained from the operator-product expansion. We apply our formalism to $B \to K$, $B \to \rho$, $B \to K^*$ and $B_s \to \phi$ FFs, by fitting the (truncated) SE/SSE to theoretical "data" from Lattice QCD and/or LCSRs in Sec. 4.4.3. Our conclusions are presented in Sec. 4.5, and some technical details are given in App.B.2.

4.2 Form Factors

In this section, we will first provide the definitions for the various $B \to L$ meson FFs in question, where L is a generic light meson, fix the notation to be used in the subsequent discussion, and introduce the SE/SSE.

4.2.1 Definition of Form Factors and Helicity Amplitudes

The form factors defined in Eqs. (1.25-1.27) constitute the standard definitions for the FFs widely used in the literature. However, here we find it convenient to work with certain linear combinations of these, dubbed helicity amplitudes in Ref. [149]. This is primarily in order to diagonalise the unitarity relations, which shall be used to derive the dispersive bounds on certain FF parameterisations. The helicity amplitudes also

have definite spin-parity quantum numbers, and this is useful when considering the contribution of excited states. In addition, they can easily be related to the universal soft FFs, appearing in the heavy-quark and/or large-energy limit (see App. B of Ref. [155]), and lead to simple expressions for the observables in $B \to L\,\ell^+\ell^-$ decays in the naive factorisation approximation. In order to simplify imposing the dispersive bounds, we also choose a particular normalisation convention and define new $B \to P$ vector FFs, for the decay to a pseudoscalar meson P, via

$$\mathcal{A}_{V,\sigma}(q^2) = \sqrt{\frac{q^2}{\lambda}}\,\varepsilon_\sigma^{*\mu}(q)\,\langle P(k)|\bar{q}\,\gamma_\mu\,b|\bar{B}(p)\rangle\,. \tag{4.1}$$

Here

$$\lambda = \big((m_B - m_P)^2 - q^2\big)\,\big((m_B + m_P)^2 - q^2\big) \equiv (t_- - q^2)(t_+ - q^2) \tag{4.2}$$

is a standard kinematic function, and $\varepsilon_\sigma^{*\mu}(q)$ are transverse ($\sigma = \pm$), longitudinal ($\sigma = 0$) or time-like ($\sigma = t$) polarisation vectors as defined in the App. B of Ref. [155]. This implies

$$\mathcal{A}_{V,0}(q^2) = f_+(q^2)\,, \qquad \mathcal{A}_{V,t}(q^2) = \frac{m_B^2 - m_P^2}{\sqrt{\lambda}}\,f_0(q^2)\,, \tag{4.3}$$

while the transverse projections vanish. Similarly, for the $B \to P$ tensor FF, we define

$$\mathcal{A}_{T,\sigma}(q^2) = (-i)\sqrt{\frac{1}{\lambda}}\,\varepsilon_\sigma^{*\mu}(q)\,\langle P(k)|\bar{q}\,\sigma_{\mu\nu}q^\nu\,b|\bar{B}(p)\rangle\,. \tag{4.4}$$

Here, the only non-zero FF is*

$$\mathcal{A}_{T,0}(q^2) = \frac{\sqrt{q^2}}{m_B + m_P}\,f_T(q^2)\,. \tag{4.5}$$

A similar analysis for the $B \to V$ vector and axial-vector FFs, for the decay to a vector meson V, yields

$$\mathcal{B}_{V,\sigma}(q^2) = \sqrt{\frac{q^2}{\lambda}}\sum_{\varepsilon(k)}\varepsilon_\sigma^{*\mu}(q)\,\langle V(k,\varepsilon(k))|\bar{q}\,\gamma_\mu(1-\gamma^5)\,b|\bar{B}(p)\rangle \tag{4.6}$$

*The newly defined tensor FF $\mathcal{A}_{T,0}(q^2)$ vanishes as $\sqrt{q^2}$, which might look somewhat artificial at first, but in light of the fact that the tensor current does not contribute to physical processes at $q^2 = 0$ we feel the definition is appropriate.

with

$$\mathcal{B}_{V,0}(q^2) = \frac{(m_B + m_V)^2\,(m_B^2 - m_V^2 - q^2)\,A_1(q^2) - \lambda\,A_2(q^2)}{2m_V\sqrt{\lambda}\,(m_B + m_V)}\,,$$

$$\mathcal{B}_{V,t}(q^2) = A_0(q^2)\,,$$

$$\mathcal{B}_{V,1}(q^2) \equiv -\frac{\mathcal{B}_{V,-} - \mathcal{B}_{V,+}}{\sqrt{2}} = \frac{\sqrt{2\,q^2}}{m_B + m_V}\,V(q^2)\,,$$

$$\mathcal{B}_{V,2}(q^2) \equiv -\frac{\mathcal{B}_{V,-} + \mathcal{B}_{V,+}}{\sqrt{2}} = \frac{\sqrt{2\,q^2}\,(m_B + m_V)}{\sqrt{\lambda}}\,A_1(q^2)\,. \tag{4.7}$$

Finally, the $B \to V$ matrix elements with tensor currents are projected on

$$\mathcal{B}_{T,\sigma}(q^2) = \sqrt{\frac{1}{\lambda}}\sum_{\varepsilon(k)} \varepsilon_\sigma^{*\mu}(q)\,\langle V(k,\varepsilon(k))|\bar{q}\,\sigma_{\mu\alpha}q^\alpha(1+\gamma^5)\,b|\bar{B}(p)\rangle \tag{4.8}$$

giving rise to the FFs

$$\mathcal{B}_{T,0}(q^2) = \frac{\sqrt{q^2}\,(m_B^2 + 3m_V^2 - q^2)}{2m_V\sqrt{\lambda}}\,T_2(q^2) - \frac{\sqrt{q^2\,\lambda}}{2m_V\,(m_B^2 - m_V^2)}\,T_3(q^2)$$

$$\mathcal{B}_{T,1}(q^2) = -\frac{\mathcal{B}_{V,-} - \mathcal{B}_{V,+}}{\sqrt{2}} = \sqrt{2}\,T_1(q^2)\,,$$

$$\mathcal{B}_{T,2}(q^2) = -\frac{\mathcal{B}_{V,-} + \mathcal{B}_{V,+}}{\sqrt{2}} = \frac{\sqrt{2}\,(m_B^2 - m_V^2)}{\sqrt{\lambda}}\,T_2(q^2)\,. \tag{4.9}$$

4.2.2 Series Expansion

Resonances

An important factor in determining the shape of the FF is the presence of low-lying resonances with appropriate quantum numbers and mass $m_{\rm R}$ in the range $t_- < m_{\rm R}^2 < t_+$. Common to several parameterisations is the inclusion of the low-lying resonance by means of a simple pole. The various descriptions differ in the modelling of the continuous part. In the following, we use the abbreviation $P(q^2) = 1 - q^2/m_R^2$. If multiple resonances are present in the given region, then $P(q^2)$ should be a product of such poles, and if no resonances are present then $P(q^2) = 1$. A summary of the relevant resonance masses is provided in Tab. 4.1.

Table 4.1: Summary of the masses of low-lying B_d and B_s resonances, using PDG values [30] and/or theoretical estimates from heavy-quark/chiral symmetry [156]. Notice that the mass values for $(0^+, 1^+)$ predicted in Ref. [156] have not been confirmed experimentally, yet. Instead the PDG quotes "effective" resonances $B_J^*(5698)$ and $B_{sJ}^*(5853)$ with undetermined spin/parity.

Transition	J^P	Mass (GeV)	J^P	Mass (GeV)	Ref.
$b \to d$	0^-	5.28	1^-	5.33	[30]
	0^+	5.63	1^+	5.68	[156]
	1^+	5.72	2^+	5.75	[30]
$b \to s$	0^-	5.37	1^-	5.42	[30]
	0^+	5.72	1^+	5.77	[156]
	1^+	5.83	2^+	5.84	[30]

Series Expansion (SE)

The SE parameterisation is derived using dispersive relations [147–149; 151]. The starting point is to extend the FFs defined in the physical range (from $q^2 = 0$ to $t_- = (m_B - m_L)^2$) to analytic functions throughout the complex $t = q^2$ plane, except for along the branch cut at the threshold for production of real BP/BV pairs at $q^2 \geq t_+ = (m_B + m_L)^2$. If low-lying resonances are present below t_+, they are accounted for by the so called Blaschke factor $B(t)$, see below. Complex analysis can then be used to map the cut t–plane onto the unit disc in terms of the coordinate $z(t)$. The variable $z(t)$ is found to be an excellent expansion parameter for the FFs. Furthermore, with an appropriately chosen normalisation function $\phi_f(t)$, one obtains simple dispersive bounds on the coefficients of the SE, see below. We will discuss the calculation of the functions $\phi_f(t)$ as well as the derivation of the dispersive bounds in greater detail in Sec. 4.3. The Series Expansion (SE) then corresponds to the following FF parameterisation,

$$f(t) = \frac{1}{B(t)\,\phi_f(t)} \sum_k \alpha_k\, z^k(t)\,, \tag{4.10}$$

with

$$z(t) \equiv z(t, t_0) = \frac{\sqrt{t_+ - t} - \sqrt{t_+ - t_0}}{\sqrt{t_+ - t} + \sqrt{t_+ - t_0}}\,. \tag{4.11}$$

Here $0 \leq t_0 < t_-$ is a free parameter which can be optimised to reduce the maximum value of $|z(t)|$ in the physical FF range,

$$t_0\big|_{\text{opt.}} = t_+ \left(1 - \sqrt{1 - \frac{t_-}{t_+}}\right) . \tag{4.12}$$

We will later see that with the optimised value for t_0, the FFs can be well described by a SE which is truncated after the second term proportional to $z(t)$. Other values of t_0 (e.g. $t_0 = 0$) are also allowed but sometimes one is then required to go to higher order in the SE.

As a crucial property, the function $z(t)$ satisfies $|z(t)| \equiv 1$ in the pair-production region, $t \geq t_+$. The Blaschke factor is thus chosen as $B(t) = z(t, m_{\text{R}}^2)$. As for $P(q^2)$ defined above, if multiple resonances are present, then $B(t)$ is a product of the corresponding Blaschke factors. Further discussion about the physical basis for the SE is found in Ref. [149].

Simplified Series Expansion (SSE)

Another form of the Series Expansion method can also be considered. Instead of the Blaschke factor $B(t)$, one can use a simple pole $P(q^2)$ to account for low-lying resonances. This idea was proposed in Ref. [146], yielding

$$f(t) = \frac{1}{P(t)} \sum_k \tilde{\alpha}_k \, z^k(t, t_0) \, . \tag{4.13}$$

It was found that the dispersive bounds can still be imposed on the coefficients $\tilde{\alpha}_k$ of the SSE. We will discuss this and other issues concerning the validity of the simplifications in the following section.

4.3 Dispersive Bounds

The FFs describe the process $B \to L$ with $L = P, V$ in the decay region $0 < q^2 < t_- = (m_B - m_L)^2$. Using crossing symmetry, they can also describe the process in the pair-production region $q^2 > (m_B + m_L)^2$. This can be exploited to obtain a bound on parameters describing the FFs. A detailed derivation of this bound can be found in

Refs. [148; 150]. Here we provide a brief outline of the argument, in order to introduce our notation and to extend the method to tensor the FFs.

The crucial observation of the idea of dispersive bounds (as it is for QCD sum rules) is the possibility to evaluate the correlator of two flavour-changing currents,

$$\Pi^X_{\mu\nu}(q^2) = i \int d^4x\, e^{i\,q\cdot x}\, \langle 0|\, \mathrm{T}\, j^X_\mu(x)\, j^{\dagger\, X}_\nu(0)\, |0\rangle \ , \tag{4.14}$$

either by an operator product expansion (OPE) or by unitarity considerations. Here the relevant currents j^X_μ are defined as[†]

$$\begin{aligned} j^V_\mu &= \bar q \gamma_\mu b\,, & j^{V-A}_\mu &= \bar q \gamma_\mu (1-\gamma^5) b\,, \\ j^T_\mu &= \bar q \sigma_{\mu\alpha} q^\alpha b\,, & j^{T+A_T}_\mu &= \bar q \sigma_{\mu\alpha} q^\alpha (1+\gamma^5) b\,. \end{aligned} \tag{4.15}$$

Furthermore, we introduce longitudinal and transverse helicity projectors,

$$P^{\mu\nu}_L(q^2) = \frac{q^\mu q^\nu}{q^2}\,, \qquad P^{\mu\nu}_T(q^2) = \frac{1}{D-1}\left(\frac{q^\mu q^\nu}{q^2} - g^{\mu\nu}\right)\,, \tag{4.16}$$

which allow us to rewrite the correlation functions in terms of Lorentz scalars,

$$\Pi^X_I(q^2) \equiv P^{\mu\nu}_I(q^2)\, \Pi^X_{\mu\nu}(q^2)\,, \qquad (I = L, T). \tag{4.17}$$

As $\Pi^X_I(q^2)$ is an analytic function, it satisfies the subtracted dispersion relation,

$$\chi^X_I(n) = \frac{1}{n!}\, \frac{d^n \Pi_X(q^2)}{dq^{2n}}\bigg|_{q^2=0} = \frac{1}{\pi} \int\limits_0^\infty dt\, \frac{\mathrm{Im}\, \Pi^X_I(t)}{(t-q^2)^{n+1}}\bigg|_{q^2=0}\,, \tag{4.18}$$

where the number of subtractions n is chosen to render the resulting function $\chi^X_I(n)$ finite.

[†]In phenomenological applications, we are only interested in the currents $j^{T+A_T}_\mu$. The connection to correlators with genuine tensor currents $j_{\mu\nu} = \bar q \sigma_{\mu\nu} q$ is given in App. D of Ref. [155].

4.3.1 Hadronic representation of the Correlator

Unitarity allows us to express $\mathrm{Im}\,\Pi_I^X(q^2)$ as the positive definite sum over all hadronic states Γ with allowed quantum numbers:

$$\mathrm{Im}\,\Pi_I^X(q^2) = \frac{1}{2}\sum_\Gamma \int d\rho_\Gamma\,(2\pi)^4\,\delta^4(q-p_\Gamma)\,P_I^{\mu\nu}\;\langle 0|\,j_\mu^X\,|\Gamma\rangle\,\langle\Gamma|\,j_\nu^{\dagger X}\,|0\rangle\;. \tag{4.19}$$

where p_Γ is the total momentum of the final state, and $d\rho_\Gamma$ contains the appropriate phase-space weighting. For a particular choice of intermediate state, $\Gamma = BL$, we define

$$\mathrm{Im}\,\Pi_{I,BL}^X(q^2) = \eta\int d\rho_{BL}\,P_I^{\mu\nu}\;\langle 0|\,j_\mu^X\,|BL\rangle\,\langle BL|\,j_\nu^{\dagger X}\,|0\rangle\;, \tag{4.20}$$

where η is an isospin-degeneracy factor for a given channel, and we relegate the contribution from phase space to the function

$$d\rho_{BL} = \frac{1}{4\pi^2}\int\frac{d^3p_B}{2E_B}\,\frac{d^3p_L}{2E_L}\,\delta^4(q-p_B-p_L)\,. \tag{4.21}$$

Clearly, this results in the inequality

$$\mathrm{Im}\Pi_{I,BL}^X(t) \le \mathrm{Im}\Pi_I^X(t)\,. \tag{4.22}$$

Now, by extending the FFs to analytic functions throughout the t–plane, except for along the branch cut at the threshold for production of real BL pairs, one can use crossing symmetry to relate the matrix elements $\langle 0|\,j^X\,|BL\rangle$ to $\langle B|\,j^X\,|L\rangle$. The latter can be rewritten in terms of FFs, as defined in Sec. 4.2. As stated earlier, we use helicity-based linear combinations of the traditional FFs, such that all production amplitudes 'diagonalise':

$$\begin{aligned}
P_T^{\mu\nu}\,\langle P|j_\mu^V|B\rangle\langle B|j_\nu^{\dagger V}|P\rangle &= \frac{\lambda}{3q^2}\,|\mathcal{A}_{V,0}|^2\;,\\
P_L^{\mu\nu}\,\langle P|j_\mu^V|B\rangle\langle B|j_\nu^{\dagger V}|P\rangle &= \frac{\lambda}{q^2}\,|\mathcal{A}_{V,t}|^2\;,\\
P_T^{\mu\nu}\,\langle P|j_\mu^T|B\rangle\langle B|j_\nu^{\dagger T}|P\rangle &= \frac{\lambda}{3}\,|\mathcal{A}_{T,0}|^2\;,
\end{aligned} \tag{4.23}$$

for B decays into pseudoscalars, and for decays into vectors,

$$P_T^{\mu\nu}\,\langle V|j_\mu^{V-A}|B\rangle\langle B|j_\nu^{\dagger,V-A}|V\rangle = \frac{\lambda}{3q^2}\sum_{i=0}^{2}|\mathcal{B}_{V,i}|^2\,,$$

$$P_L^{\mu\nu}\,\langle V|j_\mu^{V-A}|B\rangle\langle B|j_\nu^{\dagger,V-A}|V\rangle = \frac{\lambda}{q^2}\,|\mathcal{B}_{V,t}|^2\,,$$

$$P_T^{\mu\nu}\,\langle V|j_\mu^{T+A_T}b|B\rangle\langle B|j_\nu^{\dagger,T+A_T}b|V\rangle = \frac{\lambda}{3}\sum_{i=0}^{2}|\mathcal{B}_{T,i}|^2\,. \tag{4.24}$$

We can now express $\mathrm{Im}\,\Pi^X_{I,BL}$ in compact form,

$$\mathrm{Im}\,\Pi^X_{I,BL} = \eta\int d\rho_{BL}\,\frac{\lambda}{3t}\left|A_I^X\right|^2 = \frac{\eta}{48\pi}\,\frac{\lambda^{3/2}}{t^2}\left|A_I^X\right|^2\,, \tag{4.25}$$

where the $\left|A_I^X\right|^2$ can be read off (4.23,4.24),

$$\left|A_T^V\right|^2 = |\mathcal{A}_{V,0}|^2\,,\qquad \left|A_L^V\right|^2 = 3\,|\mathcal{A}_{V,t}|^2\,,\qquad \left|A_T^T\right|^2 = q^2\,|\mathcal{A}_{T,0}|^2\,, \tag{4.26}$$

for decays into pseudoscalars, and

$$\left|A_T^{V-A}\right|^2 = \sum_{i=0}^{2}|\mathcal{B}_{V,i}|^2\,,\qquad \left|A_L^{V-A}\right|^2 = 3\,|\mathcal{B}_{V,t}|^2\,,\qquad \left|A_T^{T+A_T}\right|^2 = q^2\sum_{i=0}^{2}|\mathcal{B}_{T,i}|^2\,, \tag{4.27}$$

for decays into vector mesons.

4.3.2 OPE for the Correlator

Alternatively, we can examine the correlator in Eq. (4.14), using an OPE for the T-ordered product of currents in the limit $q^2 = 0 \ll t_+$. The standard expansion takes the form [74; 75; 157]

$$i\int dx\,e^{i\,q\cdot x}\,P_I^{\mu\nu}\,\mathrm{T}\left\{j_\mu^X(x)\,j_\nu^{\dagger\,X}(0)\right\} = \sum_{k=1}^{\infty}C_{I,k}^X(q)\,\mathcal{O}_k\,, \tag{4.28}$$

where $C^X_{I,n}(q)$ are Wilson coefficients for a given current X and projector I, and $\mathcal{O}_n$ are local gauge-invariant operators, consisting of quark and gluon fields. Here, the operators

are ordered by increasing dimension k. We can use the above, to express the correlator,

$$\Pi^X_{I,\mathrm{OPE}}(q^2) = \sum_{k=1}^{\infty} C^X_{I,k}(q^2)\,\langle O_k\rangle\ . \tag{4.29}$$

Besides the identity operator, whose Wilson coefficient contains the purely perturbative contribution to the correlator, we will specifically consider the first few operators related to the non-perturbative contribution from the quark condensate $\langle m\bar{q}q\rangle$, the gluon condensate $\langle\frac{\alpha_s}{\pi}G^2\rangle$, and the mixed condensate $\langle\bar{q}\sigma gGq\rangle$. We will elaborate on our calculation of the Wilson coefficients, $C^X_{I,k}(q^2)$, later. Specifically, we must calculate the Wilson coefficients entering the functions $\chi^X_I(n)$ defined in Eq. (4.18).

4.3.3 Bounds on coefficients in the SE

Using Eq. (4.22), we find

$$\frac{1}{\pi}\int\limits_0^\infty dt\,\frac{\mathrm{Im}\,\Pi^X_{I,BL}(t)}{(t-q^2)^{n+1}}\bigg|_{q^2=0} = \frac{1}{\pi}\int\limits_{t_+}^\infty dt\,\frac{\eta\,\lambda^{3/2}(t)}{48\pi\,t^{n+3}}\left|A^X_I(t)\right|^2 \le \chi^X_I(n)\,, \tag{4.30}$$

where $\chi^X_I \equiv \chi^X_{I,\mathrm{OPE}}$ is calculated from Eq. (4.29). Mapping the pair-production region $t \ge t_+$ onto the unit circle $|z(t)| = 1$, this inequality could be written in the form

$$\frac{1}{2\pi i}\oint\frac{dz}{z}\,|\phi^X_I\,A^X_I|^2(z) \le 1 \quad\Leftrightarrow\quad \frac{1}{\pi}\int_{t_+}^\infty\frac{dt}{t-t_0}\sqrt{\frac{t_+-t_0}{t-t_+}}\,|\phi^X_I\,A^X_I|^2(t) \le 1\,, \tag{4.31}$$

where the function $|\phi^X_I(t)|^2$ can be obtained by comparing (4.31) and Eq. (4.30), and using $\lambda(t) = (t_+-t)(t_--t)$,

$$|\phi^X_I(t)|^2 = \frac{\eta}{48\pi\,\chi^X_I(n)}\,\frac{(t-t_+)^2}{(t_+-t_0)^{1/2}}\,\frac{(t-t_-)^{3/2}}{t^{n+2}}\,\frac{t-t_0}{t}\,. \tag{4.32}$$

The isospin-degeneracy factor η takes the values 3/2, 2 and 1 for $B\to\rho$, $B\to K^{(*)}$ and $B_s\to\phi$ respectively. We may now generically write the helicity-based FFs $A^X_I(t)$ as

$$A^X_I(t) = \frac{(\sqrt{-z(t,0)})^m(\sqrt{z(t,t_-)})^l}{B(t)\,\phi^X_I(t)}\,\sum_{k=0}^\infty\alpha_k\,z^k \tag{4.33}$$

with real coefficients α_k, and a Blaschke factor $B(t) = \prod_i z(t, m_{R_i}^2)$, representing poles due to sub-threshold resonances of masses m_{R_i}, and satisfying $|B(t)| = 1$ in the pair-production region. The additional factors $(\sqrt{-z(t,0)})^m$ and $(\sqrt{z(t,t_-)})^l$ have been added to take into account the unconventional normalisation of our FF functions through factors of $\sqrt{q^2}$ and $\sqrt{\lambda}$ (e.g. $m = 1$ for $\mathcal{A}_{T,0}$, and $l = -1$ for $\mathcal{A}_{V,t}$, cf. above).[‡] The function $\phi_I^X(t)$ has to be constructed in such a way that its absolute value satisfies Eq. (4.32), while Eq. (4.33) retains the analytical properties of the FF. This can easily be achieved by replacing potential poles and cuts in $\sqrt{|\phi_I^X(t)|^2}$, by making replacements of the form

$$\frac{1}{t-X} \to \frac{-z(t,X)}{t-X}\,, \tag{4.34}$$

which is allowed as $|z(t,X)| = 1$ in the pair-production region. This results in (see also [158])

$$\phi_I^X(t) = \sqrt{\frac{\eta}{48\pi\chi_I^X(n)}}\,\frac{(t-t_+)}{(t_+-t_0)^{1/4}}\left(\frac{z(t,0)}{-t}\right)^{(3+n)/2}\left(\frac{z(t,t_0)}{t_0-t}\right)^{-1/2}\left(\frac{z(t,t_-)}{t_--t}\right)^{-3/4}. \tag{4.35}$$

Inserting the parameterisation from Eq. (4.33) into Eq. (4.31), and using $|z(t,t_0)| = |z(t,m_R^2)| = |z(t,0)| = 1$, the integration $dz/z = d\varphi$ along the unit circle is trivial, yielding the desired bound on the coefficients α_k,

$$\sum_{k=0}^{\infty}\alpha_k^2 < 1\,. \tag{4.36}$$

For decays into vector mesons, using an analogous parameterisation as in Eq. (4.33) for each *individual* FF contribution in Eq. (4.27), one obtains a bound on the sum of the corresponding coefficients. As an example, let us consider $A_T^{V-A}(t)$, where we parametrise

$$\mathcal{B}_{V,0}(t) = \frac{1}{B(t)\,\sqrt{z(t,t_-)}\,\phi_T^{V-A}(t)}\sum_{k=0}^{K-1}\beta_k^{(V,0)}\,z^k\,,$$

[‡]These factors could also be considered as part of the Blaschke factor. Note that under a change of normalisation convention for the FFs, both, the so-constructed Blaschke factor as well as the function $\phi(t)$ have to be modified, while the coefficients α_k of the SE remain the same.

$$\mathcal{B}_{V,1}(t) = \frac{\sqrt{-z(t,0)}}{B(t)\,\phi_T^{V-A}(t)} \sum_{k=0}^{K-1} \beta_k^{(V,1)}\, z^k\,,$$

$$\mathcal{B}_{V,2}(t) = \frac{\sqrt{-z(t,0)}}{B(t)\,\sqrt{z(t,t_-)}\,\phi_T^{V-A}(t)} \sum_{k=0}^{K-1} \beta_k^{(V,2)}\, z^k\,, \tag{4.37}$$

resulting in the dispersive bound

$$\sum_{k=0}^{K-1} \left((\beta_k^{(V,0)})^2 + (\beta_k^{(V,1)})^2 + (\beta_k^{(V,2)})^2 \right) < 1\,. \tag{4.38}$$

4.3.4 The coefficients $\chi_I^X(n)$

In Tab. 4.2 we summarise the numerical result of our calculation of the various coefficients $\chi_I^X(n)$, which enter the functions $\phi_I^X(t)$ in the SE. We quote individual numbers for the perturbative LO and NLO results, as well as from the condensate contributions, for two different values of light-quark masses, $m = m_d$ and $m = m_s$. The number of subtractions is also indicated. Details of the calculation as well as analytical formulae for the perturbative coefficients can be found in App. B.2. As can be observed from Tab. 4.2[§], the NLO perturbative corrections are essential for a reliable estimate for the coefficients $\chi_I^X(n)$, while the quark condensate gives only small contributions, and the gluon condensate and the mixed quark-gluon condensate are negligible.

4.4 Form Factor Fits to Theoretical Data

4.4.1 Theory Input from Lattice and LCSR

As mentioned in the introduction, LCSR and Lattice are largely complementary, as they perform best in different regimes of momentum transfer q^2. It is worth mentioning that certain decays, e.g. decays to unstable hadrons, are more challenging in Lattice QCD, and in some cases only quenched results exist for a subset of the FFs. On the other hand, LCSRs provide results for all decay channels considered here, including the complete set of seven FFs for $B \to K^*$ and $B_s \to \phi$, which so far have not been fully addressed by

[§]Note that here the coefficients are evaluated at the scale of the $\overline{\text{MS}}$ b quark mass in order to consistent with previous literature

Table 4.2: Summary of OPE results for the coefficients $\chi_I^X(n)$. The following parameter values have been used [74; 159–161]: $\bar{\mu} = m_b = 4.2$ GeV, $m_d = 4.8$ MeV, $m_s = 104$ MeV, $\alpha_s = 0.2185$, $\langle \bar{d}d \rangle = (278 \text{ MeV})^3$, $\langle \bar{s}s \rangle = 0.8 \langle \bar{d}d \rangle$, $\left\langle \frac{\alpha_s}{\pi} G^2 \right\rangle = 0.038 \text{ GeV}^4$, $\langle \bar{q}\sigma gGq \rangle = (1.4 \text{ GeV})^2 \langle \bar{\text{q}}\text{q} \rangle$.

q	Correlator	Subtractions	LO	NLO	$\langle \bar{q}q \rangle$	$\left\langle \frac{\alpha}{\pi} G^2 \right\rangle$	$\langle \bar{q}\sigma gGq \rangle$	Σ
	$100 \times m_b^2 \chi^S$	2	1.265	0.589	0.029	0.001	−0.003	1.88
	$100 \times m_b^2 \chi^P$	2	1.268	0.590	0.029	0.001	−0.003	1.88
	$100 \times \chi_L^V$	1	1.262	0.211	0.029	0.001	−0.003	1.50
d	$100 \times \chi_L^A$	1	1.271	0.205	0.029	0.001	−0.003	1.50
	$100 \times m_b^2 \chi_T^V$	2	0.951	0.236	−0.029	−0.001	0.007	1.16
	$100 \times m_b^2 \chi_T^A$	2	0.948	0.237	−0.029	−0.001	0.007	1.16
	$100 \times m_b^2 \chi_T^T$	3	2.539	0.579	−0.029	−0.000	0.008	3.10
	$100 \times m_b^2 \chi_T^{AT}$	3	2.527	0.586	−0.029	−0.001	0.008	3.09
	$100 \times m_b^2 \chi^S$	2	1.233	0.571	0.024	0.001	−0.003	1.83
	$100 \times m_b^2 \chi^P$	2	1.296	0.608	0.022	0.001	−0.003	1.93
	$100 \times \chi_L^V$	1	1.172	0.229	0.023	0.000	−0.003	1.42
s	$100 \times \chi_L^A$	1	1.361	0.187	0.023	0.002	−0.003	1.57
	$100 \times m_b^2 \chi_T^V$	2	0.980	0.237	−0.022	0.000	0.005	1.20
	$100 \times m_b^2 \chi_T^A$	2	0.916	0.238	−0.024	−0.002	0.006	1.13
	$100 \times m_b^2 \chi_T^T$	3	2.652	0.569	−0.023	0.001	0.006	3.21
	$100 \times m_b^2 \chi_T^{AT}$	3	2.404	0.603	−0.024	−0.002	0.007	2.99

Lattice QCD. However, as LCSR results are only valid in the low–q^2 regime, in these cases further theoretical information is needed to extrapolate to large values of q^2, as will be discussed in the following section.

In our analysis, we will use the LCSR predictions from Refs. [71; 72], taking 3(4) points at low values of q^2 as input, see Tab. 4.3. The errors quoted are extrapolated from the value quoted for $q^2 = 0$ in the references specified in the table. Lattice data is available for $B \to \rho$ and $B \to K$ decays, and is as shown in Tab. 4.4.[¶] For those data points which have an asymmetric statistical or systematic error, in order to perform the fit, we take the FF to be the central value in this statistical or systematic range, and take half the range to be the statistical or systematic error [162].

For $B \to \rho$ and $B \to K$ decays, we use LCSR and Lattice data to interpolate between the low and high–q^2 region. The result can be compared to the case where we extrapolate to the high–q^2 region only on the basis of LCSR predictions. This procedure will gives us an idea about the confidence in the extrapolations for those cases where Lattice data is lacking.

4.4.2 Parameterisation of FFs as Series Expansion

For those channels where Lattice data is not available, it is essential to employ a FF parameterisation that takes into account the characteristic features of the FF shape as determined from the analyticity and unitarity consideration above. For every considered FF, we will therefore define a parameterisation based on the SE,

$$\mathcal{A}_{V,0}(t) = \frac{1}{B(t)\,\phi_T^V(t)} \sum_{k=0}^{K-1} \alpha_k^{(V,0)}\, z^k\,,$$

$$\mathcal{A}_{V,t}(t) = \frac{1}{B(t)\,\sqrt{z(t,t_-)}\,\phi_L^V(t)} \sum_{k=0}^{K-1} \alpha_k^{(V,t)}\, z^k\,,$$

$$\mathcal{A}_{T,0}(t) = \frac{\sqrt{-z(t,0)}}{B(t)\,\phi_T^T(t)} \sum_{k=0}^{K-1} \alpha_k^{(T,0)}\, z^k\,, \tag{4.39}$$

[¶] We are very grateful to Sara Collins of the QCDSF collaboration for providing us with specific values for $B \to K$.

Table 4.3: Overview of LCSR points used, transformed to the helicity amplitude basis.

Decay	FF	LCSR/q^2 (GeV^2)				Ref.
$B \to K$	q^2	3	6	9	12	Tab. 3, [71]
	$\mathcal{A}_{V,0}$	0.40 ± 0.05	0.48 ± 0.06	0.59 ± 0.07	-	
	$\mathcal{A}_{V,t}$	0.40 ± 0.05	0.51 ± 0.06	0.65 ± 0.08	-	
	$\mathcal{A}_{T,0}$	0.13 ± 0.01	0.22 ± 0.02	0.34 ± 0.03	-	
$B \to \rho$	q^2	3	6	9	12	Tab. 8, [72]
	$\mathcal{B}_{V,0}$	0.37 ± 0.12	0.46 ± 0.13	0.60 ± 0.14	-	
	$\mathcal{B}_{V,1}$	0.16 ± 0.01	0.27 ± 0.02	0.41 ± 0.04	-	
	$\mathcal{B}_{V,2}$	0.16 ± 0.02	0.29 ± 0.03	0.46 ± 0.04	-	
	$\mathcal{B}_{V,t}$	0.37 ± 0.04	0.46 ± 0.04	0.58 ± 0.06	-	
	$\mathcal{B}_{T,0}$	0.17 ± 0.35	0.3 ± 0.26	0.47 ± 0.23	0.71 ± 0.22	
	$\mathcal{B}_{T,1}$	0.45 ± 0.04	0.55 ± 0.05	0.69 ± 0.06	0.9 ± 0.08	
	$\mathcal{B}_{T,2}$	0.46 ± 0.04	0.58 ± 0.05	0.76 ± 0.07	1.0 ± 0.1	
$B \to K^*$	q^2	3	6	9	12	Tab. 8, [72]
	$\mathcal{B}_{V,0}$	0.45 ± 0.13	0.56 ± 0.13	0.73 ± 0.15	-	
	$\mathcal{B}_{V,1}$	0.19 ± 0.02	0.32 ± 0.03	0.49 ± 0.04	-	
	$\mathcal{B}_{V,2}$	0.20 ± 0.02	0.35 ± 0.03	0.57 ± 0.06	-	
	$\mathcal{B}_{V,t}$	0.44 ± 0.04	0.54 ± 0.05	0.67 ± 0.06	-	
	$\mathcal{B}_{T,0}$	0.23 ± 0.36	0.39 ± 0.27	0.60 ± 0.24	0.90 ± 0.22	
	$\mathcal{B}_{T,1}$	0.59 ± 0.06	0.72 ± 0.07	0.89 ± 0.08	1.2 ± 0.1	
	$\mathcal{B}_{T,2}$	0.61 ± 0.06	0.77 ± 0.07	1.0 ± 0.1	1.4 ± 0.1	
$B_s \to \phi$	q^2	3	6	9	12	Tab. 8, [72]
	$\mathcal{B}_{V,0}$	0.55 ± 0.12	0.68 ± 0.13	0.85 ± 0.14	-	
	$\mathcal{B}_{V,1}$	0.2 ± 0.02	0.34 ± 0.03	0.52 ± 0.04	-	
	$\mathcal{B}_{V,2}$	0.21 ± 0.02	0.38 ± 0.04	0.62 ± 0.06	-	
	$\mathcal{B}_{V,t}$	0.56 ± 0.04	0.68 ± 0.05	0.85 ± 0.06	-	
	$\mathcal{B}_{T,0}$	0.26 ± 0.39	0.44 ± 0.29	0.67 ± 0.26	1.0 ± 0.3	
	$\mathcal{B}_{T,1}$	0.59 ± 0.06	0.72 ± 0.07	0.89 ± 0.08	1.2 ± 0.1	
	$\mathcal{B}_{T,2}$	0.61 ± 0.06	0.77 ± 0.07	1.0 ± 0.1	1.4 ± 0.1	

Table 4.4: Overview of Lattice points used, transformed to the helicity amplitude basis. Note that specific values for $B \to \rho$ are as in Tab. 2 of Ref. [145].

Decay	q^2 (GeV^2)	FF			Ref.
$B \to K$		$\mathcal{A}_{V,0}$	$\mathcal{A}_{V,t}$	$\mathcal{A}_{T,0}$	QCDSF [67]
	14.5	0.94 ± 0.19	1.1 ± 0.2	-	
	15.6	1.1 ± 0.2	1.3 ± 0.3	-	
	16.7	1.2 ± 0.2	1.5 ± 0.3	-	
	17.9	1.4 ± 0.3	1.8 ± 0.3	-	
	19.	1.6 ± 0.3	2.3 ± 0.4	-	
	20.1	1.9 ± 0.4	$3. \pm 0.6$	-	
	21.3	2.3 ± 0.4	4.4 ± 0.8	-	
	22.4	2.9 ± 0.6	8.7 ± 1.7	-	
$B \to \rho$		$\mathcal{B}_{V,0}$	$\mathcal{B}_{V,1}$	$\mathcal{B}_{T,2}$	UKQCD [70]
	12.7	0.64 ± 0.78	0.34 ± 0.27	0.9 ± 0.18	
	13.	0.71 ± 0.72	0.39 ± 0.25	0.96 ± 0.18	
	13.5	0.8 ± 0.66	0.48 ± 0.22	1.1 ± 0.2	
	14.	0.9 ± 0.62	0.58 ± 0.19	1.2 ± 0.2	
	14.5	1.0 ± 0.6	0.68 ± 0.16	1.3 ± 0.2	
	15.	1.1 ± 0.6	0.78 ± 0.15	1.4 ± 0.2	
	15.5	1.3 ± 0.7	0.89 ± 0.15	1.6 ± 0.2	
	16.	1.4 ± 0.8	1.0 ± 0.2	1.8 ± 0.2	
	16.5	1.6 ± 0.9	1.2 ± 0.3	2.1 ± 0.2	
	17.1	1.8 ± 1.2	1.4 ± 0.4	2.4 ± 0.2	
	17.6	2.1 ± 1.5	1.7 ± 0.6	2.7 ± 0.3	
	18.2	$2.5 \pm 2.$	2.1 ± 0.9	3.3 ± 0.3	

and

$$\mathcal{B}_{V,t}(t) = \frac{1}{B(t)\,\phi_L^{V-A}(t)} \sum_{k=0}^{K-1} \beta_k^{(V,t)}\, z^k\,,$$

$$\mathcal{B}_{T,0}(t) = \frac{\sqrt{-z(t,0)}}{B(t)\,\sqrt{z(t,t_-)}\,\phi_T^{T+A_T}(t)} \sum_{k=0}^{K-1} \beta_k^{(T,0)}\, z^k\,,$$

$$\mathcal{B}_{T,1}(t) = \frac{1}{B(t)\,\phi_T^{T+A_T}(t)} \sum_{k=0}^{K-1} \beta_k^{(T,1)}\, z^k\,,$$

$$\mathcal{B}_{T,2}(t) = \frac{1}{B(t)\,\sqrt{z(t,t_-)}\,\phi_T^{T+A_T}(t)} \sum_{k=0}^{K-1} \beta_k^{(T,2)}\, z^k\,, \tag{4.40}$$

and $\mathcal{B}_{V,0-2}$ already given in Eq. (4.37). Here we have used our FF convention defined in Eqs. (4.1), (4.4), (4.6) and (4.8) along with the prefactors necessary to obtain the correct analytical behaviour of our FFs.[‖] In our fits below, we will find that in general the SE can be truncated after the first two terms, i.e. the parameter K can be set to 2. We should point out, however, that this does not necessarily imply that higher-order terms in the SE are negligible: Although $|z|^2 \ll 1$ in the semi-leptonic region, one may still have $|\alpha_2 z^2| \sim |\alpha_1 z|$ if the coefficients satisfy $\alpha_1 \ll \alpha_2 \lesssim 1$. From the theoretical point of view, this reflects an irreducible source of uncertainty. From the practical point of view, we consider the truncated series expansion as a reasonable parameterisation which is easy to implement (and easy to refine) in phenomenological studies.

For simplicity, the theoretical relations that some of the FFs fulfil at $q^2 = 0$ (see App. B of Ref. [155]) will not be implemented in the fit, as they are automatically satisfied by the rather precise input from LCSR at this point. However, the helicity-based FF definition further implies a relation between the FFs $\mathcal{B}_{V,0}$ and $\mathcal{B}_{V,2}$, and similarly between $\mathcal{B}_{T,0}$ and $\mathcal{B}_{T,2}$ at the kinematic endpoint $q^2 = t_- = (m_B - m_L)^2$,

$$\lim_{q^2\to t_-} \frac{\mathcal{B}_{V,2}(q^2)}{\mathcal{B}_{V,0}(q^2)} = \lim_{q^2\to t_-} \frac{\mathcal{B}_{T,2}(q^2)}{\mathcal{B}_{T,0}(q^2)} = \sqrt{2}\,, \tag{4.41}$$

[‖] In Refs. [151] and [146; 150], the predictions from perturbative QCD for the scaling of the FFs at large values of q^2 have been used as an additional constraint on the shape of the FFs. We have found that these constraints do not influence the FF fits in the decay region significantly. As the asymptotic behaviour of exclusive observables in QCD is still a matter of controversy, we therefore find it safer and simpler not to include these constraints in our parameterisation.

which we will implement as an additional constraints on the corresponding coefficients in the SE. From the above parameterisations, the SSE is obtained by the replacements

$$\phi_I^X(t) \to 1\,, \quad B(t) \to P(t)\,, \quad \sqrt{-z(t,0)} \to \sqrt{q^2}/m_B\,, \quad \sqrt{z(t,t_-)} \to \sqrt{\lambda}/m_B^2\,, \tag{4.42}$$

with new coefficients $\tilde{\alpha}_k$ and $\tilde{\beta}_k$.

Unitarity constraints

For the SE parameterisation, the unitarity constraints take the form

$$\sum_{k=0}^{K-1} (\alpha_k)^2 \le 1 \quad \text{for } \mathcal{A}_{V,0} \text{ and } \mathcal{A}_{T,0}, \qquad 3\sum_{k=0}^{K-1} (\alpha_k)^2 \le 1 \quad \text{for } \mathcal{A}_{V,t}, \tag{4.43}$$

and

$$\begin{aligned}
&3\sum_{k=0}^{K-1} (\beta_k^{(V,t)})^2 \le 1 \quad \text{for } \mathcal{B}_{V,t},\\
&\sum_{k=0}^{K-1} \left\{ (\beta_k^{(V,0)})^2 + (\beta_k^{(V,1)})^2 + (\beta_k^{(V,2)})^2 \right\} \le 1 \quad \text{for } \mathcal{B}_{V,0},\ \mathcal{B}_{V,1}, \text{ and } \mathcal{B}_{V,2},\\
&\sum_{k=0}^{K-1} \left\{ (\beta_k^{(T,0)})^2 + (\beta_k^{(T,1)})^2 + (\beta_k^{(T,2)})^2 \right\} \le 1 \quad \text{for } \mathcal{B}_{T,0},\ \mathcal{B}_{T,1}, \text{ and } \mathcal{B}_{T,2}.
\end{aligned} \tag{4.44}$$

For the SSE parameterisation, imposing the unitarity bound is more complicated, as shown in Ref. [146]. We repeat the derivation of this bound in order to define notation used later. One first compares the SE and SSE parameterisations:

$$\sum_{k=0}^{K-1} \alpha_k\, z^k = \Lambda(z) \sum_{k=0}^{K-1} \tilde{\alpha}_k\, z^k \tag{4.45}$$

One can simply obtain $\Lambda(z)$ by combining the prefactors from the SE expansion with the prefactors from the SSE expansion, and expressing the result as a function of $z(t,t_0)$. Since z is a small parameter, we can expand $\Lambda(z)$ in powers of z:

$$\Lambda(z) = \sum_k \zeta_k\, z^k. \tag{4.46}$$

We can therefore obtain a relation between the coefficients α_k and $\tilde{\alpha}_k$,

$$\alpha_i = \sum_{k=0}^{\min[K-1,i]} \zeta_{i-k}\,\tilde{\alpha}_k\,, \qquad 0 \le i \le K-1\,, \tag{4.47}$$

which results in bounds of the type

$$\sum_{j,k=0}^{K-1} C_{jk}\,\tilde{\alpha}_j\,\tilde{\alpha}_k \le 1\,, \tag{4.48}$$

where

$$C_{jk} = \sum_{i=0}^{K-1-\max[j,k]} \zeta_i\,\zeta_{i+|j-k|} \tag{4.49}$$

is a positive definite matrix.

4.4.3 Fitting prescription

We perform a fit to the LCSR data, as well as, where possible, a combined fit to the LCSR and Lattice data, by minimising a χ^2 function defined by

$$\chi^2(\vec{\theta}) = \Big(F_i - F(t_i,\vec{\theta})\Big)\,\big[V^{-1}\big]_{ij}\Big(F_j - F(t_j,\vec{\theta})\Big)\,, \tag{4.50}$$

where $\vec{\theta}$ contains the parameters of a given FF parameterisation, F_i are the FF values from LCSR/Lattice at given points t_i, and V_{ij} are elements of the covariance matrix as defined below.

As explained above, we will be investigating parameterisations based on the SE and SSE, where the parameters will be subject to additional constraints derived from dispersive bounds on the FFs.

- In the conventional series expansion (SE), we use (4.10), and truncate the series after the first 2 terms, such that

$$\vec{\theta} = \{\alpha_0, \alpha_1\}\,, \qquad \sum \alpha_i^2 \overset{!}{<} 1\,.$$

- The simplified series expansion (SSE) uses (4.13), with

$$\vec{\theta} = \{\tilde{\alpha}_0, \tilde{\alpha}_1\}\,, \qquad \sum_{i,j=0}^{1} C_{ij}\,\tilde{\alpha}_i\tilde{\alpha}_j \overset{!}{<} 1\,,$$

  where the matrix C_{ij} is defined in Eq. (4.49).

In constructing the covariance matrix, when we do a combined fit to LCSR and Lattice data, we assume the matrix to be block diagonal with independent blocks for Lattice and LCSR, equivalent to $\chi^2 = \chi^2_{\rm LCSR} + \chi^2_{\rm Lat}$, where

$$\chi^2_{\rm LCSR}(\vec{\theta}) = \Big(F_i - F(t_i,\vec{\theta})\Big)\,\big[V^{-1}_{\rm LCSR}\big]_{ij}\Big(F_j - F(t_j,\vec{\theta})\Big)\,, \tag{4.51}$$

and

$$\chi^2_{\rm Lat}(\vec{\theta}) = \Big(F_i - F(t_i,\vec{\theta})\Big)\,\big[V^{-1}_{\rm Lat}\big]_{ij}\Big(F_j - F(t_j,\vec{\theta})\Big)\,, \tag{4.52}$$

We consider the statistical and systematic contributions to the Lattice errors separately. Where results were not available in the literature, we received the breakdown by private communication with the authors. In obtaining the covariance matrix, we make the following conservative assumptions:

- Statistical errors of Lattice data are 50% correlated [67; 70].
- Systematic errors of Lattice data are 100% correlated [67; 70].
- Errors of LCSR data are due to parametric as well as to systematic uncertainties from different sources. In order to provide a concrete number for the χ^2 value characterising the quality of the fit, we have estimated these errors at different values t_i to be 75% correlated**.

This prescription leads to a covariance matrix $V^{ij} = \mathrm{cov}[\mathrm{t^i}, \mathrm{t^j}]$, containing

$$V^{ij}_{\rm LCSR} = \frac{1}{4}\kappa^i\kappa^j\delta_{ij} + \frac{3}{4}\kappa^i\kappa^j \qquad \text{and} \tag{4.53}$$

$$V^{ij}_{\rm Lat} = \frac{1}{2}\sigma^i\sigma^j\delta_{ij} + \frac{1}{2}\sigma^i\sigma^j + \varepsilon^i\varepsilon^j \tag{4.54}$$

**We have checked that using a 90% or 50% correlation instead, of course changes the value of χ^2, does not influence the optimal parameter values. A similar comment applies to the number of individual LCSR points used in the fit.

where σ_i are the statistical errors, ε_i are the systematic errors for the Lattice data, and κ_i are the errors for the LCSR predictions.

Minimising $\chi^2(\vec{\theta})$ then yields the best fit parameters $\vec{\theta}^*$, as well as the covariance matrix of the fit, $U_{ij} = \mathrm{cov}[\theta_\mathrm{i}, \theta_\mathrm{j}]$,

$$\left(U^{-1}\right)_{ij} = \frac{1}{2}\left.\frac{\partial^2\chi^2(\vec{\theta})}{\partial\theta_i\,\partial\theta_j}\right|_{\vec{\theta}=\vec{\theta}^*}, \tag{4.55}$$

from which we calculate the error associated to the fitted FF function:

$$\Delta F(t,\vec{\theta}^*) = \left.\frac{\partial F(t,\vec{\theta})}{\partial\theta_i}\right|_{\vec{\theta}=\vec{\theta}^*} U_{ij} \left.\frac{\partial F(t,\vec{\theta})}{\partial\theta_j}\right|_{\vec{\theta}=\vec{\theta}^*} \tag{4.56}$$

4.4.4 Results

Having established the fitting procedure, we consider FFs for the decays $B \to \rho$, $B \to K$, $B \to K^*$ and $B_s \to \phi$. We concentrate on radiative and semi-leptonic decays, as previously the dispersive bounds had not been calculated for the tensor current, so could not be applied to these decays. The phenomenological motivations for studying the chosen decays are as follows. First, they involve flavour changing neutral currents via e.g. electroweak penguins, so they are particularly sensitive to new physics. Secondly, the di-lepton signature can easily be detected at the LHC, and the three-body or four-body final state (for subsequent decays $K^* \to K\pi$ and $\phi \to KK$) involves many promising observables related to various angular distributions [52; 88; 89; 142; 152].

From the theoretical point of view, the $B \to V\gamma$ decay as well as the low-q^2 region of $B \to L\,\ell^+\ell^-$ transitions allow for a systematic inclusion of radiative corrections within the QCD factorisation approach at leading order in the $1/m_b$ expansion [47; 78]. In this region, the transition FFs (which still determine a major part of non-perturbative input) can be obtained from LCSR estimates alone. As it has been discussed, for instance, in Ref. [102; 163], the high-q^2 region may also be interesting in order to constrain NP contributions (notably to the short-distance Wilson coefficients C_9 and C_{10}), and therefore our extrapolations of LCSR results for the tensor FFs in that region will be particularly relevant for this purpose. In the following subsection, we present the results of fitting the specific FFs to both, the SE and SSE parameterisations, using LCSR and Lattice data where appropriate as discussed in Sec. 4.4.1. For the light meson masses, we use $m_K = 494$ MeV, $m_{K^*} = 892$ MeV, $m_\rho = 776$ MeV, $m_\phi = 1.02$ GeV.

***B → K* form factors:** In Figs. 4.1–4.5, we show the fit for the various $B \to K$ FFs, which enter, for instance, the radiative $B \to K\ell^+\ell^-$ and $B \to K\nu\bar{\nu}$ decays. We compare the result of the SE and SSE parameterisations using LCSR data, and investigate the changes when the Lattice data is included. The numerical results for the best-fit parameters of the SE and SSE fit are found in corresponding Tabs. 4.5–4.6. The covariance matrices for these fits can also be found in App. B.3.

Generally, both parameterisations are seen to fit the data well, and importantly, we find agreement with the Lattice predictions for $\mathcal{A}_{V,0}$ and $\mathcal{A}_{V,t}$, even when they are not included in the fit. We therefore consider our extrapolation of LCSR data for the tensor FF $\mathcal{A}_{T,0}$ to the high-q^2 region, where Lattice data does not exist, as sufficiently reliable. The quality of the fits is astonishingly good, considering the χ^2 values for only two free parameters in the expansion. The differences between the SE and SSE are only marginal, which can be traced back to the usage of the optimised value for the auxiliary parameter t_0 in Eq. (4.12). The dispersive bounds turn out to be far from being separated, and therefore they have only little impact on the FF fit. This observation is in line with other studies of heavy-to-light FFs in the literature, see e.g. [147; 151; 164].

In order to address the question of potential contributions from higher-order terms in the series expansion, we consider the LCSR prediction for the vector and tensor form factors $\mathcal{A}_{V,0}$, $\mathcal{A}_{T,0}$ and fit to a SE with $K = 3$, where the coefficient a_2 of the z^2 term in the expansion has been fixed to values between $[0.9, +0.9]$, representing almost the maximal range allowed by the unitarity constraints. The results of these fits are shown in Figs. 4.2 and 4.6. Let us first consider the case where only LCSR data is used in the fit. We observe that, as expected, the constraints from the LCSR points at low values of q^2 are not sufficient to determine the behaviour at large q^2, if higher-order terms in the SE (with no further phenomenological constraints) are allowed for. However, the behaviour of the form factor corresponding to the extreme values of a_2 does not appear very realistic (even a rough numerical estimate of coupling constants for the first low-lying resonances with the considered hadronic transition would be sufficient to exclude the curves at the margin). Therefore the associated error estimate appears too pessimistic to us. Moreover, typically, exclusive semi-leptonic branching fractions are suppressed relative to the inclusive ones by a factor of about 20. This suggests that the right-hand side of the dispersive bounds should not exceed a value of 5% (instead of 100%). Correspondingly, a realistic range of allowed a_2 values should rather be taken as $[0.25, +0.25]$, which is indicated by the thick central lines in Fig. 4.2. The associated uncertainty is only slightly larger than that obtained from the variation of (a_0, a_1) for the SE fit with $K = 2$. If,

on the other hand, the lattice information (in the case of $\mathcal{A}_{V,0}$) is taken into account, the cases with $|a_2| \gtrsim 0.25$ actually do not yield a satisfactory fit anymore, and again the error estimate of the linear fit seems to be sufficient to estimate the fit errors. In view of the generic difficulties in estimating systematic theoretical uncertainties, we thus consider the SE/SSE parameterisation with $K = 2$ and the associated error estimates as sufficiently reliable for practical applications.

Another comment applies to the scalar FFs $\mathcal{A}_{V,t}$: As shown in Tab. 4.1, the combined heavy-quark/chiral-symmetry limit considered in Ref. [156] predicts a scalar B_s resonance *below* BK-production threshold (such a state is also favoured by a Lattice computation in [165]). On the other hand, the PDG only finds resonances at masses near/above the production threshold. We have therefore chosen to compare two variants of the fit, with/without a scalar resonance.[††] As can be seen, the fit *with* a scalar resonance from [156] describes the combined Lattice/LCSR data significantly better than the fit without a low-lying resonance (where in the latter case again the dispersive bounds constrain the FF to lie systematically below the Lattice data). However, within the present uncertainties of Lattice and LCSR data, this could only be taken as a very indirect argument in favour of a scalar resonance in the anticipated mass region.

Table 4.5: $B \to K$: Fit of SE parameterisation to LCSR or LCSR/Lattice results, for $\mathcal{A}_{V,0}$ ($X = 1$), $\mathcal{A}_{V,t}$ ($X = 3$) and $\mathcal{A}_{T,0}$ ($X = 1$).

A_X	m_R	α_0	α_1	Fit to	$\chi^2_{\rm fit}$	$X\sum_i \alpha_i^2$
$\mathcal{A}_{V,0}$	5.41	-2.4×10^{-2}	6.2×10^{-2}	LCSR and Lattice	5.07×10^{-3}	4.43×10^{-3}
$\mathcal{A}_{V,t}$	-	-6.8×10^{-2}	0.20	LCSR and Lattice	0.200	0.129
$\mathcal{A}_{V,t}$	5.72	-4.8×10^{-2}	0.11	LCSR and Lattice	1.54×10^{-4}	4.34×10^{-2}
$\mathcal{A}_{V,0}$	5.41	-2.8×10^{-2}	6.0×10^{-2}	LCSR	3.94×10^{-3}	4.40×10^{-3}
$\mathcal{A}_{V,t}$	-	-6.7×10^{-2}	0.18	LCSR	1.44×10^{-3}	0.111
$\mathcal{A}_{V,t}$	5.72	-2.5×10^{-2}	7.2×10^{-2}	LCSR	0.329	5.77×10^{-3}
$\mathcal{A}_{T,0}$	5.41	-4.5×10^{-2}	8.9×10^{-2}	LCSR	0.234	2.99×10^{-2}

[††]Notice that BZ [71] use an effective resonance mass above production threshold to parametrise the scalar FFs.

Table 4.6: $B \to K$: Fit of SSE parameterisation to LCSR or LCSR/Lattice results, for $\mathcal{A}_{V,0}$ ($X = 1$), $\mathcal{A}_{V,t}$ ($X = 3$) and $\mathcal{A}_{T,0}$ ($X = 1$).

A_X	m_R	$\tilde{\alpha}_0$	$\tilde{\alpha}_1$	Fit to	χ^2_{fit}	$X \sum_{i,j} C_{i,j}\tilde{\alpha}_i\tilde{\alpha}_j$
$\mathcal{A}_{V,0}$	5.41	0.48	-1.0	LCSR and Lattice	5.15×10^{-3}	4.04×10^{-3}
$\mathcal{A}_{V,t}$	-	0.54	-1.7	LCSR and Lattice	0.904	0.142
$\mathcal{A}_{V,t}$	5.72	0.30	0.20	LCSR and Lattice	7.17×10^{-5}	5.32×10^{-2}
$\mathcal{A}_{V,0}$	5.41	0.48	-1.1	LCSR	8.15×10^{-3}	3.06×10^{-3}
$\mathcal{A}_{V,t}$	-	0.52	-1.4	LCSR	2.27×10^{-3}	9.55×10^{-2}
$\mathcal{A}_{V,t}$	5.72	0.50	-1.4	LCSR	0.940	6.51×10^{-3}
$\mathcal{A}_{T,0}$	5.41	0.28	0.35	LCSR	0.128	3.15×10^{-2}

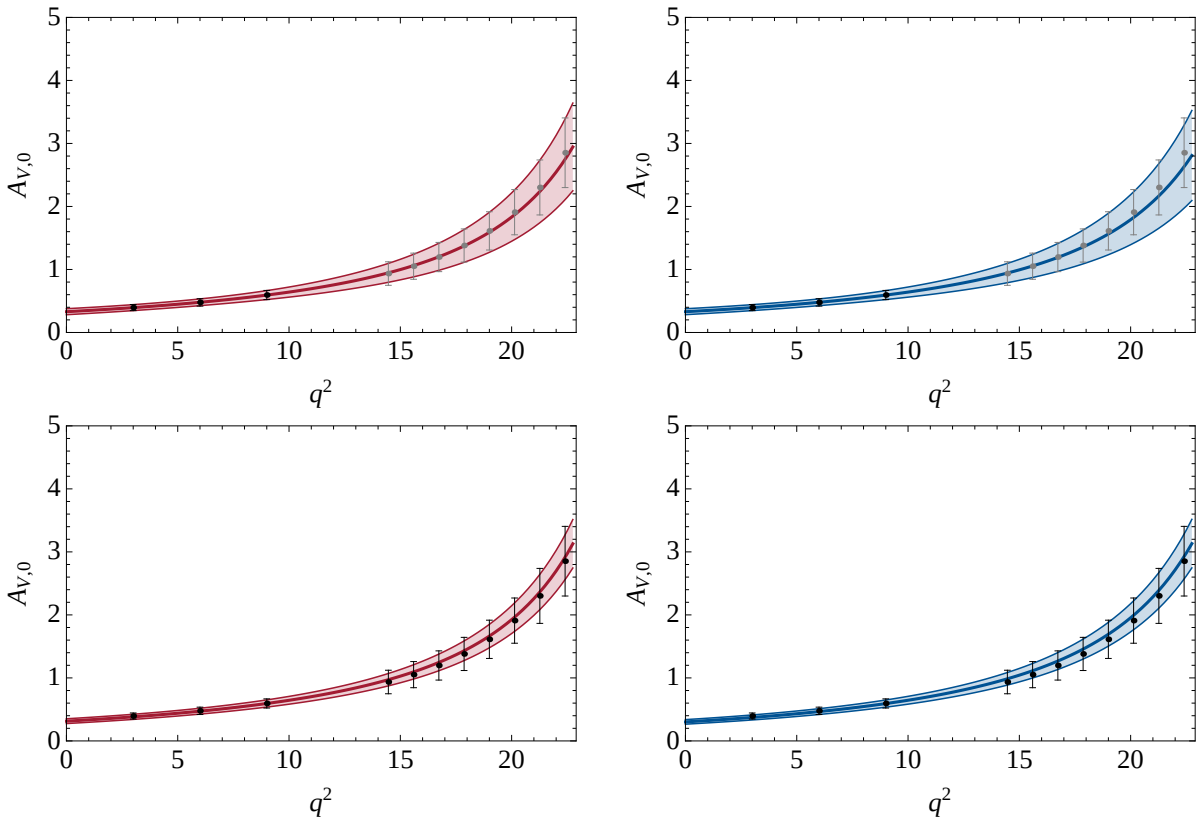

Figure 4.1: $B \to K$: Fit of SE (left) and SSE (right) parameterisations to LCSR (top) and to LCSR and Lattice (bottom) for $\mathcal{A}_{V,0}$. The LCSR and Lattice data are shown by black points with error bars in the appropriate q^2 range.

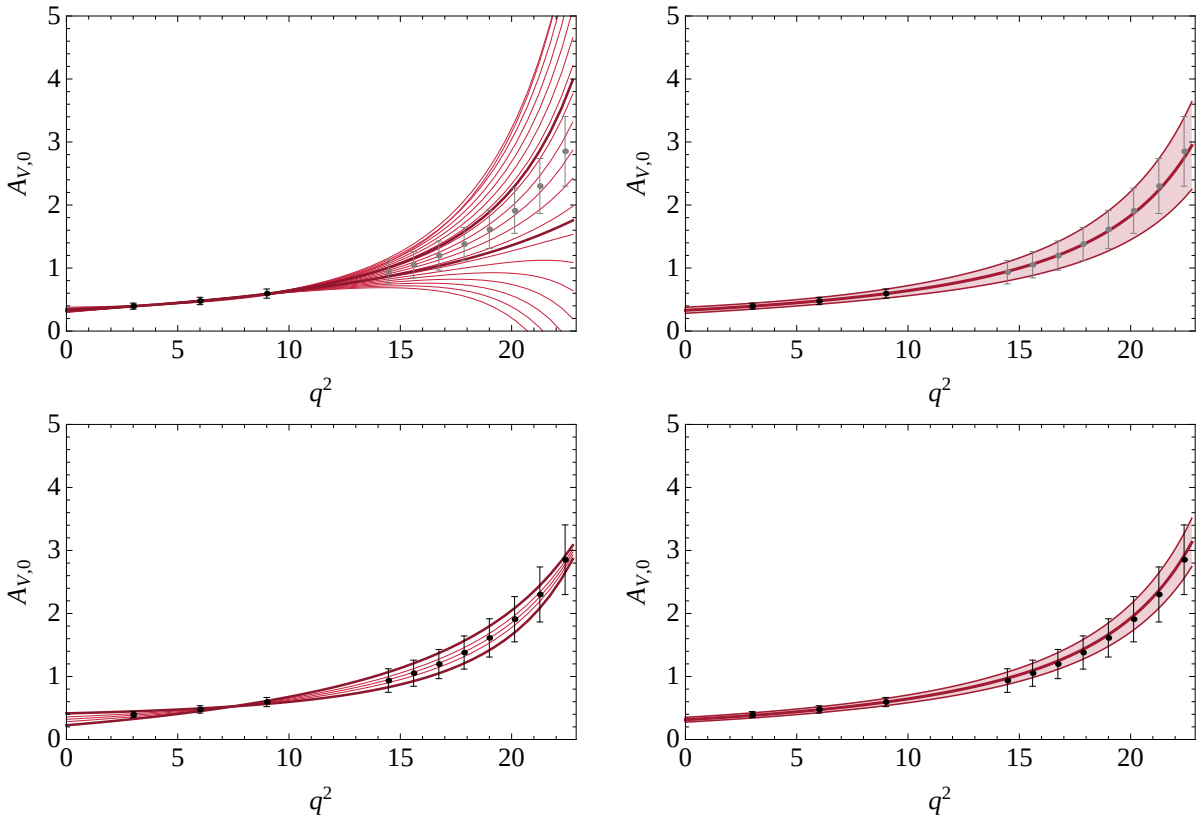

Figure 4.2: $B \to K$: Fit of the SE parameterisation to LCSR (top) and to LCSR and Lattice (bottom) for $\mathcal{A}_{V,0}$ with the parameter a_2 varied between $[-0.9, +0.9]$ (left). The thick dark lines show $a_2 = \pm 0.25$. For comparison we again show the fits truncated after a_1.

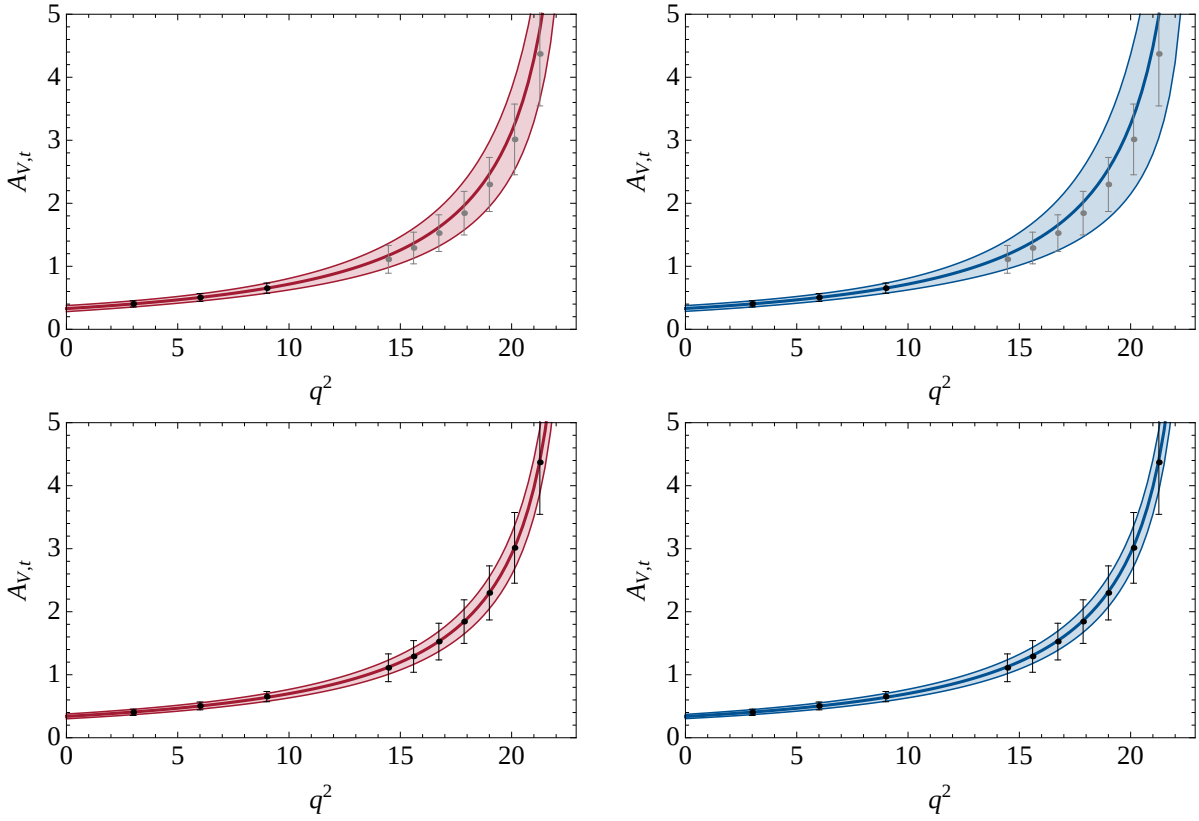

Figure 4.3: $B \to K$: Fit of SE (left) and SSE (right) parameterisations to LCSR (top) and to LCSR and Lattice (bottom) for $\mathcal{A}_{V,t}$. The LCSR and Lattice data are shown by black points with error bars in the appropriate q^2 range.

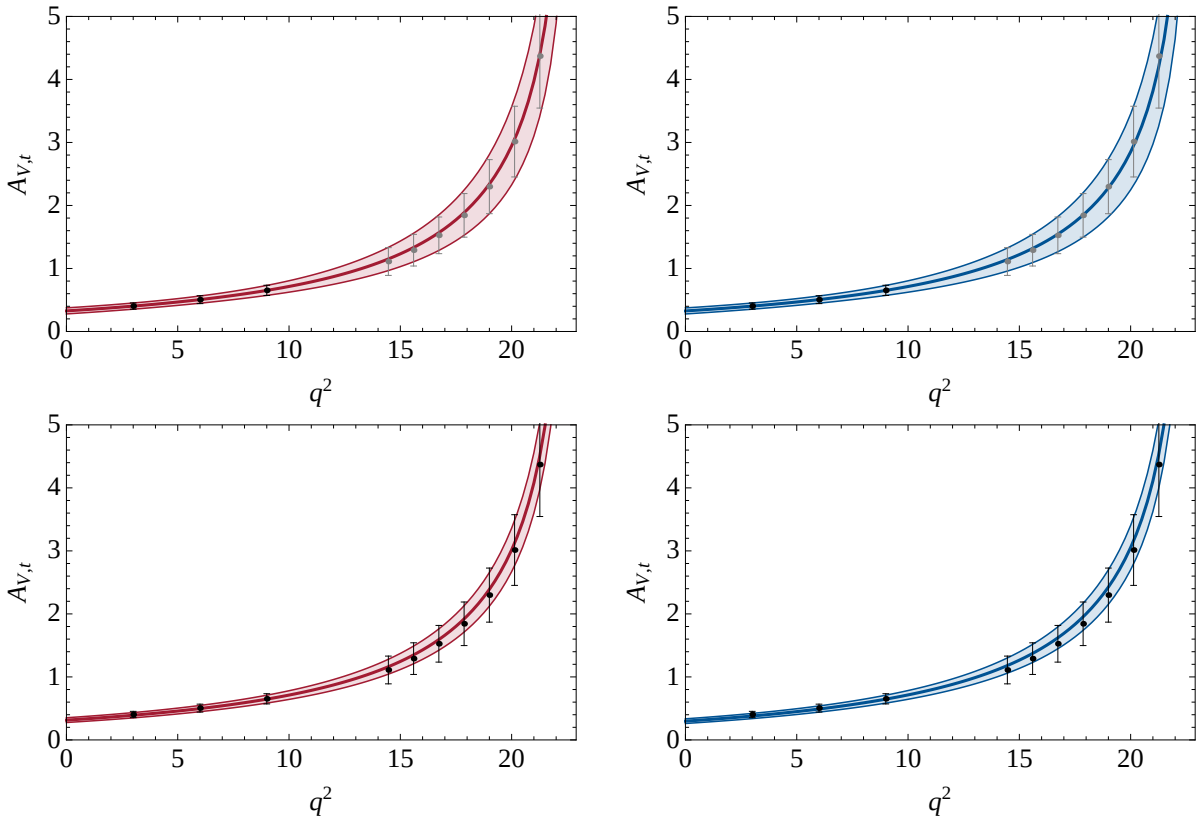

Figure 4.4: $B \to K$: The same as Fig. 4.3 but without using the scalar B_s resonance in the fit ansatz.

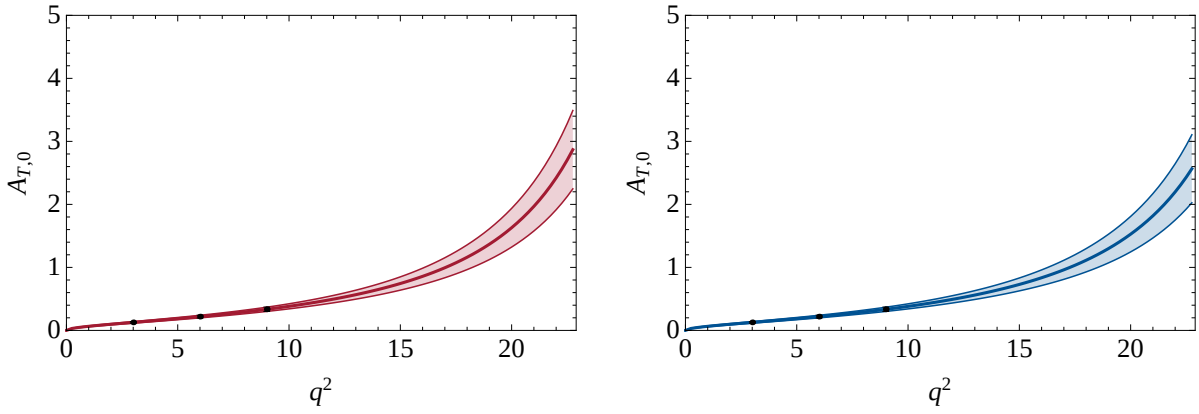

Figure 4.5: $B \to K$: Fit of SE (left) and SSE (right) parameterisations to LCSR for $\mathcal{A}_{T,0}$. The LCSR data is shown by black points with error bars.

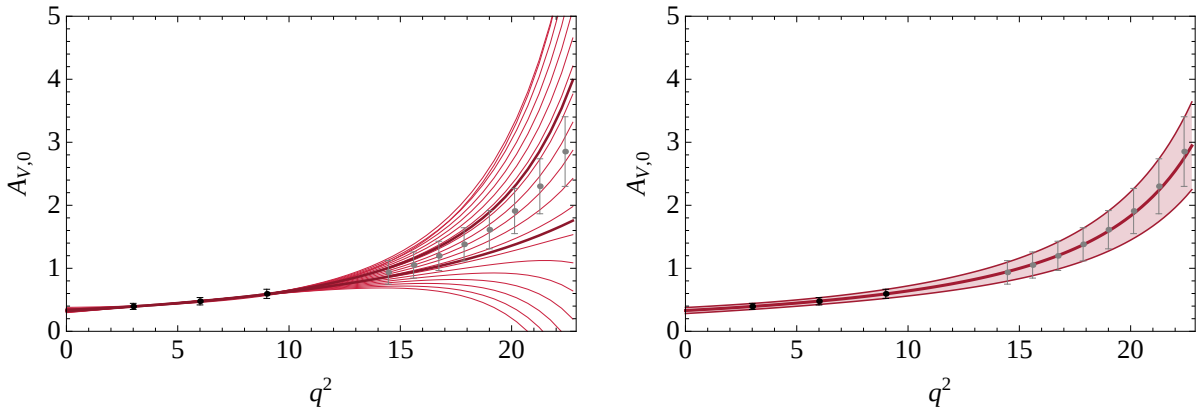

Figure 4.6: $B \to K$: Fit of the SE parameterisation to LCSR for $\mathcal{A}_{T,0}$ with the parameter a_2 varied between $[-0.9, +0.9]$ (left). The thick dark lines show $a_2 = \pm 0.25$. For comparison we again show the fit truncated after a_1.

***B → ρ* form factors:** Our FF fits for $B \to \rho$ transitions, relevant for the radiative $B \to \rho\gamma$ and $B \to \rho\ell^+\ell^-$ decays, are summarised in Figs. 4.7–4.13 and Tabs. 4.7 and 4.8, where we again compare the fit to SE and SSE parameterisations. As in the case of $B \to K$ FFs, we observe similarly good results in general for SE and SSE fits, with the dispersive bounds again playing only a minor role in restricting the coefficients of the SE/SSE. The covariance matrices for the fits can again be found in App. B.3.

Lattice results are restricted to the (axial–)vector FFs, and we again study how the fits change when the Lattice data is included: In the case of the FF $\mathcal{B}_{V,0}$, the uncertainties on the Lattice data are large, and the fit is dominated by the LCSR points at low values of q^2. Still, we find that the best-fit curve also describes the central values of the Lattice estimates well. The situation is somewhat different for $\mathcal{B}_{V,1}$, where the central values of the Lattice points do not quite agree with the extrapolation of the LCSR prediction. The fit is consistent within Lattice uncertainties, but a rather large value of χ^2, dominated by the deviations from the Lattice points, is generated. On the other hand, for $\mathcal{B}_{V,1}$ the Lattice data are competitive with the LCSR input, and we can again observe that the extrapolation of the LCSR predictions describes the Lattice points very well, while inclusion of the Lattice data in this case leads to a very precise FF description.

In the remaining cases, we provide the extrapolations for the FFs from LCSR input, as Lattice data is not currently available. Note that the uncertainties for the FF $\mathcal{B}_{T,0}$ are quite large, because we had to determine the LCSR input values from the *difference* of two FFs in Eq. (4.8). Of course, it would be desirable to directly calculate the FF $\mathcal{B}_{T,0}$ in the LCSR approach which should lead to significantly smaller uncertainties for

the input data and the extrapolation to large values of q^2. A similar comment applies to the FF $\mathcal{B}_{V,0}$.

Table 4.7: $B \to \rho$: Fit of SE parameterisation to LCSR or LCSR/Lattice results for $\mathcal{B}_{V,0-2}$ $(X = 1)$, $\mathcal{B}_{V,t}$ $(X = 3)$ and $\mathcal{B}_{T,0-2}$ $(X = 1)$.

B_X	m_R	β_0	β_1	Fit to	$\chi^2_{\rm fit}$	$X\sum_i \beta_i^2$
$\mathcal{B}_{V,0}$	5.72	-8.0×10^{-3}	2.5×10^{-2}			
$\mathcal{B}_{V,1}$	5.33	-3.5×10^{-2}	0.11	LCSR and Lattice	32.1	1.98×10^{-2}
$\mathcal{B}_{V,2}$	5.72	-2.5×10^{-2}	7.8×10^{-2}			
$\mathcal{B}_{V,0}$	5.72	-7.5×10^{-3}	1.4×10^{-2}			
$\mathcal{B}_{V,1}$	5.33	-3.7×10^{-2}	8.9×10^{-2}	LCSR	9.56×10^{-2}	1.28×10^{-2}
$\mathcal{B}_{V,2}$	5.72	-2.3×10^{-2}	5.2×10^{-2}			
$\mathcal{B}_{V,t}$	5.28	-3.2×10^{-2}	8.9×10^{-2}	LCSR	3.81×10^{-3}	2.66×10^{-2}
$\mathcal{B}_{T,0}$	5.72	-1.4×10^{-2}	-8.3×10^{-3}			
$\mathcal{B}_{T,1}$	5.33	-1.0×10^{-2}	3.4×10^{-2}	LCSR	4.18×10^{-2}	1.86×10^{-3}
$\mathcal{B}_{T,2}$	5.72	-6.3×10^{-3}	1.7×10^{-2}			

Table 4.8: $B \to \rho$: Fit of SSE parameterisation to LCSR or LCSR/Lattice results for $\mathcal{B}_{V,0-2}$ $(X = 1)$, $\mathcal{B}_{V,t}$ $(X = 3)$ and $\mathcal{B}_{T,0-2}$ $(X = 1)$.

B_X	m_R	$\tilde{\beta}_0$	$\tilde{\beta}_1$	Fit to	$\chi^2_{\rm fit}$	$X\sum_{i,j} C_{i,j}\tilde{\beta}_i\tilde{\beta}_j$
$\mathcal{B}_{V,0}$	5.72	0.26	0.14			
$\mathcal{B}_{V,1}$	5.33	0.51	-1.7	LCSR and Lattice	33.0	1.85×10^{-2}
$\mathcal{B}_{V,2}$	5.72	0.40	-0.15			
$\mathcal{B}_{V,0}$	5.72	0.26	0.50			
$\mathcal{B}_{V,1}$	5.33	0.54	-1.4	LCSR	4.34×10^{-2}	1.10×10^{-2}
$\mathcal{B}_{V,2}$	5.72	0.37	0.24			
$\mathcal{B}_{V,t}$	5.28	0.43	-1.3	LCSR	8.49×10^{-3}	2.16×10^{-2}
$\mathcal{B}_{T,0}$	5.72	0.35	0.94			
$\mathcal{B}_{T,1}$	5.33	0.52	-1.5	LCSR	3.57×10^{-2}	1.79×10^{-3}
$\mathcal{B}_{T,2}$	5.72	0.34	0.31			B

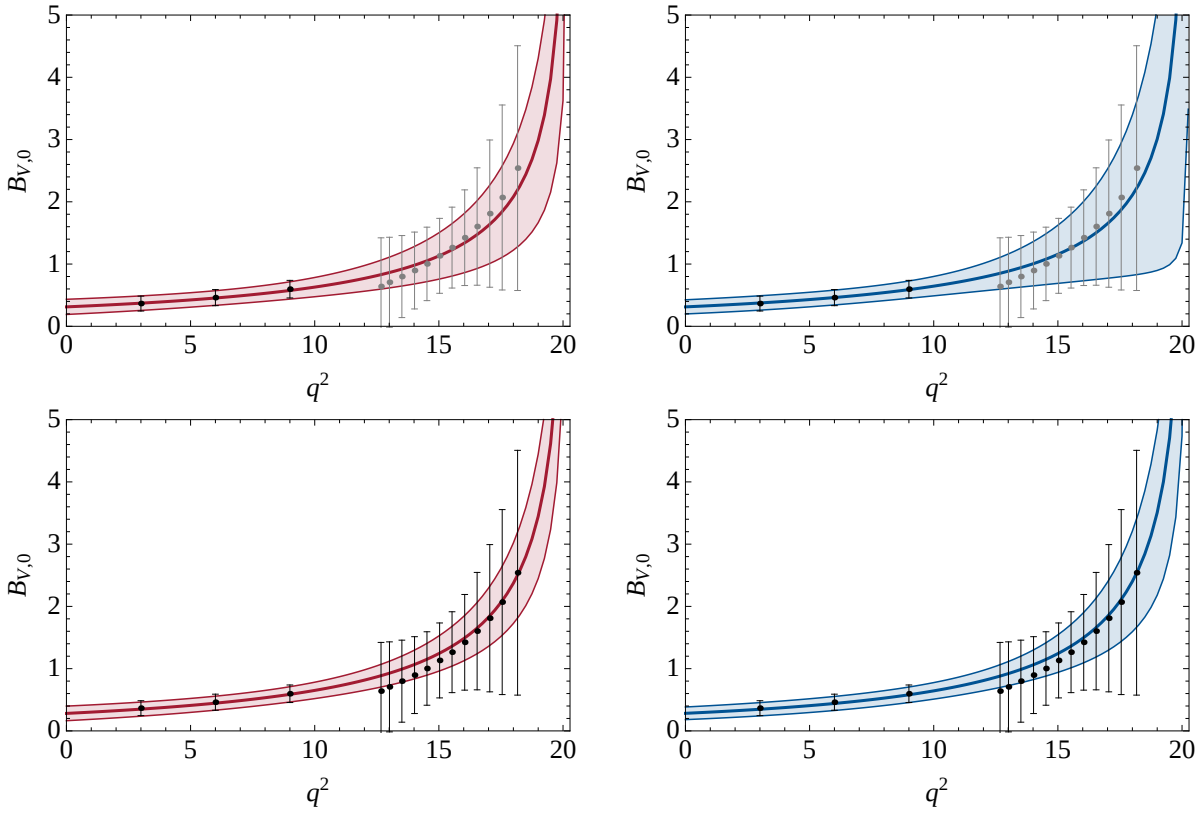

Figure 4.7: $B \to \rho$: Fit of SE (left) and SSE (right) parameterisations to LCSR (top) and to LCSR and Lattice (bottom) for $\mathcal{B}_{V,0}$. The LCSR and Lattice data are shown by black points with error bars in the appropriate q^2 range.

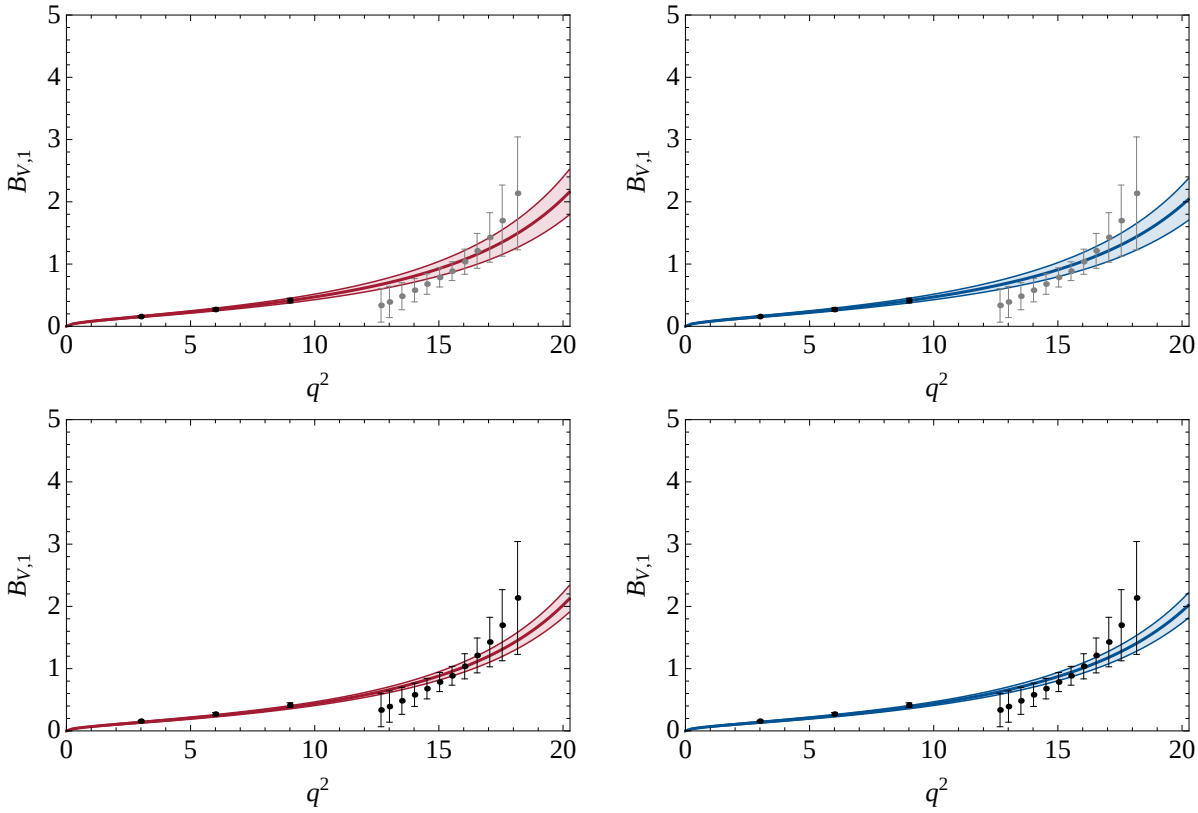

Figure 4.8: $B \to \rho$: Fit of SE (left) and SSE (right) parameterisations to LCSR (top) and to LCSR and Lattice (bottom) for $\mathcal{B}_{V,1}$. The LCSR and Lattice data are shown by black points with error bars in the appropriate q^2 range.

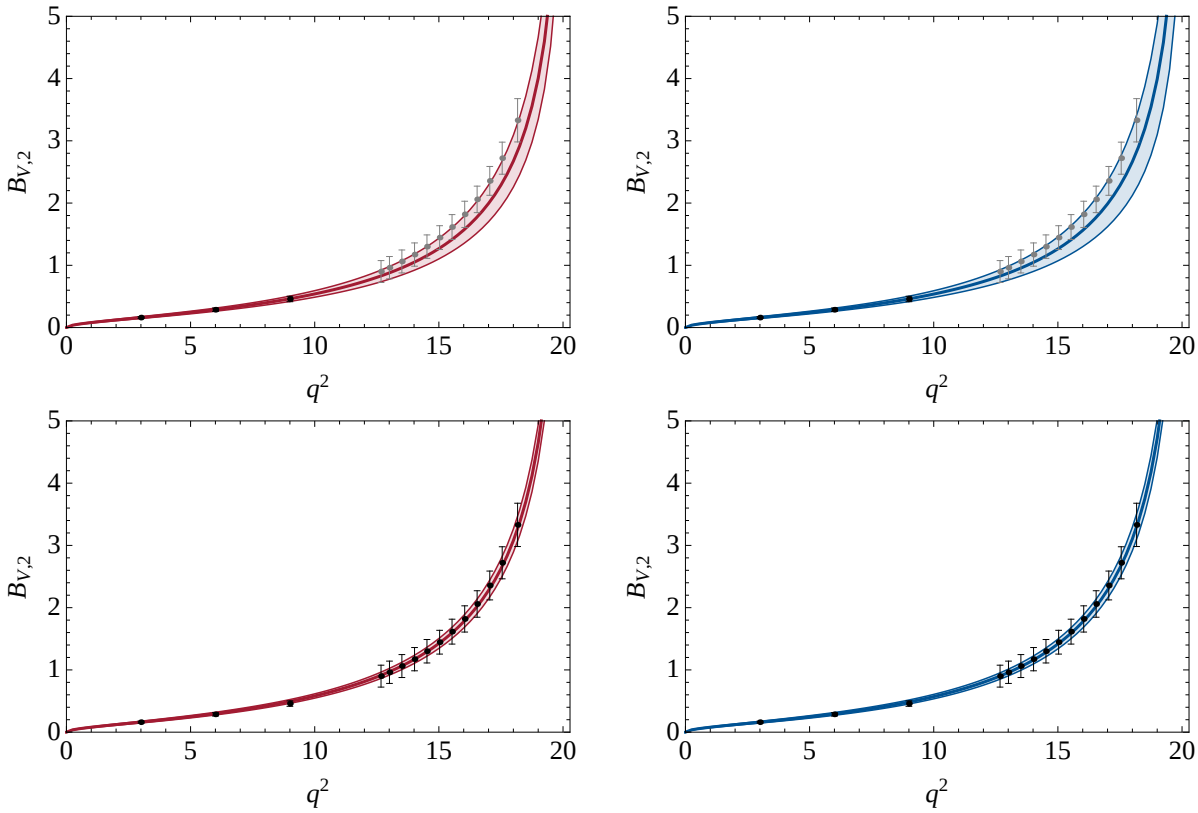

Figure 4.9: $B \to \rho$: Fit of SE (left) and SSE (right) parameterisations to LCSR (top) and to LCSR and Lattice (bottom) for $\mathcal{B}_{V,2}$. The LCSR and Lattice data are shown by black points with error bars in the appropriate q^2 range.

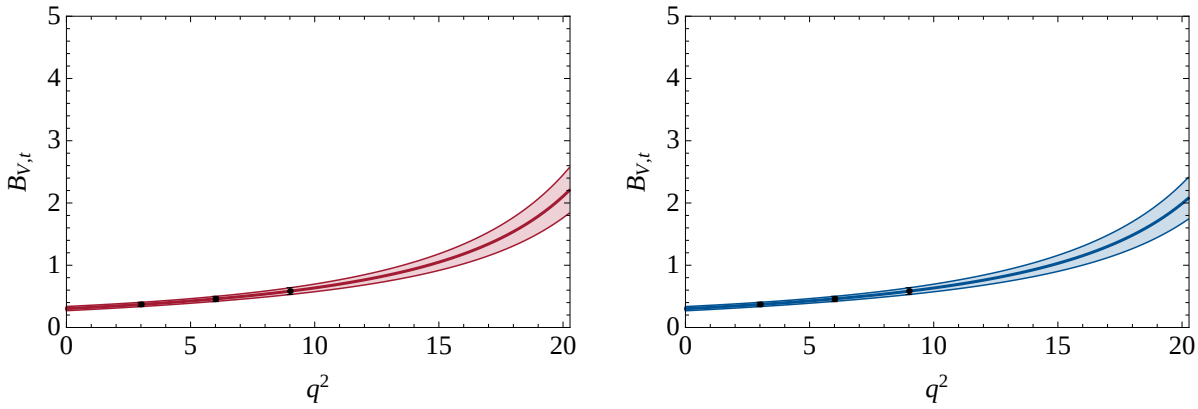

Figure 4.10: $B \to \rho$: Fit of SE (left) and SSE (right) parameterisations to LCSR for $\mathcal{B}_{V,t}$. The LCSR data is shown by black points with error bars.

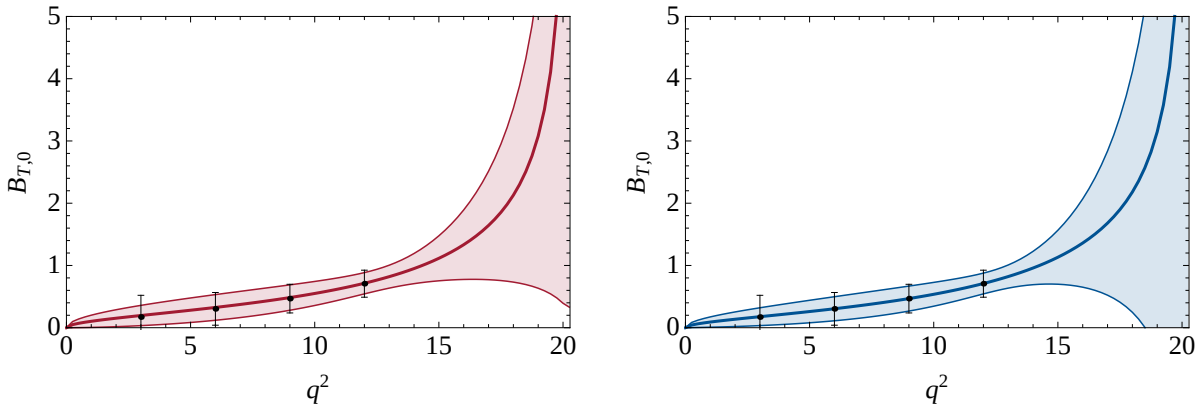

Figure 4.11: $B \to \rho$: Fit of SE (left) and SSE (right) parameterisations to LCSR for $\mathcal{B}_{T,0}$. The LCSR data is shown by black points with error bars.

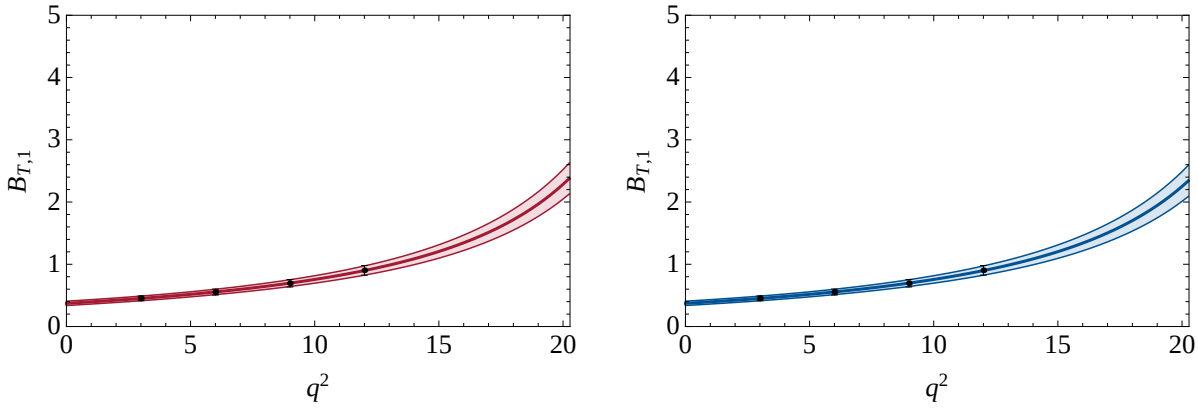

Figure 4.12: $B \to \rho$: Fit of SE (left) and SSE (right) parameterisations to LCSR for $\mathcal{B}_{T,1}$. The LCSR data is shown by black points with error bars.

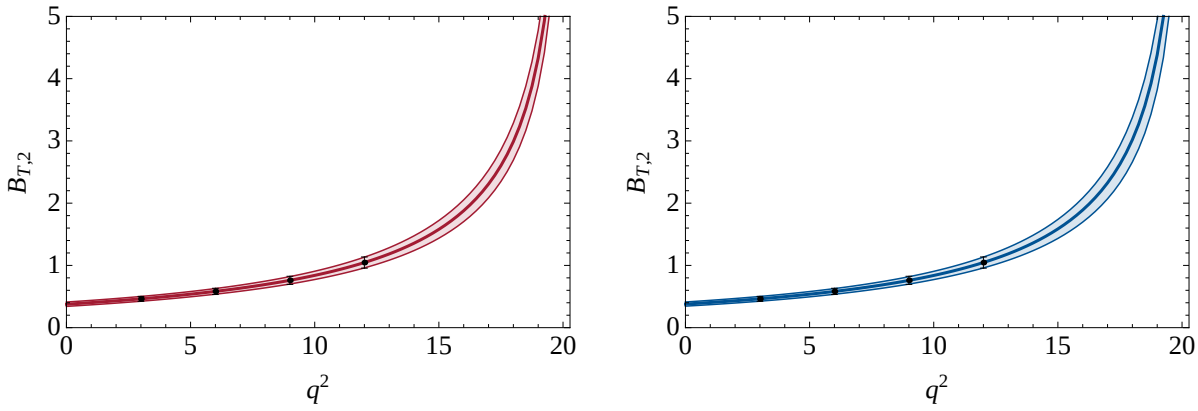

Figure 4.13: $B \to \rho$: Fit of SE (left) and SSE (right) parameterisations to LCSR for $\mathcal{B}_{T,2}$. The LCSR data is shown by black points with error bars.

B → K* and B_s → φ form factors: The analysis of $B \to K^*$ transitions is more difficult on the Lattice, as the K^*–meson is unstable. Quenched calculations on the Lattice have been attempted for the tensor FFs needed in $B \to K^*\gamma$, at $q^2 = 0$, but we do not include these results in our analysis as the other FFs for this decay have not so far been calculated. Therefore, we can only fit to the LCSR data, and our numerical results for the best-fit parameters of the SE and SSE fit are found in Tabs. 4.9 and 4.10. The covariance matrices for the fits can also be found in App. B.3.

Table 4.9: $B \to K^*$: Fit of SE parameterisation to LCSR results for $\mathcal{B}_{V,0-2}$ $(X = 1)$, $\mathcal{B}_{V,t}$ $(X = 3)$ and $\mathcal{B}_{T,0-2}$ $(X = 1)$.

B_X	m_R	β_0	β_1	Fit to	χ^2_{fit}	$X\sum_i \beta_i^2$
$\mathcal{B}_{V,0}$	5.83	-9.4×10^{-3}	1.4×10^{-2}			
$\mathcal{B}_{V,1}$	5.41	-5.0×10^{-2}	0.10	LCSR	0.149	1.86×10^{-2}
$\mathcal{B}_{V,2}$	5.83	-3.0×10^{-2}	6.8×10^{-2}			
$\mathcal{B}_{V,t}$	5.37	-4.4×10^{-2}	0.11	LCSR	1.72×10^{-3}	4.25×10^{-2}
$\mathcal{B}_{T,0}$	5.83	-1.9×10^{-2}	-1.9×10^{-2}			
$\mathcal{B}_{T,1}$	5.41	-1.4×10^{-2}	4.1×10^{-2}	LCSR	1.88×10^{-2}	3.14×10^{-3}
$\mathcal{B}_{T,2}$	5.83	-8.0×10^{-3}	2.2×10^{-2}			

Table 4.10: $B \to K^*$: Fit of SSE parameterisation to LCSR results for $\mathcal{B}_{V,0-2}$ $(X = 1)$, $\mathcal{B}_{V,t}$ $(X = 3)$ and $\mathcal{B}_{T,0-2}$ $(X = 1)$.

$B\overline{B}$ B_X	m_R	$\tilde{\beta}_0$	$\tilde{\beta}_1$	Fit to	χ^2_{fit}	$X\sum_{i,j} C_{i,j}\tilde{\beta}_i\tilde{\beta}_j$
$\mathcal{B}_{V,0}$	5.83	0.31	0.74			
$\mathcal{B}_{V,1}$	5.41	0.62	-1.4	LCSR	5.84×10^{-2}	1.63×10^{-2}
$\mathcal{B}_{V,2}$	5.83	0.45	0.35			
$\mathcal{B}_{V,t}$	5.37	0.49	-1.4	LCSR	4.63×10^{-3}	3.62×10^{-2}
$\mathcal{B}_{T,0}$	5.83	0.45	1.4			
$\mathcal{B}_{T,1}$	5.41	0.60	-1.5	LCSR	9.65×10^{-3}	2.75×10^{-3}
$\mathcal{B}_{T,2}$	5.83	0.42	0.45			

As in the case of $B \to K^*$, Lattice QCD predictions for $B_s \to \phi$ FFs are lacking, and we can only fit to the LCSR data. Our numerical results for the best-fit parameters of the SE and SSE parameterisations are found in Tabs. 4.11 and 4.12. The covariance matrices for the fits can also be found in App. B.3. In all cases, we find a good description of the LCSR input at low q^2, and from the experience in $B \to K$ and $B \to \rho$ transitions we expect the extrapolation to high q^2 to be sufficiently reliable. Still, input from Lattice computations – if feasible – for $B \to K^*$ and $B_s \to \phi$ transitions at intermediate values of q^2 would be most welcome.

Table 4.11: $B_s \to \phi$: Fit of SE parameterisation to LCSR results for $\mathcal{B}_{V,0-2}$ ($X = 1$), $\mathcal{B}_{V,t}$ ($X = 3$) and $\mathcal{B}_{T,0-2}$ ($X = 1$).

B_X	m_R	β_0	β_1	Fit to	χ^2_{fit}	$X\sum_i \beta_i^2$
$\mathcal{B}_{V,0}$	5.83	-5.8×10^{-3}	3.5×10^{-3}			
$\mathcal{B}_{V,1}$	5.41	-3.4×10^{-2}	9.6×10^{-2}	LCSR	0.124	1.29×10^{-2}
$\mathcal{B}_{V,2}$	5.83	-1.8×10^{-2}	4.7×10^{-2}			
$\mathcal{B}_{V,t}$	5.37	-3.4×10^{-2}	9.3×10^{-2}	LCSR	8.93×10^{-3}	2.96×10^{-2}
$\mathcal{B}_{T,0}$	5.83	-1.1×10^{-2}	-1.5×10^{-2}			
$\mathcal{B}_{T,1}$	5.41	-9.0×10^{-3}	3.5×10^{-2}	LCSR	4.45×10^{-2}	1.86×10^{-3}
$\mathcal{B}_{T,2}$	5.83	-4.6×10^{-3}	1.4×10^{-2}			

Table 4.12: $B_s \to \phi$: Fit of SSE parameterisation to LCSR results for $\mathcal{B}_{V,0-2}$ ($X = 1$), $\mathcal{B}_{V,t}$ ($X = 3$) and $\mathcal{B}_{T,0-2}$ ($X = 1$).

$B\overline{B}\ B_X$	m_R	$\tilde{\beta}_0$	$\tilde{\beta}_1$	Fit to	χ^2_{fit}	$X\sum_{i,j} C_{i,j}\tilde{\beta}_i\tilde{\beta}_j$
$\mathcal{B}_{V,0}$	5.83	0.37	1.1			
$\mathcal{B}_{V,1}$	5.41	0.67	-2.1	LCSR	1.44×10^{-2}	1.15×10^{-2}
$\mathcal{B}_{V,2}$	5.83	0.50	0.19			
$\mathcal{B}_{V,t}$	5.37	0.61	-1.8	LCSR	1.57×10^{-2}	2.58×10^{-2}
$\mathcal{B}_{T,0}$	5.83	0.51	1.7			
$\mathcal{B}_{T,1}$	5.41	0.66	-2.2	LCSR	3.49×10^{-2}	1.66×10^{-3}
$\mathcal{B}_{T,2}$	5.83	0.46	0.26			

4.5 Summary

We have shown that the form factors (FFs) relevant for radiative and semi-leptonic decays of B and B_s mesons into light pseudoscalar or vector mesons can be conveniently parametrised via a series expansion (SE) in the variable $z(t)$ (see the definition in Eq. (4.11)). With the current accuracy of theoretical estimates from light-cone sum rules (LCSRs) and (where available) Lattice QCD, we found that keeping only two terms in the expansion and correctly implementing the analytical behaviour due to below-threshold resonances, results in a very good description of the FFs over the whole range of momentum transfer in the physical decay region.

The coefficients of the SE are further constrained by dispersive bounds, exploiting the crossing symmetry between the physical B meson decay and the pair-production of heavy and light mesons by the considered decay current. In order to put the discussion for the various FFs on a common footing, we found it convenient to use a basis where the decay/production currents are projected by transverse, longitudinal and time-like polarisation vectors with respect to momentum transfer t. Considering the corresponding projections for the current correlators, the constraints take the simple form as indicated in Eqs. (4.43,4.44). We stress that for decays into vector mesons the dispersive bounds constrain the *sum* of (squared) coefficients for the three axial-vector FFs, as well as for the three tensor FFs. In a simultaneous fit of all FFs, these constraints are thus stronger than those for the individual FFs in that sum.

In order to determine the correct normalisation of the SE, given by the profile functions $\phi(z(t))$, we calculate the current correlators using an OPE, including NLO perturbative corrections and the leading non-perturbative contributions from quark, gluon and mixed condensates. In particular, we provide the NLO results for the perturbative contribution to the tensor-current correlation functions, which are relevant for the FFs appearing in radiative and rare semi-leptonic B decays.

With these theoretical tools at hand, we have performed numerical fits to LCSR (Lattice) predictions at low (medium) momentum transfer for all the FFs appearing in $B \to K, \rho, K^*$ and $B_s \to \phi$ transitions. We have also investigated a simplified form of the SE, where the profile functions $\phi(z(t))$ are re-expanded in powers of $z(t)$, while the dispersive bounds take a somewhat more complicated form. We find that both the standard and the simplified SE give a similarly good description of the FF functions. In those cases, where Lattice estimates of the FFs is lacking, the SE is used

to extrapolate the LCSR predictions to the high-q^2 region. Comparing fits with/without using the available Lattice data for $B \to K$ and $B \to \rho$ transitions, we judge these extrapolations to be rather reliable. Some of our results could be further improved in the future by the following: experimentally confirming a scalar B_s resonance below B–K threshold, contributing to the scalar $B \to K$ FF; decreasing the uncertainties in Lattice predictions for $B \to \rho$ axial-vector FFs; calculating LCSRs directly in the helicity basis and computing of $B \to K^*$ and $B_s \to \phi$ FFs on the Lattice with dynamical fermions.

In conclusion, we have shown that the parameterisation of heavy-to-light FFs as a truncated series expansion in $z(t)$ in combination with theoretical estimates from LCSRs and Lattice QCD is very useful, not only for the determination of the CKM element $|V_{ub}|$ from charged semi-leptonic $B \to \pi$ or $B \to \rho$ decays, but also for the description of FFs for radiative and semi-leptonic $b \to s$ and $b \to d$ transitions, which will continue to play a major role for the indirect search of new physics effects from rare flavour decays.

Chapter 5

The $B \to \pi$ Form Factor in Light-Cone Sum Rules at NNLO

5.1 Introduction

Improving the precision on $|V_{ub}|$ helps in the effort to overconstrain the sides of the unitarity triangle, one of which is given by $|V_{ub}/|V_{cb}|$, thereby testing the CKM mechanism of the Standard Model. The semi-leptonic decay $B \to \pi l \nu$ offers a determination, promising both theoretically and experimentally. Being an exclusive mode, extracting $|V_{ub}|$ requires information about the relevant hadronic matrix element, parametrised by the form factors $f_+(q^2)$ and $f_-(q^2)$ defined in Eq. (1.31).

In the limit of massless leptons, applicable to $l = e$ and μ, only $f_+(q^2)$ is required [166],

$$\frac{d\Gamma}{dq^2}(B^0 \to \pi^- l^+ \nu_l) = \frac{G_F^2 |V_{ub}|^2}{192\pi^3 m_B^3} \lambda^{3/2}(q^2) |f_+(q^2)|^2, \tag{5.1}$$

where G_F is the Fermi coupling constant and $\lambda(q^2) = (m_B^2 + m_\pi^2 - q^2)^2 - 4m_B^2 m_\pi^2$ for masses m_B and m_π of the B and π mesons respectively. Therefore the extraction of $|V_{ub}|$ relies on the theoretical prediction for $f_+(q^2)$, via Lattice QCD or LCSR. Recent calculations are summarised in Tab. 5.1.

As discussed in Ch. 4, LCSR are restricted to large recoil energies of the pion, corresponding to $q^2 \lesssim 14$ GeV, and Lattice results to small values of the pion momentum, i.e. $q^2 \gtrsim 15$ GeV. However, note that the form factor at $q^2 = 0$ was recently obtained in a quenched calculation on a very fine lattice [67]. Experimentally the q^2 distribu-

tion has been measured with increasing accuracy at CLEO [169; 170], Babar [171–173] and Belle [174]. In order to maximally exploit these theoretical and experimental results, one requires a well motivated parameterisation for the q^2 dependence of $f_+(q^2)$. There are a number of approaches, either assuming vector meson dominance as in Refs. [144; 167], using dispersive bounds to constrain the coefficients of a series expansion as in Refs. [146; 148] or using the Omnès representation as in Refs. [145; 175]. In all these, the normalisation provided by the LCSR prediction at $q^2 = 0$ plays a crucial role.

We are interested in calculating the gauge invariant subset of two-loop radiative corrections to $f_+(0)$ proportional to β_0, making the assumption, to be discussed in Sec. 5.3, that these are a good approximation to the complete next-to-next-to-leading order (NNLO) result. In addition to the motivation already mentioned, this calculation will allow us to investigate the size of these radiative corrections in view of the large two-loop corrections calculated for f_B in QCD sum rules [176; 177]. The LCSR approach to form factors involves taking the ratio of $f_B f_+(q^2)$ to f_B. We therefore test the argument that radiative corrections to these quantities should cancel in this ratio when both are calculated in sum rules. The form factor $f_+(q^2)$ has already been calculated in LCSR to high accuracy. The next-to-leading order (NLO) twist-2 corrections were calculated in Ref. [178] and the leading order (LO) corrections up to twist-4 were calculated in Ref. [179]. Since the LO twist-3 contribution was found to be large, further improvements were made by calculating the NLO corrections in Ref. [167]. A recent update where the $\overline{\text{MS}}$ mass is used in place of the pole mass for m_b can be found in Ref. [168].

The rest of this chapter is structured as follows: Sec. 5.2 contains the set-up for the calculation, including the expression for the one-loop correction at leading-twist; in Sec. 5.3 we discuss Naïve Non-abelianisation, and give details of the two-loop calculation; in Sec. 5.4 we describe the structure of the divergences of the bare result and the

Method	Collaboration	Ref.
LCSR	Ball and Zwicky	[167]
LCSR	Duplančić *et al.*	[168]
LQCD	HPQCD	[69]
LQCD	Fermilab-MILC	[66]

Table 5.1: Summary of the latest theoretical calculations of $f_+(q^2)$ in QCD sum rules on the light-cone (LCSR) and unquenched Lattice QCD (LCQD).

renormalisation procedure; a detailed analysis of our numerical results, paying particular attention to f_B and the moments of the twist-2 light-cone distribution amplitude, can be found in Sec. 5.5; finally we summarise in Sec. 5.6.

5.2 Set-up of the Calculation

The leading-order light-cone sum rule at twist-2 for $f_+(q^2)$ is derived in Ch. 1. Returning to the correlator introduced in Eq. (1.29), we now consider the perturbative corrections to the leading-twist term in the expansion about the light-cone $x^2 = 0$, as calculated to NLO in Ref. [178]. In analogy to Eq. (1.34), we express the correlator in the collinearly factorised form,

$$\Pi_\mu(p_B^2, q^2) = \sum_n \int du\, \mathcal{T}_\mu^{(n)}(u, \mu^2)\phi^{(n)}(u, \mu^2). \tag{5.2}$$

We can then obtain the twist-2 contribution using the completeness relation,

$$\bar{u}_a d_b = \frac{1}{4}\mathbb{1}_{ba}(\bar{u}d) - \frac{1}{4}(i\gamma_5)_{ba}(\bar{u}i\gamma_5 d) + \frac{1}{4}(\gamma_\mu)_{ba}(\bar{u}\gamma^\mu d) - \frac{1}{4}(\gamma_\mu\gamma_5)_{ba}(\bar{u}\gamma^\mu\gamma_5 d) + \dots . \tag{5.3}$$

Despite only being valid in four dimensions, we can use this relation as the additional terms arising in D dimensions, required for dimensional regularisation, are found to cancel with corresponding terms arising in association with the counterterms. More specifically, we obtain the leading-twist hard scattering kernel, $\mathcal{T}_\mu^{(2)}(u, \mu^2)$, using the projector

$$\frac{i}{4} f_\pi \not{p}\gamma_5 \int_0^1 du\, e^{i\bar{u}p\cdot x}\phi(u, \mu^2). \tag{5.4}$$

The tree-level term $\Pi_\mu^{(0)}$ is then found to be

$$\Pi_\mu^{(0)} = -\frac{1}{4} f_\pi\, m_b \int_0^1 du\, \phi(u, \mu^2)\, tr\{\gamma_\mu \frac{\not{p}_B - \bar{u}\not{p} + m_b}{(p_B - \bar{u}p)^2 - m_b^2}\not{p}\}, \tag{5.5}$$

where we have perturbatively expanded the leading-twist contribution to the correlator,

$$\Pi_\mu^{\mathrm{T2}} = \int du\, \mathcal{T}_\mu^{(2)}(u, \mu^2)\phi(u, \mu^2) \tag{5.6}$$

$$= \Pi_\mu^{(0)} + \frac{\alpha_s}{4\pi}\Pi_\mu^{(1)} + \left(\frac{\alpha_s}{4\pi}\right)^2 N_f\, \Pi_\mu^{(2)} \dots . \tag{5.7}$$

The $\mathcal{O}(\alpha_s)$ radiative corrections to the correlator, involving six further diagrams, were first calculated in Ref. [178],

$$\Pi_\mu^{(1)} = \frac{\mathcal{N}}{4}\int_0^1 du\,\phi(u,\mu^2)\int\frac{d^Dk}{(2\pi)^D}\frac{g^{\alpha\beta}}{k^2}F_\mu^{\rm T}, \tag{5.8}$$

where the normalisation $\mathcal{N}$ is defined as

$$\mathcal{N} = -i\,(4\pi)^2\,C_F f_\pi\,m_b. \tag{5.9}$$

$F_\mu^{\rm T}$ contains the total contribution of the traces and fermionic propagators for the weak-vertex correction, B-vertex correction, box, b quark self-energy and light quark self-energy diagrams. We do not include the gluon propagator in $F_\mu^{\rm T}$ for reasons that will become clear later. To be explicit, we define $F_\mu^{\rm T}$ to be

$$F_\mu^{\rm T} = F_\mu^{\rm WV} + F_\mu^{\rm BV} + F_\mu^{\rm BX} + F_\mu^{\rm SE} + F_\mu^{\rm LSE}, \tag{5.10}$$

where the contribution of individual diagrams in Feynman gauge are found to be

$$F_\mu^{\rm WV} = tr\{\gamma_\alpha\frac{\not k - u\not p}{(k-up)^2}\gamma_\mu\frac{\not q - \not k + u\not p + m_b}{(q-k+up)^2-m_b^2}\gamma_\beta\frac{\not p_B - \bar u\not p + m_b}{(p_B-\bar up)^2-m_b^2}\not p\} \tag{5.11}$$

$$F_\mu^{\rm BV} = tr\{\gamma_\mu\frac{\not p_B - \bar u\not p + m_b}{(p_B-\bar up)^2-m_b^2}\gamma_\alpha\frac{-\not p_B - \not k + \bar u\not p - m_b}{(p_B+k-\bar up)^2-m_b^2}\frac{\not k - \bar u\not p}{(k-\bar up)^2}\gamma_\beta\not p\} \tag{5.12}$$

$$F_\mu^{\rm BX} = tr\{\gamma_\alpha\frac{u\not p - \not k}{(up-k)^2}\gamma_\mu\frac{\not p_B - \bar u\not p - \not k + m_b}{(p_B-\bar up-k)^2-m_b^2}\frac{\not k + \bar u\not p}{(k+\bar up)^2}\gamma_\beta\not p\} \tag{5.13}$$

$$F_\mu^{\rm SE} = tr\{\gamma_\mu\frac{\not p_B - \bar u\not p + m_b}{(p_B-\bar up)^2-m_b^2}\gamma_\alpha\frac{-\not p_B + \bar u\not p + \not k - m_b}{(p_B-\bar up-k)^2-m_b^2}\gamma_\beta\frac{\not p_B - \bar u\not p + m_b}{(p_B-\bar up)^2-m_b^2}\not p\}. \tag{5.14}$$

As in previous calculations, we take the limit that the light quarks are massless, i.e. $p^2 = 0$, such that the self-energy diagrams for the external light quarks only contribute logarithmic terms in dimensional regularisation, which we will return to in Sec. 5.4. As stated earlier, the diagrams for the $\mathcal{O}(\alpha_s)$ corrections have all been calculated by a number of authors in the past so here we will only discuss the technical details for the $\mathcal{O}(\alpha_s^2\beta_0)$ corrections. We also will not discuss details of the higher twist calculations, which can be found in Ref. [167], although these will be incorporated in our numerical analysis.

5.3 Radiative Corrections at Order $\alpha_s^2\beta_0$

In analogy with QED, where the running of the β-function is connected to the photon polarisation, Brodsky, Lepage and Mackenzie had the idea that one can associate the running of the QCD β-function with fermion loop insertions in the lowest order corrections, provided the tree-level diagram does not contain any gluons. The running of the β-function for QCD is given by $\beta = \alpha_s/(4\pi)\,\beta_0 + \ldots$ where $\beta_0 = 11C_A - 2/3\,N_f$. The scale of the lowest order correction can therefore be set by demanding that this contribution to the two-loop correction vanishes, a procedure known as BLM scale setting [180].

In Ref. [181], it was observed that in a number of cases where the left-over part of the two-loop correction could be calculated e.g. higher order corrections to observables from hadronic vacuum polarisation and to the pole mass, it was found to be small in comparison to the fermion-loop contribution. Here a technique labelled Naive Non-abelianisation (NNA) was proposed, where "the non-abelian theory is estimated by replacing the leading term in the β-functions of the large-N_f abelian theory by its non-abelian counterpart". Further, in Refs. [182; 183], a generalisation of the BLM scale setting was proposed, whereby fermion loop insertions in the lowest order corrections were re-summed to all orders. The one-loop running of α_s has the potential to generate large corrections, and by setting the scale in this way one can reduce the uncertainty of an observable due to the lack of exact higher order results.

BLM scale-setting and NNA are not entirely distinct techniques, however, in BLM scale-setting the left-over part of the two-loop correction is not required to be small, but NNA asserts that this is the case. We therefore calculate fermion-loop insertions in $\mathcal{O}(\alpha_s)$ diagrams and replace N_f in the resulting expressions by $-(3/2)\beta_0 \equiv N_f - 33/2$. According to the NNA philosophy, this is a good approximation to the complete two-loop result. The corrections take the form,

$$\Pi_\mu^{(2)} = \mathcal{N} \int_0^1 du\, \phi(u,\mu^2) \int \frac{d^Dk}{(2\pi)^D} \frac{\Gamma(\epsilon)\Gamma(2-\epsilon)^2}{\Gamma(4-2\epsilon)} \left(\frac{-k^2}{4\pi\mu^2}\right)^{-\epsilon} \frac{1}{k^2} \left(g^{\alpha\beta} - \frac{k^\alpha k^\beta}{k^2}\right) F_\mu^{\mathrm{T}}, \tag{5.15}$$

where F_μ^{T} is as defined in Eq. (5.10). The relevant Feynman diagrams are shown in Fig. 5.1. The calculation is similar to the one-loop case, however, the additional fermion loop induces two important changes. Firstly, the tensor structure of the gluon propagator

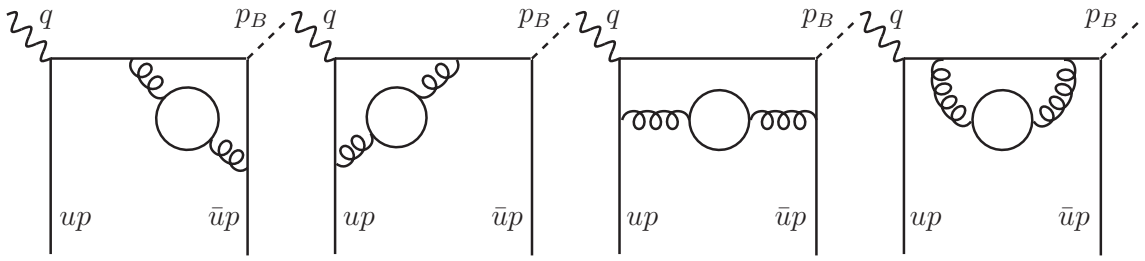

Figure 5.1: Feynman diagrams for $\mathcal{O}(\alpha_s^2\beta_0)$ corrections to Π_μ^{T2}. From left to right, the B-vertex correction, weak vertex correction, box and b quark self-energy diagrams are shown. The external quarks are on-shell with momenta as indicated and the dashed line represents the B meson.

changes from the form

$$\frac{-ig^{\alpha\beta}}{k^2} \to \frac{-i}{k^2}\left(g^{\alpha\beta} - \frac{k^\alpha k^\beta}{k^2}\right) \tag{5.16}$$

resulting in additional terms in the trace (although these cancel in the sum of all diagrams due to gauge invariance [184]). Secondly, the factor $\Gamma(\epsilon)$ means that the integrals must be expanded to a higher order in ϵ. The increased complexity of the calculation is slightly compensated by the fact that we set $q^2 = 0$. More specifically, we perform the traces using the mathematica package FeynCalc [185], and calculate the integrals using Feynman parameters to rearrange them such that we can apply the useful formula found in Ref. [44]. We then expand the hypergeometric functions using the mathematica package HypExp [186]. The resulting expression must then be simplified and rearranged into a form facilitating the convolution with the distribution amplitude, a task which requires the use of a number of known di- and tri-logarithmic identities, for example,

$$\begin{aligned}\mathrm{Li}_3(z) =& -\mathrm{Li}_3\left(\frac{z}{z-1}\right) - \mathrm{Li}_3\left(\frac{1}{1-z}\right) + \frac{1}{3}\log^3(1-z) - \frac{1}{2}\log(-z)\log^2(1-z) \\ & - \frac{1}{6}\pi^2\log(1-z) + \zeta(3)\,, \quad z \notin (1,\infty)\end{aligned} \tag{5.17}$$

$$\mathrm{Li}_3(z) = \mathrm{Li}_3\left(\frac{1}{z}\right) - \frac{1}{6}\log^3(-z) - \frac{i\,\pi}{2}\left(\sqrt{\frac{z-1}{z}}\sqrt{\frac{z}{z-1}} - 1\right)\log^2(z) - \frac{1}{6}\pi^2\log(-z) \tag{5.18}$$

5.4 Structure of the Divergences

The bare $\mathcal{O}(\alpha_s^2 N_f)$ results, containing both infra-red (IR) and ultra-violet (UV) divergences, are treated in naïve dimensional regularisation, with totally anti-commuting γ_5, renormalising the UV divergences in the $\overline{\text{MS}}$ scheme. As mentioned earlier, although the light quark self energy diagrams vanish, the UV and IR divergences arising from these diagrams cannot be neglected:

$$\begin{aligned}\Pi_\mu^{(2),\text{LSE}} &= \mathcal{N}\int_0^1 du\,\phi(u,\mu^2)\int\frac{d^Dk}{(2\pi)^D}\frac{\Gamma(\epsilon)\Gamma(2-\epsilon)^2}{\Gamma(4-2\epsilon)}\left(\frac{-k^2}{4\pi\mu^2}\right)^{-\epsilon}\frac{1}{k^2}\left(g^{\alpha\beta}-\frac{k^\alpha k^\beta}{k^2}\right)F_\mu^{\text{LSE}}\\ &= \frac{1}{2}C_F\,N_f\,\Pi_\mu^{(0)}\left(\frac{1}{\epsilon_{\text{UV}}}-\ln\frac{m_B^2}{\mu_{\text{UV}}^2}-\frac{1}{\epsilon_{\text{IR}}}+\ln\frac{m_B^2}{\mu_{\text{IR}}^2}\right),\end{aligned} \tag{5.19}$$

where $D = 4 - 2\epsilon$, and we distinguish between the UV and IR scales μ_{UV} and μ_{IR}.

On adding all the diagrams together, we first perform the gluon self-energy renormalisation using the $\mathcal{O}(\alpha_s N_f)$ contribution to the corresponding renormalisation constant $Z_{3\text{YM}}$, multiplied by $\Pi_\mu^{(1)}$, where [44]

$$Z_{3\text{YM}}^{(2n_f)} = -\frac{\alpha_s}{4\pi}C_F N_f\left(\frac{2}{3\epsilon}\right). \tag{5.20}$$

This results in a counter-term of the form

$$\Pi_\mu^{(2),\text{CT}} = \mathcal{N}\int_0^1 du\,\phi(u,\mu^2)\int\frac{d^Dk}{(2\pi)^D}\left(\frac{1}{6\epsilon}\right)\frac{1}{k^2}\left(g^{\alpha\beta}-\frac{k^\alpha k^\beta}{k^2}\right)F_\mu^{\text{T}}. \tag{5.21}$$

The remaining UV poles can be removed by mass renormalisation, using the $\mathcal{O}(\alpha_s^2 N_f)$ contribution to the renormalisation constants Z_m,

$$Z_m^{(2n_f)} = \left(\frac{\alpha_s}{4\pi}\right)^2 C_F N_f\left(-\frac{1}{\epsilon^2}+\frac{5}{6\epsilon}\right). \tag{5.22}$$

The result is now UV finite, and we factorise the remaining IR divergences into the form of a renormalisation constant which we will refer to as $Z_T^{(2n_f)}$.

In order to achieve a complete cancellation of the IR divergences, one must consider the renormalisation group (RG) running of the bare DA. This can be expressed in terms

of the evolution kernel $V(u,v)$, defined by

$$\mu^2 \frac{d}{d\mu^2}\phi(u,\mu^2) = \int_0^1 dy\, V(u,v)\phi(y,\mu^2). \tag{5.23}$$

It was first calculated to two-loop accuracy in Refs. [187; 188]. We require the contribution at $\mathcal{O}(\alpha_s^2 N_f)$,

$$V(u,v) = \frac{\alpha_s}{2\pi}\, V_0(u,v) + \left(\frac{\alpha_s}{2\pi}\right)^2 \tfrac{1}{2} N_f\, C_F\, V_N(u,v) + \dots\,, \tag{5.24}$$

where expressions for $V_0(u,v)$ and $V_N(u,v)$ can be found in Ref. [188], and the ellipses indicate other $\mathcal{O}(\alpha_s^2)$ and higher order terms. This RG running arises due to the UV singularity of the DA, which can be expressed in terms of the renormalisation function $Z_\phi(u,v)$, related to $V(u,v)$ via (see Ref. [184])

$$V(u,v) = -\frac{1}{Z_\phi(u,v)}\left(\mu^2 \frac{\partial}{\partial \mu^2} Z_\phi(u,v)\right). \tag{5.25}$$

$Z_\phi^{(2n_f)}(u,v)$, i.e. the $\mathcal{O}(\alpha_s^2 N_f)$ contribution to $Z_\phi(u,v)$, can be expressed in terms of $V_N(u,v)$ by

$$Z_\phi^{(2n_f)}(u,v) = \left(\frac{\alpha_s}{4\pi}\right)^2 C_F N_f \frac{V_N(u,v)}{\epsilon}. \tag{5.26}$$

Note that, as we use the asymptotic DA, the contribution due to $V_0(u,v)$ vanishes on convolution with the DA, and therefore we neglect the terms $\sim V_0(u,v)/\epsilon^2$. On explicit calculation, when the IR scale is set to be equal to the factorisation scale, we find that the UV divergence of the DA ($Z_\phi^{(2n_f)}(u,v)$) cancels the IR divergence of the hard scattering kernel ($Z_T^{(2n_f)}$) exactly at $\mathcal{O}(\alpha_s^2 N_f)$. Therefore $Z_T^{(2n_f)}$ can be absorbed into the DA, as discussed in detail in Ref. [189]. Note that replacing the $\overline{\text{MS}}$ mass for m_b by the pole mass [190] removes all UV scale dependence of our result. All remaining scale dependence is therefore given by the factorisation scale, which in the following will be denoted by μ.

5.5 Results

Now, having shown that our results for the perturbative corrections at $\mathcal{O}(\alpha_s^2 N_f)$ are UV and IR finite, we can proceed to analyse how this affects the value of the form factor

at zero recoil, $f_+(0)$. First we require predictions for the twist-2, 3 and 4 light-cone distribution amplitudes. We then must extract the spectral density from the correlation function Π_μ. Finally we need the QCD sum rules result for the B meson decay constant f_B. We will discuss these steps before coming to the numerical analysis.

5.5.1 Distribution Amplitudes

Light-cone distribution amplitudes (DA's) describe the matrix elements of non-local operators expanded about the light-cone i.e. $x^2 = 0$. They contain the distribution of the momentum fraction of partons in the hadron's infinite momentum frame. The theory of DA's is well known (see e.g. Ref. [191]). They are ordered by twist and at leading-twist the pion DA $\phi(u,\mu)$ in the Fock-Schwinger or light-cone gauge is defined by

$$\langle \pi(p)|\bar{u}(0)\gamma_\mu\gamma_5\, d(x)|0\rangle = -if_\pi p_\mu \int_0^1 du\, e^{i\bar{u}p\cdot x}\phi(u,\mu^2). \tag{5.27}$$

Due to the conformal symmetry of QCD broken by radiative corrections, the leading-twist pion DA can be expressed in terms of a partial wave expansion in conformal spin,

$$\phi(u,\mu^2) = 6u(1-u)\sum_{n=0}^{\infty} a_n(\mu^2)C_n^{3/2}(2u-1). \tag{5.28}$$

In the case of the pion, the odd moments are zero by G-parity. This expansion is usually truncated, as the higher moments are suppressed due to the highly oscillatory behaviour of the Gegnbauer polynomials. However, the truncation is only justified if the hard scattering kernel $\mathcal{T}_\mu^{(n)}$ is slowly varying and non-singular for all u [192]. We include the DA up to a_4 for the $\mathcal{O}(\alpha_s)$ contribution, but use the asymptotic DA (i.e. $\phi(u,\infty) = 6u(1-u)$) for the $\mathcal{O}(\alpha_s^2\beta_0)$ contribution as the effect of $a_{2,4}(\mu)$ at this order in the perturbative expansion should be negligible*.

As we also include the previously calculated twist-3 and 4 contributions in our analysis, the corresponding DA's are required. The definitions of these can be found in Ref. [167] where it is shown that, for a given twist, the two and three particle distribution amplitudes can be related by an equation of motion resulting in a reduced number of independent parameters: $\eta_{3,4}$ and $\omega_{3,4}$. These parameters, along with a_n are known

*This can be inferred from Fig. 1 of Ref. [166], where the respective size of different contributions in a_n to $f_+(q^2)$ were shown as a function of q^2

γ_{a^n}	γ_{η_3}	γ_{ω_3}	γ_{η_4}	γ_{ω_4}
$4C_F\left(\psi(n+2)+\gamma_E-\frac{3}{4}-\frac{1}{2(n+1)(n+2)}\right)$	$\frac{16}{3}C_F+C_A$	$-\frac{25}{6}C_F+\frac{7}{3}C_A$	$\frac{8}{3}C_F$	$-\frac{8}{3}C_F+\frac{10}{3}C_A$

Table 5.2: One-loop anomalous dimensions of the parameters a_n, $\eta_{3,4}$ and $\omega_{3,4}$ describing the DAs [167; 193].

to renormalise multiplicatively to leading log accuracy [192],

$$c(\mu^2) = c(\mu_0^2)\left(\frac{\alpha_s(\mu^2)}{\alpha_s(\mu_0^2)}\right)^{\gamma_c/\beta_0} \tag{5.29}$$

where μ_0 is the initial scale at which the parameter has been calculated, γ_c are the one-loop anomalous dimensions for the parameter $c = a_n$, $\eta_{3,4}$ or $\omega_{3,4}$, as defined in Tab. 5.2. Since we calculate the hard scattering kernel to $\mathcal{O}(\alpha_s^2 N_f)$, we should take the scale dependence of the twist-2 DA to the same order. This involves adding the term $2C_F V_N(u,v)\ln(\mu^2/\mu_0^2)\Pi_\mu^{(0)}$ to the result for $\Pi_\mu^{(2)}$, where V_N is as defined in Eq. 5.24.

5.5.2 Spectral Density

Having obtained a finite total result for the twist-2 contribution to Π_μ, we need to extract the imaginary part to obtain the spectral density which enters in the sum rule. As in Eq. (1.30), we define Π_+^{T2} in terms of Π_μ^{T2} via

$$\Pi_\mu^{\mathrm{T2}} = (p_B+p)_\mu \Pi_+^{\mathrm{T2}}(p_B^2,q^2) + (p_B-p)_\mu \Pi_-^{\mathrm{T2}}(p_B^2,q^2). \tag{5.30}$$

It is then straightforward to extract the relevant spectral density

$$\rho_{\mathrm{T2}} = \frac{1}{\pi}\mathrm{Im}\Pi_+^{\mathrm{T2}}. \tag{5.31}$$

An expression for the NNLO correction to ρ_{T2} is given explicitly in App. C. In order to obtain the $\mathcal{O}(\alpha_s^2\beta_0)$ result, N_f in ρ_{T2} should be replaced by $-3/2\,\beta_0$. Including the contributions at twist-3 to one-loop accuracy and twist-4 to leading order accuracy,

$$\rho_{\Pi_+}(s,0) = \lim_{q^2\to 0}(\rho_{\mathrm{T2}} + \rho_{\mathrm{T3}} + \rho_\sigma + \rho_{\mathrm{p}} + \rho_{\mathrm{T4}}^{2p} + \rho_{\mathrm{T2}}^{3p}), \tag{5.32}$$

where ρ_{T3}, ρ_σ and ρ_{p} are contributions at twist-3 and $\rho_{\mathrm{T4}}^{2(3)p}$ are contributions at twist-4 as defined in Ref. [167]. An additional twist-4 term, $\mathrm{T4}_c$ cannot be expressed via a dispersion relation so must be included separately. Therefore, on taking the Borel transformation of Π_+, we have

$$\hat{B}\Pi_+ = \int_{m_b^2}^{\infty} ds\, \rho_{\Pi_+}(s,0) e^{-s/M^2} + \mathrm{T4}_c^{(0)}. \tag{5.33}$$

where we have defined $\mathrm{T4}_c^{(0)}$ via

$$\mathrm{T4}_c^{(0)} = \lim_{q^2 \to 0} T4_c. \tag{5.34}$$

5.5.3 Decay Constant f_B

The sum rule is now given by

$$f_+(0) = \frac{1}{m_B^2 f_B} \left(\int_{m_b^2}^{s_0} ds\, \rho_{\Pi_+}(s,0) e^{(m_B^2 - s)/M^2} + \mathrm{T4}_c\, e^{m_B^2/M^2} \right), \tag{5.35}$$

such that in order to obtain a numerical result for $f_+(0)$, f_B is required as input. For consistency we use the QCD sum rules result, also calculated to $\mathcal{O}(\alpha_s^2\beta_0)$, in the hope that there will be a cancellation of radiative corrections as well as the dependence on other input parameters such as m_b and μ. The full $\mathcal{O}(\alpha_s^2)$ corrections were analysed in Refs. [176] (and [177]), and were found to be large. The sum rule for f_B is given by

$$f_B = \frac{1}{m_B^2} \left(\int_{m_b^2}^{s_0} ds\, \rho_{\mathrm{pert}}(s) e^{(m_B^2 - s)/M^2} + C_{\bar{q}q} \langle \bar{q} q \rangle + C_{\bar{q}Gq} \langle \bar{q} \sigma_g G q \rangle \right)^{\frac{1}{2}}, \tag{5.36}$$

where $C_{\bar{q}q}$ and $C_{\bar{q}Gq}$ are Wilson coefficients for the OPE in terms of the quark and mixed condensates respectively [194; 195], and $\rho_{\mathrm{pert}}(s)$ can be expanded in $\alpha_s(\mu)$,

$$\rho_{\mathrm{pert}}(s) = \rho_{\mathrm{pert}}^{(0)}(s) + \frac{\alpha_s}{4\pi} \rho_{\mathrm{pert}}^{(1)}(s) + \left(\frac{\alpha_s}{4\pi} \right)^2 N_f \rho_{\mathrm{pert}}^{(2)}(s) \ldots. \tag{5.37}$$

The tree level result is trivially found to be

$$\rho_{\mathrm{pert}}^{(0)}(s) = \frac{N_c}{8\pi^2} m_b^2\, s \left(1 - \frac{m_b^2}{s} \right)^2. \tag{5.38}$$

Parameter	Value	Ref.	Parameter	Value	Ref.
m_π	139.6 MeV	[30]	f_π	130.4 MeV	[30]
η_3	0.015	[193]	ω_3	-3	[193]
η_4	10	[193]	ω_4	0.2	[193]
$\langle\bar{q}q\rangle$	$(-0.24 \pm 0.01)^3\,\text{GeV}^3$	[167]	$\langle\bar{q}\sigma gGq\rangle$	$0.8\,\langle\bar{q}q\rangle$	[167]

Table 5.3: Summary of values of parameters used in the numerical analysis. Note the quark condensate is given at the scale 1 GeV.

The $\mathcal{O}(\alpha_s)$ result $\rho^{(1)}_{\text{pert}}(s)$ can be obtained from Ref. [196]. The full $\mathcal{O}(\alpha_s^2)$ corrections to $\rho_{\text{pert}}(s)$, in the case that the light quark is massless, have been calculated in Refs. [197] and [198]. An analytical calculation of all diagrams was not feasible, so Padé approximations and conformal mapping were used to obtain semi-numerical results, which the authors have kindly provided in publically available code. We can express $\rho^{(2)}_{\text{pert}}(s)$ in terms of the quantity $R^{(2),s}_{FL}(s)$ defined in Ref. [197] using

$$\rho^{(2)}_{\text{pert}}(s) = C_F\, m_b^2\, s\, R^{(2),s}_{FL}(s). \tag{5.39}$$

To obtain the $\mathcal{O}(\alpha_s^2\beta_0)$ result, N_f in $\rho_{\text{pert}}(s)$ should be replaced by $-3/2\,\beta_0$. The result for $R^{(2),s}_{FL}(s)$ is given at the scale m_b, and the pole mass is used for the b quark. We must therefore include the $\mathcal{O}(\alpha_s^2\beta_0)$ corrections which arise on re-expressing $\alpha_s(m_b)$ in terms of $\alpha_s(\mu)$, and take the form

$$\Delta\rho^{(2)}_{\text{pert}}(s) = C_F \ln\frac{m_b}{\mu}\,\rho^{(1)}_{\text{pert}}(s) \tag{5.40}$$

This results in a sum rule for f_B largely independent of the renormalisation scale μ.

5.5.4 Numerical Analysis

The LCSR approach requires a careful choice of numerical values for the continuum limit s_0 and the Borel parameter M^2. Note that we rescale the Borel parameter by $\langle u\rangle^{-1}$ as defined in Ref. [167], as it was found that the effective Borel parameter in the tree-level sum rule is uM^2_{LC} rather than M^2_{LC} corresponding to M^2 in Eq. (5.35). The continuum threshold s_0 is chosen such that the continuum contribution is approximately 25-30% of the B contribution. The role of the Borel transformation is to ensure the effects of

Set	$m_b\,(\mathrm{GeV})$	$s_0\,(\mathrm{GeV}^2)$	$M^2\,(\mathrm{GeV}^2)$	$f_B(\mathrm{MeV})$
1	4.78	34.1	4.0	0.181
2	4.84	33.2	4.0	0.162
3	4.90	32.4	4.0	0.144

Table 5.4: Values of f_B along with the associated Borel parameter (M^2) and continuum threshold (s_0) for three values of m_b. The three parameter sets are used in the final analysis of $f_+(0)$.

higher states are sufficiently suppressed, reducing the impact of the assumption of quark-hadron duality, and improving the convergence of OPE. The rescaled Borel parameter M^2 is therefore fixed to ensure the sum rule is flat in the range 4-10 GeV^2. We find that treating the sum rules for $f_B f_+(0)$ and f_B separately results in a value $f_+(0)$ which exhibits little dependence on, but a clear extremum as a function of these parameters. We also ensure that the sum rule for m_B, which can be obtained by differentiating the sum rule for f_B or $f_+(0)$ by $1/M^2$, is fulfilled to 0.1% [167]. The values s_0 and M^2 used for f_B and $f_B f_+(0)$ are specified in Tabs. 5.4 and 5.5.

From Eq. (5.28) it is clear that making numerical predictions for the twist-2 pion DA comes down to determining the moments of the conformal expansion. This is not straightforward, as they can only be calculated by non-perturbative methods, such as QCD sum rules or Lattice QCD. The first QCD sum rules calculation, by Chernyak and Zhitnitsky [199], found $a_2(0.5\,\mathrm{GeV}) = 2/3$ which was larger than expected. However this calculation employed local condensates, and later LCSR calculations [191] and QCD sum rules calculations with non-local condensates yielded smaller values [200]. More recently, Lattice QCD has made predictions for $a_2(2\,\mathrm{GeV})$, first in the quenched approximation [201], and later with dynamical fermions in Refs. [202; 203]. Combining these Lattice results with experimental constraints, i.e. measurements of the $\gamma\gamma^*\pi$ form factor at CLEO [204] up to 9 GeV^2 and CELLO [205] in the low q^2 regime, one can obtain an estimate for $a_4(\mu)$ [206]. In order to account for the present uncertainty on these moments, we present our results for five possible values of $a_2(2\,\mathrm{GeV}) = \{0.0, 0.1, 0.2, 0.3, 0.4\}$, keeping a_4 fixed at 0, which is compatible with all current determinations. We also explored the affect of a non-zero a_4, taking the conservative range of values $a_4(2\,\mathrm{GeV}) = \{-0.1, 0.0, 0.1\}$.

Parameters describing the twist-3 and 4 DA's η_3, ω_3, η_4 and ω_4 were introduced in Sec. 5.5.1. These were first calculated in QCD sum rules [191], using nonlocal operator

	Set 1		Set 2		Set 3	
$a_2(2\,\text{GeV})$	$s_0\,(\text{GeV}^2)$	$f_+(0)$	$s_0\,(\text{GeV}^2)$	$f_+(0)$	$s_0\,(\text{GeV}^2)$	$f_+(0)$
0.0	33.9	$0.246^{+0.010}_{-0.011}$	32.7	$0.232^{+0.012}_{-0.013}$	31.7	$0.214^{+0.015}_{-0.015}$
0.1	34.6	$0.270^{+0.010}_{-0.011}$	33.2	$0.259^{+0.012}_{-0.013}$	32.0	$0.243^{+0.015}_{-0.015}$
0.2	35.6	$0.294^{+0.010}_{-0.011}$	33.7	$0.286^{+0.013}_{-0.013}$	32.4	$0.272^{+0.017}_{-0.016}$
0.3	36.9	$0.316^{+0.010}_{-0.011}$	34.4	$0.312^{+0.013}_{-0.013}$	32.6	$0.301^{+0.018}_{-0.017}$
0.4	39.1	$0.337^{+0.009}_{-0.011}$	35.2	$0.337^{+0.013}_{-0.013}$	32.9	$0.328^{+0.019}_{-0.018}$

Table 5.5: Results for $f_+(0)$ and associated continuum threshold for the three parameter sets defined in Tab. 5.4, keeping the Borel parameter fixed at $M^2 = 8.0\,\text{GeV}^2$, and $a_4(2\,\text{GeV}) = 0.0$

$a_4(2\,\text{GeV})$	$s_0\,(\text{GeV}^2)$	$f_+(0)$
-0.1	32.8	$0.283^{+0.014}_{-0.014}$
0.0	33.9	$0.286^{+0.013}_{-0.013}$
0.1	35.1	$0.286^{+0.012}_{-0.012}$

Table 5.6: Results demonstrating the dependence of $f_+(0)$ on a_4 for parameter set 2 defined in Tab. 5.4, keeping the Borel parameter fixed at $M^2 = 8\,\text{GeV}^2$, and $a_2(2\,\text{GeV}) = 0.2$

product expansion and conformal expansion, and the updated values from Ref. [193], summarised in Tab. 5.3, are used in our numerical analysis. The error on each of these parameters is approximately 50%. The condensates are also required as input; we use $\langle\bar{q}q\rangle$ as in Tab. 5.3, $\langle\bar{q}\sigma gGq\rangle = 0.8\,\langle\bar{q}q\rangle$, and we neglect the gluon condensate as its contribution is comparably small.

The b quark mass required is the pole mass m_b, calculated at $\mathcal{O}(\alpha_s^2\beta_0)$ from the running quark mass. The RG improved b quark mass, in the potential substraction scheme (see Ref. [128]) was calculated at NNLO from sum rules in Ref. [127] to be $m_b^{\text{PS}}(2\,\text{Gev}) = 4.52 \pm 0.06\,\text{GeV}$, as in Tab. 5.3. The central pole mass used in our numerical analysis is calculated to be 4.84 GeV at $\mathcal{O}(\alpha_s^2\beta_0)$, a good approximation to the full two-loop result 4.81 GeV. It is also in agreement with the full two-loop result for the pole mass obtained from the $\overline{\text{MS}}$ mass, $4.79^{+0.19}_{-0.08}$ GeV [30]. We carry out the analysis for each of three parameter sets, defined in Tab. 5.4 for $m_b = \{4.78, 4.84, 4.90\}$ GeV.

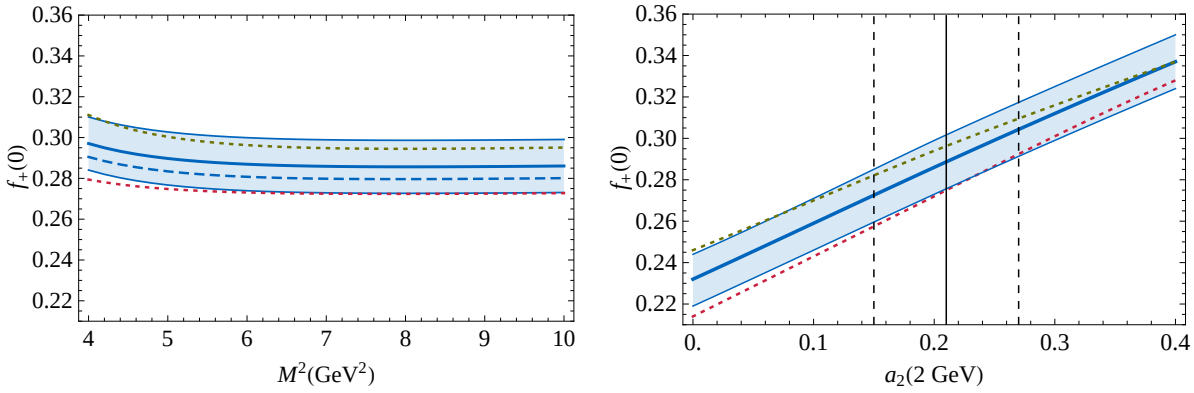

Figure 5.2: Results for $f_+(0)$, including the twist-2 $\mathcal{O}(\alpha_s^2\beta_0)$ corrections (blue), for central values of input parameters. In both plots dotted lines show $f_+(0)$ for $m_b = 4.78$ GeV (upper green) and for $m_b = 4.90$ GeV (lower red). The left-hand plot provides a comparison with the previous result [167] (dashed blue), as a function of the Borel parameter M^2. The right-hand plot shows $f_+(0)$ as a function of $a_2(2\,\text{GeV})$, where the vertical lines indicate the recent Lattice prediction for a_2 (central) with errors (dashed) [203].

Finally the factorisation scale μ is chosen to be the typical virtuality of the b quark, $\sqrt{m_B^2 - m_b^2}$. The uncertainty on $f_+(0)$ can then be obtained by varying s_0 and M^2, the various input parameters as indicated in Tab. 5.3 and the factorisation scale. We find that the dominant uncertainties on $f_+(0)$ arise due to varying the following:

- the continuum threshold s_0 by $\pm 0.5\,\text{GeV}^2$ and the Borel parameter M_2 by $\pm 1.2\,\text{GeV}^2$ for both $f_+(0)f_B$ and f_B;
- the condensates as indicated in Tab. 5.3;
- the twist-3 parameter η_3 by $\pm 50\%$;
- the factorisation scale in the range $\mu/2$ to 2μ.

The uncertainties arising from each of the above are calculated independently, and then added in quadrature. These are summarised along with our results for $f_+(0)$ in Tab. 5.5 for each of the parameter sets defined in Tab. 5.4 and for values of $a_2(2\,\text{GeV})$ as indicated. The uncertainties are seen to be small, approximately 4-7%, and could be further improved by better determinations of the condensates and the twist-3 parameters from, for example, Lattice QCD. In Tab. 5.6 we demonstrate that a_4 has a small effect $\sim 1\%$, justifying our central value $a_4 = 0$ in Tab. 5.5. Note that for certain values of $a_2(2\,\text{GeV})$ and m_b, i.e. $a_2(2\,\text{GeV}) = 0.4$ in Set 1 and $a_2(2\,\text{GeV}) = 0.0$ in Set 3, the sum rule for $f_B f_+(0)$ only exhibits an extremum for values of the continuum threshold outside the optimal range described earlier, such that the result is probably less reliable.

We compare our result for $f_+(0)$, including the twist-2 $\mathcal{O}(\alpha_s^2\beta_0)$ corrections, to the previous result [167] in the left-hand plot of Fig. 5.2. Despite the large $\mathcal{O}(\alpha_s^2\beta_0)$ corrections to f_B mentioned earlier, there is little change in $f_+(0)$, only $\sim 2\%$. This observation reinforces the reliability of the light-cone sum rule approach to the calculation of form factors, as it seems that the results are stable with respect to higher order corrections. It also acts as confirmation that the QCD sum rules result for f_B should be used in preference to the Lattice QCD result in LCSR calculations of the form factors. By interpolating between the results in Tab. 5.5, we obtain $f_+(0)$ as a function of $a_2(2\,\text{GeV})$, as shown in the right-hand plot of Fig. 5.2. Here the most recent Lattice prediction for $a_2(2\,\text{GeV})$ is highlighted. The sensitivity of $f_+(0)$ to a_2 is clear. However, this plot should allow our result for $f_+(0)$ to be easily obtained on more precise Lattice results for a_2 becoming available.

5.6 Summary

In this chapter we have calculated the $\mathcal{O}(\alpha_s^2\beta_0)$ corrections to $f_+(0)$ at leading-twist in QCD sum rules on the light-cone. We have shown that in spite of large positive NNLO corrections to the QCD sum rules result for f_B, the LCSR prediction for the form factor $f_+(0)$ only increases by $\sim 2\%$, as seen in Fig. 5.2 (left-hand plot). This increases our confidence in the stability of LCSR calculations for form factors with respect to radiative corrections. We have performed a comprehensive numerical analysis of our result, including twist-3 contributions at NLO and twist-4 contributions at LO. We find the main sources of theoretical uncertainty are due to a_2 and m_b, and therefore have presented our results for values $a_2(2\,\text{GeV}) = \{0.0, 0.1, 0.2, 0.3, 0.4\}$ and $m_b = \{4.78, 4.84, 4.90\}$ GeV, as seen in Tab. 5.5. Our assumption $a_4 = 0$ is justified in Tab. 5.6 where the maximal effect of a_4 on the result is seen to be of order 1%. The remaining uncertainty is found to be, at most, of order 7%, which could be reduced in the future by the determination of the condensates and twist-3 parameters on the Lattice. Our central results from Tab. 5.5 were presented in Fig. 5.2 (right-hand plot) as a function of $a_2(2\,\text{GeV})$. We hope that, when improved calculations of the leading moment of the π DA become available, this will allow instant access to our numerical prediction for $f_+(0)$. We stress that our approach to $f_+(0)$ in LCSR is complementary to Lattice QCD calculations of $f_+(q^2)$ as the latter are more applicable to the region of large q^2. Future analyses taking both into account, as in Refs [146; 175], should then facilitate an improved determination of the CKM matrix element $|V_{ub}|$.

Chapter 6

Conclusion

This thesis is dedicated to the study of observables for $B \to K^* \mu^+ \mu^-$ and form factors for radiative and semi-leptonic B decays. In Ch. 2 we examined the angular distribution of $B \to K^* \mu^+ \mu^-$, and identified sets of observables, the $S_i^{(a)}$'s and $A_i^{(a)}$'s, emphasising CP-conserving and CP-violating effects respectively. Our predictions for these in the SM, calculated at NLO in QCD factorisation using the LCSR full form factors, were shown in Figs. 2.2 and 2.3, where the $S_i^{(a)}$'s were found to be numerically significant, whereas the $A_i^{(a)}$'s, being doubly Cabibbo suppressed, are close to zero. In particular, the plots of S_4, S_5 and S_6^s as a function of q^2 were seen to exhibit a zero-crossing point in the range $1 - 6$ GeV^2, insensitive to hadronic effects, and these points were shown in Figs. 2.4 to be sensitive to model independent New Physics effects. We also found that S_6^c is zero in the SM, only arising in NP models where scalar operators contribute. Therefore this observable can be used along with the branching ratio for $B_s \to \mu^+ \mu^-$ to distinguish between the effects of scalar and pseudoscalar operators, as seen in Fig. 2.5, thus probing the possibility of an additional Higgs doublet.

We then investigated the potential to study this angular distribution in the first few years at LHCb in Ch. 3, identifying three observables in particular which can be measured with relatively little angular information, $A_{\rm FB}$, $F_{\rm L}$ and S_5. By considering the current constraints on the NP contribution to the Wilson coefficients relevant to this decay, we showed that by measuring these observables with $2\,{\rm fb}^{-1}$ at LHCb, the parameter space would be considerably reduced, as seen in Figs. 3.8. In addition we found that S_5 and its zero crossing play an interesting and complementary role here, as seen in Figs. 3.7.

In Ch. 4 we studied the extrapolation of the form factors (FFs) for $B \to K^{(*)}, \rho$ and $B_s \to \phi$ decays. Considering two parameterisations, the series expansion and the

simplified series expansions as defined in Eqs. (4.10,4.13), we used dispersive bounds to constrain the coefficients of these expansions. This involved a new NLO calculation of the bound for the tensor form factors required for radiative decays. Comparing fits of the $B \to K, \rho$ form factors to LCSR with and without using the available Lattice data (in Figs. 4.1 to 4.1 for $B \to K$ and Figs. 4.7 to 4.13 for $B \to \rho$) gives us confidence in the reliability of these extrapolations for those channels where Lattice data is lacking. These parameterisations for the FFs will be useful not only for the determination of $|V_{ub}|$ from $B \to \pi, \rho\, l\nu$, but also rare radiative decays e.g. $B \to \rho/K^{(*)}\, l^+ l^-$ for the indirect search of new physics effects.

Finally in Ch. 5 we calculated the $\mathcal{O}(\alpha_s^2 \beta_0)$ corrections to $f_+(0)$ at leading-twist in QCD sum rules on the light-cone. In spite of large positive NNLO corrections to the QCD sum rules result for f_B, the LCSR prediction for the form factor $f_+(0)$ only increases by $\sim 2\%$, as seen in Fig. 5.2 (left-hand plot). This increases our confidence in the stability of LCSR calculations for form factors with respect to radiative corrections. We presented our results in a range of values of $a_2(2\,\text{GeV})$ and m_b, the main sources of theoretical uncertainty, as seen in Tab. 5.5 and Fig. 5.2 (right-hand plot). Future analyses taking both into account, as in Refs [146; 175], should then facilitate an improved determination of the CKM matrix element $|V_{ub}|$. We hope that, in conjunction with measurements of exclusive radiative and semi-leptonic B decays at LHCb and future B-factories, this work will help in the effort not only to test the SM, but also to explore the structure of TeV scale physics.

Appendix A

Angular Coefficients

Here we provide the relations between the angular coefficients, $I_i^{(s/c)}$, and the auxiliary functions defined in Eq. (3.4). The $I_i^{(s/c)}$'s were defined in Chapter 2, as in Ref. [52], in terms of the transversity amplitudes $A_{\perp/\parallel}$, A_0 and A_t. These transversity amplitudes are projections of the decay amplitude onto various combinations of helicity states of the $K^*$and the virtual gauge boson. The projections can be achieved by contracting $\mathcal{T}_\mu^{1/2}$ with the virtual gauge boson polarisation vector. We use four basis vectors for the virtual gauge boson polarisation vector corresponding to transverse ($\pm$), longitudinal (0) and timelike (t) states, and three basis vectors for the virtual gauge boson polarisation vector corresponding to transverse ($\pm$) and longitudinal (0) states. One first extracts the helicity amplitudes H_+, H_- and H_0 using the basis polarisation vectors +,-,0 respectively for both the $K^*$and the virtual gauge boson. H_t is found by taking the longitudinal polarisation vector for the $K^*$and the timelike polarisation vector for the virtual gauge boson. Using the relations

$$A_{\perp/\parallel} = \frac{H_+ \mp H_-}{\sqrt{2}} \tag{A.1}$$

and $A_0 = H_0$, $A_t = H_t$, one then obtains expressions for the transversity amplitudes in terms of $A(q^2)$ to $S(q^2)$,

$$A_\perp^i(q^2) = \sqrt{2\,\lambda}\, N\, m_B\, c_i(q^2) \tag{A.2}$$

$$A_\parallel^i(q^2) = -\sqrt{2}\, N\, m_B\, a_i(q^2) \tag{A.3}$$

$$A_0^i(q^2) = \frac{N\, m_B}{\hat{m}_{K^*}\sqrt{\hat{q}^2}}\left(-\frac{1-\hat{m}_{K^*}^2-\hat{q}^2}{2}\, a_i(q^2) + \lambda\, b_i(q^2)\right) \tag{A.4}$$

$$A_t(q^2) = \frac{N\, m_B\sqrt{\lambda}}{\hat{m}_{K^*}\sqrt{\hat{q}^2}}\left(F(q^2) - (1-\hat{m}_{K^*})G(q^2) - \hat{q}^2 H(q^2)\right), \tag{A.5}$$

where $i = L/R$. We use the standard normalisation and definitions following Ref. [106],

$$\beta = \sqrt{1 - \frac{4m_\mu^2}{q^2}} \tag{A.6}$$

$$\lambda = 1 + \hat{m}_{K^*}^4 + \hat{q}^4 - 2\left(\hat{q}^2 + \hat{m}_{K^*}^2\left(1 + \hat{q}^2\right)\right) \tag{A.7}$$

$$N = \left(\frac{G_F^2\,\alpha^2}{3 \cdot 2^{10}\pi^5\, m_B}|V_{ts}V_{tb}^*|^2 q^2\,\lambda^{1/2}\,\beta\right)^{\frac{1}{2}}, \tag{A.8}$$

where α is the electromagnetic coupling constant and G_F is the Fermi constant. In the above definitions of the transversity amplitudes, the functions $a_{L/R}(q^2)$, $b_{L/R}(q^2)$, $c_{L/R}(q^2)$, are analogous to those defined in Ref. [105].

$$a_{L/R}(q^2) = B(q^2) \mp F(q^2) \tag{A.9}$$

$$b_{L/R}(q^2) = \frac{1}{2}\left(C(q^2) \mp G(q^2)\right) \tag{A.10}$$

$$c_{L/R}(q^2) = \frac{1}{2}\left(A(q^2) \mp E(q^2)\right). \tag{A.11}$$

Using the above it is possible to compare the predictions of Eqs. (3.4) to the standard results in the literature, and are found to agree with those given in Chapter 2 [52].

Appendix B

Dispersive Bounds and Fit Results

B.1 Kinematics and Polarisation Vectors

In the following, we consider a B-meson decaying in its rest frame to a final-state meson travelling in the z-direction. The polarisation vectors for a (virtual) vector state, with 4-momentum $q^\mu = (q^0, 0, 0, -|\vec{q}\,|)$, are defined as

$$\begin{aligned} \varepsilon_\pm^\mu(q) &= \mp\frac{1}{\sqrt{2}}\,(0, 1, \mp i, 0)\,, \qquad \varepsilon_0^\mu(q) = \frac{1}{\sqrt{q^2}}\,(|\vec{q}\,|, 0, 0, -q^0)\,, \\ \varepsilon_t^\mu(q) &= \frac{1}{\sqrt{q^2}}\,q^\mu\,. \end{aligned} \tag{B.1}$$

In particular, for the decay of a B-meson at rest into a light meson with mass m_L and momentum $\vec{k}$, we have

$$q^0 = m_B - E = \frac{m_B^2 - m_L^2 + q^2}{2m_B}\,, \qquad |\vec{q}\,| = |\vec{k}\,| = \frac{\sqrt{\lambda}}{2m_B}\,, \tag{B.2}$$

with λ defined in (4.2). We also define the linear combinations

$$\varepsilon_1^\mu(q) = \frac{\varepsilon_-^\mu(q) - \varepsilon_+^\mu(q)}{\sqrt{2}} = (0, 1, 0, 0)\,, \qquad \varepsilon_2^\mu(q) = \frac{\varepsilon_-^\mu(q) + \varepsilon_+^\mu(q)}{\sqrt{2}} = (0, 0, i, 0)\,. \tag{B.3}$$

In the same way, the polarisation vectors for an on-shell K^* meson with momentum $k^\mu = (E, 0, 0, |\vec{k}\,|)$ are given as

$$\varepsilon_\pm^\mu(k) = \mp\frac{1}{\sqrt{2}}(0, 1, \pm i, 0)\,, \qquad \varepsilon_0^\mu(k) = \frac{1}{m_{K^*}}(|\vec{k}\,|, 0, 0, E)\,. \tag{B.4}$$

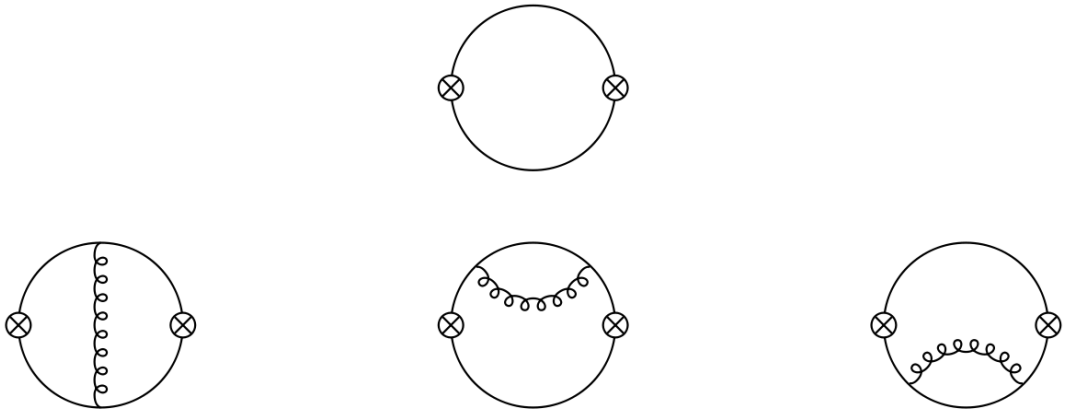

Figure B.1: One- and two-loop diagrams contributing to the correlation function. The crossed circle indicates the insertion of the corresponding scalar, vector or tensor currents. The counter-term diagrams related to the fermion self-energies are not shown.

B.2 Calculation of Wilson Coefficients χ_I^X

As explained in Sec. 4.3.2, the correlator in Eq. (4.14) can be calculated using an OPE,

$$\Pi^X_{I,\mathrm{OPE}}(q^2) = \sum_{k=1}^{\infty} C^X_{I,k}(q^2) \langle O_k \rangle \ . \tag{B.1}$$

where $C^X_{I,n}(q)$ are Wilson coefficients for a given current X and projector I, and $\mathcal{O}_n$ are local gauge-invariant operators, consisting of quark and gluon fields. The operators are ordered by increasing dimension k. Besides the identity operator, whose Wilson coefficient contains the purely perturbative contribution to the correlator, we include the first few operators related to the non-perturbative contribution from the quark condensate $\langle m\bar{q}q\rangle$, the gluon condensate $\langle \frac{\alpha_s}{\pi} G^2\rangle$, and the mixed condensate $\langle \bar{q}\sigma gGq\rangle$. The contributions of the condensates to the scalar and vector correlators were calculated to all orders in the quark mass and lowest order in the coupling constant in [207]. This was extended to the tensor correlators in App. C.2 of Ref. [155]. Here we calculate the one- and two-loop diagrams (see Fig. B.1) contributing to the perturbative part of the correlation functions, as described below.

More specifically, we require $\chi^X_I(n)$ defined in Eq. (4.30), where n is the necessary number of subtractions, for the scalar, vector and tensor correlators, which can be obtained by making use of a Taylor expansion of the Wilson coefficients at $q^2 = 0$. This expansion greatly simplifies the calculation, allowing one to eliminate external momenta in the propagators and to use tensor reduction and recursion relations to express the two-loop integrals in terms of two fundamental master integrals. We find it useful to

present the result in terms of the dimensionless variable

$$v \equiv \frac{M-m}{M+m}\,, \tag{B.2}$$

where M and m are the masses of the heavy and light quark in the loop. We further define the functions

$$\begin{aligned}
f_1(v) &\equiv \frac{1-v^2}{v}\,\mathrm{atanh}(v)\,,\\
f_2(v) &\equiv \frac{1}{v}\,\ln\left(\frac{1-v}{1+v}\right) - \frac{2}{1-v}\,\ln\left(\frac{1+v}{2}\right) - \frac{2}{1+v}\,\ln\left(\frac{1-v}{2}\right)\,,\\
f_3(v) &\equiv \frac{1}{v}\,\mathrm{Li}_2\left(\frac{4v}{(1+v)^2}\right) - \frac{1}{v}\,\mathrm{Li}_2\left(-\frac{4v}{(1-v)^2}\right) - \frac{4\,(1+v^2)}{v^2}\,\mathrm{atanh}^2(v)\,,
\end{aligned} \tag{B.3}$$

which are symmetric under the exchange of light and heavy quarks ($v \to -v$), and take finite values in the limits $v \to \{-1, 0, 1\}$. From our results for the scalar, vector and tensor currents given below, one can obtain expressions for the currents with opposite parity by making the substitution $v \to 1/v$. Note that our expressions for scalar and vector currents coincide with [207]; the results for the tensor currents are new.

B.2.1 Scalar Correlator

For the correlator of two scalar currents, we obtain

$$\chi^S(2)\Big|_{\mathrm{LO}} = \frac{(3+v^2)(3v^2-1)}{64\pi^2(M+m)^2\,v^4} \overset{v\to 1}{\to} \frac{1}{8\pi^2 M^2}\,,$$

$$\begin{aligned}
\chi^S(2)\Big|_{\mathrm{NLO}} = \frac{\alpha_s C_F}{4\pi}\,\frac{1}{64\pi^2(M+m)^2\,v^4}\Bigg\{ & 6\Big(3f_1\,(1-v^2)^2\\
& +(3+v^2)(3v^2-1)\Big)\left(f_2\,(1-v^2) - 4\,\log\left(\frac{m+M}{\mu}\right)\right)\\
& -f_1^2\left(11v^4-50v^2+23\right) + f_1\left(47v^4-126v^2+103\right)\\
& +4\,f_3\,v^2\,(5v^2-1) + 2\left(29v^4+65v^2-40\right)\Bigg\}
\end{aligned} \tag{B.4}$$

$$\overset{v\to 1}{\to} \frac{1}{8\pi^2 M^2}\,\frac{\alpha_s C_F}{4\pi}\left(-24\,\log\left(\frac{M}{\mu}\right) + \frac{2\pi^2}{3} + \frac{27}{2}\right). \tag{B.5}$$

B.2.2 Vector Correlator

For the different projections of the correlator of two vector currents, we obtain

$$\chi_L^V(1)\Big|_{\rm LO} = \frac{(3+v^2)(3v^2-1)}{64\pi^2\,v^2} \overset{v\to 1}{\to} \frac{1}{8\pi^2}\,, \tag{B.6}$$

$$\begin{aligned}\chi_L^V(1)\Big|_{\rm NLO} &= \frac{\alpha_s C_F}{4\pi}\frac{1}{64\pi^2\,v^2}\Bigg\{ f_1^2\left(25v^4+14v^2-23\right)\\ &\quad +2f_1\left(19v^4-6v^2+23\right)\\ &\quad +4f_3\,v^2\left(5v^2-1\right)-23+14v^2+13v^4\Bigg\}\end{aligned}$$

$$\overset{v\to 1}{\to} \frac{\alpha_s C_F}{4\pi}\frac{1}{8\pi^2}\left(\frac{1}{2}+\frac{2\pi^2}{3}\right)\,, \tag{B.7}$$

and

$$\chi_T^V(2)\Big|_{\rm LO} = \frac{-21v^6+53v^4+13v^2+3}{512\pi^2\,(M+m)^2\,v^4} \overset{v\to 1}{\to} \frac{3}{32\pi^2M^2}\,, \tag{B.8}$$

$$\begin{aligned}\chi_T^V(2)\Big|_{\rm NLO} &= \frac{\alpha_s C_F}{4\pi}\frac{-1}{1536\pi^2\,(M+m)^2\,v^4}\Bigg\{ f_1^2\left(803v^6-863v^4-155v^2-73\right)\\ &\quad 2f_1\left(677v^6-741v^4+279v^2+73\right)\\ &\quad 4f_3\,v^2\left(19v^4-86v^2-5\right)-73-323v^2-755v^4+551v^6\Bigg\}\end{aligned}$$

$$\overset{v\to 1}{\to} \frac{\alpha_s C_F}{4\pi}\frac{3}{32\pi^2M^2}\left(\frac{25}{6}+\frac{2\pi^2}{3}\right)\,. \tag{B.9}$$

B.2.3 Tensor Correlator

The relevant projection of the tensor current gives rise to

$$\chi_T^T(3)\big|_{LO} = \frac{-9f_1\left(v^2-1\right)^2\left(3v^2+1\right)+4\left(-9v^6+21v^4+v^2+3\right)}{256\pi^2\left(m+M\right)^2v^4}$$

$$\overset{v\to 1}{\to} \frac{1}{4\pi^2 M^2} \tag{B.10}$$

$$\begin{aligned}\chi_T^T(3)\big|_{NLO} \;=\; & \frac{\alpha_s C_F}{4\pi}\,\frac{1}{384\pi^2(M+m)^2v^4}\Bigg\{12\big(3(v^2-1)^2(3v^2+1)f_1-3\\ & -v^2-21v^4+9v^6\big)\left(f_2\,(1-v^2)-4\,\log\left(\frac{m+M}{\mu}\right)\right)\\ & -f_1^2\left(766v^6-598v^4-142v^2-218\right)\\ & -f_1\left(1091v^6-1137v^4+297v^2+325\right)\\ & -8f_3\,v^2\left(7v^4-26v^2-5\right)+107+69v^2+469v^4-325v^6\Bigg\}\end{aligned} \tag{B.11}$$

$$\overset{v\to 1}{\to} \frac{\alpha_s C_F}{4\pi}\,\frac{1}{4\pi^2 M^2}\left(\frac{10}{3}+\frac{2\pi^2}{3}+8\log\left(\frac{M}{\mu}\right)\right)\,. \tag{B.12}$$

B.3 Covariance Matrices

Here we give the covariance matrices as defined in (4.55) for the parameters corresponding to the best-fit parameters in Tables 4.5 to 4.12.

***B → K* form factor fit:**

- The fit of $B \to K$ FFs to LCSR data alone gives the covariances matrices:

	SE	SSE
$\mathcal{A}_{V,0}$	$\begin{pmatrix} 1.56\times10^{-5} & -1.04\times10^{-4} \\ -1.04\times10^{-4} & 9.59\times10^{-4}\end{pmatrix}$	$\begin{pmatrix} 4.39\times10^{-3} & -2.91\times10^{-2} \\ -2.91\times10^{-2} & 0.266\end{pmatrix}$
$\mathcal{A}_{V,t}^{\text{no res.}}$	$\begin{pmatrix} 1.19\times10^{-4} & -7.87\times10^{-4} \\ -7.87\times10^{-4} & 6.98\times10^{-3}\end{pmatrix}$	$\begin{pmatrix} 7.17\times10^{-3} & -4.75\times10^{-2} \\ -4.75\times10^{-2} & 0.423\end{pmatrix}$
$\mathcal{A}_{V,t}$	$\begin{pmatrix} 6.27\times10^{-6} & -2.72\times10^{-5} \\ -2.72\times10^{-5} & 2.19\times10^{-4}\end{pmatrix}$	$\begin{pmatrix} 2.61\times10^{-3} & -1.08\times10^{-2} \\ -1.08\times10^{-2} & 8.86\times10^{-2}\end{pmatrix}$
$\mathcal{A}_{T,0}$	$\begin{pmatrix} 2.1\times10^{-5} & -6.55\times10^{-5} \\ -6.55\times10^{-5} & 5.37\times10^{-4}\end{pmatrix}$	$\begin{pmatrix} 7.63\times10^{-4} & 6.3\times10^{-4} \\ 6.3\times10^{-4} & 8.32\times10^{-3}\end{pmatrix}$

- For the fit of scalar/vector $B \to K$ FFs to LCSR and Lattice data, we obtain the covariance matrices:

	SE	SSE
$\mathcal{A}_{V,0}$	$\begin{pmatrix} 1.48 \times 10^{-5} & -9.81 \times 10^{-5} \\ -9.81 \times 10^{-5} & 8.76 \times 10^{-4} \end{pmatrix}$	$\begin{pmatrix} 6.26 \times 10^{-3} & -4.15 \times 10^{-2} \\ -4.15 \times 10^{-2} & 0.382 \end{pmatrix}$
$\mathcal{A}_{V,t}^{\text{no res.}}$	$\begin{pmatrix} 4.82 \times 10^{-5} & -2.03 \times 10^{-4} \\ -2.03 \times 10^{-4} & 1.6 \times 10^{-3} \end{pmatrix}$	$\begin{pmatrix} 3.08 \times 10^{-3} & -1.39 \times 10^{-2} \\ -1.39 \times 10^{-2} & 0.11 \end{pmatrix}$
$\mathcal{A}_{V,t}$	$\begin{pmatrix} 6.21 \times 10^{-5} & -4.11 \times 10^{-4} \\ -4.11 \times 10^{-4} & 3.75 \times 10^{-3} \end{pmatrix}$	$\begin{pmatrix} 3.45 \times 10^{-3} & -2.37 \times 10^{-2} \\ -2.37 \times 10^{-2} & 0.261 \end{pmatrix}$

$B \to \rho$ form factor fit:

- Fitting to LCSR data alone, the covariance matrices for the $B \to \rho$ FFs are given by:

	SE	SSE
$\mathcal{B}_{V,0}$	$\begin{pmatrix} 4.15 \times 10^{-6} & -3.2 \times 10^{-5} \\ -3.2 \times 10^{-5} & 7.93 \times 10^{-4} \end{pmatrix}$	$\begin{pmatrix} 5.26 \times 10^{-3} & -4.33 \times 10^{-2} \\ -4.33 \times 10^{-2} & 1.57 \end{pmatrix}$
$\mathcal{B}_{V,1}$	$\begin{pmatrix} 1.57 \times 10^{-5} & -1.28 \times 10^{-4} \\ -1.28 \times 10^{-4} & 1.92 \times 10^{-3} \end{pmatrix}$	$\begin{pmatrix} 3.29 \times 10^{-3} & -2.7 \times 10^{-2} \\ -2.7 \times 10^{-2} & 0.396 \end{pmatrix}$
$\mathcal{B}_{V,2}$	$\begin{pmatrix} 6.45 \times 10^{-6} & -5.23 \times 10^{-5} \\ -5.23 \times 10^{-5} & 7.98 \times 10^{-4} \end{pmatrix}$	$\begin{pmatrix} 1.83 \times 10^{-3} & -1.42 \times 10^{-2} \\ -1.42 \times 10^{-2} & 0.274 \end{pmatrix}$
$\mathcal{B}_{V,t}$	$\begin{pmatrix} 1.19 \times 10^{-5} & -9.76 \times 10^{-5} \\ -9.76 \times 10^{-5} & 1.42 \times 10^{-3} \end{pmatrix}$	$\begin{pmatrix} 2.19 \times 10^{-3} & -1.81 \times 10^{-2} \\ -1.81 \times 10^{-2} & 0.258 \end{pmatrix}$
$\mathcal{B}_{T,0}$	$\begin{pmatrix} 1.01 \times 10^{-5} & 1.29 \times 10^{-4} \\ 1.29 \times 10^{-4} & 1.72 \times 10^{-2} \end{pmatrix}$	$\begin{pmatrix} 6.49 \times 10^{-3} & 9.63 \times 10^{-2} \\ 9.63 \times 10^{-2} & 15.3 \end{pmatrix}$
$\mathcal{B}_{T,1}$	$\begin{pmatrix} 7.45 \times 10^{-7} & -4.16 \times 10^{-6} \\ -4.16 \times 10^{-6} & 5.21 \times 10^{-5} \end{pmatrix}$	$\begin{pmatrix} 1.86 \times 10^{-3} & -9.82 \times 10^{-3} \\ -9.82 \times 10^{-3} & 0.13 \end{pmatrix}$
$\mathcal{B}_{T,2}$	$\begin{pmatrix} 2.7 \times 10^{-7} & -1.41 \times 10^{-6} \\ -1.41 \times 10^{-6} & 1.89 \times 10^{-5} \end{pmatrix}$	$\begin{pmatrix} 8.09 \times 10^{-4} & -2.15 \times 10^{-3} \\ -2.15 \times 10^{-3} & 6.88 \times 10^{-2} \end{pmatrix}$

- For the fit of vector and axial-vector $B \to \rho$ FFs to LCSR and Lattice data, the covariance matrices read:

	SE	SSE
$\mathcal{B}_{V,0}$	$\begin{pmatrix} 2.62\times10^{-6} & -1.35\times10^{-5} \\ -1.35\times10^{-5} & 5.35\times10^{-4} \end{pmatrix}$	$\begin{pmatrix} 2.86\times10^{-3} & -5.12\times10^{-3} \\ -5.12\times10^{-3} & 0.796 \end{pmatrix}$
$\mathcal{B}_{V,1}$	$\begin{pmatrix} 5.72\times10^{-6} & -3.08\times10^{-5} \\ -3.08\times10^{-5} & 9.15\times10^{-4} \end{pmatrix}$	$\begin{pmatrix} 1.24\times10^{-3} & -7.07\times10^{-3} \\ -7.07\times10^{-3} & 0.193 \end{pmatrix}$
$\mathcal{B}_{V,2}$	$\begin{pmatrix} 1.99\times10^{-6} & -3.02\times10^{-6} \\ -3.02\times10^{-6} & 2.26\times10^{-4} \end{pmatrix}$	$\begin{pmatrix} 5.21\times10^{-4} & 1.52\times10^{-3} \\ 1.52\times10^{-3} & 6.4\times10^{-2} \end{pmatrix}$

***B* → *K** form factor fit:** The covariance matrices for the $B \to K^*$ FFs are given by:

	SE	SSE
$\mathcal{B}_{V,0}$	$\begin{pmatrix} 4.38\times10^{-6} & -3.12\times10^{-5} \\ -3.12\times10^{-5} & 1.08\times10^{-3} \end{pmatrix}$	$\begin{pmatrix} 4.85\times10^{-3} & -3.26\times10^{-2} \\ -3.26\times10^{-2} & 1.85 \end{pmatrix}$
$\mathcal{B}_{V,1}$	$\begin{pmatrix} 1.94\times10^{-5} & -1.63\times10^{-4} \\ -1.63\times10^{-4} & 3.06\times10^{-3} \end{pmatrix}$	$\begin{pmatrix} 3.\times10^{-3} & -2.54\times10^{-2} \\ -2.54\times10^{-2} & 0.467 \end{pmatrix}$
$\mathcal{B}_{V,2}$	$\begin{pmatrix} 1.01\times10^{-5} & -8.52\times10^{-5} \\ -8.52\times10^{-5} & 1.59\times10^{-3} \end{pmatrix}$	$\begin{pmatrix} 2.42\times10^{-3} & -1.87\times10^{-2} \\ -1.87\times10^{-2} & 0.456 \end{pmatrix}$
$\mathcal{B}_{V,t}$	$\begin{pmatrix} 1.79\times10^{-5} & -1.53\times10^{-4} \\ -1.53\times10^{-4} & 2.75\times10^{-3} \end{pmatrix}$	$\begin{pmatrix} 2.24\times10^{-3} & -1.93\times10^{-2} \\ -1.93\times10^{-2} & 0.34 \end{pmatrix}$
$\mathcal{B}_{T,0}$	$\begin{pmatrix} 1.63\times10^{-5} & 3.6\times10^{-4} \\ 3.6\times10^{-4} & 2.41\times10^{-2} \end{pmatrix}$	$\begin{pmatrix} 9.38\times10^{-3} & 0.246 \\ 0.246 & 17.7 \end{pmatrix}$
$\mathcal{B}_{T,1}$	$\begin{pmatrix} 1.17\times10^{-6} & -6.23\times10^{-6} \\ -6.23\times10^{-6} & 9.82\times10^{-5} \end{pmatrix}$	$\begin{pmatrix} 2.26\times10^{-3} & -1.12\times10^{-2} \\ -1.12\times10^{-2} & 0.191 \end{pmatrix}$
$\mathcal{B}_{T,2}$	$\begin{pmatrix} 4.04\times10^{-7} & -2.07\times10^{-6} \\ -2.07\times10^{-6} & 3.4\times10^{-5} \end{pmatrix}$	$\begin{pmatrix} 1.12\times10^{-3} & -2.27\times10^{-3} \\ -2.27\times10^{-3} & 0.11 \end{pmatrix}$

***$B_s \to \phi$* form factor fit:** The covariance matrices for the $B_s \to \phi$ FFs are given by:

	SE	SSE
$\mathcal{B}_{V,0}$	$\begin{pmatrix} 1.16 \times 10^{-6} & -8.32 \times 10^{-6} \\ -8.32 \times 10^{-6} & 3.47 \times 10^{-4} \end{pmatrix}$	$\begin{pmatrix} 4.56 \times 10^{-3} & -2.81 \times 10^{-2} \\ -2.81 \times 10^{-2} & 1.98 \end{pmatrix}$
$\mathcal{B}_{V,1}$	$\begin{pmatrix} 8.44 \times 10^{-6} & -7.79 \times 10^{-5} \\ -7.79 \times 10^{-5} & 1.63 \times 10^{-3} \end{pmatrix}$	$\begin{pmatrix} 3.37 \times 10^{-3} & -3.15 \times 10^{-2} \\ -3.15 \times 10^{-2} & 0.643 \end{pmatrix}$
$\mathcal{B}_{V,2}$	$\begin{pmatrix} 3.6 \times 10^{-6} & -3.26 \times 10^{-5} \\ -3.26 \times 10^{-5} & 7.08 \times 10^{-4} \end{pmatrix}$	$\begin{pmatrix} 2.91 \times 10^{-3} & -2.38 \times 10^{-2} \\ -2.38 \times 10^{-2} & 0.662 \end{pmatrix}$
$\mathcal{B}_{V,t}$	$\begin{pmatrix} 6.61 \times 10^{-6} & -6.07 \times 10^{-5} \\ -6.07 \times 10^{-5} & 1.28 \times 10^{-3} \end{pmatrix}$	$\begin{pmatrix} 2.05 \times 10^{-3} & -1.9 \times 10^{-2} \\ -1.9 \times 10^{-2} & 0.394 \end{pmatrix}$
$\mathcal{B}_{T,0}$	$\begin{pmatrix} 7.03 \times 10^{-6} & 1.75 \times 10^{-4} \\ 1.75 \times 10^{-4} & 1.04 \times 10^{-2} \end{pmatrix}$	$\begin{pmatrix} 1.41 \times 10^{-2} & 0.406 \\ 0.406 & 25.2 \end{pmatrix}$
$\mathcal{B}_{T,1}$	$\begin{pmatrix} 6.39 \times 10^{-7} & -3.91 \times 10^{-6} \\ -3.91 \times 10^{-6} & 6.67 \times 10^{-5} \end{pmatrix}$	$\begin{pmatrix} 3.37 \times 10^{-3} & -1.93 \times 10^{-2} \\ -1.93 \times 10^{-2} & 0.35 \end{pmatrix}$
$\mathcal{B}_{T,2}$	$\begin{pmatrix} 1.63 \times 10^{-7} & -8.97 \times 10^{-7} \\ -8.97 \times 10^{-7} & 1.69 \times 10^{-5} \end{pmatrix}$	$\begin{pmatrix} 1.64 \times 10^{-3} & -3.86 \times 10^{-3} \\ -3.86 \times 10^{-3} & 0.187 \end{pmatrix}$

Appendix C

Spectral Density

In analogy to Eq. (5.7), we can perturbatively expand the twist-2 spectral density,

$$\rho_{\mathrm{T2}} = \rho_{\mathrm{T2}}^{(0)} + \frac{\alpha_s}{4\pi}\,\rho_{\mathrm{T2}}^{(1)} + \left(\frac{\alpha_s}{4\pi}\right)^2 N_f\,\rho_{\mathrm{T2}}^{(2)} \ldots . \tag{C.1}$$

Our NNLO correction $\rho_{\mathrm{T2}}^{(2)}$ then takes the form,

$$\begin{aligned}
\rho_{\mathrm{T2}}^{(2)} = f_\pi C_F \Bigg\{ & \frac{5m_b^3(m_b^2-s)}{3s^3}\log^3\left(1-\frac{m_b^2}{s}\right) \\
& + \left(\frac{9m_b^3(m_b^2-s)}{s^3}\log\left(\frac{s}{m_b^2}\right) - \frac{m_b(m_b^2-s)\,(20m_b^4-42s\,m_b^2+7s^2)}{2s^4}\right)\log^2\left(1-\frac{m_b^2}{s}\right) \\
& + \left(\frac{9m_b^3(m_b^2-s)}{s^3}\log^2\left(\frac{s}{m_b^2}\right) - \frac{2m_b\,(36m_b^6-47s\,m_b^4+35s^2m_b^2-6s^3)}{3s^4}\log\left(\frac{s}{m_b^2}\right) + \right. \\
& \left. \frac{m_b(m_b^2-s)\,(32m_b^4-10\pi^2 s\,m_b^2-428s\,m_b^2+79s^2)}{6s^4} - \right. \\
& \left. \frac{14m_b^3(m_b^2-s)}{s^3}\mathrm{Li}_2\left(\frac{m_b^2}{s}\right)\right)\log\left(1-\frac{m_b^2}{s}\right) + \\
& \frac{m_b^3(m_b^2-s)}{3s^3}\log^3\left(\frac{s}{m_b^2}\right) - \frac{m_b^3\,(48m_b^4-134s\,m_b^2+107s^2)}{6s^4}\log^2\left(\frac{s}{m_b^2}\right) - \\
& \frac{6m_b^3(m_b^2-s)}{s^3}\log^2\left(\frac{m_b^2}{s}-1\right) + \\
& \log\left(\frac{\mu}{2}\right)\left(- \frac{2m_b^3(m_b^2-s)}{s^3}\log^2\left(1-\frac{m_b^2}{s}\right) + \right. \\
& \left. \left(-\frac{4m_b^3(m_b^2-s)}{s^3}\log\left(\frac{s}{m_b^2}\right) - \frac{2m_b(m_b^2-s)}{s^2}\right)\log\left(1-\frac{m_b^2}{s}\right) - \right.
\end{aligned}$$

$$\frac{2m_b^3(m_b^2-s)}{s^3}\log^2\left(\frac{s}{m_b^2}\right)-$$

$$\frac{2m_b^3}{s^2}\log\left(\frac{s}{m_b^2}\right)+\frac{2m_b^3\left(-15+\pi^2\right)\left(m_b^2-s\right)}{3s^3}\Bigg)+$$

$$\frac{2m_b(m_b^2-s)\left(8m_b^4-8s\,m_b^2+s^2\right)}{s^4}\log\left(\frac{s}{m_b^2}-1\right)+$$

$$\frac{2m_b\left(6m_b^6+22s\,m_b^4-19s^2m_b^2-s^3\right)}{s^4}\mathrm{Li}_2\left(\frac{m_b^2}{s}\right)+$$

$$\log\left(\frac{s}{m_b^2}\right)\Bigg(-\frac{m_b\left(-32m_b^6-8\pi^2s\,m_b^4+484s\,m_b^4+8\pi^2s^2m_b^2-239s^2m_b^2+24s^3\right)}{6s^4}-$$

$$\frac{8m_b^3(m_b^2-s)}{s^3}\log\left(\frac{s}{m_b^2}-1\right)-\frac{18m_b^3(m_b^2-s)}{s^3}\mathrm{Li}_2\left(\frac{m_b^2}{s}\right)\Bigg)$$

$$+\log\left(\frac{\mu}{m_b^2}\right)\Bigg(-\frac{2m_b^3(m_b^2-s)}{s^3}\log^2\left(1-\frac{m_b^2}{s}\right)+$$

$$\left(\frac{2m_b(m_b^2-s)\left(4m_b^4-10s\,m_b^2+s^2\right)}{s^4}-\frac{8m_b^3(m_b^2-s)}{s^3}\log\left(\frac{s}{m_b^2}\right)\right)\log\left(1-\frac{m_b^2}{s}\right)-$$

$$\frac{2m_b(m_b^2-s)\left(\pi^2m_b^2-27m_b^2+9s\right)}{3s^3}+\frac{2m_b^3\left(4m_b^4-14s\,m_b^2+9s^2\right)}{s^4}\log\left(\frac{s}{m_b^2}\right)+$$

$$\frac{12m_b^2m_b(m_b^2-s)}{s^3}\mathrm{Li}_2\left(\frac{m_b^2}{s}\right)\Bigg)+$$

$$\frac{6m_b^3(m_b^2-s)}{s^3}\mathrm{Li}_3\left(1-\frac{m_b^2}{s}\right)-\frac{10m_b^3(m_b^2-s)}{s^3}\mathrm{Li}_3\left(\frac{m_b^2}{s}\right)+$$

$$\frac{m_b}{9s^4}\Bigg(18\pi^2m_b^6-137\pi^2s\,m_b^4+363s\,m_b^4-216s\,\zeta(3)m_b^4+98\pi^2s^2m_b^2-$$

$$561s^2m_b^2+216s^2\zeta(3)m_b^2-3\pi^2s^3+198s^3\Bigg)\Bigg\} \tag{C.2}$$

Bibliography

[1] P. W. Higgs, *Broken symmetries and the mass of gauge bosons*, *Phys. Rev. Lett.* **13** (1964) 508–509.

[2] S. L. Glashow, *Partial Symmetries of Weak Interactions*, *Nucl. Phys.* **22** (1961) 579–588.

[3] S. Weinberg, *A Model of Leptons*, *Phys. Rev. Lett.* **19** (1967) 1264–1266.

[4] M. Gell-Mann, *A Schematic Model of Baryons and Mesons*, *Phys. Lett.* **8** (1964) 214–215.

[5] S. Weinberg, *Nonabelian Gauge Theories of the Strong Interactions*, *Phys. Rev. Lett.* **31** (1973) 494–497.

[6] M. Y. Han and Y. Nambu, *Three-triplet model with double SU(3) symmetry*, *Phys. Rev.* **139** (1965) B1006–B1010.

[7] D. J. Gross and F. Wilczek, *Ultra-violet behaviour of non-abelian gauge theories*, *Phys. Rev. Lett.* **30** (1973) 1343–1346.

[8] H. D. Politzer, *Reliable perturbative results for strong interactions?*, *Phys. Rev. Lett.* **30** (1973) 1346–1349.

[9] H. Fritzsch, M. Gell-Mann and H. Leutwyler, *Advantages of the Color Octet Gluon Picture*, *Phys. Lett.* **B47** (1973) 365–368.

[10] J. R. Ellis, G. Giudice, M. L. Mangano, I. Tkachev and U. Wiedemann, *Review of the Safety of LHC Collisions*, *J. Phys.* **G35** (2008) 115004 [0806.3414].

[11] S. Pokorski, *Phenomenological guide to physics beyond the standard model*, hep-ph/0502132.

[12] M. Drees, *An Introduction to supersymmetry*, hep-ph/9611409.

[13] **ATLAS** Collaboration, G. Aad *et. al.*, *The ATLAS experiment at the CERN large hadron collider*, *JINST* **3** (2008) S08003.

[14] **CMS** Collaboration, G. L. Bayatian *et. al.*, "CMS physics: Technical design report." CERN-LHCC-2006-001.

[15] **LHC*b*** Collaboration, A. A. Alves *et. al.*, *The LHC*b *Detector at the LHC*, *JINST* **3** (2008) S08005.

[16] **ATLAS** Collaboration, B. Epp, *B physics with ATLAS and CMS*, *PoS* **2008LHC** (2008) 078.

[17] M. K. Gaillard and B. W. Lee, *Rare Decay Modes of the K-Mesons in Gauge Theories*, *Phys. Rev.* **D10** (1974) 897.

[18] A. J. Buras, W. Slominski and H. Steger, *B Meson Decay, CP Violation, Mixing Angles and the Top Quark Mass*, *Nucl. Phys.* **B238** (1984) 529.

[19] M. E. Peskin and D. V. Schroeder, *An Introduction to quantum field theory*, . Reading, USA: Addison-Wesley (1995) 842 p.

[20] G. Isidori, Y. Nir and G. Perez, *Flavor Physics Constraints for Physics Beyond the Standard Model*, 1002.0900.

[21] N. Cabibbo, *Unitary Symmetry and Leptonic Decays*, *Phys. Rev. Lett.* **10** (1963) 531–533.

[22] M. Kobayashi and T. Maskawa, *CP Violation in the Renormalizable Theory of Weak Interaction*, *Prog. Theor. Phys.* **49** (1973) 652–657.

[23] S. L. Glashow, J. Iliopoulos and L. Maiani, *Weak Interactions with Lepton-Hadron Symmetry*, *Phys. Rev.* **D2** (1970) 1285–1292.

[24] J. H. Christenson, J. W. Cronin, V. L. Fitch and R. Turlay, *Evidence for the 2 pi Decay of the k(2)0 Meson*, *Phys. Rev. Lett.* **13** (1964) 138–140.

[25] **BABAR** Collaboration, B. Aubert *et. al.*, *Observation of CP violation in the B^0 meson system*, *Phys. Rev. Lett.* **87** (2001) 091801 [hep-ex/0107013].

[26] **Belle** Collaboration, K. Abe *et. al.*, *Observation of large CP violation in the neutral B meson system*, *Phys. Rev. Lett.* **87** (2001) 091802 [hep-ex/0107061].

[27] G. C. Branco, L. Lavoura and J. P. Silva, *CP violation*, *Int. Ser. Monogr. Phys.* **103** (1999) 1–536.

[28] L. Wolfenstein, *Parametrization of the Kobayashi-Maskawa Matrix*, *Phys. Rev. Lett.* **51** (1983) 1945.

[29] A. J. Buras, M. E. Lautenbacher and G. Ostermaier, *Waiting for the top quark mass, $K^+ \to \pi^+ \nu\bar{\nu}$, $B_s^0 - \bar{B}_s^0$ mixing and CP asymmetries in B decays*, *Phys. Rev.* **D50** (1994) 3433–3446 [hep-ph/9403384].

[30] **Particle Data Group** Collaboration, C. Amsler *et. al.*, *Review of particle physics*, *Phys. Lett.* **B667** (2008) 1.

[31] **UTfit** Collaboration, M. Bona *et. al.*, *Standard Model analysis of the unitarity triangle*, *Nuovo Cim.* **123B** (2008) 666–673.

[32] **CKMfitter Group** Collaboration, J. Charles *et. al.*, *CP violation and the CKM matrix: Assessing the impact of the asymmetric B factories*, *Eur. Phys. J.* **C41** (2005) 1–131 [hep-ph/0406184].

[33] C. Balazs, M. S. Carena, A. Menon, D. E. Morrissey and C. E. M. Wagner, *Overview of Electroweak Baryogenesis*, *ECONF* **C0508141** (2005) ALCPG0333.

[34] A. J. Buras, *Weak Hamiltonian, CP violation and rare decays*, hep-ph/9806471.

[35] C. Bobeth, M. Misiak and J. Urban, *Photonic penguins at two loops and m_t-dependence of $BR(B \to X_s l^+ l^-)$*, *Nucl. Phys.* **B574** (2000) 291–330 [hep-ph/9910220].

[36] C. Bobeth, A. J. Buras, F. Kruger and J. Urban, *QCD corrections to $\bar{B} \to X_{d,s}\nu\bar{\nu}$, $\bar{B}_{d,s} \to \ell^+\ell^-$, $K \to \pi\nu\bar{\nu}$ and $K_L \to \mu^+\mu^-$ in the MSSM*, *Nucl. Phys.* **B630** (2002) 87–131 [hep-ph/0112305].

[37] K. G. Chetyrkin, M. Misiak and M. Munz, *Weak radiative B-meson decay beyond leading logarithms*, *Phys. Lett.* **B400** (1997) 206–219 [hep-ph/9612313].

[38] C. G. Bollini and J. J. Giambiagi, *Dimensional Renormalization: The Number of Dimensions as a Regularizing Parameter*, *Nuovo Cim.* **B12** (1972) 20–25.

[39] J. F. Ashmore, *A Method of Gauge Invariant Regularization*, *Lett. Nuovo Cim.* **4** (1972) 289–290.

[40] G. M. Cicuta and E. Montaldi, *Analytic renormalization via continuous space dimension*, *Nuovo Cim. Lett.* **4** (1972) 329–332.

[41] M. S. Chanowitz, M. Furman and I. Hinchliffe, *The Axial Current in Dimensional Regularization*, *Nucl. Phys.* **B159** (1979) 225.

[42] W. A. Bardeen, A. J. Buras, D. W. Duke and T. Muta, *Deep Inelastic Scattering Beyond the Leading Order in Asymptotically Free Gauge Theories*, *Phys. Rev.* **D18** (1978) 3998.

[43] G. 't Hooft, *Dimensional regularization and the renormalization group*, *Nucl. Phys.* **B61** (1973) 455–468.

[44] P. Pascual and R. Tarrach, *QCD: Renormalization for the Practitioner*, *Lect. Notes Phys.* **194** (1984) 1–277.

[45] P. Gambino, M. Gorbahn and U. Haisch, *Anomalous dimension matrix for radiative and rare semileptonic B decays up to three loops*, *Nucl. Phys.* **B673** (2003) 238–262 [hep-ph/0306079].

[46] M. Gorbahn and U. Haisch, *Effective Hamiltonian for non-leptonic $|\Delta(F)| = 1$ decays at NNLO in QCD*, *Nucl. Phys.* **B713** (2005) 291–332 [hep-ph/0411071].

[47] M. Beneke, T. Feldmann and D. Seidel, *Systematic approach to exclusive $B \to Vl^+l^-$, $V\gamma$ decays*, *Nucl. Phys.* **B612** (2001) 25–58 [hep-ph/0106067].

[48] M. Artuso *et. al.*, *B, D and K decays*, *Eur. Phys. J.* **C57** (2008) 309–492 [0801.1833].

[49] M. Ciuchini, G. Degrassi, P. Gambino and G. F. Giudice, *Next-to-leading QCD corrections to $B \to X_s\gamma$ in supersymmetry*, *Nucl. Phys.* **B534** (1998) 3–20 [hep-ph/9806308].

[50] A. J. Buras, P. Gambino, M. Gorbahn, S. Jager and L. Silvestrini, *Universal unitarity triangle and physics beyond the standard model*, *Phys. Lett.* **B500** (2001) 161–167 [hep-ph/0007085].

[51] W. Altmannshofer, A. J. Buras and P. Paradisi, *Low Energy Probes of CP Violation in a Flavor Blind MSSM*, *Phys. Lett.* **B669** (2008) 239–245 [0808.0707].

[52] W. Altmannshofer *et. al.*, *Symmetries and Asymmetries of $B \to K^*\mu^+\mu^-$. Decays in the Standard Model and Beyond*, *JHEP* **01** (2009) 019 [0811.1214].

[53] **CDF** Collaboration, T. Aaltonen *et. al.*, *First Flavor-Tagged Determination of Bounds on Mixing- Induced CP Violation in $B_s^0 \to J/\psi\phi$ Decays*, *Phys. Rev. Lett.* **100** (2008) 161802 [0712.2397].

[54] **D0** Collaboration, V. M. Abazov *et. al.*, *Measurement of B_s^0 mixing parameters from the flavor-tagged decay $B_s^0 \to J/\psi\phi$*, *Phys. Rev. Lett.* **101** (2008) 241801 [0802.2255].

[55] B. O. Lange, M. Neubert and G. Paz, *Theory of charmless inclusive B decays and the extraction of V(ub)*, *Phys. Rev.* **D72** (2005) 073006 [hep-ph/0504071].

[56] M. Antonelli *et. al.*, *Flavor Physics in the Quark Sector*, 0907.5386.

[57] **Heavy Flavor Averaging Group** Collaboration, E. Barberio *et. al.*, *Averages of b−hadron and c−hadron Properties at the End of 2007*, 0808.1297.

[58] M. Bona *et. al.*, *SuperB: A High-Luminosity Asymmetric e^+e^- Super Flavor Factory. Conceptual Design Report*, 0709.0451.

[59] **UTfit** Collaboration, M. Bona *et. al.*, *The unitarity triangle fit in the standard model and hadronic parameters from lattice QCD: A reappraisal after the measurements of $\Delta(m_s)$ and BR($B \to \tau\nu/\tau$)*, *JHEP* **10** (2006) 081 [hep-ph/0606167].

[60] **CLEO** Collaboration, R. Ammar *et. al.*, *Evidence for penguins: First observation of $B \to K^*(892)$ gamma*, *Phys. Rev. Lett.* **71** (1993) 674–678.

[61] P. Ball and R. Zwicky, *Time-dependent CP asymmetry in $B \to K^*\gamma$ as a (quasi) null test of the standard model*, *Phys. Lett.* **B642** (2006) 478–486 [hep-ph/0609037].

[62] J. Dickens, V. Gibson, C. Lazzeroni and M. Patel, "A study of the sensitivity to the forward-backward asymmetry in $B_d \to K^{*0}\mu^+\mu^-$ decays at LHC*b*.".

[63] P. Ball and V. M. Braun, *Use and misuse of QCD sum rules in heavy-to-light transitions: The decay $B \to \rho e\nu$ reexamined*, *Phys. Rev.* **D55** (1997) 5561–5576 [hep-ph/9701238].

[64] S. J. Brodsky and G. P. Lepage, *Exclusive processes in quantum chromodynamics*, *Adv. Ser. Direct. High Energy Phys.* **5** (1989) 93–240.

[65] R. Akhoury, G. F. Sterman and Y. P. Yao, *Exclusive semileptonic decays of B mesons into light mesons*, *Phys. Rev.* **D50** (1994) 358–372.

[66] J. A. Bailey *et. al.*, *The $B \to \pi\ell\nu$ semileptonic form factor from three-flavor lattice QCD: A Model-independent determination of $|V_{ub}|$*, *Phys. Rev.* **D79** (2009) 054507 [0811.3640].

[67] **QCDSF** Collaboration, A. Al-Haydari *et. al.*, *Semileptonic form factors $D \to \pi, K$ and $B \to \pi, K$ from a fine lattice*, *Eur. Phys. J.* **A43** (2010) 107–120 [0903.1664].

[68] C. Bernard *et. al.*, *Visualization of semileptonic form factors from lattice QCD*, *Phys. Rev.* **D80** (2009) 034026 [0906.2498].

[69] E. Dalgic *et. al.*, *B Meson Semileptonic Form Factors from Unquenched Lattice QCD*, *Phys. Rev.* **D73** (2006) 074502 [hep-lat/0601021].

[70] **UKQCD** Collaboration, K. C. Bowler, J. F. Gill, C. M. Maynard and J. M. Flynn, *$B \to \rho l \nu$ form factors in lattice QCD*, *JHEP* **05** (2004) 035 [hep-lat/0402023].

[71] P. Ball and R. Zwicky, *New Results on $B \to \pi$, K, η Decay Formfactors from Light- Cone Sum Rules*, *Phys. Rev.* **D71** (2005) 014015 [hep-ph/0406232].

[72] P. Ball and R. Zwicky, *$B_{d,s} \to \rho, \omega, K^*, \phi$ Decay Form Factors from Light-Cone Sum Rules Revisited*, *Phys. Rev.* **D71** (2005) 014029 [hep-ph/0412079].

[73] P. Colangelo and A. Khodjamirian, *QCD sum rules, a modern perspective*, hep-ph/0010175.

[74] M. A. Shifman, A. I. Vainshtein and V. I. Zakharov, *QCD and Resonance Physics. Sum Rules*, *Nucl. Phys.* **B147** (1979) 385–447.

[75] M. A. Shifman, A. I. Vainshtein and V. I. Zakharov, *QCD and Resonance Physics: Applications*, *Nucl. Phys.* **B147** (1979) 448–518.

[76] I. I. Balitsky, V. M. Braun and A. V. Kolesnichenko, *Radiative Decay $\Sigma^+ \to p\gamma$ in Quantum Chromodynamics*, *Nucl. Phys.* **B312** (1989) 509–550.

[77] V. L. Chernyak and I. R. Zhitnitsky, *B meson exclusive decays into baryons*, *Nucl. Phys.* **B345** (1990) 137–172.

[78] M. Beneke, T. Feldmann and D. Seidel, *Exclusive radiative and electroweak $b \to d$ and $b \to s$ penguin decays at NLO*, *Eur. Phys. J.* **C41** (2005) 173–188 [hep-ph/0412400].

[79] M. Beneke and T. Feldmann, *Symmetry-breaking corrections to heavy-to-light B meson form factors at large recoil*, *Nucl. Phys.* **B592** (2001) 3–34 [hep-ph/0008255].

[80] B. Grinstein, M. J. Savage and M. B. Wise, *$B \to X_s e^+ e^-$ in the Six Quark Model*, *Nucl. Phys.* **B319** (1989) 271–290.

[81] A. J. Buras, M. Misiak, M. Munz and S. Pokorski, *Theoretical uncertainties and phenomenological aspects of $B \to X_s \gamma$ decay*, *Nucl. Phys.* **B424** (1994) 374–398 [hep-ph/9311345].

[82] **BELLE** Collaboration, J. T. Wei *et. al.*, *Measurement of the Differential Branching Fraction and Forward-Backword Asymmetry for B-¿K(*)l+l-*, *Phys. Rev. Lett.* **103** (2009) 171801 [0904.0770].

[83] G. Eigen, *Exclusive $b \to s(d)\ell\ell$ Decays*, 0807.4076.

[84] **CDF** Collaboration, T. Aaltonen *et. al.*, *Search for the Rare Decays $B^+ \to \mu^+\mu^- K^+$, $B^0 \to \mu^+\mu^- K^{*0}(892)$, and $B_s^0 \to \mu^+\mu^-\phi$ at CDF*, *Phys. Rev.* **D79** (2009) 011104 [0804.3908].

[85] G. Hiller and F. Kruger, *More model-independent analysis of $b \to s$ processes*, *Phys. Rev.* **D69** (2004) 074020 [hep-ph/0310219].

[86] A. Ali, P. Ball, L. T. Handoko and G. Hiller, *A comparative study of the decays $B \to (K, K^*)l^+l^-$ in Standard Model and supersymmetric theories*, *Phys. Rev.* **D61** (2000) 074024 [hep-ph/9910221].

[87] A. Ali, G. Kramer and G.-h. Zhu, *$B \to K^*l^+l^-$ in soft-collinear effective theory*, *Eur. Phys. J.* **C47** (2006) 625–641 [hep-ph/0601034].

[88] C. Bobeth, G. Hiller and G. Piranishvili, *CP Asymmetries in bar $B \to \bar{K}^*(\to \bar{K}\pi)\bar{\ell}\ell$ and Untagged $\bar{B}_s$, $B_s \to \phi(\to K^+K^-)\bar{\ell}\ell$ Decays at NLO*, *JHEP* **07** (2008) 106 [0805.2525].

[89] U. Egede, T. Hurth, J. Matias, M. Ramon and W. Reece, *New observables in the decay mode $\bar{B} \to \bar{K}^{*0}l^+l^-$*, *JHEP* **11** (2008) 032 [0807.2589].

[90] C. S. Kim and T. Yoshikawa, *Systematic Analysis of $B \to K\pi l^+l^-$ Decay through Angular Decomposition*, 0711.3880.

[91] **Tevatron Electroweak Working Group** Collaboration, T. Aaltonen *et. al.*, *Combination of CDF and D0 results on the mass of the top quark*, 0808.1089.

[92] D. Becirevic, V. Lubicz and F. Mescia, *An estimate of the $B \to K^*\gamma$ form factor*, *Nucl. Phys.* **B769** (2007) 31–43 [hep-ph/0611295].

[93] S. Meinel, R. Horgan, L. Khomskii, L. C. Storoni and M. Wingate, *Moving NRQCD and $B \to K^*\gamma$*, *PoS* **LAT2007** (2007) 377 [0710.3101].

[94] P. Ball and V. M. Braun, *Exclusive semileptonic and rare B meson decays in QCD*, *Phys. Rev.* **D58** (1998) 094016 [hep-ph/9805422].

[95] T. Onogi, *Heavy flavor physics from lattice QCD*, *PoS* **LAT2006** (2006) 017 [hep-lat/0610115].

[96] P. Ball and R. Zwicky, *$|V_{td}/V_{ts}|$ from $B \to V\gamma$*, *JHEP* **04** (2006) 046 [hep-ph/0603232].

[97] M. Steinhauser, *Precise Determinations of the Charm Quark Mass*, 0809.1925.

[98] P. Ball and R. Zwicky, *SU(3) breaking of leading-twist K and K* distribution amplitudes: A reprise*, *Phys. Lett.* **B633** (2006) 289–297 [hep-ph/0510338].

[99] P. Ball and R. Zwicky, *Operator relations for SU(3) breaking contributions to K and K* distribution amplitudes*, *JHEP* **02** (2006) 034 [hep-ph/0601086].

[100] P. Ball and G. W. Jones, *Twist-3 distribution amplitudes of K^* and ϕ mesons*, *JHEP* **03** (2007) 069 [hep-ph/0702100].

[101] P. Ball, V. M. Braun and A. Lenz, *Twist-4 Distribution Amplitudes of the K^* and ϕ Mesons in QCD*, *JHEP* **08** (2007) 090 [0707.1201].

[102] B. Grinstein and D. Pirjol, *Precise $|V_{ub}|$ determination from exclusive B decays: Controlling the long-distance effects*, *Phys. Rev.* **D70** (2004) 114005 [hep-ph/0404250].

[103] F. Kruger, L. M. Sehgal, N. Sinha and R. Sinha, *Angular distribution and CP asymmetries in the decays $\overline{B} \to K^-\pi^+e^-e^+$ and $\overline{B} \to \pi^-\pi^+e^-e^+$*, *Phys. Rev.* **D61** (2000) 114028 [hep-ph/9907386].

[104] B. Grinstein and D. Pirjol, *The forward-backward asymmetry in $B \to K\pi l^+ l^-$ decays*, *Phys. Rev.* **D73** (2006) 094027 [hep-ph/0505155].

[105] C. S. Kim, Y. G. Kim, C. Lu and T. Morozumi, *Azimuthal angle distribution in $B \to K^*(\to K\pi) l^+ l^-$ at low invariant $m_{l^+l^-}$ region*, *Phys. Rev.* **D62** (2000) 034013 [hep-ph/0001151].

[106] F. Krüger and J. Matias, *Probing new physics via the transverse amplitudes of $B^0 \to K^{*0}(\to K^-\pi^+)\ell^+\ell^-$ at large recoil*, *Phys. Rev.* **D71** (2005) 094009 [hep-ph/0502060].

[107] A. Faessler, T. Gutsche, M. A. Ivanov, J. G. Korner and V. E. Lyubovitskij, *The Exclusive rare decays $B \to K(K^*)\bar{\ell}\ell$ and $B_c \to D(D^*)\bar{\ell}\ell$ in a relativistic quark model*, *Eur. Phys. J. direct* **C4** (2002) 18 [hep-ph/0205287].

[108] E. Lunghi and J. Matias, *Huge right-handed current effects in $B \to K^*(K\pi)l^+l^-$ in supersymmetry*, *JHEP* **04** (2007) 058 [hep-ph/0612166].

[109] D. Seidel, *Analytic two-loop virtual corrections to $b \to dl^+l^-$*, *Phys. Rev.* **D70** (2004) 094038 [hep-ph/0403185].

[110] G. Buchalla, G. Hiller and G. Isidori, *Phenomenology of nonstandard Z couplings in exclusive semileptonic $b \to s$ transitions*, *Phys. Rev.* **D63** (2000) 014015 [hep-ph/0006136].

[111] ***BABAR*** Collaboration, B. Aubert *et. al.*, *Angular distributions in the decays $B \to K^* l^+ l^-$*, 0804.4412.

[112] Belle Collaboration, J. T. Wei *et. al.*, *Measurement of the differential branching fraction and forward-backward asymmetry for $B \to K^{(*)} l^+ l^-$*, *Phys. Rev. Lett.* **103** (2009) 171801 [0904.0770].

[113] T. Feldmann and J. Matias, *Forward-backward and isospin asymmetry for $B_d \to K^{*0}\mu^+\mu^-$ decay in the Standard Model and in supersymmetry*, *JHEP* **01** (2003) 074 [hep-ph/0212158].

[114] A. J. Buras, *Minimal flavor violation*, *Acta Phys. Polon.* **B34** (2003) 5615–5668 [hep-ph/0310208].

[115] M. Blanke, A. J. Buras, D. Guadagnoli and C. Tarantino, *Minimal Flavour Violation Waiting for Precise Measurements of ΔM_s, S_{psiphi}, A^s_{SL}, $|V_{ub}|$, γ and $B^0_{s,d} \to \mu^+\mu^-$*, *JHEP* **10** (2006) 003 [hep-ph/0604057].

[116] **CDF** Collaboration, T. Aaltonen *et. al.*, *Search for $B^0_s \to \mu^+\mu^-$ and $B^0_d \to \mu^+\mu^-$ decays with $2fb^{-1}$ of $p\bar{p}$ collisions*, *Phys. Rev. Lett.* **100** (2008) 101802 [0712.1708].

[117] A. Ali, T. Mannel and T. Morozumi, *Forward backward asymmetry of dilepton angular distribution in the decay $b \to sl^+l^-$*, *Phys. Lett.* **B273** (1991) 505–512.

[118] G. Burdman, *Short distance coefficients and the vanishing of the lepton asymmetry in $B \to Vl^+l^-$*, *Phys. Rev.* **D57** (1998) 4254–4257 [hep-ph/9710550].

[119] W. Reece and U. Egede, "Performing the full angular analysis of $\overline{B}_d \to \overline{K}^{*0}\mu^+\mu^-$ at LHC*b*." CERN-LHCb-2008-041.

[120] F. Jansen, N. Serra, G. Y. Smit and N. Tuning, "Determination of the forward-backward asymmetry in the decay $B_d \to K^{*0}\mu^+\mu^-$ with an unbinned counting analysis." CERN-LHCb-2009-003, May, 2009.

[121] U. Egede, "Angular correlations in the $\overline{B}_d \to \overline{K}^{*0}\mu^+\mu^-$ decay." CERN-LHCb-2007-057.

[122] D. J. Lange, *The* EvtGen *particle decay simulation package*, *Nucl. Instrum. Meth.* **A462** (2001) 152–155.

[123] P. Ball. private communication, 2007.

[124] Q.-S. Yan, C.-S. Huang, W. Liao and S.-H. Zhu, *Exclusive semileptonic rare decays $B \to (K, K^{*0})l^+l^-$ in supersymmetric theories*, *Phys. Rev.* **D62** (2000) 094023 [hep-ph/0004262].

[125] **Particle Data Group** Collaboration, C. Amsler *et. al.*, *Review of particle physics*, *Phys. Lett.* **B667** (2008) 1.

[126] A. Signer, *The charm quark mass from non-relativistic sum rules*, *Phys. Lett.* **B672** (2009) 333–338 [0810.1152].

[127] A. Pineda and A. Signer, *Renormalization Group Improved Sum Rule Analysis for the Bottom Quark Mass*, *Phys. Rev.* **D73** (2006) 111501 [hep-ph/0601185].

[128] M. Beneke, *A quark mass definition adequate for threshold problems*, *Phys. Lett.* **B434** (1998) 115–125 [hep-ph/9804241].

[129] T. Appelquist, H.-C. Cheng and B. A. Dobrescu, *Bounds on universal extra dimensions*, *Phys. Rev.* **D64** (2001) 035002 [hep-ph/0012100].

[130] P. Colangelo, F. De Fazio, R. Ferrandes and T. N. Pham, *Exclusive $B \to K^{(*)}l^+l^-$, $B \to K^{(*)}\nu\bar{\nu}$ and $B \to K^*\gamma$ transitions in a scenario with a single universal extra dimension*, *Phys. Rev.* **D73** (2006) 115006 [hep-ph/0604029].

[131] E. Gabrielli and S. Khalil, *On the $B \to X_s l^+l^-$ decays in general supersymmetric models*, *Phys. Lett.* **B530** (2002) 133–141 [hep-ph/0201049].

[132] C. Bobeth, A. J. Buras and T. Ewerth, *$\bar{B} \to X_s l^+l^-$ in the MSSM at NNLO*, *Nucl. Phys.* **B713** (2005) 522–554 [hep-ph/0409293].

[133] ***BABAR*** Collaboration, B. Aubert *et. al.*, *Measurements of branching fractions, rate asymmetries, and angular distributions in the rare decays $B \to Kl^+l^-$ and $B \to K^*l^+l^-$*, *Phys. Rev.* **D73** (2006) 092001 [hep-ex/0604007].

[134] **CDF** Collaboration, "Search for $B_s^0 \to \mu^+\mu^-$ and $B_d^0 \to \mu^+\mu^-$ decays with $3.7 fb^{-1}$ of $p\bar{p}$ collisions." CDF Public Note 9892, 2009.

[135] **BABAR** Collaboration, B. Aubert *et. al.*, *Measurement of the $B \to X_s\ell^+\ell^-$ branching fraction with a sum over exclusive modes*, *Phys. Rev. Lett.* **93** (2004) 081802 [hep-ex/0404006].

[136] **Belle** Collaboration, M. Iwasaki *et. al.*, *Improved measurement of the electroweak penguin process $B \to X_s l^+l^-$*, *Phys. Rev.* **D72** (2005) 092005 [hep-ex/0503044].

[137] A. Ghinculov, T. Hurth, G. Isidori and Y. P. Yao, *The rare decay $B \to X_s l^+ l^-$ to NNLL precision for arbitrary dilepton invariant mass*, *Nucl. Phys.* **B685** (2004) 351–392 [hep-ph/0312128].

[138] D. Guetta and E. Nardi, *Searching for new physics in rare $B \to \tau$ decays*, *Phys. Rev.* **D58** (1998) 012001 [hep-ph/9707371].

[139] P. Gambino and P. Giordano, *Normalizing inclusive rare B decays*, *Phys. Lett.* **B669** (2008) 69–73 [0805.0271].

[140] **Heavy Flavor Averaging Group (HFAG)** Collaboration, E. Barberio *et. al.*, *Averages of B–hadron properties at the end of 2006*, 0704.3575.

[141] M. Bauer, S. Casagrande, U. Haisch and M. Neubert, *Flavor Physics in the Randall-Sundrum Model: II. Tree- Level Weak-Interaction Processes*, 0912.1625.

[142] A. Bharucha and W. Reece, *Constraining new physics with B to K* mu+ mu- in the early LHC era*, 1002.4310.

[143] **LHC*b*** Collaboration, B. Adeva *et. al.*, *Roadmap for selected key measurements of LHC*b, 0912.4179.

[144] D. Becirevic and A. B. Kaidalov, *Comment on the heavy $\to$ light form factors*, *Phys. Lett.* **B478** (2000) 417–423 [hep-ph/9904490].

[145] J. M. Flynn and J. Nieves, *$|V_{ub}|$ from exclusive semileptonic $B \to \pi$ decays revisited*, *Phys. Rev.* **D76** (2007) 031302 [0705.3553].

[146] C. Bourrely, I. Caprini and L. Lellouch, *Model-independent description of $B \to \pi l \nu$ decays and a determination of $|V_{ub}|$*, *Phys. Rev.* **D79** (2009) 013008 [0807.2722].

[147] M. C. Arnesen, B. Grinstein, I. Z. Rothstein and I. W. Stewart, *A precision model independent determination of $|V_{ub}|$ from $B \to \pi e \nu$*, *Phys. Rev. Lett.* **95** (2005) 071802 [hep-ph/0504209].

[148] C. G. Boyd, B. Grinstein and R. F. Lebed, *Constraints on form-factors for exclusive semileptonic heavy to light meson decays*, *Phys. Rev. Lett.* **74** (1995) 4603–4606 [hep-ph/9412324].

[149] C. G. Boyd and M. J. Savage, *Analyticity, shapes of semileptonic form factors, and $\bar{B} \to \pi \ell \bar{\nu}$*, *Phys. Rev.* **D56** (1997) 303–311 [hep-ph/9702300].

[150] I. Caprini, L. Lellouch and M. Neubert, *Dispersive bounds on the shape of $\bar{B} \to D^{(*)} l \bar{\nu}$ form factors*, *Nucl. Phys.* **B530** (1998) 153–181 [hep-ph/9712417].

[151] T. Becher and R. J. Hill, *Comment on form factor shape and extraction of $|V_{ub}|$ from $B \to \pi \ell \nu$*, *Phys. Lett.* **B633** (2006) 61–69 [hep-ph/0509090].

[152] C. Bobeth, G. Hiller and G. Piranishvili, *Angular Distributions of $B \to K ll$ Decays*, *JHEP* **12** (2007) 040 [0709.4174].

[153] M. Bartsch, M. Beylich, G. Buchalla and D. N. Gao, *Precision Flavour Physics with $B \to K \nu \bar{\nu}$ and $B \to K \ell^+ \ell^-$*, *JHEP* **11** (2009) 011 [0909.1512].

[154] P. Ball, $|V_{ub}|$ *from UTangles and* $B \to \pi\ell\nu$, *Phys. Lett.* **B644** (2007) 38–44 [hep-ph/0611108].

[155] A. Bharucha, T. Feldmann and M. Wick, *Theoretical and Phenomenological Constraints on Form Factors for Radiative and Semi-Leptonic B-Meson Decays*, 1004.3249.

[156] W. A. Bardeen, E. J. Eichten and C. T. Hill, *Chiral Multiplets of Heavy-Light Mesons*, *Phys. Rev.* **D68** (2003) 054024 [hep-ph/0305049].

[157] V. A. Novikov, M. A. Shifman, A. I. Vainshtein and V. I. Zakharov, *Operator expansion in quantum chromodynamics beyond perturbation theory*, *Nucl. Phys.* **B174** (1980) 378.

[158] R. J. Hill, *The modern description of semileptonic meson form factors*, hep-ph/0606023.

[159] C. Bernard *et. al.*, *Status of the MILC light pseudoscalar meson project*, *PoS* **LAT2007** (2007) 090 [0710.1118].

[160] R. Williams, C. S. Fischer and M. R. Pennington, *Extracting the* $\bar{q}q$ *condensate for light quarks beyond the chiral limit in models of QCD*, 0704.2296.

[161] M. V. Polyakov and C. Weiss, *Mixed quark-gluon condensate from instantons*, *Phys. Lett.* **B387** (1996) 841–847 [hep-ph/9607244].

[162] G. D'Agostini, *Asymmetric Uncertainties: Sources, Treatment and Potential Dangers*, physics/0403086.

[163] C. Bobeth, G. Hiller and D. van Dyk, *The Benefits of* $B \to K^* l^+ l^-$ *Decays at Low Recoil*, *JHEP* **07** (2010) 098 [1006.5013].

[164] S. Descotes-Genon and A. Le Yaouanc, *Parametrisations of the* $D \to Kl\nu$ *form factor and the determination of* $\hat{g}$, *J. Phys.* **G35** (2008) 115005 [0804.0203].

[165] **UKQCD** Collaboration, A. M. Green, J. Koponen, C. McNeile, C. Michael and G. Thompson, *Excited B mesons from the lattice*, *Phys. Rev.* **D69** (2004) 094505 [hep-lat/0312007].

[166] P. Ball and R. Zwicky, $|V_{ub}|$ *and constraints on the leading-twist pion distribution amplitude from* $B \to \pi\ell\nu$, *Phys. Lett.* **B625** (2005) 225–233 [hep-ph/0507076].

[167] P. Ball and R. Zwicky, $B \to \pi, K, \eta$ *decay formfactors from light-cone sum rules*, hep-ph/0406261.

[168] G. Duplancic, A. Khodjamirian, T. Mannel, B. Melic and N. Offen, $|V_{ub}|$ *determination using* $B \to \pi$ *form factor from light-cone sum rule*, *J. Phys. Conf. Ser.* **110** (2008) 052026.

[169] **CLEO** Collaboration, S. B. Athar *et. al.*, *Study of the* q^2 *dependence of* $B \to \pi l\nu$ *and* $B \to \rho(\omega) l\nu$ *decay and extraction of* $|V_{ub}|$, *Phys. Rev.* **D68** (2003) 072003 [hep-ex/0304019].

[170] **CLEO** Collaboration, N. E. Adam *et. al.*, *A Study of Exclusive Charmless Semileptonic B Decay and* $|V_{ub}|$, *Phys. Rev. Lett.* **99** (2007) 041802 [hep-ex/0703041].

[171] **BABAR** Collaboration, B. Aubert *et. al.*, *Study of $B \to \pi \ell \nu$ and $B \to \rho \ell \nu$ decays and determination of $|V_{ub}|$*, *Phys. Rev.* **D72** (2005) 051102 [hep-ex/0507003].

[172] **BABAR** Collaboration, B. Aubert *et. al.*, *Measurements of $B \to \{\pi, \eta, \eta'\} \ell \nu_\ell$ Branching Fractions and Determination of $|V_{ub}|$ with Semileptonically Tagged B Mesons*, *Phys. Rev. Lett.* **101** (2008) 081801 [0805.2408].

[173] **BABAR** Collaboration, and others, *Study of $B \to \pi l \nu$ and $B \to \rho l \nu$ Decays and Determination of $|V_{ub}|$*, 1005.3288.

[174] **Belle** Collaboration, I. Adachi *et. al.*, *Measurement of exclusive $B \to X_u l \nu$ decays using full- reconstruction tagging at Belle*, 0812.1414.

[175] J. M. Flynn and J. Nieves, *$|V_{ub}|$ from Exclusive Semileptonic $B \to \pi$ Decays*, *Phys. Lett.* **B649** (2007) 269–274 [hep-ph/0703284].

[176] M. Jamin and B. O. Lange, *f_B and f_{B_s} from QCD sum rules*, *Phys. Rev.* **D65** (2002) 056005 [hep-ph/0108135].

[177] A. A. Penin and M. Steinhauser, *Heavy-light meson decay constant from QCD sum rules in three-loop approximation*, *Phys. Rev.* **D65** (2002) 054006 [hep-ph/0108110].

[178] E. Bagan, P. Ball and V. M. Braun, *Radiative corrections to the decay $B \to \pi e \nu$ and the heavy quark limit*, *Phys. Lett.* **B417** (1998) 154–162 [hep-ph/9709243].

[179] A. Khodjamirian, R. Ruckl, S. Weinzierl, C. W. Winhart and O. I. Yakovlev, *Predictions on $B \to \pi \bar{l} \nu / l$, $D \to \pi \bar{l} \nu / l$ and $D \to K \bar{l} \nu / l$ from QCD light-cone sum rules*, *Phys. Rev.* **D62** (2000) 114002 [hep-ph/0001297].

[180] S. J. Brodsky, G. P. Lepage and P. B. Mackenzie, *On the Elimination of Scale Ambiguities in Perturbative Quantum Chromodynamics*, *Phys. Rev.* **D28** (1983) 228.

[181] D. J. Broadhurst and A. G. Grozin, *Matching QCD and HQET heavy - light currents at two loops and beyond*, *Phys. Rev.* **D52** (1995) 4082–4098 [hep-ph/9410240].

[182] M. Beneke and V. M. Braun, *Naive nonAbelianization and resummation of fermion bubble chains*, *Phys. Lett.* **B348** (1995) 513–520 [hep-ph/9411229].

[183] P. Ball, M. Beneke and V. M. Braun, *Resummation of $(\beta_0 \, alpha_s)^n$ corrections in QCD: Techniques and applications to the tau hadronic width and the heavy quark pole mass*, *Nucl. Phys.* **B452** (1995) 563–625 [hep-ph/9502300].

[184] B. Melic, B. Nizic and K. Passek, *BLM scale setting for the pion transition form factor*, *Phys. Rev.* **D65** (2002) 053020 [hep-ph/0107295].

[185] R. Mertig, M. Bohm and A. Denner, *FEYN CALC: Computer algebraic calculation of Feynman amplitudes*, *Comput. Phys. Commun.* **64** (1991) 345–359.

[186] T. Huber and D. Maitre, *HypExp 2, Expanding Hypergeometric Functions about Half- Integer Parameters*, *Comput. Phys. Commun.* **178** (2008) 755–776 [0708.2443].

[187] G. R. Katz, *Two Loop Feynman Gauge Calculation of the Meson Nonsinglet Evolution Potential*, *Phys. Rev.* **D31** (1985) 652.

[188] S. V. Mikhailov and A. V. Radyushkin, *Evolution Kernels in QCD: Two Loop Calculation in Feynman Gauge*, *Nucl. Phys.* **B254** (1985) 89.

[189] E. Braaten, *QCD Corrections to Meson - Photon Transition Form-Factors*, *Phys. Rev.* **D28** (1983) 524.

[190] R. Tarrach, *The Pole Mass in Perturbative QCD*, *Nucl. Phys.* **B183** (1981) 384.

[191] V. M. Braun and I. E. Filyanov, *QCD Sum Rules in Exclusive Kinematics and Pion Wave Function*, *Z. Phys.* **C44** (1989) 157.

[192] P. Ball and A. N. Talbot, *Models for light-cone meson distribution amplitudes*, *JHEP* **06** (2005) 063 [hep-ph/0502115].

[193] P. Ball, *Theoretical update of pseudoscalar meson distribution amplitudes of higher twist: The nonsinglet case*, *JHEP* **01** (1999) 010 [hep-ph/9812375].

[194] T. M. Aliev and V. L. Eletsky, *On Leptonic Decay Constants of Pseudoscalar D and B Mesons*, *Sov. J. Nucl. Phys.* **38** (1983) 936.

[195] E. Bagan, P. Ball, V. M. Braun and H. G. Dosch, *QCD sum rules in the effective heavy quark theory*, *Phys. Lett.* **B278** (1992) 457–464.

[196] C. A. Dominguez and N. Paver, *How large is f_B from QCD sum rules?*, *Phys. Lett.* **B269** (1991) 169–174.

[197] K. G. Chetyrkin and M. Steinhauser, *Heavy-light current correlators at order α_s^2 in QCD and HQET*, *Eur. Phys. J.* **C21** (2001) 319–338 [hep-ph/0108017].

[198] K. G. Chetyrkin, J. H. Kuhn and M. Steinhauser, *Heavy quark current correlators to $\mathcal{O}(\alpha_s^2)$*, *Nucl. Phys.* **B505** (1997) 40–64 [hep-ph/9705254].

[199] V. L. Chernyak and A. R. Zhitnitsky, *Asymptotic Behavior of Exclusive Processes in QCD*, *Phys. Rept.* **112** (1984) 173.

[200] S. V. Mikhailov and A. V. Radyushkin, *The Pion wave function and QCD sum rules with nonlocal condensates*, *Phys. Rev.* **D45** (1992) 1754–1759.

[201] L. Del Debbio, M. Di Pierro and A. Dougall, *The second moment of the pion light cone wave function*, *Nucl. Phys. Proc. Suppl.* **119** (2003) 416–418 [hep-lat/0211037].

[202] V. M. Braun *et. al.*, *Moments of pseudoscalar meson distribution amplitudes from the lattice*, *Phys. Rev.* **D74** (2006) 074501 [hep-lat/0606012].

[203] **RBC** Collaboration, P. A. Boyle *et. al.*, *Parton Distribution Amplitudes and Non-Perturbative Renormalisation*, *PoS* **LATTICE2008** (2008) 165 [0810.1669].

[204] **CLEO** Collaboration, J. Gronberg *et. al.*, *Measurements of the meson photon transition form factors of light pseudoscalar mesons at large momentum transfer*, *Phys. Rev.* **D57** (1998) 33–54 [hep-ex/9707031].

[205] **CELLO** Collaboration, H. J. Behrend *et. al.*, *Studies of multi - hadronic final states in photon-photon interactions*, *Z. Phys.* **C51** (1991) 365–376.

[206] N. G. Stefanis, *New vistas of the meson structure in QCD from low to high energies*, *Nucl. Phys. Proc. Suppl.* **181-182** (2008) 199–203 [0805.3117].

[207] M. Jamin and M. Münz, *Current correlators to all orders in the quark masses*, *Z. Phys.* **C60** (1993) 569–578 [hep-ph/9208201].